Treatment Of Fluoride Containing Water Using Adsorption And Precipitation Followed By Microfiltration

Thesis submitted in partial fulfillment of the

requirements for the Degree

of

DOCTOR OF PHILOSOPHY

by

Aparajita Goswami

Department of Chemical Engineering
Indian Institute of Technology Guwahati
Guwahati – 781039, India
March, 2013

Dedication

To My beloved father

"Late Jagannath Goswami"

for whom I have become what I am today.

Department of Chemical Engineering
Indian Institute of Technology Guwahati
Guwahati 781039, India

CERTIFICATE

This is to certify that the thesis entitled "**Treatment Of Fluoride Containing Water Using Adsorption And Precipitation Followed By Microfiltration**", being submitted by Ms Aparajita Goswami for the award of PhD degree, is a record of bonafide research carried out by her at the Chemical Engineering Department, Indian Institute of Technology Guwahati, under my guidance and supervision. The work documented in this thesis has not been submitted to any other University or Institute for the award of any degree or diploma.

(Dr. Mihir Kumar Purkait)
Associate Professor
Department of Chemical Engineering
Indian Institute of Technology Guwahati
Guwahati 781039

Acknowledgement

I would like to express my gratitude to all those who in different ways helped me in completing this research work within the time span of four years directly or indirectly. To begin with, I wish to express my deepest acknowledgement to my supervisor, **Dr. Mihir Kumar Purkait** for providing me inspiring and valuable guidance throughout the entire course of this work. I am indebted to him for his useful suggestions and constant encouragement throughout the entire period. He taught me how to write and improve the quality of a journal paper and the thesis. I thank him for his patience and amicable nature. It has been a great privilege to work with him. The experience of working with him, I strongly believe, will have far-reaching influence in my future life.

I express my gratitude and indebtedness to Dr. V.S. Moholkar, head, Chemical Engineering Department, Dr. P. Saha, Ex-head, Chemical Engineering Department, and Dr. A.K. Ghosal, Ex-head, Chemical Engineering Department, for providing me with the necessary laboratory and Departmental facilities.

I am grateful to all the members of my doctoral committee, Dr. S.K. Mazumdar and Dr. C. Das of Chemical Engineering Department and Dr. B. Pradhan of Civil Engineering Department for their supports and valuable suggestions throughout my doctoral program.

I am thankful to all the staff members of **Central Instruments Facility** for allowing me to utilize their experimental resources which was essential in my research work. I am also thankful to all present and ex-staff members of the Chemical Engineering Department for their genuine help and support during the entire period of this work.

I am also grateful to all the faculty members of Chemical Engineering Department for their useful suggestions and help at various stages of this work. I am thankful to my senior research scholars, Barun, Deba da, Bandana mam, Kabita mam and Ujwala for their friendly behavior and assistance. I also wish to extend my deep sense of appreciation to all my research colleagues for their friendly support and timely assistance whenever I needed for. Working with them was really a pleasant experience for me. Thanks to all those lab-mates in the department including the present and past M. Tech students for their help in different forms.

I also wish to extend my loving thanks to my family, my brother and my sister and all the family members for their constant moral supports. I have no word to thank **GOD** who is my strength and wisdom.

Finally, I express my enormous gratitude and indebtedness to my husband, **Ranjan, my sister in law Sangeeta** and **my mother in law** for their utmost care, immense sacrifice, unlimited patience and constant endorsement at all stages of this work during these period. This work would not have been possible to complete without their support.

Indian Institute of Technology Guwahati ***(Aparajita Goswami)***

March, 2013

Abstract

Scarcity of drinking water is a major problem in present world. Although lots of water sources are available, source of drinking water is very limited due to contamination of water. The most harmful contaminant present in water includes fluoride, arsenic, iron and nitrate/ nitrite. The fluoride contamination covers almost all parts of the world. India is also affected severely by this contaminant. Seventeen states of India are affected by fluorosis, which is a fluoride bearing disease. Small amount of fluoride is important for the development of teeth and bone. But its excess content may cause several diseases to human as well as animals. Therefore researcher focused on their research for efficient defluoridation techniques. Various techniques like adsorption, chemical coagulation - precipitation, membrane separation, ion-exchange and hybrid techniques were investigated in detail. Unfortunately the performance of all the processes remains unsatisfactory due the unique properties of fluoride. Considering the fundamental aspect of fluoride removal, the present work is focused on few defluoridation techniques.

Three different techniques viz., adsorption, chemical precipitation and chemical precipitation followed by microfiltration were investigated for effective removal of fluoride from water. Adsorption study was carried out with four different adsorbents like pyrophyllite, acidic alumina, schwertmannite and nanomagnetite aggregated schwertmannite. The adsorbents were characterized by XRD, BET, FTIR, FESEM and VSM to know its structure, surface area, functional groups present, morphology and magnetic property respectively. Several parameters like contact time, initial fluoride concentration, adsorbent dose, pH,

temperature, stirring speed, presence of other ions were studied in detailed. Thermodynamic and kinetic study was carried out to know the nature and mechanism of adsorption. Equilibrium isotherm was studied with Langmuir, Freundlich, Temkin and DR isotherm models. The performance of the adsorbents in terms of adsorption capacity was observed in the following order; pyrophyllite < acidic alumina < schwertmannite < nanomagnetite aggregated schwertmannite. All the adsorbents are regenerated and a process design calculation was made in order to preliminary asses the adsorbent requirement.

Chemical precipitation method was used to remove fluoride from water. Three different precipitating agents: calcium chloride, calcium hydroxide and calcium nitrate were selected to precipitate fluoride ion from water. The parameters such as effect of molar ration, pH and presence of other ions effect on the extent of fluoride removal was studied in detailed. The precipitate formed during this technique was characterized by FESEM, EDX and XRD to know its composition and physical nature. However, the rate of settling was very low due to smaller size and lesser amount of fluoride precipitate. Hence, microfiltration (MF) was chosen as a combinational technique to remove fluoride precipitate from the precipitation chamber.

Inorganic microfiltration membrane was prepared by paste method and sintered at 950^{o}C. The membrane was characterized using standard technique. The prepared MF membrane was of circular shape having 52.5 mm diameter and 0.5 mm width and placed in a batch cell. Fluoride removal efficiency of prepared MF membrane was observed at various operating conditions and results are reported in details. Precipitation followed by microfiltration experiments was conducted and the performances in term of permeate flux and

extent of fluoride removal was investigated. It was observed that the prepared microfiltration membrane was efficient in retaining the suspended particulates formed during the chemical precipitation process. In addition to this, the retained particulates over the ceramic membrane surface were characterized using SEM, XRD and EDX. It was observed that the hybrid technique can successfully remove fluoride from contaminated drinking water. Apart from defluoridation experiments, copper (II) oxide nanoparticle was synthesized and used for arsenic removal from aqueous medium. It was seen that the arsenic removal capacity of the said adsorbent is much better than the several conventional adsorbent.

Summary

In this study, different techniques for defluoridation of water were investigated. Four different adsorbents viz; pyrophyllite, acidic alumina, schwertmannite and nanomagnetite aggregated schwertmannite were used for defluoridation of water. Different precipitating agents such as calcium chloride, calcium hydroxide and calcium nitrate were used to precipitate and remove fluoride from water. A microfiltration membrane was prepared and used for the separation of byproducts obtained from chemical precipitation method of defluoridation. Apart from these adsorbent, copper (II) oxide nanoparticles were synthesized and used for the removal of arsenic from contaminated drinking water.

The thesis is organized in the following chapters:

Chapter 1: Introduction

Chapter 2: Adsorbent Preparation and Characterization

Chapter 3: Removal of Fluoride Using Various Adsorbents

Chapter 4: Chemical Treatment Followed by Microfiltration for Defluoridation

Chapter 5: Removal of Arsenic Using Copper (II) Oxide Nanoparticles

Chapter 6: Conclusions and Scope of Future Works

Keeping in mind the broad objectives of the work, the present thesis is organized as follows.

Chapter 1 gives an overview of the problem undertaken in this work. A brief overview of fluoride and its harmful effects are discussed in this chapter. It also explains the salient features of different defluoridation techniques used to reduce fluoride content in water. The

chapter subsequently represents detailed literature review of different processes, its advantages and limitations and selection of a particular technique of defluoridation. Different adsorbents, their advantages and performances towards defluoridation are explained. The occurrence and various health effects of arsenic are also explained in this section. The removal of arsenic using various techniques is reported well. Finally, the broad objectives of the present work are mentioned in **Chapter 1**.

Complete description of the experimentations involved during adsorbent preparation and their characterization techniques are reported in **Chapter 2**. The characterization results of different adsorbents are also discussed here. **Chapter 3** explains separately the details of experimentations involved during adsorption of fluoride from synthetic fluoride contaminated water using different adsorbents including results and discussion thereon. Effect of different adsorption parameters on the extent of adsorption is reported. Details of kinetics, equilibrium and thermodynamic behavior of adsorption are discussed. Spent adsorbents are regenerated and a process calculation for designing of an adsorber for defluoridation is also presented in this chapter.

The chemical precipitation technique for defluoridation was adopted and the results are elaborated in **Chapter 4**. The preparation and characterization of microfiltration membrane is also described here. Precipitation followed by microfiltration technique was adopted for defluoridation and discussed in **Chapter 4**. The removal of arsenic using copper (II) nanoparticle is discussed in **Chapter 5**. Finally, conclusions and future recommendations drawn from this study are summarized in **Chapter 6**.

List of Tables

Table number	Caption	Page number
Table 1.1	Fluoride concentration in agricultural crops and edible items [21]	6
Table 1.2	Effects of fluoride in water on human health [20]	8
Table 1.3	Fluoride Concentrations in Different States of India [22]	11
Table 1.4	Analysis results of selected groundwater samples of Guwahati [34]	13
Table 1.5	Advantages and disadvantages of different fluoride removal techniques	22
Table 3.1	Experimental conditions for different adsorbents used for defluoridation of water	76
Table 3.2	Thermodynamic parameters of fluoride adsorption on pyrophyllite at different temperatures	95
Table 3.3	External mass transfer coefficient for the adsorption of fluoride at 24^{o}C	97
Table 3.4	Different kinetic model parameters at 24^{o}C	101
Table 3.5	Langmuir and Freundlich isotherm constants for the adsorption of fluoride on pyrophyllite at 24^{o}C	106
Table 3.6	Thermodynamic parameters for fluoride adsorption using acidic alumina	117
Table 3.7	Different kinetic model parameters at 25 ^{o}C for fluoride adsorption	119

Table 3.8	Langmuir and Freundlich isotherm constants for fluoride adsorption on acidic alumina	121
Table 3.9	Thermodynamic parameters for fluoride adsorption on Sh	131
Table 3.10	Kinetic model parameters for fluoride adsorption on Sh	132
Table 3.11	Equilibrium isotherm constants of Langmuir, Freundlich, Temkin and DR isotherms for fluoride adsorption	136
Table 3.12	Thermodynamic parameters for fluoride adsorption on Sh	145
Table 3.13	Various kinetic model parameters at 25 ^{o}C on NMSh	148
Table 3.14	Langmuir, Freundlich, Temkin and DR isotherm constants for fluoride adsorption on NMSh	150
Table 3.15	Comparison of fluoride adsorption capacities of different adsorbents	160
Table 4.1	Composition of ceramic microfiltration membrane	179
Table 4.2	EDX analysis of the synthesized membrane before and after corrosion test	195
Table 4.3	Experimental condition of fluoride removal by MF membrane	196
Table 4.4	Removal performance of fluoride by hybrid technique	201
Table 4.5	Quality of chemical precipitation solution and permeate of MF	204
Table 5.1	Effect of competing anions on arsenic adsorption	220
Table 5.2	Thermodynamic parameters for arsenic adsorption	221

Table 5.3	Various kinetic model parameters for arsenic adsorption at 25^{o}C	225
Table 5.4	Comparison of arsenic adsorption capacity of copper (II) oxide with some reported adsorbents	228
Table 5.5	Langmuir and Freundlich isotherm constants for arsenic adsorption	228
Table ER1:	Values of uncertainties estimated in PWF measurements for membranes prepared at 950 ^{o}C and operated at 310 kPa of transmembrane pressure	243

List of Figures

Figure number	Caption	Page number
Fig. 1.1	Countries with endemic fluorosis due to excess fluoride in drinking water	10
Fig. 1.2	Map showing the distribution of fluoride in guwahati city. Location of fluoride-affected areas: 1, Bonda; 2, Narengi; 3, Birkuchi; 4, Saatgaon; 5, Boidangbori; 6, Hengerabari; 7, Sixmile; 8, Beltola; 9, Hatigaon; 10, Bashistha; 11, Khanapara; 12, Lokhra Chariali; 13, Saukuchi; 14, Chandmari; 15, Noonmati and 16, Mathgharia	14
Fig. 2.1	Structure of pyrophyllite molecule [1]	45
Fig. 2.2	Pore size distribution of pyrophyllite	53
Fig. 2.3	X-ray diffraction of pyrophyllite molecule	53
Fig. 2.4	FTIR of pyrophyllite molecule	54
Fig. 2.5	Particle size distribution of pyrophyllite	55
Fig. 2.6	pH_{ZPC} of pyrophyllite	56
Fig. 2.7	Pore size distribution of acidic alumina	57
Fig. 2.8	XRD of acidic alumina	58
Fig. 2.9	FTIR of acidic alumina	59
Fig. 2.10	SEM picture of acidic alumina	59
Fig. 2.11	Particle size distribution of acidic alumina	60

Fig. 2.12	pH_{ZPC} of acidic alumina	61
Fig. 2.13	Pore size distribution of Sh	62
Fig. 2.14	XRD of Sh	63
Fig. 2.15	FESEM image of Sh	64
Fig. 2.16	FTIR of Sh	65
Fig. 2.17	Particle size distribution of Sh	66
Fig. 2.18	Pore size distribution of NMSh	67
Fig. 2.19	XRD of NMSh and magnetite particles	68
Fig. 2.20	FESEM picture of NMSh	69
Fig. 2.21	FTIR of NMSh	70
Fig. 2.22	VSM of magnetite, NMSh and Sh	71
Fig. 2.23	pH_{ZPC} of NMSh	72
Fig. 3.1	Single stage batch reactor design scheme	88
Fig. 3.2a	Effect of contact time on fluoride adsorption by pyrophyllite	90
Fig. 2b	Effect of initial fluoride concentration on the adsorption rate	91
Fig. 3.3	Variation of fluoride adsorption with adsorbent dose	92
Fig 3.4	Effect of pH on the percentage adsorption of fluoride	94
Fig. 3.5	Effect of temperature on the extent of adsorption of fluoride	95
Fig. 3.6	Effect of stirring on the percentage adsorption of fluoride	98
Fig. 3.7	Effect of other ions on the extent of adsorption of fluoride	99
Fig. 3.8	Pseudo second order kinetic model for the adsorption of fluoride	102
Fig. 3.9	Intra particle diffusion model for adsorption of fluoride	103

Fig. 3.10	Langmuir and Freundlich adsorption isotherms for fluoride adsorption	105
Fig. 3.11	Volume of fluoride contaminated water treated with unit mass of pyrophyllite (Adsorbent mass (M) against volume of solution treated (L))	107
Fig. 3.12	Effect of contact time on fluoride adsorption using acidic alumina	109
Fig. 3.13	Variation of adsorbent dose on the removal of fluoride	110
Fig. 3.14	Effect of pH on the percentage adsorption of fluoride using acidic alumina	112
Fig. 3.15	Effect of stirring speed on fluoride adsorption	113
Fig. 3.16	Effect of other anions on fluoride adsorption	115
Fig. 3.17	Effect of temperature on fluoride adsorption	116
Fig. 3.18	Kinetics of acidic alumina adsorbed fluoride (a) Pseudo second order (b) Intra particle diffusion	118
Fig. 3.19	Various adsorption isotherms for fluoride adsorption on acidic alumina	120
Fig. 3.20	Volume of treated water using unit mass of acidic alumina	123
Fig. 3.21	Effect of contact time on fluoride adsorption by Sh	125
Fig. 3.22	Variation of adsorbent dose on residual fluoride concentration	126
Fig. 3.23	Effect of pH on the percentage adsorption of fluoride using Sh	128
Fig. 3.24	Fluoride removal in presence of various co-ions	130
Fig. 3.25	Effect of temperature on fluoride removal efficiency	131
Fig. 3.26	Kinetics of Sh adsorbed fluoride (a) Pseudo first order (b) Pseudo	133

	second order (c) Intra particle diffusion	
Fig. 3.27	Adsorption isotherms of Sh - fluoride system	135
Fig. 3.28	Variation of volume of fluoride free water using Sh	137
Fig. 3.29	Effect of contact time on fluoride adsorption by NMSh	139
Fig. 3.30	Residual fluoride concentration with varying adsorbent dose	140
Fig. 3.31	Effect of pH on the percentage adsorption of fluoride using NMSh	141
Fig.3.32	Effect of stirring speed on fluoride adsorption	142
Fig. 3.33	Presence of co-anions on the extent of fluoride adsorption	143
Fig. 3.34	Effect of temperature on fluoride adsorption	144
Fig. 3.35	Kinetics of NMSh adsorbed fluoride system (a) Pseudo second order kinetic model (b) Intra particle diffusion model	146
Fig. 3.36	Adsorption isotherms of NMSh - fluoride system	149
Fig. 3.37	Volume treated water using NMSh	151
Fig. 4.1	Effect of molar ratio on fluoride precipitation	173
Fig. 4.2	Effect of pH on fluoride precipitation	174
Fig. 4.3	Variation of fluoride precipitation for different calcium salts	174
Fig. 4.4	Effect of other ions on fluoride precipitation	176
Fig. 4.5	Characterization of precipitate formed during chemical precipitation. (a) FESEM picture of precipitate, (b) EDX of the precipitate, (c) XRD and (d) particle size distribution of precipitate	177
Fig. 4.6	Schematic representation of the membrane preparation procedure	180
Fig. 4.7	Experimental set up used for water permeation experiment	183

	1: Feed inlet 2:Valve 3: Membrane cell 4: Regulator 5: Compressed air cylinder 6: Membrane 7: Permeate collector 8: Weighing balance	
Fig. 4.8	XRD diagram of kaolin powder	186
Fig. 4.9	Particle size distribution for kaolin, quartz, $CaCO_3$ and feldspar	187
Fig. 4.10	TGA-DTA curve of membrane powder	188
Fig. 4.11	XRD patterns of membrane powder at various sintering temperatures	190
Fig. 4.12	Top surface SEM images of prepared membrane at 950^{o}C sintering temperature	191
Fig. 4.13	Pore size distributions (based on SEM) of prepared ceramic membranes at 950^{o}C	192
Fig. 4.14	Variation of membrane porosity and structural density with varing sintering temperatures	193
Fig. 4.15	Variation of pure water flux with time during compaction study	194
Fig. 4.16	Fluoride removal by MF membrane (a) 10 mg/L initial fluoride solution (b) 5 mg/L initial fluoride solution	197
Fig. 4.17	Variation of permeate flux with time during the MF technique	198
Fig. 4.18	Schematic figure of combination technique	199
	1: Magnetic needle; 2: Stirring plate; 3: Precipitation bath; 4: Outlet; 5: Membrane cell; 6: Regulator; 7: Compressed air cylinder; 8: Permeate collector	
Fig. 4.19	Flux variation after separation of chemical precipitate	202

Fig. 5.1a	TEM picture of copper (II) oxide nanoparticles before adsorption	213
Fig. 5.1b	Pore size distribution of copper (II) oxide nanoparticles	214
Fig. 5.1c	XRD of copper (II) oxide nanoparticles	214
Fig. 5.1d	Fourier transform infrared spectroscopy of copper (II) oxide nanoparticles.	215
Fig. 5.2a	Effect of contact time on arsenic adsorption (inset: Effect of initial arsenic concentration on adsorption rate).	216
Fig. 5.2b	Variation of adsorbent dose on the removal of arsenic	217
Fig. 5.2c	Effect of pH on the percentage adsorption of arsenic (inset: pH_{ZPC} of copper (II) oxide nanoparticles)	218
Fig. 5.3	Intra particle diffusion kinetic model for the adsorption of arsenic	226
Fig. 5.4	Equilibrium isotherm model for arsenic adsorption	227
Fig. 5.5	Volume of arsenic contaminated water treated with unit mass of adsorbent (inset: Adsorbent mass (M) against volume of solution treated (L)).	230

CONTENTS

	Page No.
Dedication	i
Certificate	ii
Acknowledgement	iii-iv
Abstract	v-vii
Summary	viii-ix
List of Tables	x-xii
List of Figures	xiii-xviii
Contents	xix-xxi
Chapter 1 Introduction	**1-43**
1.1 Background	1
1.2 Occurrences and sources of fluoride	2
1.3 Health effects and permissible limit of fluoride	7
1.4 Global scenario of fluoride contamination	9
1.4.1 World scenario	9
1.4.2 Indian scenario	10
1.4.3 Assam scenario	12
1.5 Defluoridation techniques	14
1.5.1 Chemical process	15
1.5.2 Physical process	16
1.6 Advantages and disadvantages of different processes	22
1.7 Various combinational techniques for defluoridation	25
1.8 Occurrence, sources and health effects of arsenic	26
1.9 Various arsenic removal techniques	28
1.10 Aim of the current research	29
1.11 References	30
Chapter 2 Adsorbent Preparation and Characterization	**44-73**
2.1 Different adsorbents used in defluoridation of water	44
2.2 Characterization of adsorbents	48
2.3 Adsorbent characterization results	52

2.3.1 Pyrophyllite	52
2.3.2 Acidic alumina	56
2.3.3 Schwertmannite (Sh)	61
2.3.4 Nanomagnetite aggregated schwertmannite (NMSh)	66
2.4 Summary	72
2.5 References	73
Chapter 3 Removal of fluoride using various adsorbents	**74-169**
3.1 Materials and experimental methods	74
3.2 Fluoride removal by Pyrophyllite	89
3.3 Fluoride removal by Acidic alumina	108
3.4 Fluoride removal by schwertmannite	124
3.5 Fluoride removal by Nanomagnetite aggregated schwertmannite	138
3.6 Performance analysis of various adsorbents used for fluoride removal	152 161
3.7 Summary	164
3.8 References	
Chapter 4: Chemical Treatment Followed by Microfiltration for Defluoridation	**170-208**
4.1 Chemical treatment method	170
4.1.1 Experimental methods	171
4.1.2 Mechanism of fluoride removal	171
4.1.3 Performance of chemical treatment method	172
4.1.4 Characterization of precipitate	176
4.2 Membrane filtration technique	178
4.2.1. Raw materials	178
4.2.2. Membrane preparation	179
4.2.3 Characterization techniques	181
4.2.4 Fluoride removal by microfiltration membrane	195
4.3 Chemical treatment followed by microfiltration	198
4.3.1 Experimental procedure	199
4.3.2 Experimental results of hybrid technique	200

4.4 Summary	204
4.5 References	206
Chapter 5 Removal of Arsenic Using Copper (II) Oxide Nanoparticles	**209-232**
5.1 Experimental	209
5.1.1 Materials	209
5.1.2 Preparation of Cupper (II) oxide nanoparticles.	210
5.1.3 Method	210
5.1.4 Characterization techniques and measurement	211
5.2 Results and discussion	212
5.2.1 Characterization of adsorbent	212
5.2.2 Effect of contact time and initial concentration	215
5.2.3 Adsorbent dose effect	217
5.2.4 pH effect	218
5.2.5 Stirring speed effect	219
5.2.6 Competing anions	219
5.2.7 Temperature effect and thermodynamic study	220
5.2.8 Kinetic study	222
5.2.9 Equilibrium study	226
5.2.10 Regeneration of adsorbent	229
5.2.11 Process calculation	229
5.3 Summary	230
5.4. References	231
Chapter 6 Conclusions and Scope of Future Works	**233-240**
Error Analysis	241-243
Bibliography	244-246
Appendix A	247-258

Chapter 1

Introduction

This chapter discusses the problem associated with the discharge of fluoride bearing water from various industries and natural sources into the surrounding environment. A brief overview of fluoride and its harmful effects are discussed in this chapter. Salient features of different defluoridation techniques used to reduce fluoride content in water are explained. Detailed literature review of different processes and their advantages, limitations and selection of a particular technique of defluoridation are reported. The presence of arsenic, its health effects and various techniques for arsenic removal is also discussed. The objective and the organization of thesis work are highlighted at the end of this chapter.

1.1 Background

Drinking water scarcity is a major problem in present world. Although abundant sources of groundwater as well as surface water are available, sources of drinking water is very much limited due to contamination of water. Water is contaminated either due to some natural calamities or some anthropogenic activities of human. The major contaminants include heavy metals such as iron, arsenic, lead, mercury, chromium, cadmium and many more, inorganic ions such as fluoride, nitrate, chloride, perchlorate and sulfate and different coloring effluents coming from dye industry, textile and paper industries. All these contaminants impart severe health effects on human. Among all these contaminants, fluoride is considered as one of the most harmful and toxic

contaminant present in water. Fluoride is an ionic form of elemental fluorine. Fluorine is considered as the most highly reactive element of halogen family. Small amounts of it are found in seawater, bone, teeth and in ground water mainly as fluoride ion. Most of the fluoride are associated with monovalent cations such as NaF and KF is water soluble, while the one formed with divalent cations such as CaF_2 and PbF_2 is generally insoluble.

1.2 Occurrences and sources of fluoride

Fluoride occurrence in groundwater is a natural phenomenon, influenced by the local and regional geologic setting and hydro-geological conditions of the region. Fluoride occurs abundantly in the earth's crust as a component of rocks and minerals. Naturally fluoride is present as a natural constituent of rocks in the form of fluorite, fluorospar or calcium fluoride (CaF_2), apatite or rock phosphate $[Ca_3F(PO_4)_3]$, cryolite (Na_3AlF_6), magnesium fluoride (MgF_2), and as a replacement of ions in the crystal lattice of mica and many other minerals [3, 4] and released into the groundwater by slow dissolution of such rocks and minerals [1, 2]. Chemically, fluoride and OH ions are negatively charged and also have almost similar ionic sizes. Hence, during the chemical reaction, fluoride ion can easily replace OH ions present in rocks and enriched its concentration in rocks and minerals. Whenever carbonate and bicarbonate rich water passed through such type of rocks, fluoride ion is released due to some chemical reactions (Reaction 1.1 and 1.2) and percolates to the ground water and increases its concentration [5].

$$CaF_2 + Na_2CO_3 \rightarrow CaCO_3 + 2F^- + 2Na^+ \qquad (1.1)$$

$$CaF_2 + 2NaHCO_3 \rightarrow CaCO_3 + 2Na^+ + 2F^- + H_2O + CO_2 \quad (1.2)$$

The dissolution of fluoride from geologic formations occurs through the rain water and repeated irrigation of agricultural lands. As rain water percolates through the soil, it comes in contact with the rocks and minerals in the aquifer materials. Due to the acid in the soil, dissolution of fluoride from the country rocks occurs. Dissolution of fluoride in groundwater itself may also contribute to the fluoride contamination phenomenon. The fluoride content in groundwater becomes higher in summer season due to a drop in the water level. The higher concentration of fluoride in the summer may be further attributed to the higher dissolution of fluoride, which may be due to the presence of air in the minerals/rocks cavities, which indicates that oxygen in the cavities of the geologic formation catalyzes the fluoride dissolution process. The evidence suggests that, as the groundwater level gradually drops below the earth's crust, a greater concentration of fluoride is found in the water because of greater dissolution of fluoride from rocks and soil.

Industries are also a very important source of groundwater contamination. The effluents and other by-products of industries often constitute sources of groundwater pollution. Industries that release significant quantities of fluoride in process waste streams include fluorosilicone acid and fluorocarbon polymer synthesis, gasoline production and manufacture's of coke, ceramic, cement, enamel, fiber glass, electronics, pesticides and fertilizers, surface heating operations, metal etching (with hydrofluoric acid) and wood preservatives [6]. Fluoride discharged from fertilizer manufacturing processes is typically in the form of silicon tetra fluoride, as a result of processing of phosphate rock. Power plant boiler cleaning wastes may contain fluoride due to its presence in the cleaning

formulation. Both fluorspar and limestone are among the basic fluxing materials used in steel making. Air pollution control scrubbers water from steel manufacturing in basic oxygen, open hearth and electric arc furnaces as well as in the sintering plant is the principal source of fluoride-containing waste water from this industry. The primary aluminum processing industry uses the fluoride compound cryolite as a catalyst in bauxite ore reduction, the gaseous fluoride resulting from this process are discharged directly in to the atmosphere or the fluoride into aqueous waste streams from wet scrubbing of the process fumes [7]. Average fluoride values for aluminum reduction plants are reported as 107–145 mg/L in wastewater streams. It has been observed that the number of echinocytes increases, depending on the duration of fluoride exposure among the workers in aluminum smelters [8]. Fluoride concentrations ranging from 1,000–3,000 mg/L have been reported for a glass manufacturing process. Glass and plating wastes typically contain fluoride in the form of hydrogen fluoride or fluoride ion, depending on the pH of the waste. A high amount of fluoride has been reported in the groundwater in the vicinity of the aluminum industry [3, 9]. The main sources of fluoride in brickworks are local clay and burning of coal. Malhotra et al. [10] and Clarke et al. [11] have also reported fluoride contamination in groundwater due to by-products of brick kilns.

Nonpoint sources of groundwater pollution also contribute fluoride to ground water to some extent. Modern agricultural practices that involve the application of fertilizers coupled with pesticides which contain about 1–3% fluoride also contribute fluoride to groundwater [12]. The use of phosphatic fertilizers might also be one of the factors contributing to high fluoride concentration, which is being leached down to the groundwater by irrigation return flow [13, 14]. Irrigation with water containing small

amounts of fluoride ion would tend to concentrate these ions in the soil. If the calcium ions are removed as calcite, fluoride ions will either be absorbed or co-precipitated with calcite. If the carbonate concentration is high enough to precipitate calcium as calcite without concomitant removal of fluoride ions, these ions may move down to the water front and ultimately join the main groundwater body [15]. The U.S. Environmental Protection Agency [16] has recommended 1 mg/L of fluoride in irrigation water for continuous use but up to 15 mg/L of fluoride for short term use (20 years) on fine soils. The production of fly ash is another important nonpoint source of fluoride contamination. More than 150 million tonnes of fly ash one produced annually worldwide from the combustion of coal in power plants [17]. At least half of this amount is disposed of by landfill, thus contributing to environmental pollution due to leaching of fluoride. In addition to this, smoke particles from the aluminum industry, brickworks, and volcanoes also contain traces of fluoride [11, 18, 19]. Fluoride in the atmosphere has been detected near Agra, India, due to the presence of about 16 brickworks in that area [13]. A possibility of groundwater contamination may exist due to traces of fluoride in the atmosphere during the rainy season. The Geological Survey of India has also brought out considerable data which reveal that fluorite, topaz, apatite, rock phosphates, phosphatic nodules and phosphorites are widespread in India and contain high percentages of fluoride. As a result of their rich mineral content, fluoride leaches out and contaminates not only the groundwater but the soil as well, thereby contaminating agricultural crops also.

Besides water, fluoride is also found in agricultural crops and other edible items. It is well recognized that fluoride enters the human body through various foods, though

the data available in India are rather scanty. The information that is available is based on the analysis of food or agricultural crops in certain regions. Thus, data, from a specific location may not be applicable to other regions due to the varying concentration of fluoride in water and soil. Table 1.1 shows the fluoride concentration in different agricultural crops and other edible items [20].

Table 1.1: Fluoride concentration in agricultural crops and edible items [21]

Food item	**Fluoride concentration (mg Kg)$^{-1}$**	**Food item**	**Fluoride concentration (mg Kg^{-1})**
Cereals:		**Nuts and oil seeds:**	
Wheat	4.6	Almond	4.0
Rice	5.9	Coconut	4.4
Maize:		Mustard seeds	5.7
Pulses and legumes	5.6	Groundnut	5.1
Green gram dal	2.5	**Beverages:**	
Red gram dal	3.7	Tea	60–112
Soyabean	4.0	Aerated drinks	0.77–1.44
Vegetables:		**Spices and condiments:**	
Cabbage	3.3	Corriander	2.3
Tomato	3.4	Garlic	5.0
Cucumber	4.1	Turmeric	3.3
Lady finger	4.0		
		Food from animal sources:	
Spinach	2.0	Mutton	3.0–3.5
Lettuce	5.7	Beef	4.0–5.0
Mint	4.8	Pork	3.0–4.5
Potato	2.8	Fishes	1.0–6.5
Carrot	4.1	**Others:**	
Fruits:		Rock salts	200.0–250.0
Mango	3.7	Areca but (supari)	3.8–12.0
Apple	5.7	Beetle leaf (pan)	7.8–12.0
Guava	5.1	Tobacco	3.2–38

In addition to foodstuffs, fluoride has also been reported in cosmetics and drugs. The use of drugs containing sodium fluoride for osteoporosis, otosteosclerosis, and dental caries is very common. Different brands of toothpaste contain excessive amounts of fluoride. Fluoride enters into the circulation directly from the oral cavity through the fine blood vessels of the mouth. Fluoride is a persistent bio accumulator; even small amounts that enter through fluoride toothpaste one guaranteed entry in children as well as adults, and the cumulative effects of fluoride are a matter of serious concern.

1.3 Health effects and permissible limit of fluoride

Fluoride in drinking water has appeared as serious problem and around 200 million people, from 25 nations of the world over, are under the dreadful fate of fluorosis [21]. Fluorosis is an endemic disease due to long term intake of excessive fluoride. So far two main kinds of fluorosis, namely dental fluorosis and skeletal fluorosis have been identified. Fluorosis occurs due to the presence of fluoride in both high (>1.5 mg/L) and low (<0.6 mg/L) concentration in drinking water, with identified health effect and benefits for human beings. Teeth mottling which is characterized initially by opaque white patches on the teeth and in advanced stages leads to dental fluorosis (teeth display brown to black staining) followed by pitting of teeth surfaces [22, 23]. High manifestations of dental fluorosis are mostly found in children up to the age of 12 years. Skeletal fluorosis is a bone disease exclusively caused by consumption of fluoride more than 3 mg/L [24]. Mild cases of skeletal fluorosis cause slight problems. However, in serious cases, skeletal fluorosis results in unbearable pain as well as severe damage to bones and joints [25]. Crippling skeletal fluorosis can occur when the water supply

contains more than 10 mg/L of fluoride. The severity of fluorosis depends on the concentration of fluoride in the drinking water, daily intake, continuity and duration of exposure and climatic conditions. The health impact of fluoride on human being is summarized in Table 1.2.

Table 1.2: Effects of fluoride in water on human health [20]

Fluoride concentration (mg/L)	**Effects**
<1.0	Safe limit
1.0-3.0	Dental fluorosis
3.0-4.0	Stiffened and brittle bones and joints
4.0-6.0 above	Deformities in knee and hip bones and finally paralysis making the person unable to walk or stand in straight posture, crippling fluorosis

Since fluoride has dual significance on human health, World Health Organization (WHO) recommends that water containing a minimum of 0.6 mg/L fluoride and a maximum of 1.5 mg/L fluoride is considered safe for drinking purposes [26]. This permissible limit varies according to the climatic condition of a place. Hence every country of the world has different permissible limits based on their geography, temperature and humidity. The standard of the United States is between 0.6 and 0.9 mg/L and that of India is 0.6 and 1.2 mg/L in drinking water [27].

Therefore, by considering the climatic and other above said conditions the World Health Organization (WHO) has set a limit range between 0.5 to 1.5 mg/L [26]. According to Indian standards the safe limit is 0.6 - 1.2 mg/L and it is the same in China and Bangladesh. According to United States standards it is in between 0.6 and 0.9 mg/L [26]. Apart from fluorosis, excess fluoride consumption often leads to urinary tract manifestations, allergic manifestations, gastro intestinal problems, neurological and muscular problems, cancer, brain damage, Alzheimer's syndrome and thyroid disorder [27, 28].

1.4 Global scenario of fluoride contamination

1.4.1 World scenario

Presence of excess amount of fluoride in drinking water is often reported in many countries all over the world. There are more than 20 developed and developing nations that are endemic for fluorosis. These are Argentina, USA, Morocco, Algeria, Libya, Egypt, Jordan, Turkey, Iran, Iraq, Kenya, Tanzania, S. Africa, China, Australia, New Zealand, Japan, Canada, Saudi Arabia, Persian Gulf, Sri Lanka, Syria, India. One of the worst effected countries is China, where ground water as well as air is polluted from fluoride. In China, about 38 million people are reported to suffer from dental fluorosis and about 1.7 million from skeletal fluorosis [28].

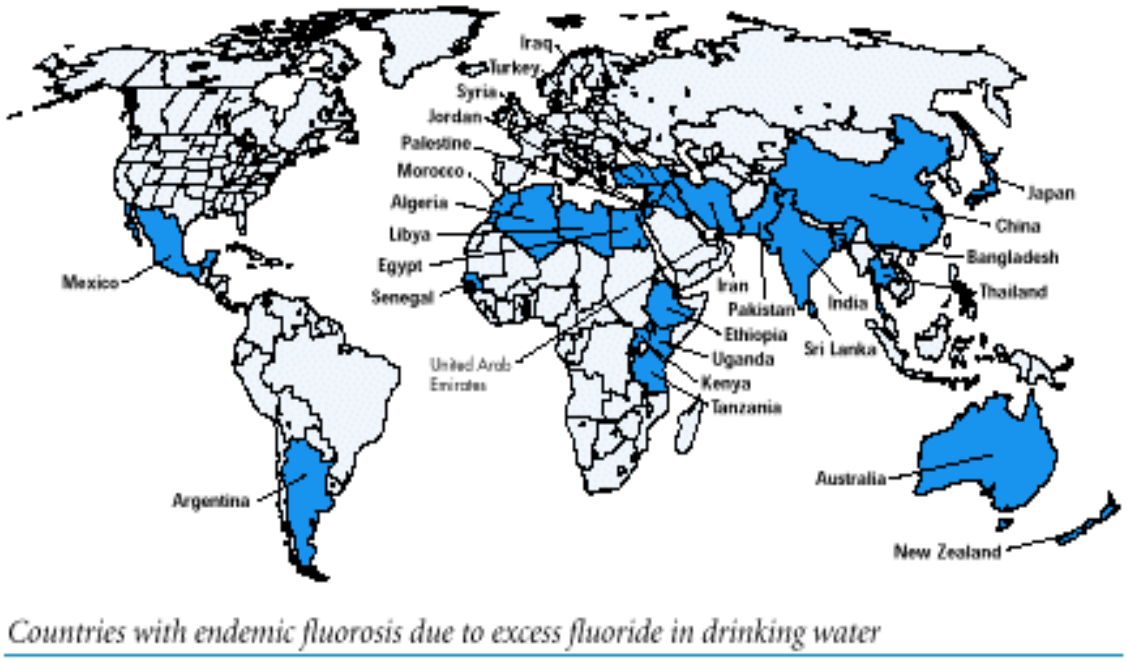

Figure 1.1: Countries with endemic fluorosis due to excess fluoride in drinking water

1.4.2 Indian scenario

In India, it was first detected in Nellore district of Andhra Pradesh in 1937. Since then considerable work has been done in different parts of India to explore the fluoride laden water sources and their impacts on human as well on animals. At present, it has been estimated that fluorosis is prevalent in 17 states of India out of 32 states. The fluoridated states include Andhra Pradesh, Assam, Bihar, Delhi, Gujarat, Haryana, Jammu and Kashmir, Karnataka, Kerala, Madhya Pradesh, Maharashtra, Orissa, Punjab, Rajasthan, Tamil Nadu, Uttar Pradesh, and West Bengal. Table 1.3 gives Fluoride concentrations in different states of India.

Table 1.3: Fluoride Concentrations in Different States of India [22]

States	Districts	Range of fluoride concentration (mg/L)
Assam	Karbianglong, Nagaon	0.2-18.1
Andhra Pradesh	All districts except Adilabad, Nizamabad, West Godhavari, Visakhapattnam, Vijzianagaram, Srikakulam	0.11-20.0
Bihar	Palamu, Daltonganj, Gridh, Gaya, Rohtas, Gopalganj, Paschim, Champaran	0.6-8.0
Delhi	Kanjhwala, Najafgarh, Alipur	0.4-10.0
Gujarat	All districts except Dang	1.58-31.0
Haryana	Rewari, Faridabad, Karnal, Sonipat, Jind, Gurgaon, Mohindergarh, Rohtak, Kurukshetra, Kaithal,Bhiwani, Sirsa, Hisar	0.17-24.7
Jammu and Kashmir	Doda	0.05-4.2
Karnataka	Dharwad, Gadag, Bellary, Belgam, Raichur, Bijapur, Gulbarga, Chitradurga, Tumkur, Chikmagalur,Manya, Banglore, Mysore	0.2-18.0
Kerala	Palghat, Allepy, Vamanapuram, Alappuzha	0.2-2.5
Maharashtra	Chandrapur, Bhandara, Nagpur, Jalgaon,	0.11-10.2

	Bulduna, Amravati, Akola, Yavatmal, Nanded, Sholapur	
Madhya Pradesh	Shivpuri, Jabua, Mandla, Dindori, Chhindwara, Dhar, Vidhisha, Seoni, Sehore, Raisen and Bhopal	0.08-4.2
Orrissa	Phulbani, Koraput, Dhenkanal	0.6-5.7
Punjab	Mansa, Faridcot, Bhatinda, Muktsar, Moga, Sangrur, Ferozpur, Ludhiana, Amritsar, Patila, Ropar,Jallandhar, Fatehgarh sahib	0.44-6.0
Rajasthan	All the 32 districts	0.2-37.0
Tamilnadu	Salem, Periyar, Dharampuri, Coimbatore, Tiruchirapalli, Vellore, Madurai, Virudunagar	1.5-5.0
Uttar Pradesh	Unnao, Agra, Meerut, Mathura, Aligarh, Raibareli, Allahabad	0.12-8.9
West Bengal	Birbhum, Bhardaman, Bankura	1.5-13.0

1.4.3 Assam scenario

Ground water of Assam is also contaminated by fluoride. The worst affected district is Karbi Anglong. The fluoride level in ground water collected from Bagpani of Bagpani area, Karbi-Anglong district [30] was found to be 8.02 mg/L and in another sample collected from Nopak-Killing of Bagpani area, it was 14.36 mg/L. People of these areas are suffering from dental as well as skeletal fluorosis. Dutta et al. [31] studied the

ground water samples for fluoride and found high level in some parts of Nagaon, Marigaon and Golaghat districts. Dutta et al. [32] studied the fluoride level in the ground water of small tea garden in Sunitpur district of Assam and found the range from 0.17 to 5.602 ppm. Borah et al. [33] reported the fluoride concentration 0.0912 - 0.228 mg/L in the Tinsukia town master plan area of Tinsukia district, which is one of the neighboring district of the Dibrugarh district. Fluoride is also present in some places of Guwahati city. The water analysis report of some selected areas of Guwahati city are presented in Table 4. Figure 1.2 shows the fluoride contaminated areas of Guwahati city.

Table 1.4: Analysis results of selected groundwater samples of Guwahati [34]

Sample no.	Sample location	Source	Ca^{2+} (ppm)	Mg^{2+} (ppm)	Na^{+} (ppm)	K^{+} (ppm)	Fe^{2+} (ppm)	Zn^{2+} (ppm)	F^{-} (ppm)	Cl^{-} (ppm)	SO_4^{2-} (ppm)	NO_3^{-} (ppm)	Ortho-phosphate (ppm)	TH (ppm)	Total alka-linity (ppm)
001	Chandmari colony	HT (PH)	10.4	7.2	29.2	7.3	0.15	0.02	2.67	7	120	1.1	6.15	55.7	244
018	Hatigarh Chariali	DTW	3.5	8.1	24.3	6.6	1.48	_	1.13	5	170	1.1	6.86	42.1	224
022	Narengi	DTW	26.5	26.1	32.8	12.0	0.05	0.09	1.07	106	155	112.3	6.44	173.6	154
023	Birkuchi	HT	2.4	0.2	84.2	6.2	0.32	0.08	6.88	9	265	2.4	4.63	7.0	176
025	Narengi	HT	4.1	2.2	99.9	6.6	0.78	0.01	4.67	7	245	4.7	5.44	19.1	220
040	Saatgaon	HT	1.5	2.5	63.2	6.6	2.16	0.01	2.75	7	155	13.3	7.24	13.8	249
041	Saatgaon	DTW	9.4	5.0	74.4	6.1	0.12	0.03	2.25	52	1610	1.1	5.72	43.8	205
044	Kalyan kuchi	HT (PH)	6.3	5.7	82.0	7.1	3.09	0.05	2.00	5	205	8.0	5.20	39.0	259
076	Kalapahar	HT (PH)	8.3	12.8	65.2	3.1	0.37	0.03	0.35	120	530	113.5	5.87	73.6	56
084	Lalganesh	HT	11.0	13.0	33.5	3.6	0.49	0.08	0.90	9	160	5.0	8.34	81.1	317
089	Saukuchi	DTW	6.9	5.7	56.4	6.2	0.16	0.06	3.75	7	215	1.0	8.76	40.7	215
103	Beltola Chariali	HT	6.3	6.8	31.2	3.3	3.16	–	1.00	5	175	6.0	7.19	43.7	171
124	Sixmile	HT	16.9	10.6	36.6	4.1	–	1.97	2.20	–	120	210.3	4.68	85.9	34
131	Sixmile	DTW	5.9	4.1	42.8	10.9	0.17	0.44	4.31	8	130	10.3	4.39	31.7	215
197	Birkuchi	HT (PH)	7.9	8.4	31.9	5.7	4.23	0.04	1.11	9	275	1.0	6.96	54.4	259
198	Birkuchi	HT	9.2	10.6	30.6	5.9	0.75	0.23	1.50	9	325	0.8	6.63	66.4	268
200	Saatgaon	DTW	8.0	7.0	97.0	6.1	0.17	0.05	2.50	7	150	1.1	7.30	48.6	322
202	Saatgaon	DTW	6.5	3.2	54.3	4.5	1.49	0.32	4.40	9	150	2.5	9.07	29.3	317
204	Bagharbari	DTW	5.9	5.7	41.7	6.7	0.04	0.04	1.50	7	125	1.3	4.82	38.3	229
209	Rukminigaon	HT (PH)	6.9	5.4	40.8	5.2	1.70	0.05	1.65	7	150	3.6	6.39	39.7	220
217	Hatigaon	HT (PH)	8.3	7.4	32.9	3.5	0.01	0.04	1.13	5	135	3.0	7.26	51.2	229
219	Hatigaon	DTW	9.0	7.3	37.2	4.8	0.02	0.06	1.08	9	130	4.0	6.00	52.3	244
234	Dipar Bil	Lake	10.0	7.3	28.6	10.4	0.72	–	0.42	31	370	2.2	3.78	55.2	151
235	Brahmaputra	River	10.4	5.7	4.5	1.2	0.25	–	0.18	3	175	1.2	4.45	49.6	88
WHO guideline values[11]			–	–	200	–	0.3	5	1.5	250	400	45	–	500	–

Distribution of Fluoride in Guwahati [34]

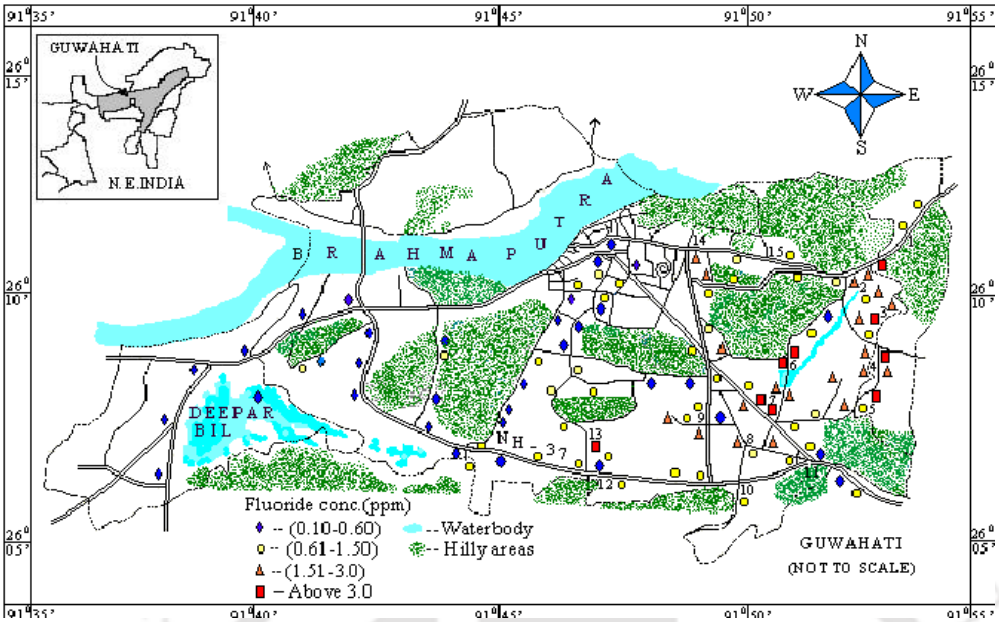

Figure 1.2: Map showing the distribution of fluoride in guwahati city. Location of fluoride-affected areas: 1, Bonda; 2, Narengi; 3, Birkuchi; 4, Saatgaon; 5, Boidangbori; 6, Hengerabari; 7, Sixmile; 8, Beltola; 9, Hatigaon; 10, Bashistha; 11, Khanapara; 12, Lokhra Chariali; 13, Saukuchi; 14, Chandmari; 15, Noonmati and 16, Mathgharia

1.5 Defluoridation techniques

To maintain the WHO permissible limit, various defluoridation techniques are used to treat fluoride contaminated water. All the defluoridation techniques are mainly divided in two categories; physical process and chemical process. Physical process includes adsorption, ion exchange and membrane separation techniques. Chemical process includes chemical coagulation- precipitation and electro-coagulation techniques. A small overview of each process is discussed in the proceeding section.

1.5.1 Chemical process

Chemical process includes chemical coagulation precipitation process which is also called Nalgonda technique and electro coagulation process.

Chemical coagulation - precipitation

Chemical precipitation method is the most common method of fluoride removal from water. This is a two step process. In the first step, precipitation occurs by adding lime which is followed by a second step where alum is added to cause coagulation. When alum is added to water, essentially two reactions occur. In the first reaction, alum reacts with some of the alkalinity to produce insoluble aluminium hydroxide [$Al(OH)_3$]. In the second reaction, alum reacts with fluoride ions present in the water. The best fluoride removal is accomplished at pH range of 5.5–7.5 [35]. The process undergoes the following reactions:

$$Ca(OH)_2 \rightarrow Ca^{2+} + 2OH^- \qquad (1.1)$$

$$Ca^{2+} + 2F^- \rightarrow CaF_2 \downarrow \qquad (1.2)$$

Electro-coagulation

In electrocoagulation process, an applied potential generates the coagulant species in situ as the sacrificial metal anode (aluminium or iron) dissolves, while hydrogen is simultaneously evolved at the cathode. Coagulant species aggregate the suspended particles or precipitate and adsorb dissolved contaminants. Tiny bubbles of hydrogen and oxygen that are formed during electrolysis of water, collide with air bubbles which compel to float the pollutant particles. Choice of electrode material depends on various

criteria such as low-cost, low-oxidation potential, inertness towards the system under consideration, etc. Different electrodes were reported in the literature like carbon [36], mild steel [37], iron [38], graphite titanium [39] and aluminium [40, 41]. Aluminium was reported to be very effective and successful in fluoride removal at favorable operating conditions [41].

1.5.2 Physical process

This category includes adsorption, ion exchange and membrane based technology. The summary of each technique is described below.

Adsorption:

Adsorption is a physical process and it is considered as cheap and easy handling process. The selection of adsorbents should be economic, easily available, easy handling and must have good fluoride adsorption behavior. Lots of adsorbents are reported in the literature such as some biological materials, natural clay materials, agricultural waste materials, metal oxides and hydroxides, calcium and iron based adsorbents. The adsorbents like plaster of paris [42], granular red mud [43], pyrophyllite [2], PCB [44], γ – alumina [45], acidic alumina [46], calcium aluminate [47], protonated cross-linked chitosan particles [48], hydroxyapatite [49], granular ceramic [50] and many other adsorbents are employed for fluoride removal. Apart from these adsorbents, nano sized adsorbents such as nano alumina [51], Fe–Al–Ce nano-adsorbent [52] and others are some of the nano adsorbents which are used in defluoridation of water. Although lot of adsorbents were reported in the literature, researchers are still finding for a better, efficient and cost effective adsorbent which will helpful in treating fluoride contaminated

water. Hence, in this study, we concentrate mainly on the adsorption process of defluoridation.

Ion exchange:

Ion exchange is a physical process similar to adsorption. In this technique, fluoride can be removed from water supplies with a strongly basic anion-exchange resin containing quaternary ammonium functional groups. The removal takes place according to the following reaction:

$$\text{Matrix-}NR_3^+Cl^- + F^- \rightarrow \text{Matrix-}NR_3^+F^- + Cl^-$$

The fluoride ions replace the chloride ions of the resin. This process continues until all the sites on the resin are occupied by fluoride. The resin is then backwashed with water that is supersaturated with dissolved sodium chloride salt. New chloride ions then replace the fluoride ions leading to recharge of the resin and starting the process again. The driving force for the replacement of chloride ions from the resin is the stronger electro negativity of the fluoride ions. Meenakshi and Viswanathan [53] studied Indion FR10 and Ceralite IRA 400 resin as defluoridating agent. The same author also studied metal ion incorporation in ion exchange resin [54] used as fluoride removing agent from water.

Membrane based technologies:

Membrane based techniques mainly comprise of reverse osmosis (RO), nanofiltration (NF), dialysis and electro-dialysis which are getting attractive in separation and purification technology. In the recent years, RO membrane process has emerged as a preferred alternative to provide safe drinking water without posing the problems

associated with other conventional methods. RO is a physical process in which the contaminants are removed by applying pressure on the feed water to direct it through a semipermeable membrane. The process is the reverse of natural osmosis as a result of the applied pressure to the concentrated side of the membrane, which overcomes the natural osmotic pressure. RO membrane rejects ions based on size and electrical charge. RO produces water of extremely high purity. Some applications of reverse osmosis to purification of water are discussed by Schneiter and Middlebrooks [55], Fu et al. [56] and Arora et al. [57]. Ndiaye et al. [58] studied fluoride removal from effluents using RO technique. It was observed that the rejection of fluoride ion was typically higher than 98%, considering that the RO membrane was fully regenerated after each set of experiments. The factors influencing the membrane selection are cost, recovery, rejection, raw water characteristics and pretreatment. Efficiency of the process is governed by different factors such as raw water characteristics, pressure, temperature and regular monitoring and maintenance.

Nanofiltration makes use of the same overall phenomenon as reverse osmosis. For nanofiltration, the membranes have slightly larger pores than those used for reverse osmosis and offer less resistance to passage both of solvent and of solutes. As a consequence, pressures required are much lower, energy requirements are less, removal of solutes is much less exhaustive and flows are faster. The selectivity of nanofiltration relative to reverse osmosis is a particular advantage and much experimental and theoretical research is being devoted to obtaining a clearer idea of the mechanism of solute retention to facilitate production and selection of targeted membranes as well as optimization of conditions [59, 60, 61]. Retention of solutes is attributed mainly to steric

and charge effects [59] and although fluoride is a very small ion it is more strongly hydrated than other monovalent anions because of its high charge density and the consequent steric effect leads to fluoride being more strongly retained on nanofiltration membranes than competing monovalent anions such as chloride or nitrate, a particular advantage in defluoridation of brackish waters. Lhassani et al. [62] studied the selective demineralization of water by nanofiltration especially with respect to its application to the defluoridation of brackish water. Generally both ceramic and polymeric membranes are used in RO and NF techniques. But the application of polymeric membrane is more than that of ceramic membrane. Generally ceramic membranes are widely used in MF and UF techniques. A brief overview of ceramic membrane is described below.

Ceramic membrane – an overview

Ceramic membranes are widely used in microfiltration and ultrafiltration techniques. Alumina [63, 64], zirconia [65], titania [66] and silica [67] based ceramic membranes with high chemical, mechanical and thermal stability and longer life time [68] are found to be useful in different membrane based applications. However, the cost of these membranes is very high compared to polymeric membranes. This is primarily due to the higher cost of the inorganic precursors (alumina, zirconia, titania, silica) as well as very high sintering temperature (more than 1100 ^{o}C) [63 - 67] required for the fabrication of membrane. Due to these two key issues, the economic competitiveness of the inorganic membranes has not been appreciable till date to drive their industrial sustainability.

To circumvent the higher costs of inorganic membranes, existing and ongoing research in the preparation of low cost inorganic membranes is dovetailed towards the usage of low cost inorganic precursors and lower sintering temperatures (below 1000^{o}C). However, these variants in ceramic membrane research need to guarantee cheaper membranes that have the inherent ability to provide stable on time performance and life time, in similarity to the existing expensive ceramic membranes.

Recently, much work has been reported for the fabrication of inorganic membranes using cheaper raw materials such as apatite powder [69], fly ash [70], natural raw clay [71], dolomite [72] and kaolin [73, 74, 75]. However, the sintering temperature used in these works was more than 1100 ^{o}C and the average pore size of the membranes was more than 1μm. In this regard, it is well known that MF membranes with pore size in the submicron range (0.1 to 0.5 μm) are preferable for the industrial application to obtain excellent solute separation efficiency. Presently, surface modification technique is used to prepare submicron size membrane from micron size MF membrane. In this method, various inorganic precursors such as zeolite [76, 77], zirconia, alumina [76] and titania [78] are coated over the membrane surface, separately. However, the fabrication of such multilayer ceramic membranes involve a tedious cycle of sintering processes, which further contributes to the cost of the membrane [76, 77]. Therefore, there exist a necessity to develop alternate formulations using low cost precursors and low sintering temperature for the preparation of submicron range ceramic membrane with average pore size around 100 to 500 nm to further the industrialization of ceramic membranes.

Ceramic membranes are found to suitable in different process applications such as desalinations [71], high temperature membrane reactor [79], membrane bioreactor, food

processing, colored effluent treatment, drinking water purification, treatment of industrial waste water [80]. Among all of these, the treatment of waste water using membrane technology in industrial systems appears more relevant and the need of the hour due to stricter and tighter environmental and health legislations.

Advantages of ceramic membranes over polymeric membranes

The advantages of inorganic membranes have been recognized for a long time. In fact, studies of the use of some inorganic membranes such as platinum and porous glass were evident even in the last century. The operable temperature limits of inorganic membranes are obviously much higher than those of organic polymeric membranes. The majority of organic membranes begin to deteriorate structurally around 100°C. Thermal stability of membranes is becoming not only a technical problem but also an economic issue. Inorganic membranes generally can withstand organic solvents, chlorine and other chemicals better than organic membranes. This also permits the use of more effective and yet corrosive cleaning procedures and chemicals. Many organic membranes are susceptible to microbial attack during applications. This is not the case with inorganic types, particularly ceramic membranes. In addition, inorganic membranes in general do not suffer from the mechanical instability of many organic membranes where the porous support structure can undergo compaction under high pressures and cause decrease in permeability.

1.6 Advantages and disadvantages of different processes

Table 1.5: Advantages and disadvantages of different fluoride removal techniques

Technique	**Adsorption**	**Ion Exchange**	**Coagulation- Precipitation**	**Membrane Process**
Remarks	**Adsorbents:** Activated alumina, activated carbon, calcite, activated saw dust, activated coconut shell carbon and activated fly ash, groundnut shell, coffee husk, rice husk, bone	strongly basic anion-exchange resin containing quaternary ammonium functional groups is used	**<u>Nalgonda technique:</u>** In first step, precipitation occurs by lime dosing which is followed by a second step in which alum is added to cause coagulation.	NF and RO is generally used for fluoride removal

	charcoal, activated soil sorbent, etc.			
Advantage	The process can remove fluoride up to 90%. Treatment is cost-effective	Removes fluoride up to 90–95%. Retains the taste and colour of water intact.	The two-step process has been claimed as the most effective technique by NEERI Under **Rajiv Gandhi Drinking Water Mission**, several fill and draw (F&D) type and hand pump attached (HPA) plants based on Nalgonda technique have come up in rural areas for which design and technology has been developed by NEERI.	The process is highly effective for fluoride removal. Membranes also provide an effective barrier to suspended solids, all inorganic pollutants, organic micropollutants, pesticides It works under wide pH range. No interference by other ions is observed.
Disadvantage	The process is highly dependent on pH Presence of	Efficiency is reduced in presence of other ions. The technique is	The process removes only a smaller portion of fluoride (18–33%) in the form of precipitates and converts a greater	The process is expensive in comparison to other options

	sulfate, phosphate or carbonate results in ionic competition	expensive because of the cost of resin,	portion of ionic fluoride (67–82%) into soluble aluminum fluoride complex ion, and therefore this technology is erroneous. Silicates have adverse effect on defluoridation by Nalgonda Technique	

1.7 various combinational techniques for defluoridation

Based on the comparison table, researchers thought that better separation was achieved by combining two or more processes. Although various conventional techniques of water purification described earlier are being used at present to solve the problem of groundwater pollution, none of them is user-friendly and cost-effective technique due to some or the other limitation and has either no or very long pay back period. There are several combination techniques reported in the literature which are helpful in separation processes. Dhale and Mahajani [81] used an integrated process including nanofiltration and wet oxidation to treat a disperse dye bath waste. In another study [82], a combination of coagulation, adsorption and ultrafiltration was used for the treatment of a primary effluent. Combination of adsorption and membrane based processes in the treatment of process wastewater were reported in literature. Baudin et al. [83] used a combination of adsorption and ultrafiltration for the treatment of surface water in 12 full-scale drinking water treatment plants in Europe. Later on, Meier et al. [84] used a combination of adsorption and nanofiltration for the treatment of severely contaminated wastewater. In another recent work [85], the combination of adsorption and ultrafiltration was used in the treatment of colored wastewaters.

Zuoa et al, 2008 [86] has studied a combined electrocoagulation and electroflotation for removal of fluoride from drinking water. Fluoride distribution in electrocoagulation defluoridation process is investigated by Zhu et al. [87]. According to Lu and Liu [88], a hybrid precipitation – microfiltration process was studied for the removal of fluoride as well as phosphate. In this technique, first calcium salts are used to precipitate the fluoride and that fine precipitate was filtered through MF membrane in a

cross flow set up. Particle size of the precipitate formed during chemical precipitation would definitely determine the type of filtration process to be combined with the existing process. It was found that particle size of the precipitate were in the range of 0.72 to 10 μm. It was therefore realized that microfiltration may be a suitable process rather than ultrafiltration, nanofiltration or reverse osmosis. Hence, in the present work, microfiltration membranes were prepared according to the requirement. Chemical precipitation followed by microfiltration is adopted to remove fluoride ion from drinking water. Detail discussions on chemical precipitation, preparation of inorganic microfiltration membrane and its application in the separation of precipitate have been discussed in chapter 4.

1.8 Occurrences, sources and health effects of arsenic

Occurrences and sources

Presence of arsenic in underground water has been reported from different parts of India. In many cases, the water sources have been rendered unsafe for human consumption. Therefore, there is a need to focus greater attention on the future impact of water resources planning and development taking into consideration all the related issues. The toxicity scale of arsenic decreases in the following order: arsine > inorganic arsenic(III) > organic arsenic(III) > inorganic arsenic(V) > organic arsenic(V) > arsonium compounds and elemental arsenic. The carcinogenic and mutagenic effects of arsenic have been established.

Health effects of arsenic

Effects of arsenic on human health are classified as acute and sub acute which are typically reversible and chronic effects. Acute and sub acute poisoning results from ingestion of large quantities of arsenic with lower exposure time whereas, chronic poisoning occurs due to consumption of arsenic contaminated water for a long time period. Arsenocosis is caused by drinking arsenic-tainted groundwater. The disease causes many problems including vomiting and diarrhea, abdominal pain, muscular pain, skin rashes and swelling of the eyelids, feet and hands. Arsenocosis ultimately affects the heart, lungs, and kidneys and can be fatal. Hematological effects including anemia and leukaemia and peripheral neuropathy might occur after weeks or month of exposure to high doses of arsenic (0.04 mg/Kg.day or higher). Consumption of large arsenic at a time may also cause stomach pain, nausea, vomiting or diarrhoea which may lead to shock, coma and even death. It has also been reported by many researchers that chronic arsenic poisoning causes hypertension, peripheral vascular diseases, cardiac vascular diseases, respiratory diseases, diabetes mellitus, malignancies including cancer of the lungs, bladder, kidney, liver, uterus and skin. The skin is quite sensitive to arsenic and skin lesion (hyperkeratosis and dyspigmentation) has been observed even at the exposure levels in the range of 5–10**µ**g/L arsenic in drinking water.

Arsenic affected areas

Countries like Bangladesh [89], China, India [90], United States, Chile, Taiwan, Vietnam [91, 92], Mexico, Argentina [93], Poland, Canada, Hungary, New Zealand and Japan [94] are affected with arsenic contamination. Among these, Bangladesh and West

Bengal of India are highly arsenic polluted areas where arsenic concentration in water is much higher than that of WHO limit (10 μg/L) [95]. Naturally, arsenic occurs in different oxidation states. In water, it may appear in both organic and inorganic forms. Inorganic forms of arsenic such as As (III) and As (V) are the most harmful to human health. As (III) is significantly more toxic and mobile than As (V). It is more difficult to remove by conventional treatment methods. Therefore, most purification techniques require pre-oxidation of As (III) to As (V) for effective arsenic removal, causing added complexity.

1.9 Various arsenic removal techniques

Various technologies for removing arsenic from contaminated water have been developed, including oxidation- precipitation [96], coagulation - flocculation-filtration [97], adsorption [98], ion exchange and membrane filtration like reverse osmosis [99] and nanofiltration [100]. Each of the above processes has its own advantages and disadvantages which make the difficulty to select a suitable process. The disadvantages of traditional methods are high cost (coagulation - flocculation–filtration, oxidation and nanofiltration), high sludge production (coagulation - flocculation, electrochemical treatment), membrane fouling (nanofiltration) and constant monitoring of the ions concentration (ion exchange) [101]. Comparing all the disadvantages of above mentioned processes, adsorption is considered as one of the most popular method for arsenic removal from aqueous solutions, and is currently considered as an efficient and economic method for water treatment. Similar to ion exchange, constant monitoring would be required for adsorption water treatment. The cost of the process only depends on the cost of the adsorbent. Mohan and Pittmann discussed applications of different adsorbents,

including their advantages and disadvantages [102]. Adsorbents, such as activated alumina [103], activated carbon [104], various iron oxides/hydroxides [105], synthetic zeolites [106], hydrous titanium dioxide (TiO_2) [107] are used in arsenic removal. Apart from these, adsorbents derived from biological origin, industrial by products/wastes are also contributing good performance towards arsenic removal. Since arsenic is a poison for human, researchers are more concentrated on the development of new technology as well as new adsorbents which are cheap, active and rapid towards arsenic ingestion. These objectives are fulfilled with the development of nano size adsorbents which has high surface area as well as high tendency to adsorb toxic arsenic from water. Nano particles are derived from metals and metal oxides such as titanium dioxide [108], metal oxide nanomaterials [109], cupric oxide [110], nano-iron (hydr) oxide impregnated granulated activated carbon [111], synthetic nanostructured Fe (III)–Cr (III) mixed oxide [112]. Very few literatures are available on arsenic removal using nanoparticles. Hence, one of the objectives of this research work is to cover a complete adsorption study on arsenic removal using copper (II) oxide nanoparticles.

1.10 Aim of the current research

The entire research work is taken up for the followings objectives

- To investigate the performance of pyrophyllite and acidic alumina for defluoridation of water.

- To synthesis iron based adsorbent i.e. schwertmannite for defluoridation of water.

- To synthesis nanomagnetite and its aggregation on the surface of schwertmannite as adsorbent for defluoridation.
- To study the chemical precipitation followed by microfiltration technique for defluoridation.
- To synthesize copper (II) oxide nanoparticles for the removal of arsenic from water.

The thesis is organized subsequently in 6 chapters.

1.11 References

[1] Biswas, K., Gupta, K., Ghosh, U.C., 2009. Adsorption of fluoride by hydrous iron(III)–tin(IV) bimetal mixed oxide from the aqueous solutions. Chem. Eng. J. 149, 196–206.

[2] Goswami, A., Purkait, M.K., 2011. Kinetic and Equilibrium study for the fluoride adsorption using Pyrophyllite. Sep.Sci.Tech. 46, 1797-1807.

[3] Das, S., Mehta, B.C., Das, P.K., Srivastava, S.K., Samanta, S.K., 1998. Source of high fluoride in groundwater around Angul, Dhenkenal district, Orissa. Poll. Res. 17, 385–392.

[4] Das, S., Mehta, B.C., Das, P.K., Srivastava, S.K., Samanta, S.K., 1999. Sources of high fluoride in ground water around Angul, Dhenkenal district, Orissa. Poll. Res.18, 21–28.

[5] Saxena, V.K., Ahmed, S., 2001. Dissolution of Fluoride in groundwater: a water-rock interaction study. Environ. Geol. 40, 1084-1087.

[6] Chand, D., 1999. Fluoride and human health - cause for concern. Indian J. Environ. Prot. 19, 81–89.

[7] Samal, U.N., 1988. Dental fluorosis in school children in the vicinity of aluminium factory in India. Fluoride 21, 137–141.

[8] Susheela, A.K., 1991. Prevention and Control of Fluorosis: Technical Information for raining cum Awareness Camp for Doctors, Public Health Engineers and other Officers. Published by National Technology Mission of Drinking Water, New Delhi.

[9] Sun, Z., Cheng, Y., Zhou, J., Wei, R., 1998. Research on the effect of fluoride pollution in atmosphere near an aluminium electrolysis plant on regional fall wheat growth. Proc. Annu. Meet., Air Waste Manag. , Assoc. 91st TPE 09/P1-TPE 09P/7.

[10] Malhotra, S.K., Verma, A.N., Kulshreshtha, K., 1998. Fluoride and fluorosis in India—I. Drinking water source, contamination in Utter Pradesh. Poll. Res. 17, 311–315.

[11] Clarke, M.L., Harvey, D.G., Humphrevs, D.J., 1981. Veterinary Toxicology, 2nd Edn. Bailliere Tindal & CassleLtd., London, 48–54.

[12] Suresh, T., 1996. Fluoride in ground water of Chiknaya Kanahalli Taluk, Tumkur district, Karnataka. Proc. Work-shop on Challenges in Groundwater Development, Madras, pp. 185–187.

[13] Jain, C.K., Ali, I., Sharma, M.K., 1999. Fluoride contamination in ground water—Indian scenario. Indian J. Environ. Prot.19, 260–266.

[14] Sudarshan, V., Reddy, B.R., 1991. Pollution of fluoride in groundwater and its impact on environment and socio-economic status of the people—a case study in Sivannagudem area. Indian J. Environ. Prot.11, 185–192.

[15] Handa, B.K., 1979. Effect of return irrigation flows from irrigated land on the chemical composition of ground water from shallow unconfined aquifers. Prog. Water Tech. 11, 337–49.

[16] EPA Report., 1976. National Interim Primary Drinking Water Regulation. EPA Publication No. EPA-570/9-76-003.

[17] Piekos, R., Paslawska, S., 1998. Leaching characteristics of fluoride from coal fly ash. Fluoride 31, 188–192.

[18] Malhotra, S.K., Verma, M., Verma, A.N., Kulshreshtha,K., 1997. Fluoride and fluorosis in India—3. Osteo-dental fluorosis in school going children in Allahabad city (U.P.). Chemistry & Biology of Herbal Medicine. 203–210.

[19] Hakresh, C., Jain, C., 2005. Fluoride contamination in groundwater. Water Encyclopedia, Wiley online library.

[20] Meenakshi, Maheshwari, R.C., 2006. Fluoride in drinking water and its removal. J.Hazard.Mater. B137, 456-463.

[21] Garg, A., Vinod, K. R., Suthar, S., Singh, S., Sheoran, A., 2008. Environ. Geol. DOI 10.1007/s00254-008-1636-y.

[22] Rwenyonyi, C.M., Birkeland, J M., Haugejorden, O., Bjorvatn, K., 2000. Clin Oral Investig. 4, 157-161. DOI: 10.1007/PL00010677.

[23] Vieira, Hanocock, R., Eggertsson, H., Everett, E.T., Grynpas, M.D., 2005.Calcif Tissue Int. 76, 17-25.

[24] Krishnamachari, K.A., 1986. Prog Food Nutr Sci. 10, 279-314.

[25] Teotia, S.P.S., Teotia, M., 1988. Fluoride. 21, 39-44.

[26] World Health Organization (WHO), 2008. Guidelines for Drinking water Quality, third ed., vol. 1. WHO, Geneva.

[27] ISI (1983). Indian standard specification for drinking water.India: Indian Standard Institution, New Delhi.

[28] Chinoy, N.J., 1991. Effects of fluoride on physiology of animals and human beings. Indian J. Environ. Toxicol. 1, 17–32.

[29] Harrison, P.T.C., 2005. Fluoride in water: a UK perspective. J. Fluorine Chem. 126, 1448–1456.

[30] Chakraborti, D., 2000. Fluorosis in Assam. Curr. Sci., 78, 1421-1423.

[31] Dutta, R.K., Saikia, G., Das, B., Bezboruah, C., Das H.B., Dube, S.N., 2010. Fluoride Contamination in Groundwater of Central Assam, India. Asian J. Water Environ. And Poll. 2, 1199-1208.

[32] Dutta, J., Nath, M., Chetia, M., Mishra, A.K., 2010. Monitoring of Fluoride Concentration in Ground Water of Small Tea Gardens in Sunitpur District, Assam, India: Correlation with Physico-Chemical Parameters. Int. J. Chem. Tech. Res. 2, 1200.

[33] Borah, J., Saikia, D., 2011. Estimation of the Concentration of Fluoride in the Ground Water of Tinsukia Master Plan Area of the Tinsukia District. Scholars Res. Lib. 3, 202-206.

[34] Das, B., Talukdar, J., Sarma, S., Gohain, B., Dutta, R.K., Das, H.B., Das, S.C., 2003. Fluoride and other inorganic constituents in groundwater of Guwahati, Assam, India. Current Sci. 85, 10.

[35] Potgeiter, J.H., 1990. An experimental assessment of the efficiency of different defluoridation methods. Chem. SA. 317–318.

[36] Gallegos, A.A., Pletcher, D., 1999. The removal of low level organics via hydrogen peroxide formed in a reticulated vitreous carbon cathode cell. Part 2: The removal of phenols and related compounds from aqueous effluents. Electrochim. Acta. 44, 2483–2492.

[37] Golder, A.K., Hridaya, N., Samanta, A.N., Ray, S., 2005. Electrocoagulation of methylene blue and eosin yellowish using mild steel electrodes. J. Hazard. Mater. 127, 134–140.

[38] Yildiz, Y.S., Koparal, A.S., Irdemdez, S., Keskinler, B., 2007. Electrocoagulation of synthetically prepared waters containing high concentration of NOM using iron cast electrodes. J. Hazard. Mater. 139, 373–380.

[39] Hernández, I.L., Barrera-Díaz, C., Roa-Morales, G., Bilyeu, B., Ureña-Núñez, F., 2007. A combined electrocoagulation–sorption process applied to mixed industrial wastewater. J. Hazard. Mater. 144, 240–248.

[40] Bi, S., Wang, C., Cao, Q., Zhang, C., 2004. Studies on the mechanism of hydrolysis and polymerization of aluminium salts in aqueous solution: Correlations between the Core-links model and Cage-like Keggin-Al13 model. Coord. Chem. Rev. 248, 441–455.

[41] Ghosh, D., Medhi, C.R., Purkait, M.K., 2008. Treatment of fluoride contaminated drinking water by electrocoagulation using monopolar and bipolar electrode connection. Chemosphere, 73 1393 – 1400.

[42] Gopal, V., Elango, K.P., 2007. Equilibrium, kinetic and thermodynamic studies of adsorption of fluoride onto plaster of Paris. J. Hazard. Mater. 141, 98–105.

[43] Tor, A., Danaoglu, N., Arslan, G., Cengeloglu, Y., 2009. Removal of fluoride from water by using granular red mud: Batch and column studies. J. Hazard. Mater. 164, 271– 278.

[44] Viswanathan, N., Sundaram, C.S., Meenakshi, S., 2009. Removal of fluoride from aqueous solution using protonated chitosan beads. J. Hazard. Mater. 161, 423–430.

[45] Lee, G., Chen, C., Yang, S.T., Ahn, W.S., 2010. Enhanced adsorptive removal of fluoride using mesoporous alumina. Microp. Meso. Mat. 127, 152–156.

[46] Goswami, A., Purkait, M.K., 2012. The defluoridation of water by acidic alumina. Chem. Eng. Res. Des. 9 0, 2316–2324.

[47] Sakhare, N., Lunge, S., Rayalu, S., Bakardjiva, S., Subrt, J., Devotta, S., Labhsetwar, N., 2012. Defluoridation of water using calcium aluminate material. Chem. Eng. J. 203, 406–414.

[48] Huang, R., Yang, B., Liu, Q., Ding, K., 2012. Removal of fluoride ions from aqueous solutions using protonated cross-linked chitosan particles, J. Fluorine Chem. 141, 29–34.

[49] Nie, Y., Hu, C., Kong, C., 2012. Enhanced fluoride adsorption using Al (III) modified calcium hydroxyapatite. J. Hazard. Mat. 233– 234, 194– 199.

[50] Chen, N., Zhang, Z., Fenga, C., Sugiura, N., Li, M., Chen, R., 2010. Fluoride removal from water by granular ceramic adsorption. Colloid. Interf. Sci. 348, 579–584.

[51] Kumar, E., Bhatnagara, A., Kumar, U., Sillanpää, M., 2011. Defluoridation from aqueous solutions by nano-alumina: Characterization and sorption studies. J. Hazard. Mat. 186,1042–1049.

[52] Chen, L., Wang, T.J., Wu, H.X., Jin, Y., Zhang, Y., Dou, X.M., 2011. Optimization of a Fe–Al–Ce nano-adsorbent granulation process that used spray coating in a fluidized bed for fluoride removal from drinking water. Powder Technol. 206, 291–296.

[53] Meenakshi, S., Viswanathan, N., 2007. Identification of selective ion-exchange resin for fluoride sorption. J. Col. Inter. Sci. 308, 438–450.

[54] Viswanathan, N., Meenakshi, S., 2009. Role of metal ion incorporation in ion exchange resin on the selectivity of fluoride. J. Hazard. Mater. 162, 920–930.

[55] Schneiter, R.W., Middlebrooks, E.J., 1983. Arsenic and fluoride removal from groundwater by reverse osmosis. Environ. Int. 9, 289–291.

[56] Fu, P., Ruiz, H., Lozier, J., Thompson, K., Spangenberg, C., 1995. A pilot study on groundwater natural organics removal by low-pressure membranes. Desalination 102, 47–56.

[57] Arora, M., Maheshwari, R.C., Jain, S.K., Gupta, A., 2004. Use of membrane technology for potable water production. Desalination 170, 105–112.

[58] Ndiaye, P.I., Moulin, P., Dominguez, L., Millet, J.C., Charbit, F., 2005. Removal of fluoride from electronic industrial effluent by RO membrane separation. Desalination 173, 25–32.

[59] Diawara, C.K., 2008. Nanofiltration process efficiency in water desalination. Sep. Purif. Rev. 37, 303–325.

[60] Hu, K., Dickson, J.M., 2006. Nanofiltration membrane performance on fluoride removal from water. J. Membra. Sci. 279, 529–538.

[61] Bason, S., Ben-David, A., Oren, Y., Freger, V., 2006. Characterization of ion transport in the active layer of RO and NF polyamide membranes. Desalination 199, 31–33.

[62] Lhassani, A., Rumeau, M., Benjelloun, D., Pontie, M., 2001. Selective demineralization of water by nanofiltration: application to the defluorination of brackish water. Water Res. 35, 3260–3264.

[63] DeFriend, K.A., Wiesner, M.R., Barron, A.R., 2003. Alumina and aluminate ultra-filtration membranes derived from alumina nanoparticles, J. Membra. Sci. 224, 11 - 28.

[64] Gestel, T.V., Vandecasteele, C., Buekenhoudt, A., Dotremont, C., Luyten, J., Leysen, R., Bruggen, B.V., Maesc, G., 2002. Alumina and titania multilayer membranes for nanofiltration: preparation, characterization and chemical stability. J. Membra. Sci. 207, 73 - 89.

[65] Falamaki, C., Afarani, M.S., Aghaie, A., 2004. Initial sintering stage pore growth mechanism applied to the manufacture of ceramic membrane supports. J. Europ. Cer. Soci. 24, 2285 - 2292.

[66] Wang, Y.H., Tian, T.F., Liu, X.Q., Meng, G.Y., 2006. Titania membrane preparation with chemical stability for very hash environments applications. J. Membra. Sci. 280, 261 - 269.

[67] Yoshino, Y., Suzuki, T., Nair, B.N., Taguchi, H., Itoh, N., 2005. Development of tubular substrates, silica based membranes and membrane modules for hydrogen separation at high temperature. J. Membra. Sci. 267, 8 - 17.

[68] Sourirajan, S., 1970. Reverse Osmosis, Logos Press, London.

[69] Masmoudia, S., Larbot, A., Feki, H.E., Amara, R.B., 2007. Elaboration and characterisation of apatite based mineral supports for microfiltration and ultrafiltration membranes. Cer. Inter. 33, 337 - 344.

[70] Saffaj, N., Younssi, S.A., Albizane, A., Messouadi, A., Bouhria, M., Persin, M., Cretin, M., Larbot, A., 2004. Preparation and characterization of ultra-filtration membranes for toxic removal from wastewater. Desalination 168, 259 - 263.

[71] Saffaj, N., Persin, M., Younsi, S.A., Albizane, A., Cretin, M., Larbot, A., 2006. Elaboration and characterization of micro-filtration and ultra-filtration membranes deposited on raw support prepared from natural Moroccan clay: Application to filtration of solution containing dyes and salts. Appl. Clay Sci. 31, 110 - 119.

[72] Bouzerara, F., Harabi, A., Achour, S., Larbot, A., 2006. Porous ceramic supports for membranes prepared from kaolin and doloma mixtures. J. Eur. Ceram. Soc. 26, 1663 - 1671.

[73] Belouatek, A., Benderdouche, N., Addou,A., Ouagued,A., Bettahar, N., 2005. Preparation of inorganic supports for liquid waste treatment. Micropor. Mesopor. Mater. 85, 163 - 168.

[74] Almandoza, M.C., Marchese, J., Prádanos, P., Palacio, L., Hernández, A., 2004. Preparation and characterization of non-supported micro-filtration membranes from aluminosilicates. J. Membra. Sci. 241, 95 - 103.

[75] Nandi, B.K., Uppaluri, R., Purkait, M.K., 2008. Preparation and characterization of low cost ceramic membranes for microfiltration applications. App. Clay Sci. 42, 102 - 110.

[76] Workneh, S., Shukla, A., 2008. Synthesis of sodalite octahydrate zeolite-clay composite membrane and its use in separation of SDS. J. Membra. Sci. 309, 189 - 195.

[77] Potdar, A., Sukla, A., Kumar, A., 2002. Effect of gas phase modification of analcime zeolite composite membrane on separation of surfactant by ultra-filtration. J. Membra. Sci. 210, 209 - 225.

[78] Das, R., Dutta, B.K., 1999. Permeation and Separation Characteristics of Supported Alumina and Titania Membranes. Sep. Sci. Technol. 34, 609 - 625.

[79] Vivanpatarakij, S., Laosiripojana, N., Arpornwichanop, A., Assabumrungrat, S., 2009. Performance improvement of solid oxide fuel cell system using palladium membrane reactor with different operation modes. Chem. Eng. J. 146, 112 - 119.

[80] Luque, S., Gómez, D., Álvarez, J.R., 2008. Industrial Applications of Porous Ceramic Membranes (Pressure-Driven Processes). Membra. Sci. Technol. 13, 177 – 216.

[81] Dhale, A.D., Mahajani, V.V., 2000. Studies on treatment of disperse dye waste: membrane-wet oxidation process. Waste Manage. 20, 85-92.

[82] Abdessemed, D., Nezzal, G., 2002. Treatment of primary effluent by coagulation-adsorption- ultrafiltration for reuse. Desalination 152, 367-373.

[83] Baudin, I., Chevalier, M.R., Anselme, C., Cornu, S., Laine, J.M., 1997. L'Apie and Vigneux case studies: First months of operation. Desalination 113, 273-275.

[84] Meier, J., Melin, T., Eilers, L.H., 2002. Nanofiltration and adsorption on powdered adsorbent as process combination for the treatment of severely contaminated wastewater. Desalination 146, 361-366.

[85] Pigmon, H.M., Brasquet, C.F., Cloiree, P.L., 2003. Adsorption of dyes onto activated carbon cloths: approach of adsorption mechanisms and coupling of ACC with ultrafiltration to treat colored wastewaters. Sep. Puri. Technol. 31, 3-11.

[86] Zuoa, Q., Chena, X., Li, W., Chen, G., 2008. Combined electrocoagulation and electroflotation for removal of fluoride from drinking water. J. Hazard. Mater.159, 452–457.

[87] Zhu, J., Zhao, H., Ni, J., 2007. Fluoride distribution in electrocoagulation defluoridation process. Sep. Purif. Technol. 56, 184-191.

[88] Lu, N.C., Liu, J.C., 2010. Removal of phosphate and fluoride from wastewater by a hybrid precipitation - microfiltration process. Sep. Purif. Tech. 74, 329 - 335.

[89] Harvey, C.F., Ashfaque, K.N., Yu, W., Badruzzaman, A.B.M., Ali, M.A., Oates, P.M., Michael, H.A., Neumann, R.B., Beckie, R., Islam, S., Ahmed, M.F., 2006. Groundwater dynamics and arsenic contamination in Bangladesh. Chem. Geol. 228, 112–136.

[90] Chatterjee, A., Das, D., Mandal, B.K., Chowdhury, T.R., Samanta, G., Chakraborty, D., 1995. Arsenic in groundwater in six districts of West Bengal, India. Analyst, 120, 643-650.

[91] Berg, M., Tran, H.C., Nguyen, T.C., Pham, H.V., Schertenleib, R., Giger, W., 2001. Arsenic Contamination of Groundwater and Drinking Water in Vietnam: A Human Health Threat. Environ. Sci. Technol. 35, 2621–2626.

[92] Hug, S.J., Leupin, O.X., Berg, M., 2008. Bangladesh and Vietnam: Different Groundwater Compositions Require Different Approaches to Arsenic Mitigation. Environ. Sci. Technol. 42, 6318–6323.

[93] Bundschuh, J., Farias, B., Martin, R., Storniolo,A., Bhattacharya, P., Cortes, J., Bonorino, G., Albouy, R., 2004. Groundwater arsenic in the Chaco-Pampean Plain, Argentina: case study from Robles county, Santiago del Estero Province. Appl. Geochem. 19, 231–243.

[94] Smedley, P.L., Kinniburgh, D.G., A review of the source, behaviour and distribution of arsenic in natural waters. Appl. Geochem. 17, 517–568.

[95] WHO (Ed.), 2004. Guidelines for Drinking-Water Quality, 3rd ed., World Health Organization, Geneva.

[96] Leupin, O.X., Hug, S.J., 2005. Oxidation and removal of arsenic (III) from aerated groundwater by filtration through sand and zero-valent iron. Water Res. 39, 1729–1740.

[97] Hansen, H.K., N´u˜nez, P., 2006. Grandon, Electrocoagulation as a remediation tool for wastewaters containing arsenic. Miner. Eng. 19, 521–524.

[98] Jegadeesan, G., Mondal, K., Lalvani, S.B., 2005. Arsenate remediation using nanosized modified zerovalent iron particles. Environ. Prog. 24, 289–296.

[99] Ning, R.Y., 2002.Arsenic removal by reverse osmosis. Desalination. 143, 237–241.

[100] Kim, D.H., Kim, K.W., Cho, J., 2006. Removal and transport mechanisms of arsenics in UF and NF membrane processes. J.Water Health. 4, 215–223.

[101] Owlad, M., Aroua, M.K., Daud, W.A.W., Baroutian, S., 2009. Removal of hexavalent Chromium - contaminated water and wastewater: a review. Water Air Soil Pollut. 200, 59–77.

[102] Mohan, D., Pittmann Jr., C.U., 2007. Arsenic removal from water/wastewater using adsorbents—A critical review. J. Hazard. Mater. 142, 1–53.

[103] Lin, T.F., Wu, J.K., 2001. Adsorption of arsenite and arsenate within activated alumina grains: equilibrium and kinetics. Water Res. 35, 2049–2057.

[104] Daus, B., Wennrich, R., Weiss, H., 2004. Sorption materials for arsenic removal from water: a comparative study. Water Res. 38, 2948–2954.

[105] Banerjee, K., Amy, G.L., Prevost, M., Nour, S., Jekel, M., Gallagher, P.M., Blumenschein, C.D., 2008. Kinetic and thermodynamic aspects of adsorption of arsenic onto granular ferric hydroxide (GFH). Water Res. 42, 3371–3378.

[106] Chutia, P., Kato, S., Kojima, T., Satokawa, S., 2009. Arsenic adsorption from aqueous solution on synthetic zeolites. J. Hazard. Mat. 162, 440–447.

[107] Pirilä, M., Martikainen, M., Ainassaari, K., Kuokkanen, T., Keiski, R.L., 2011. Removal of aqueous As(III) and As(V) by hydrous titanium dioxide. J. Colloid Interf. Sci. 353, 257–262.

[108] Deedar, N., Irfan, A., Ishtiaq Q.A., 2009. Evaluation of the adsorption potential of titanium dioxide nanoparticles for arsenic removal. J. Environ. Sci. 21, 402–408.

[109] Hristovski, K., Baumgardner, A., Westerhoff, P., 2007. Selecting metal oxide nanomaterials for arsenic removal in fixed bed columns: From nanopowders to aggregated nanoparticle media. J. Hazard. Mat. 147, 265–274.

[110] Martinson, C.A., Reddy, K.J., 2009. Adsorption of arsenic (III) and arsenic (V) by cupric oxide nanoparticles. J. Colloid Interf. Sci. 336, 406–411.

[111] Hristovski, K.D., Westerhoff, P.K., Möller, T., Sylvester, P., 2009. Effect of synthesis conditions on nano-iron (hydr)oxide impregnated granulated activated carbon. Chem. Eng. J. 146, 237–243.

[112] Basu, T., Ghosh, U.C., 2011. Influence of groundwater occurring ions on the kinetics of As (III) adsorption reaction with synthetic nanostructured Fe(III)–Cr(III) mixed oxide. Desalination. 266, 25–32.

Chapter 2

Adsorbent Preparation And Characterization

This chapter gives the complete description of the experimentations involved during adsorbent preparation and their characterization techniques. The characterization results of different adsorbents are also discussed here.

2.1 Different adsorbents used in defluoridation of water

In this study, four different adsorbents were chosen and used as defluoridating adsorbent. Pyrophyllite, acidic alumina, schwertmannite and nanomagnetite aggregated schwertmannite were chosen as adsorbents for treating fluoride contaminating water. A brief description of each adsorbent and its characterization was discussed below.

Pyrophyllite

Pyrophyllite is basically a non-swelling hydrous aluminum silicate with the chemical formula of $AlSi_2O_5OH$. A schematic diagram of the structure of pyrophyllite is given in Figure 2.1 [1]. It belongs to the family of silicate minerals that are composed of three infinite layers formed by the sharing of oxygen ions at three corners of the silica tetrahedra. A layer of octahedrally coordinated $Al-OH$ ions holds the two layers of tetrahedrally coordinated $Si-O$ ions together as a three - layer sheet [2]. Since this three-layer unit is electrically balanced as neutral on the basal plane due to the very small ionic substitution, the crystal is held together by Van der Waals forces, which are

comparatively weak with respect to the primary covalent or ionic forces that hold the atoms in the unit layers together [3]. Consequently, easy cleavage takes place along the plane of the layers.

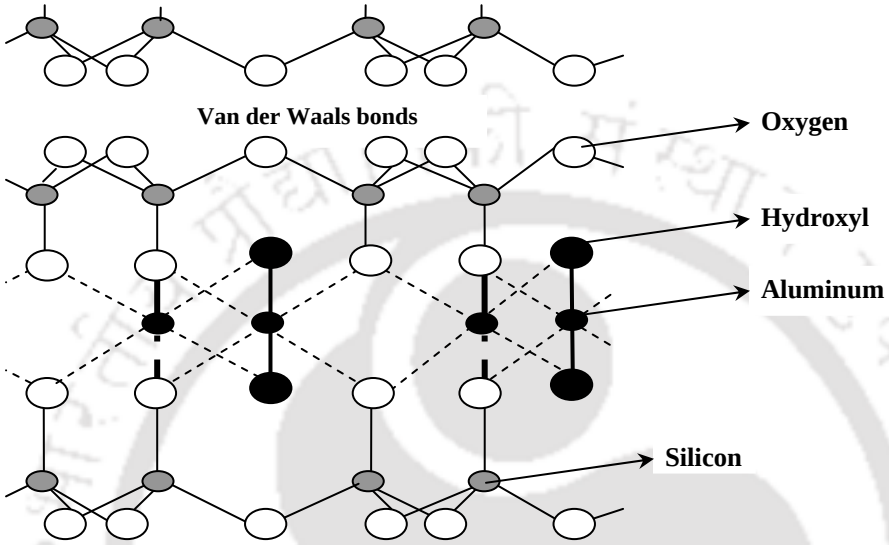

Figure 2.1: Structure of pyrophyllite molecule [1]

Physically pyrophyllite is a white, micaceous and feels greasy compound. Generally it is used as a raw material in ceramics and refractory industries due to its high refractive behaviour, low thermal and electrical conductivity, low expansion coefficient, low hot-load deformation, low reversible thermal expansion and low bulk density, excellent reheating stability and high resistance to corrosion by molten metals and basic slags [4]. In this study, pyrophyllite used was purchased from National chemicals, India and used directly as an adsorbent for fluoride removal.

Acidic alumina

In this study, acidic alumina was purchased from Merck, India and used directly as adsorbent for defluoridation of water. Generally alumina (aluminium oxide) is an amphoteric oxide with chemical formula Al_2O_3. In the present study, alumina used was acidic in nature. When neutral alumina is treated with acid e.g. HCl, acidic alumina is formed according to the following reaction [5]:

Alumina. $HOH + HCl \rightarrow$ Alumina. $HCl + HOH$ ***Reaction 1***

In absence of hydroxyl ion (i.e., slightly acidic feed solution), if acidic alumina is in contact with fluoride (F^-) ion, it displaces chloride (Cl^-) ion as in reaction 2.

Alumina. $HCl + NaF \rightarrow$ Alumina. $HF + NaCl$ ***Reaction 2***

To regenerate the fluoride containing adsorbent, a dilute solution of the most preferred hydroxide ion, in terms of $NaOH$ is used. The regeneration occurs according to reaction 3.

Alumina. $HF + 2NaOH \rightarrow$ Alumina. $NaOH + NaF + H_2O$ ***Reaction 3***

Since alumina acts as both cation and anion exchanger, Na^+ ions are exchanged for hydrogen when Na^+ ion is in excess in the regenerating solution and H^+ is absent (high pH). To restore the fluoride removal capacity, the basic alumina is in contacted with an excess of dilute HCl (reaction 4).

Alumina. $NaOH + 2HCl \rightarrow$ Alumina. $HCl + NaCl + HOH$ ***Reaction 4***

The acidic alumina (alumina. HCl), is now ready for another fluoride adsorption cycle. Based on this mechanism, acidic alumina is considered as a better adsorbent for fluoride removal.

Schwertmannite

Schwertmannite (Sh) which is an iron oxyhydroxysulfate was selected as defluoridation adsorbent. It exists naturally as geo-material and can also be synthesized in laboratory. Synthetic Sh has a probable formula of $Fe_8O_8(OH)_6SO_4$. Presence of OH^- group in Sh considers it as a fluoride adsorbing adsorbent.

Preparation of Sh

Sh was prepared by wet chemical process where urea was used as a neutralizing agent [6]. The urea solution was prepared by dissolving 150 g of urea into 500 mL of distilled water, and $Fe_2(SO_4)_3$ solution was made by dissolving about 25 g of $Fe_2(SO_4)_3.5H_2O$ in 500 mL of distilled water. The $Fe_2(SO_4)_3$ solution was preheated at 70^{o}C in a beaker and urea solution was added drop wise for about 2–4 hrs. Precipitates were formed and filtered with Whatmann filter paper. The residue obtained was dried at temperature less than 40 ^{o}C and the dried powder was considered as adsorbent for fluoride removal.

Nanomagnetite aggregated schwertmannite (NMSh)

Preparation of NMSh

The procedure for the formation of nanomagnetite aggregated schwertmannite consists of two steps. Step 1 includes the formation of nanomagnetite particles by chemical precipitation method and step 2 covers the production of schwertmannite using wet chemical process where the nanomagnetite particles are embedded on it. Magnetite nanoparticles were prepared by co-precipitation from a mixture of $FeCl_2$ and $FeCl_3$ (1: 2 molar ratio) throughout the slow addition of diluted NH_3 solution. Schwertmannite,

which is an iron oxide hydroxide adsorbent, was generated by homogenous hydrolysis of $Fe_2(SO_4)_3.nH_2O$ using urea as a neutral agent. After dissolving about 12.5 g of $Fe_2(SO_4)_3.5H_2O$ in 250 mL of distilled water, the solution was preheated at about 70°C and slowly stirred for 10 min. 5 mL of the slurry containing the fresh nanomagnetite particles was added to the solution and 250 mL of 5M urea solution was added drop-wise for about 2–4 hrs into the solution. When precipitating of crystals begun, the color of the solution was changed from red to brownish yellow and the reaction was continued until half of the initial solution was vaporized. After solid–liquid separation, solid part was rinsed for removal of impurities. Then the yielded material was dried below 40°C. The dried material is now ready for fluoride adsorption.

2.2 Characterization of adsorbents

Four adsorbents (pyrophyllite, acidic alumina, schwertmannite and nanomagnetite aggregated schwertmannite) considered in this work were characterized to know its structure, surface area, pore size distribution and other properties. Following techniques were used to study the adsorbent characterization.

✓ **Brunauer, Emmett and Teller (BET) surface area measurement**

A BET surface analyzer (SA 3100, Beckman Coulter, USA) was used to measure surface area and porosity of a solid (adsorbent). Before measurement, each sample was degassed using helium gas at a specified temperature for 2 hrs. Then the gas adsorption technique was performed by the addition of a known volume of gas (adsorbate), typically nitrogen, to a solid material in a sample vessel at cryogenic temperature (77 K). The BET

and Langmuir surface area, BJH adsorption and desorption, pore size distribution, t- plot, total pore volume and more were obtained from the adsorption isotherm.

✓ **X-ray powder diffraction (XRD)**

X-ray powder diffraction (XRD) is a rapid analytical technique primarily used for phase identification of a crystalline material and can provide information on unit cell dimensions. The structural analysis of adsorbents was recorded using XRD(D8 ADVANCE, Bruker Axs). Powder X-ray diffraction of the adsorbents were recorded by a diffractometer operating with a Cu Kα radiation source and nano bragg mode. The XRD analysis result is recorded from 5° to 90° with a step increase rate of 0.05^{o} per second. The spectrum of the analyzed adsorbents showed broad and diffuse peaks. Therefore, the identification of peaks with such broad humps is a well known confirmed characteristic of phases which are amorphous or poorly crystalline in nature.

✓ **Scanning electron microscopy (SEM) and energy dispersive X-Ray (EDX)**

The morphology of the adsorbents were analyzed by SEM, whereas elemental information of the adsorbents were recorded using EDX. Furthermore, it is mention worthy that before SEM analysis the sample was finely grinded and coated with the Au inside a plasma chamber operated under vacuum for 135 seconds with a leakage current of 4 mA. This was done to ensure the less possibility of charging during the analysis. Sample was analyzed under the application of the probe current of 94 pA and at different magnifications with the primary electron hitting the sample with energy of 10 kV – 15 kV. EDX is an integrated part of the scanning electron microscopy where energy

dispersion according to the element was calibrated with a standard Co (cobalt) sample before the analysis.

✓ **Fourier transform infrared spectroscopy (FTIR)**

Fourier transform infrared spectroscopy (FTIR, Make: Perkin Elmer, USA, Model: LR 64912C) was used to analyze the organic functional groups of the adsorbent. The adsorbent was mixed with potassium bromide properly and pressed under 5 Ton weight for 10 seconds to prepare the pellet necessary for analysis. Furthermore, the pellet was subjected to the Infrared spectra and scans were recorded with wave numbers ranging from 4000 to 450 cm^{-1}. Different peaks at different wave numbers were leveled and matched with the standard data available for certain identified bond stretching. Some peaks were not been identified due to the lack of standard data related to our work. Nonetheless, the available data well matched with the experimental results which are presented in this chapter.

✓ **Laser particle size analyzer (LPSA)**

The particle size distribution of adsorbents was evaluated using a laser particle size analyzer (Malvern, Mastersizer 2000, UK). Laser-diffraction-size analysis is based on the principle that particles of a given size diffract light through a given angle, the angle increasing with decreasing size. A narrow beam of monochromatic light from a He-Ne laser, λ = 633 nm, is passed through a suspension and the diffracted light is focused onto a detector. This senses the angular distribution of scattered light energy. A lens placed between the illuminated sample with the detector at its focal point focuses the undiffracted light to a point at the center and leaves only the surrounding diffraction

pattern, which does not vary with particle movement. Thus, a stream of particles was passed through the beam to generate a stable diffraction pattern and the optimized particle size distribution plot was obtained and stored in an online computer.

✓ **Vibrating sample magnetometer (VSM)**

The magnetic behaviour of the adsorbent was detected by VSM (Lakeshore 7410). A vibrating sample magnetometer or VSM is a scientific instrument that measures magnetic properties of a sample. A sample is placed inside a uniform magnetic field to magnetize the sample. The sample is then physically vibrated sinusoidally, typically through the use of a piezoelectric material. The induced voltage in the pickup coil is proportional to the sample's magnetic moment, but does not depend on the strength of the applied magnetic field. In a typical setup, the induced voltage is measured through the use of a lock-in amplifier using the piezoelectric signal as its reference signal. By measuring in the field of an external electromagnet, the hysteresis curve of the adsorbent material is obtained.

✓ **Zero point charge (pH_{ZPC})**

The zero point charge (pH_{ZPC}) of adsorbent describes the pH value at which the surface charge of the adsorbent is zero. This is an important property of adsorbents. The pH_{ZPC} used for adsorption experiment was determined for all the four adsorbents by using solid to liquid ratio of 1:1000. For this, 0.1 g of adsorbent was added to 100 mL of 0.01M $NaCl$ solution with varying pH from 2 to 12 and stirred for 48 hrs. The suspensions were filtered through whatmann filter paper and the final pH values were measured again. The

final pH of the solution was plotted against initial pH and the value of pH_{ZPC} was determined separately for all the adsorbents considered in this study.

2.3 Adsorbent characterization results

The detailed analysis of characterization results is summarized below separately for four adsorbents.

2.3.1 Pyrophyllite

- ✓ ***Surface area***

The specific surface area of the pyrophyllite determined from BET surface area analyzer was 424 m^2/g. Figure 2.2 showed the pore size distribution curve of adsorbent based on the nitrogen equilibrium adsorption isotherm at 77 K. It may be found from this figure that the pyrophyllite exhibited a wide distribution of pores. About 91.7% of total pores were in the range of pore diameter below 40 nm with total pore volume of 0.394 mL/g nm, indicating a very high mesopore volume. The second fraction of pores appeared in the field from 40 to 100 nm. In this range, the pore volume was 0.001 mL/g nm with only 8.3% of the total pore volume indicating the existence of the macropores. Pyrophyllite was found insoluble in acid and water in the temperature range considered in this study.

- ✓ ***XRD***

The X-ray diffraction (XRD) pattern of pyrophyllite was shown in Figure 2.3. From the XRD spectrum, it was observed that pyrophyllite used in the work was amorphous in nature.

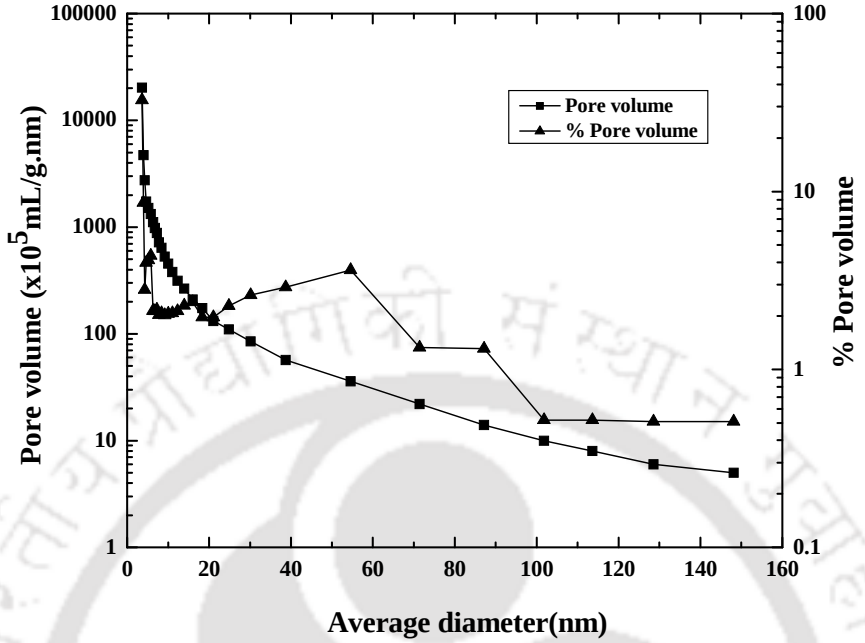

Figure 2.2: Pore size distribution of pyrophyllite

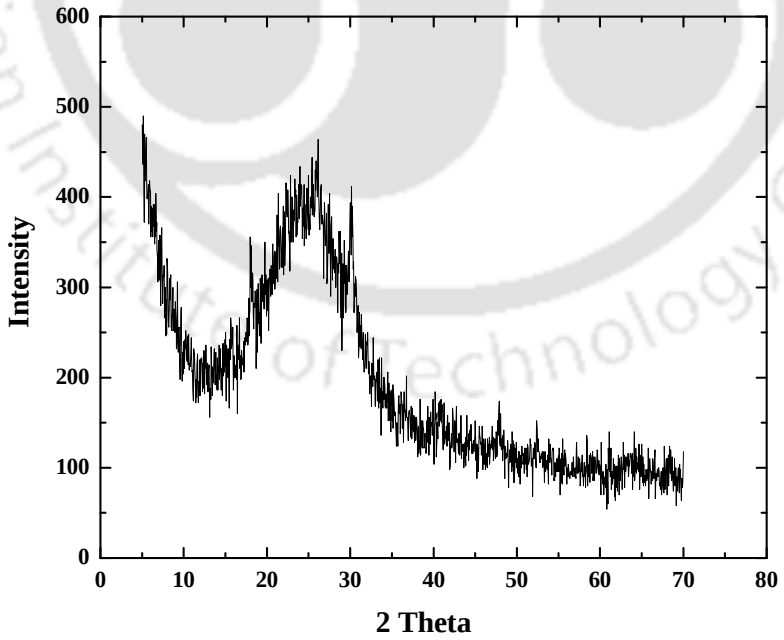

Figure 2.3: X-ray diffraction of pyrophyllite molecule

✓ ***FTIR***

The FTIR spectra were used to analyze the bonds present in pyrophyllite. The FTIR spectra of pyrophyllite were shown in Figure 2.4. According to the spectra, the band at 3431 cm^{-1} corresponds to OH^- stretching vibrations of OH groups bonded to Al ions within layer structure. Another prominent absorption feature related to H_2O deformation is expressed at 1645 cm^{-1}. The bands at 1282 and 1027 cm^{-1} was due to $Si-O$ stretching vibrations. OH bending vibration of $Al-OH$ groups were found at wavelength 888 cm^{-1}.

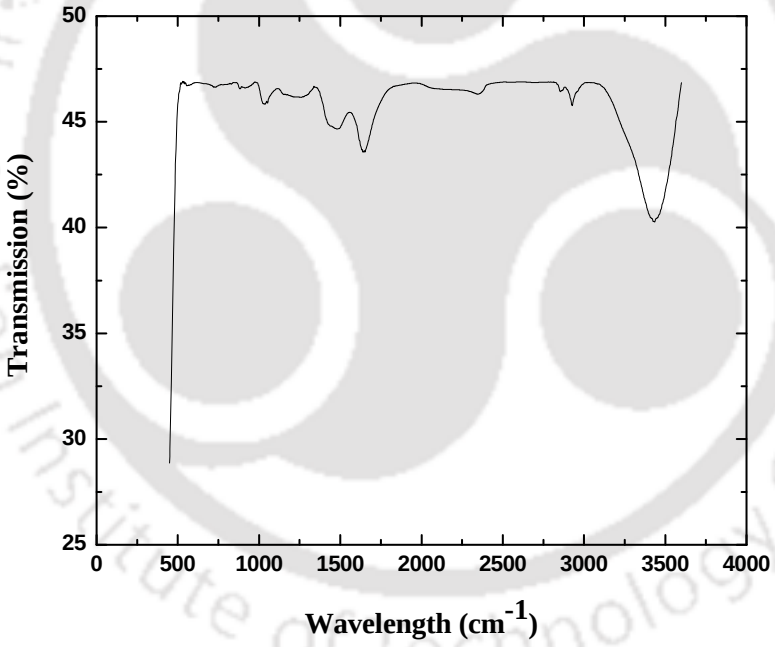

Figure 2.4: FTIR of pyrophyllite molecule

✓ ***Particle size distribution***

The particle size distribution of pyrophyllite was determined by LPSA and shown in Figure 2.5. The size of the pyrophyllite particles vary in the range of 0.65 μm to 778.1

µm. More than 88% particles were of below 200 µm. Average particle size of the adsorbent was 116.7µm.

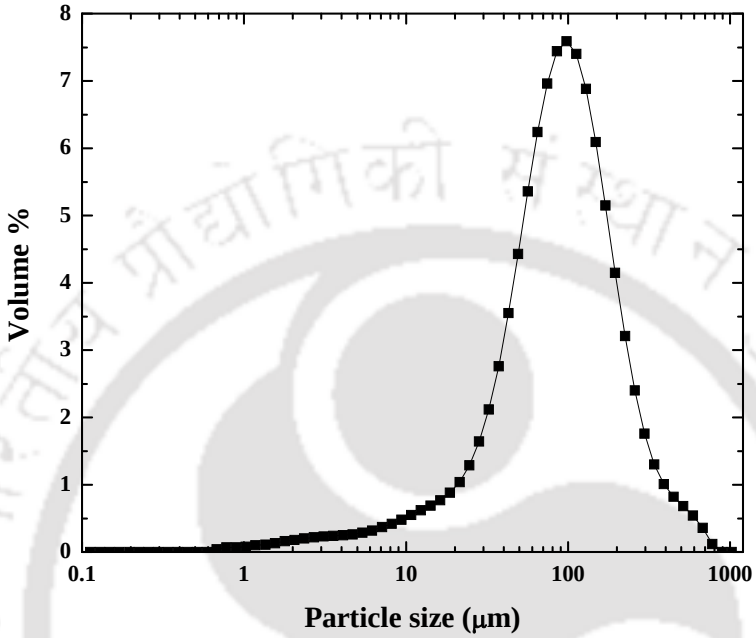

Figure 2.5: Particle size distribution of pyrophyllite

✓ **pH_{ZPC}**

The zero point charge (pH_{ZPC}) of pyrophyllite was plotted in Figure 2.6. From the figure, it was observed that with increase in initial pH of the solution, the final pH of the solution was also increasing slowly. At pH range 5.9 to 10, the final pH of the solution was almost constant at pH value 5.12 which indicated the neutral charge of the adsorbent at that pH range. Hence it may be concluded that the pH_{ZPC} value of pyrophyllite was at pH 5.12.

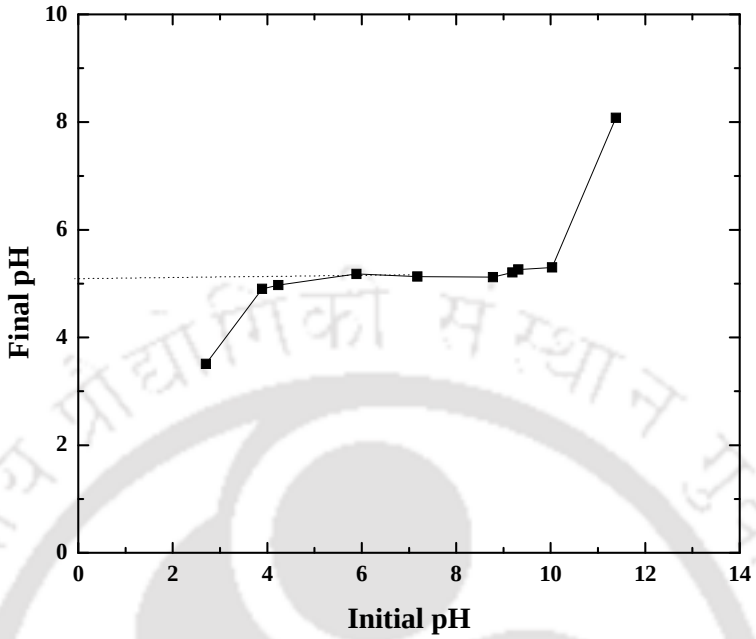

Figure 2.6: pH_{ZPC} of pyrophyllite

2.3.2 Acidic alumina

- ✓ ***Surface area***

The pore size distribution of acidic alumina was obtained from BET surface area analyzer and plotted in Figure 2.7. From the figure, it was found that the acidic alumina exhibited a wide distribution of pores. About 84.19% of total pores were in the range of pore diameter below 40 nm with total pore volume of 0.554 mL/g nm, indicating a very high mesopore volume. The second fraction of pores appeared in the range from 50 to 150 nm. In this range, the pore volume was 0.004 mL/g nm with only 15.81% of the total pore volume indicating the existence of the macropores. It was also observed that the specific surface area of alumina was 144.27 m^2/g.

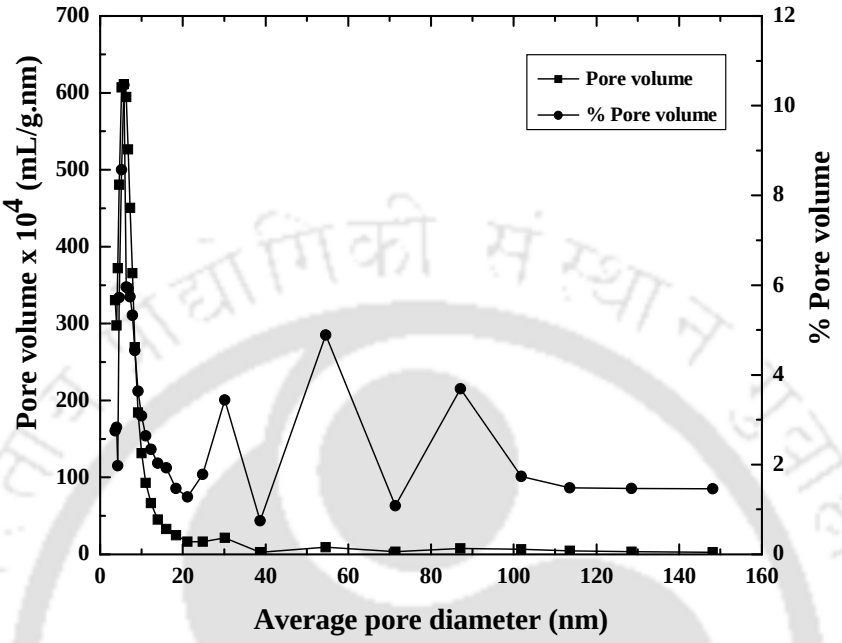

Figure 2.7: Pore size distribution of acidic alumina

✓ ***XRD***

The XRD pattern of acidic alumina was recorded and presented in Figure 2.8. The XRD pattern was matched with that of single phase aluminum oxide with broad peaks at $2\theta = 32.4^o$, 36.9^o, 39.1^o, 42.8^o, 45.1^o and 67.3^o which were matched with JCPDS file no. 00-047-1770. From the figure, it was observed that the used adsorbent was crystalline in nature.

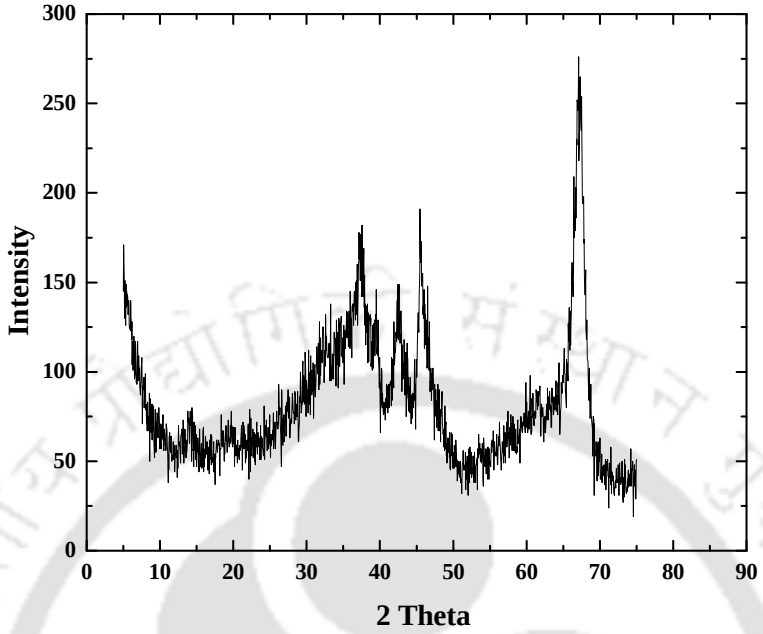

Figure 2.8: XRD of acidic alumina

✓ ***FTIR***

Figure 2.9 showed the FTIR spectra of acidic alumina which was used as adsorbent for defluoridation of water. The band at 3453.4 cm^{-1} corresponds to OH^- stretching vibrations of weakly H-bonded OH of water and a significantly broadened stretching vibration band at 3440 cm^{-1} is assigned to the formation of the $O-H \bullet\bullet\bullet F$ bond indicating the presence of hydrogen bonding. The bands at around 1644.4 cm^{-1} can be attributed to inter layer water molecules, with the stretching vibration disturbed by the presence of water molecules in the sample.

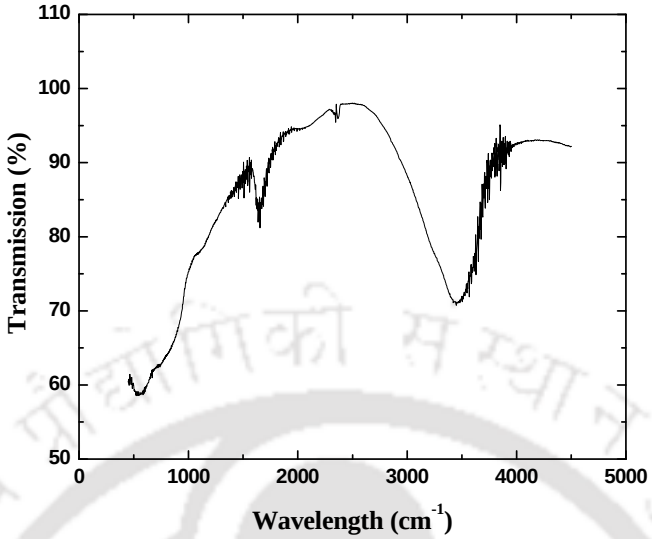

Figure 2.9: FTIR of acidic alumina

✓ **SEM**

Figure 2.10 showed the SEM picture of acidic alumina. SEM picture confirmed that the adsorbent is composed of some irregular shape particles.

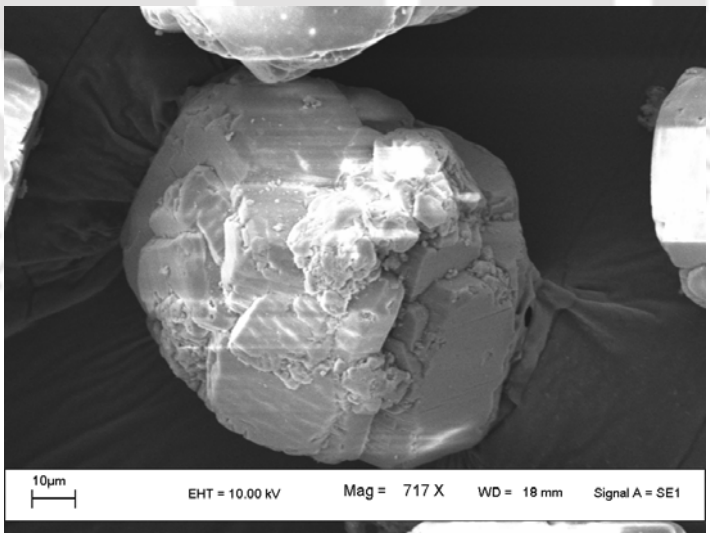

Figure 2.10: SEM picture of acidic alumina

✓ **Particle size distribution**

Figure 2.11 showed the particle size distribution of acidic alumina using LPSA. It was observed from the figure that the particle size was varied in the range of 52.5 μm to 240 μm. More than 98.7% particles were found below 200 μm. The average particle size of the adsorbent was 109.2 μm which confirmed that the adsorbent was consisted of microparticles.

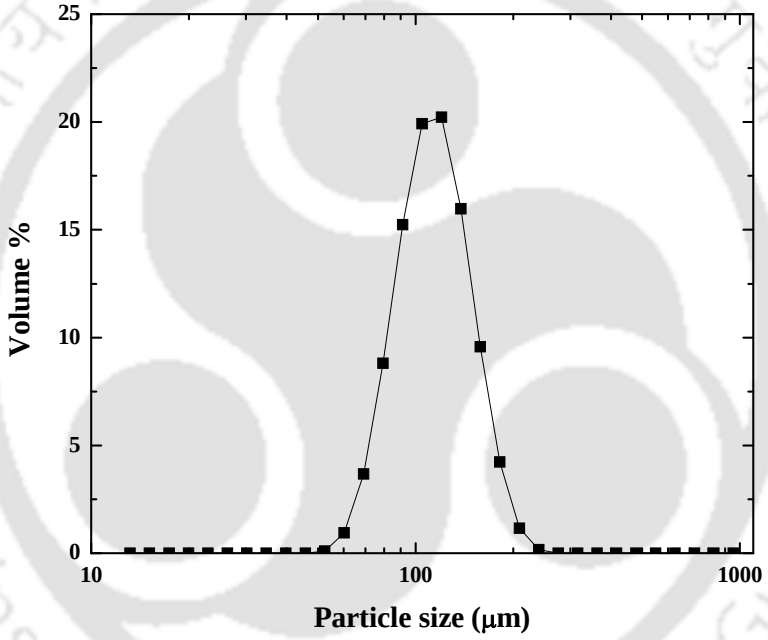

Figure 2.11: Particle size distribution of acidic alumina

✓ **pH_{ZPC}**

The point of zero charge (pH_{ZPC}) of acidic alumina was plotted in Figure 2.12. From the figure it was observed that with increase in initial pH, the final pH was increased slowly. At initial pH range of 4.9 to 10, the final pH of the solution was almost constant which indicates the neutral charge of the adsorbent at that pH range.

It was observed that pH_{ZPC} value of alumina was at pH 5.1 which concluded that the adsorbent surface had a positive charge (weekly cationic) in aqueous medium.

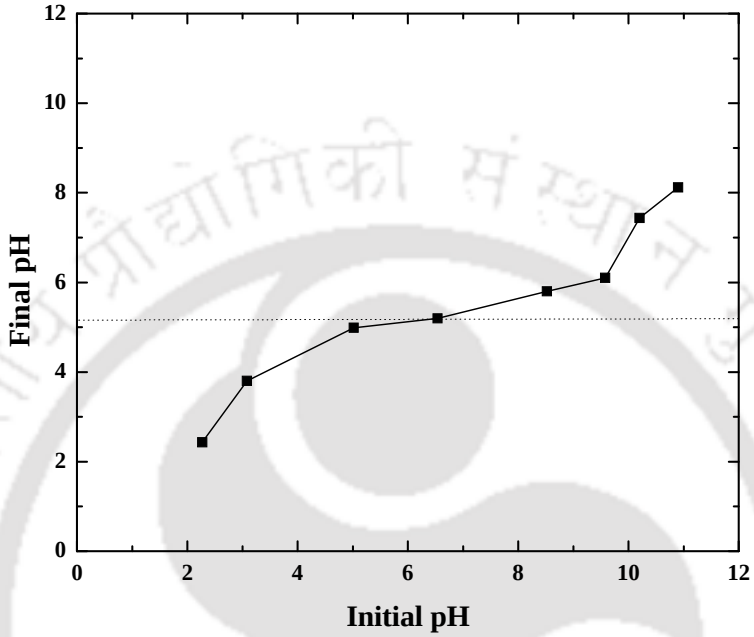

Figure 2.12: pH_{ZPC} of acidic alumina

2.3.3 Schwertmannite

✓ ***Surface area***

BET surface area analyzer was used to determine the specific surface area, pore volume and pore size distribution of Sh. The specific surface area of Sh used for defluoridation was 360.39 m^2/g. The wide distribution of pores of Sh was observed from Figure 2.13. From the figure, it was observed that about 84.25% of total pores were in the range of pore diameter below 40 nm with total pore volume of 0.18275 mL/g.nm, indicating a very high mesopore volume. In the second fraction, pores appeared in the range of 50 to 150 nm. In this range, only 15.76% of total pores were

found with pore volume 0.00141 mL/g.nm which indicate the existence of macropores.

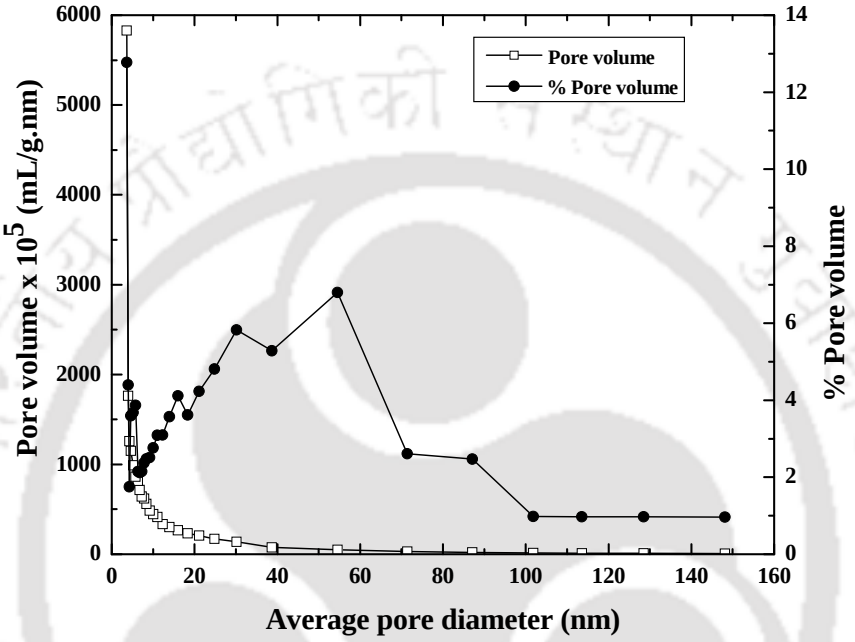

Figure 2.13: Pore size distribution of Sh

✓ ***XRD***

The XRD pattern gives an idea about the structure of an adsorbent. The XRD plot of Sh was shown in Figure 2.14. It was noticed that no specific peak was observed in the XRD pattern which indicated the amorphous nature of the prepared adsorbent.

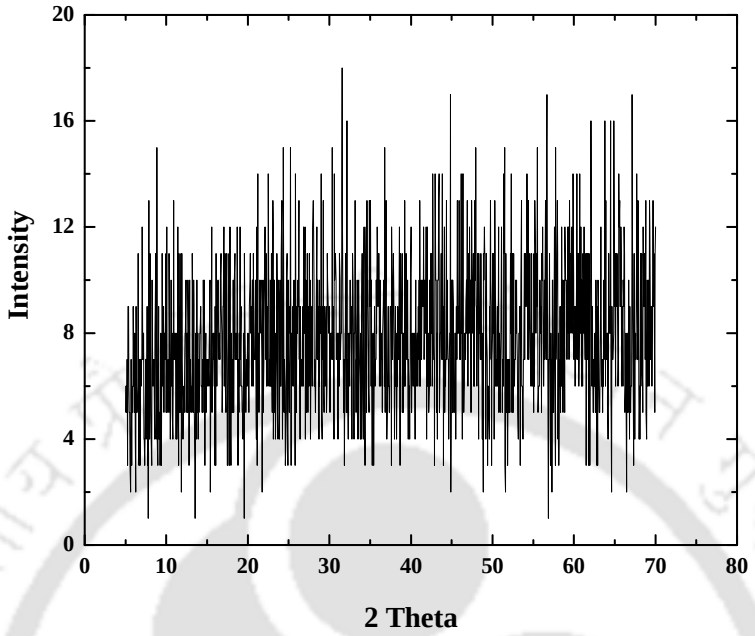

Figure 2.14: XRD of Sh

✓ ***Morphology study***

Figure 2.15 showed the FESEM picture of Sh. The Sh is known as a poorly crystalline iron oxide hydroxide that consists of spherical to ellipsoidal particles with hedge-hog like aggregates and several mm in size. The needle-like structures with average width and thickness of 2 – 4 nm and length of 60 – 90 nm radiate from the particle surfaces to devote "pincushion" morphology to this material [7].

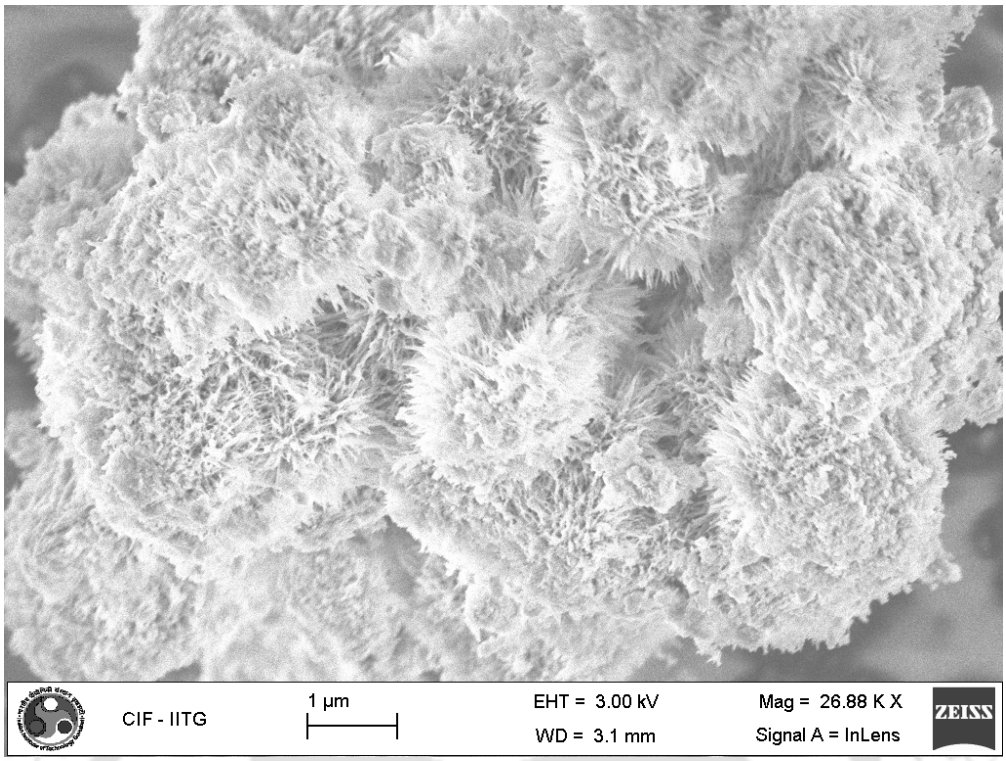

Figure 2.15: FESEM image of Sh

✓ **FTIR**

The FTIR spectrum of Sh was shown in Figure 2.16. The infrared spectrum of the sample is dominated by a broad, OH-stretching band centered at 3300 cm^{-1}. Another prominent absorption feature related to H_20 deformation is expressed at 1634 cm^{-1}. Intense bands at 1124, and 1063 cm^{-1} reflect a strong splitting of the ν_3 (SO_4) fundamental due to the formation of a bidentate bridging complex between SO_4 and Fe. This complex may result from the replacement of OH groups by SO_4 at the mineral surface through ligand exchange or by the formation of linkages within the structure during nucleation and subsequent growth of the crystal. Related features due to the presence of structural SO_4 include bands at 976 and 608 cm^{-1} that can be assigned to ν_1 (SO_4) and ν_4(SO_4), respectively. Vibrations at 704 cm^{-1} are attributed to

Fe-O stretch; however, assignment of the former is tentative because similar bands in the iron oxyhydroxides usually occur at lower frequencies. A broad absorption shoulder in the 800 to 880 cm^{-1} range is apparent in some specimens and is related to OH deformation [δ(OH)].

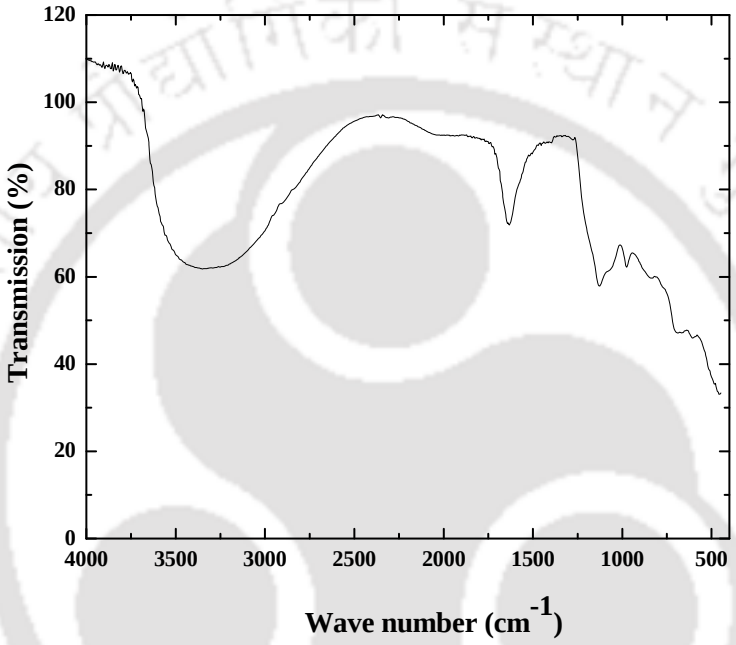

Figure 2.16: FTIR of Sh

✓ ***Particle size distribution***

The particle size distribution of prepared adsorbent was shown in Figure 2.17. The particle size of Sh was varied in the range of 3.3 µm to 1259 µm which concluded wide distribution range of particles. It was also observed that more than 72.6% particles were below 200 µm with average particle size of 150.3 µm.

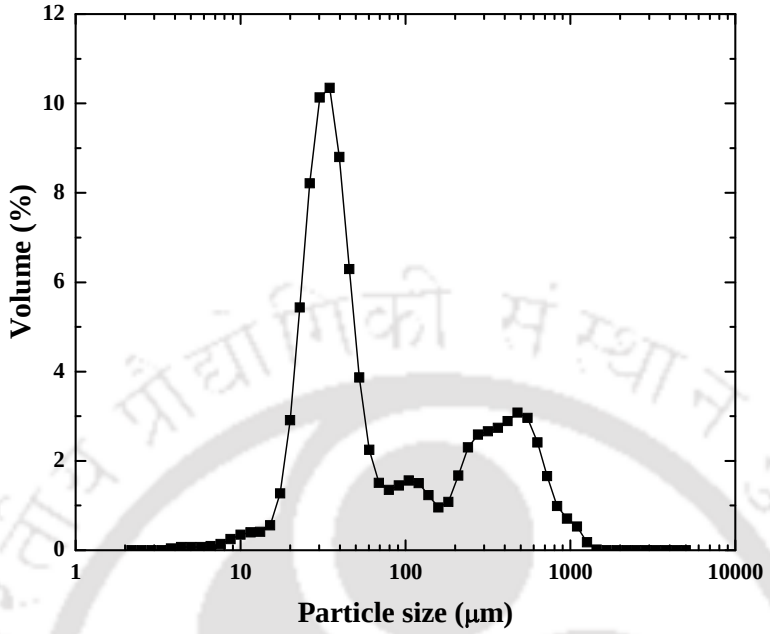

Figure 2.17: Particle size distribution of Sh

2.3.4 Nanomagnetite aggregated schwertmannite (NMSh)

✓ ***Surface area***

The BET surface area of NMSh was 276.15 m^2/g. The pore size distribution of the adsorbent was plotted in Figure 2.18. It was observed from the figure that NMSh exhibited a wide distribution of pores. About 79.28% of total pores were in the range of pore diameter below 40 nm with total pore volume of 0.139 mL/g nm, indicating a very high mesopore volume. The second fraction of pores appeared in the field from 50 to 150 nm. In this range, the pore volume was 0.00195 mL/g nm with only 20.72% of the total pore volume indicating the existence of the macropores.

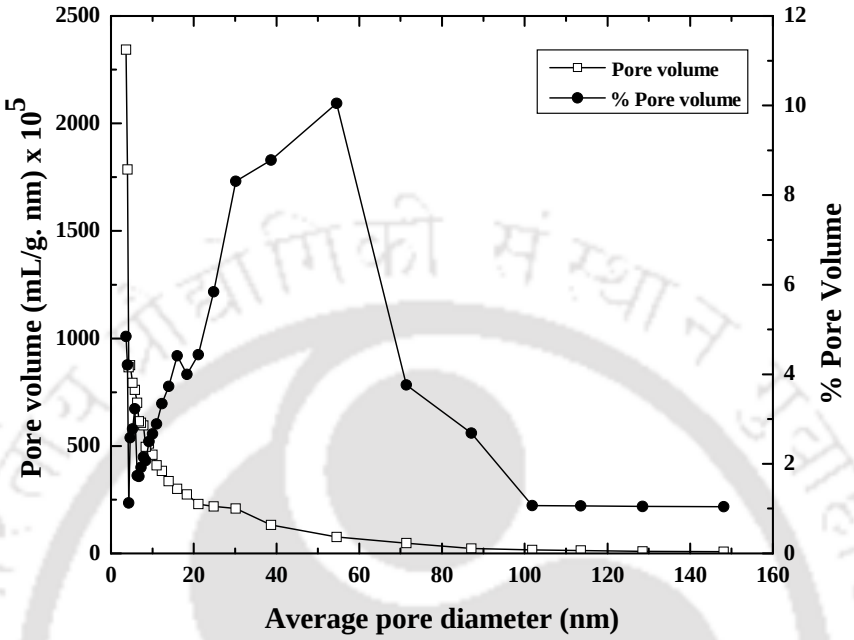

Figure 2.18: Pore size distribution of NMSh

✓ **XRD**

The XRD patterns (Figure 2.19) showed the crystal structure of the new adsorbent. The new adsorbent particles showed no peaks related with the added magnetite. This was because of a quite small amount of the nanomagnetite particles aggregated into the new adsorbent structure where the ratio of the magnetite particles to the schwertmannite ranged from 3–5%. The XRD pattern concluded that no crystallographic structure was observed in the new adsorbent.

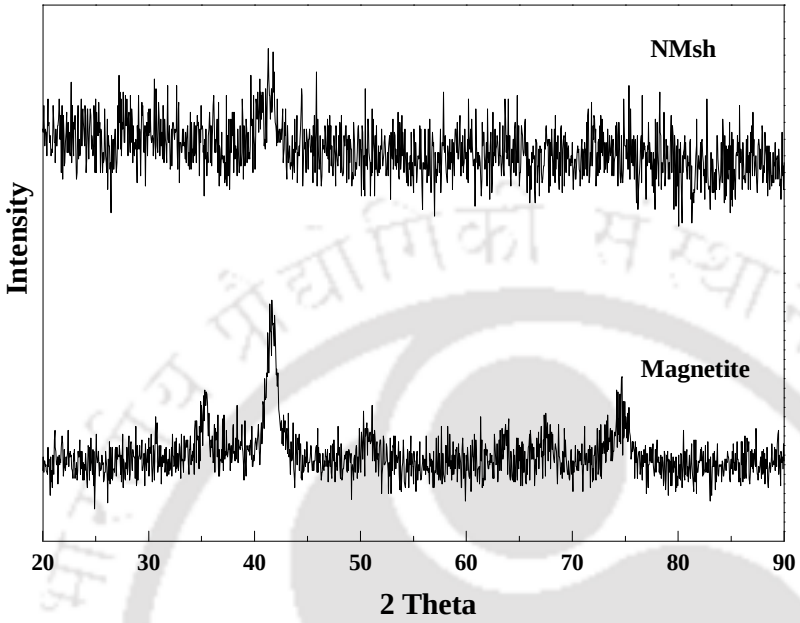

Figure 2.19: XRD of NMSh and magnetite particles

✓ **FESEM**

Figure 2.20 showed the FESEM picture of the adsorbent aggregated with magnetite nanoparticles. It was clearly observed, that the needle-like surface structure of the schwertmannite observed in Figure 2.15 has almost disappeared after addition of nanomagnetite over Sh surface.

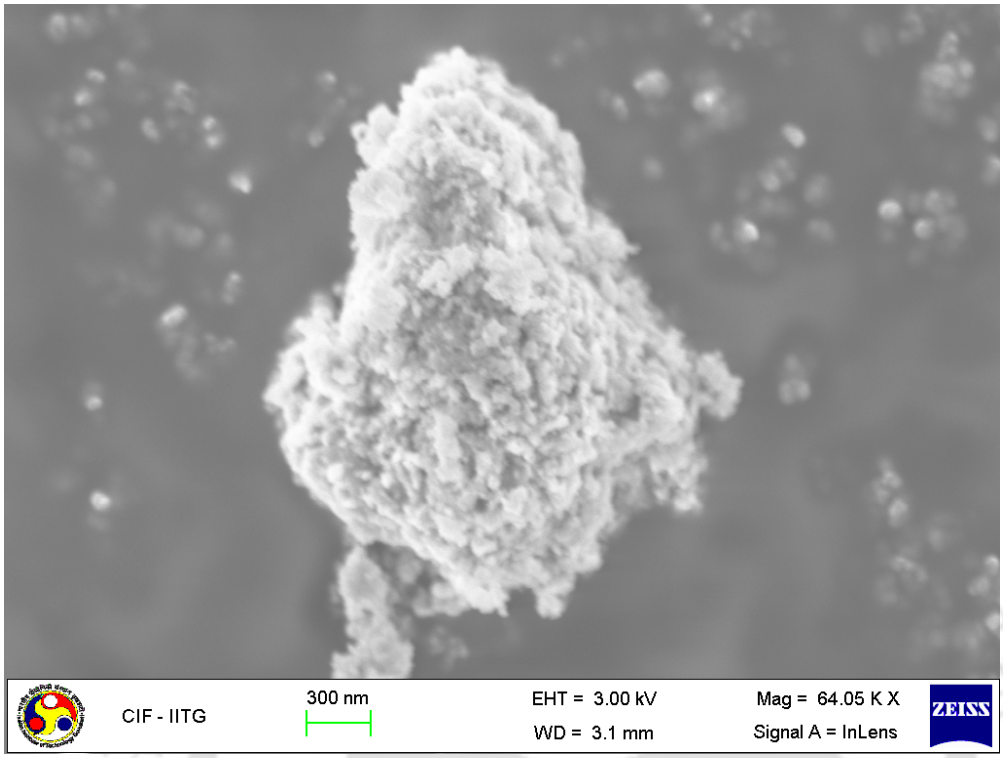

Figure 2.20: FESEM picture of NMSh

✓ **FTIR**

Figure 2.21 showed the FTIR of NMSh used for fluoride adsorption. It was observed from the figure that the infrared spectrum of the sample is dominated by a broad OH-stretching band which is confirmed by the band centered at 3430 cm^{-1}. The band at 1625 cm^{-1} showed the prominent absorption feature related to H_20 deformation. Intense bands at 1377 and 1123 cm^{-1} represent a strong splitting of ν_3 (SO_4) bond which form a bidentate bridging complex between SO_4 and Fe. This complex is formed due to the replacement of OH groups by SO_4 at the mineral surface through ligand exchange. The bands at 973 and 619 cm^{-1} can be assigned due to the presence of structural SO_4. The vibrations at 701 and 505 cm^{-1} are attributed to Fe-O stretch and the absorption band at 861cm^{-1} is related to OH deformation.

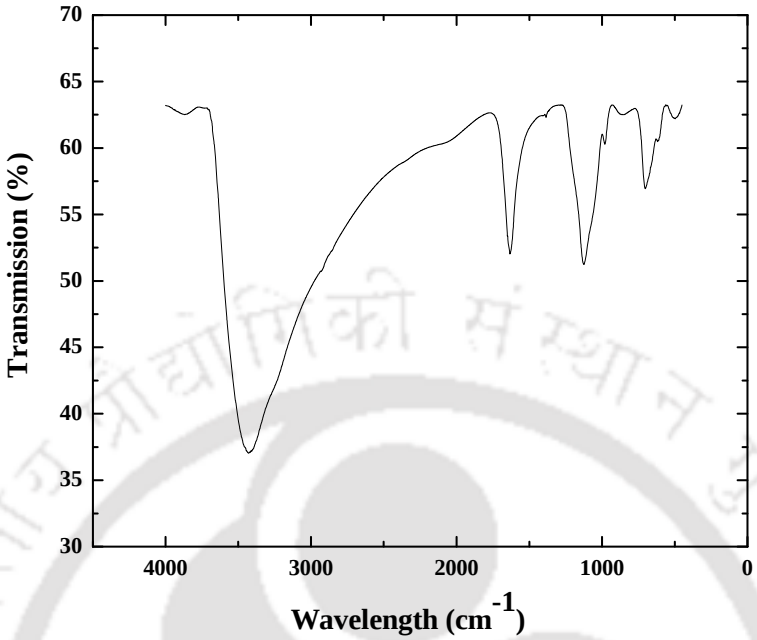

Figure 2.21: FTIR of NMSh

✓ **VSM**

Figure 2.22 showed the VSM of the NMSh, magnetite and Sh respectively. From the figure, it was found that ordinary schwertmannite (Sh) is paramagnetic in nature. From the magnetization curve, it was observed that by aggregating nanomagnetite particles in the ordinary schwertmannite, the new adsorbent has appeared as a composite of ferromagnetic and paramagnetic materials which improves the nature of the adsorbent.

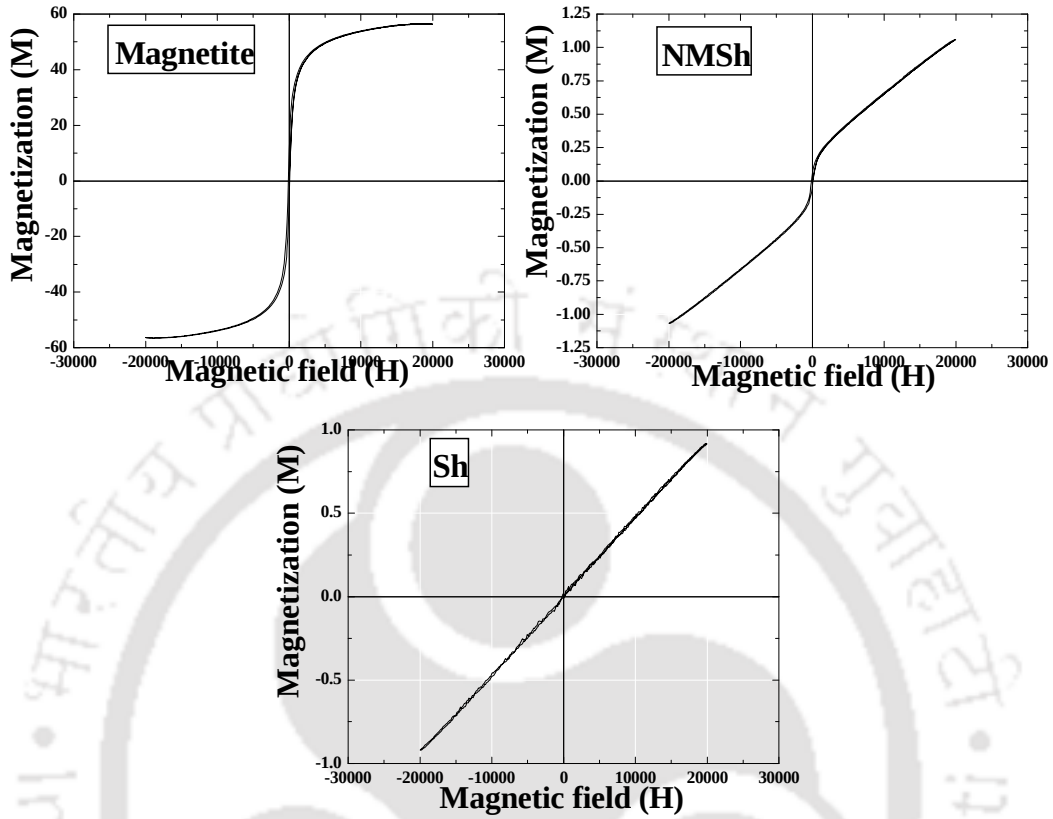

Figure 2.22: VSM of magnetite, NMSh and Sh

✓ ***pH_{ZPC}***

The point of zero charge (pH_{ZPC}) of NMSh was plotted in Figure 2.23. It was observed that the final pH of the solution is almost constant at pH 3.6 for an initial pH range of 4.2 - 9.5 which indicates the neutral charge of the adsorbent at that pH range. Hence zero point charge (pH_{ZPC}) value of NMSh was at pH 3.6 which concluded that the adsorbent surface is weekly cationic in aqueous medium.

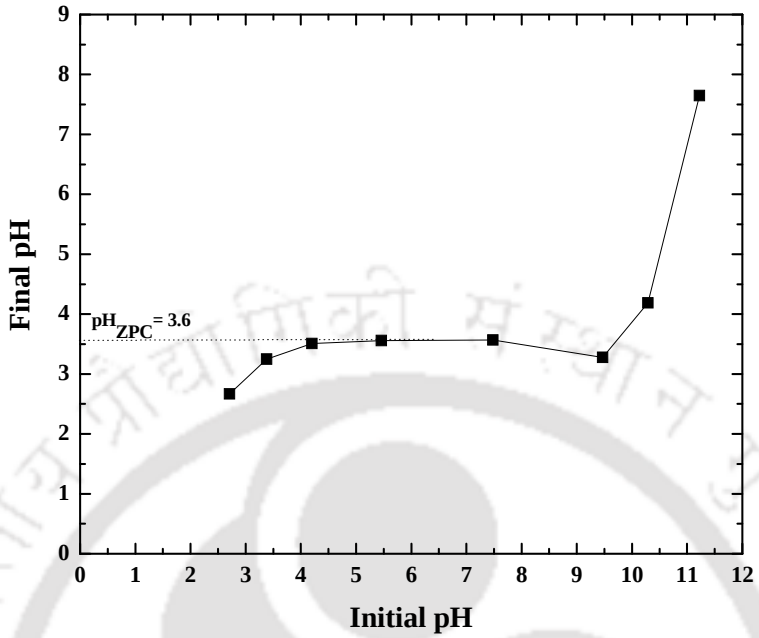

Figure 2.23: pH$_{ZPC}$ of NMSh

2.4 Summary

Fluoride is a very toxic element and it is very difficult to remove from water using conventional adsorbent like activated charcoal. Considering the fluoride removal mechanism, two adsorbents (pyrophyllite and acidic alumina) were selected and two adsorbents (Sh and NMSh) were prepared. All the adsorbents were characterized by surface area, pore size distribution, XRD, FTIR and pH$_{ZPC}$. All the four adsorbents contain OH^- group in its structure which was confirmed by the FTIR. From the above study, it may be concluded that all the four adsorbents had macro as well as mesopores in its structure. The surface area of pyrophyllite, acidic alumina, Sh and NMSh was measured as 424, 144.27, 360.39 and 276.15 m^2/g, respectively. From the XRD study, it

was concluded that pyrophyllite, Sh and NMSh had amorphous structure whereas acidic alumina is crystalline in nature with an average particle diameter of 109.2 μm. All the adsorbent were used to remove fluoride from aqueous medium and discussed separately in Chapter 3.

2.5 References

1. Ciullo, P.A., Thompson, C.S., 1994. Industrial Minerals and Rocks, Society for Mining, Metallurgy and Exploration. D.D. Carr (Ed.), Littleton, Co., 815-818.
2. Hu, Y., Liu, X., Xu, Z., 2003. Role of crystal structure in flotation separation of diaspore from kaolinite, pyrophyllite and illite. Miner. Eng. 16, 219-227.
3. Keren, R., Sparks, D.L., 1995. The Role of Edge Surfaces in Flocculation of 2:1 Clay Minerals. Soil Sci. Soc. Am. J. 59, 430-435.
4. Bentayeb, A., Amouric, M., Olives, J., Dekayir, A., Nadiri, A., 2003. XRD and HRTEM characterization of pyrophyllite from Morocco and its possible applications. Appl. Clay Sci. 22, 211-221.
5. Clifford, D., Matson, J., Kennedy, R., 1978. Activated alumina: Rediscovered "adsorbent" for fluoride, humic acids and silica. Ind. Wat. Eng. 15, 6-12.
6. Eskandarpour, A., Sassa, K., Bando, Y., Okido, M., Asai, S., 2006. Magnetic Removal of Phosphate from Wastewater Using Schwertmannite. Materials Transactions. 47, 1832-1837.
7. Bigham, J.M., Carlson, L., Murad, E., 1994. Schwertmannite, a new iron oxyhydroxysulphate from Pyhäsalmi, Finland, and other localities. Mineralogical Magazine. 58, 641-648.

Chapter 3

Removal of fluoride using various adsorbents

This chapter gives the complete description of the experimentations involved during adsorption of fluoride from fluoride contaminated water using different adsorbents including results and discussion thereon. It discusses the effect of different parameters on the adsorption of fluoride, thermodynamic behavior of adsorption, various isotherms. The entire chapter is divided into seven sections. The Adsorption experimental procedure is summarized in section 3.1. Adsorption results are discussed in section 3.2 to section 3.5 for four different adsorbents and a comparative analysis of the performance of four adsorbents is reported in section 3.6. Section 3.7 describes the summary obtained for defluoridation using four adsorbents.

3.1 Materials and experimental methods

Materials used

The synthetic fluoride solution was prepared by using sodium fluoride (NaF) which was purchased from Titan biotech Ltd, India. The adsorbents like pyrophyllite and acidic alumina used in this study were purchased from National Chemicals, India and Merck, India respectively. The chemicals, $Fe_2(SO_4)_3.5H_2O$ and urea were used to synthesize schwertmannite and $FeCl_2$, $FeCl_3$ and NH_3 were used to synthesize nanomagnetite particles. pH of the solution was maintained by adding 0.1N HCl and 0.1

N $NaOH$ and was obtained from Merck, India. The salts Na_2CO_3, KCl, Na_2SO_4, $NaNO_3$, NH_4HCO_3 and $NaH_2PO_4.H_2O$ were used to study the effect of presence of other ions in fluoride contaminated water. All these chemicals were analytical grade and purchased from Merck, India.

Experimental methods

All the batch adsorption experiments were carried out using 100 mL fluoride solution in 250 mL conical flasks at ambient temperature using different adsorbents discussed in Chapter 2. Variation of extent of fluoride adsorption is observed by agitating different fluoride concentrations with a specified dose of adsorbent, separately at room temperature. Different amounts of adsorbent were used to observe its effect on fluoride adsorption. The adsorption experiments were carried out at different pH values to know the optimum pH of the process. Different temperatures and stirring speeds were also used to know the adsorption behavior of the system. Effect of fluoride adsorption in presence of other ions was also studied with varying concentrations (100-500 mg/L) of chloride, sulphate, nitrate, phosphate, bicarbonate and carbonate ion, prepared from its sodium and ammonium salts. The samples were collected at certain time intervals and filtered with a whatmann filter paper. The adsorption kinetics, thermodynamic parameters and isotherm study was carried out. The detail procedure of adsorption kinetics, thermodynamic parameters and isotherm study were discussed below. A regeneration study was carried out in order to reuse the adsorbents for better economy of the process. Finally, a process design calculation was proposed to know the amount of adsorbent required for efficient removal of fluoride from aqueous medium. Duplicate experiments

were carried out for all the operating variables studied and only the average values are taken into consideration.

The amount of fluoride adsorbed per unit weight of adsorbent at time t, q (mg/g) and fluoride removal efficiency, R were calculated as

$$q_t = \frac{(C_o - C_t)}{M} \times V \qquad (3.1)$$

$$R = \frac{(C_o - C_t)}{C_o} \times 100 \qquad (3.2)$$

Where, C_0 is the initial fluoride concentration (mg/L), C_t is the concentration of fluoride at any time *t*, V is the volume of solution (L) and M is the mass of adsorbent (g).

Operating conditions

Different important parameters such as initial fluoride concentration, adsorption time, pH and temperature of the fluoride contaminated water used for adsorption process. All the experimental conditions considered in this study are shown in Table 3.1.

Table 3.1: Experimental conditions for different adsorbents used for defluoridation of water

Parameters	**Pyrophyllite**	**Acidic alumina**	**Sh**	**NMSh**
Contact time (minute)	Upto 120	Upto 120	Upto 120	Upto 120
Initial fluoride concentration (mg/L)	4-10	5-15	5-15	5-15
Adsorbent dose (g/L)	1- 6	1- 5	1- 4	1- 4
pH	2.8-11.2	2.2-10.7	2.7-11.4	2.6-11.8
Temperature (^oC)	24-60	25-55	30-50	25-55

Instruments used

Fluoride ion meter

The fluoride concentration was measured with a specific ion electrode (EC-FO-03) with total ionic strength adjustment buffer (TISAB) solution. TISAB was prepared by adding 58 g sodium chloride, 57 mL glacial acetic acid, 4 g CDTA (trans-1, 2-Diaminocyclohexane tetracetic acid) and 37.5 g *NaOH* in 1000 mL distilled water. To maintain pH to 5.25, 5 M *NaOH* was added drop wise. TISAB was added to the samples to de-complex the fluoride present in the solution. The fluoride samples and the fluoride standard solutions were diluted 1:1 with TISAB solution and prepared for measurement.

pH meter

A pH meter (Make: Century Instruments (P) Ltd., Chandigarh, India) was used to determine the pH of solution. The meter was first calibrated using three different buffers of pH 4, pH 7 and pH 9.2. Each time the meter was thoroughly washed with de-ionized water before and after the dipping inside the buffer solutions.

Conductivity meter

The conductivity of solution in the EC bath was measured using a digital conductivity meter (Make: Electronics Pvt. Ltd., India, Model: VS1) before and after the treatment to match with the recommendable limit of 0.2 mmhos [1]. The conductivity meter was also calibrated by matching the known conductivity of 0.1(N) KCl solutions given in the manual supplied by the manufacturer. After the calibration, the conductivity meter was thoroughly washed with de-ionized water and soaked with the tissue paper without touching the coated detector inside the meter.

Thermodynamic study

Thermodynamic parameters such as free energy change, enthalpy change and entropy change were calculated to evaluate the thermodynamic feasibility and the spontaneous nature of the process. Following equations were used to determine the thermodynamic parameters [2]

$$\Delta G^0 = \Delta H^0 - T\Delta S^0 \qquad (3.3)$$

$$\log(\frac{q_e m}{C_e}) = \frac{\Delta S^0}{2.303R} + \frac{-\Delta H^0}{2.303RT} \qquad (3.4a)$$

For unit adsorbent mass, equation 3.4a became

$$\log(\frac{q_e}{C_e}) = \frac{\Delta S^0}{2.303R} + \frac{-\Delta H^0}{2.303RT} \qquad (3.4b)$$

where q_e is the amount of fluoride adsorbed per unit mass of adsorbent (mg/g), C_e is equilibrium concentration (mg/L), m is the adsorbent mass (g/L) and T is temperature in Kelvin. $\frac{q_e}{C_e}$ is called the adsorption affinity. The values of Gibb's free energy (ΔG^0) had been calculated by knowing the enthalpy of adsorption (ΔH^0) and entropy of adsorption (ΔS^0) and ΔH^0 was obtained from a plot of $\log(\frac{q_e}{C_e})$ versus $\frac{1}{T}$, from equation (3.4b). Once these two parameters were obtained, ΔG^0 was determined from equation (3.3).

In order to further support the assertion that physical adsorption is the predominant mechanism, the values of activation energy (E_a) and sticking probability (S^*) [2] were estimated from the experimental data. They were calculated using a modified Arrhenius type equation related to surface coverage (θ) as follows [3]:

$$S^* = (1-\theta)e^{-(E_a/RT)} \qquad (3.5)$$

The S^* is a function of the adsorbate/adsorbent system under investigation, its value lies in the range $0 < S^* < 1$ and is dependent on the temperature of the system. The parameter S^* indicates the potentiality of an adsorbate to remain on the adsorbent. The θ can be calculated from the following equation:

$$\theta = [1 - C_e / C_o] \qquad (3.6)$$

The activation energy (E_a) and sticking probability (S^*) were estimated from a plot of $\ln(1-\theta)$ vs $1/T$.

Adsorption kinetics

To express the mechanism of fluoride adsorption on the adsorbent surface, different kinetic model equations were used to analyze the adsorption data to determine the related kinetic parameters. Following kinetic model equations were used to analyze the present adsorption data to determine the related kinetic parameters.

Pseudo first order kinetic model

This model assumed that the rate of change of solute uptake with time was directly proportional to difference in saturation concentration and the amount of solid uptake with time. In most cases the adsorption reaction preceded by diffusion through a boundary, the kinetics followed the pseudo first order rate equation. The rate constant of adsorption was expressed as a first-order rate expression given as [4].

$$\frac{dq_t}{dt} = k_1(q_e - q_t) \qquad (3.7)$$

Where q_t and q_e are the amount of fluoride adsorbed (mg/g) at contact time t (min) and at equilibrium, k_1 is the pseudo first order rate constant (min^{-1}). After integrating with the boundary conditions at initial time ($t = 0$), $q_t = 0$ and at any time ($t > 0$), amount of fluoride adsorbed was q_t and rearranging equation (3.7), the rate law for a pseudo-first-order reaction became

$$q_t = q_e\{1-\exp(-k_1 t)\} \qquad (3.8)$$

Taking 'ln' on both sides and then plot of $\ln(q_e - q_t)$ versus t should gave a straight line with slope of $-k_1$ and intercept $\ln q_e$ which allows calculation of adsorption rate constant k_1 and equilibrium adsorption capacity $q_{e,cal}$.

Pseudo second order kinetic model

Adsorption process with chemisorption being the rate-control followed pseudo second order model. The sorption kinetics may be represented by pseudo second order model [5] as

$$\frac{dq_t}{dt} = k_2(q_e - q_t)^2 \qquad (3.9a)$$

Where k_2 is the equilibrium rate constant for pseudo second order sorption (g/mg min). Integrating equation (3.9a) using the boundary conditions at t = 0, q_t = 0 and at any time t, amount of fluoride adsorbed was q_t, equation (3.9a) became

$$\frac{1}{(q_e - q_t)} = \frac{1}{q_e} + k_2 t \qquad (3.9b)$$

Equation (2.9b) is the integrated rate law for a pseudo second order reaction. Rearranging rate law gives

$$\frac{t}{q_t} = \frac{1}{k_2 q_e^{\ 2}} + \frac{t}{q_e} \qquad (3.10)$$

The value of q_e and the pseudo-second-order rate constant, k_2 can be calculated from the slope and intercept of the straight line obtained from the plot of $\frac{t}{q_t}$ versus t. The initial adsorption rate can be obtained as $\frac{t}{q_t}$ when t approaches zero:

$$h_o = k_2 q_e^2 \qquad (3.11)$$

where h_o is the initial adsorption rate (mg/(g time)).

Intra particle diffusion model

The adsorbate moves from the solution phase to the surface of the adsorbent particles in several steps. The overall adsorption process may be controlled by one or more steps (e.g., film or external diffusion, pore diffusion, surface diffusion and adsorption on the pore surface, or a combination of more than one step). In a rapidly stirred batch process of adsorption, the diffusive mass transfer can be related by an obvious diffusion coefficient, which will fit experimental adsorption rate data. Normally, a process is diffusion-controlled if its rate is dependent on the rate at which components diffuse toward each other. The possibility of intraparticle diffusion was explored using the intraparticle diffusion model [6]:

$$q_t = k_i t^{0.5} + I \qquad (3.12)$$

Where, q_t is the fraction of fluoride uptake (mg/g) at time t, k_i is the intra particle diffusion rate constant (mg/g $\min^{0.5}$) and I is the intercept (mg/g) related to the thickness of the boundary layer. The larger the value of I, the greater the boundary-layer effect. According to this model, if adsorption of a solute is controlled by the intra particle diffusion process, a plot of q_t versus $t^{0.5}$ gives a straight line.

Adsorption equilibrium

Adsorption equilibrium isotherms describe the relation between adsorbate concentration and its accumulating capacity of adsorbate on the adsorbent surface at constant temperature. So, in order to optimize the design of an adsorption system to remove fluoride from water, it is essential to establish the most appropriate isotherm correlation for the equilibrium curve. Accordingly, the conformity experimental results with four of the most conventional isotherm models viz. Langmuir, Freundlich, Temkin and Dubinin–Rasdushkevich (DR) isotherms were considered for this adsorption system.

Langmuir isotherm

Langmuir isotherm is based on the assumption that there is a finite number of binding sites which are homogeneously distributed over the adsorbent surface. These binding sites bear the same affinity for adsorption of a single molecular layer and there is no interaction between adsorbed molecules. The equation of Langmuir isotherm [7] is represented as:

$$q_e = \frac{Q_0 b C_e}{1 + b C_e} \qquad (3.13)$$

Where C_e (mg/L) and q_e (mg/g) are the liquid phase concentration and solid phase concentration of adsorbate at equilibrium, respectively. The adsorption capacity q_{max} (mg/g) is the amount of adsorbate at complete monolayer coverage and b (L/mg) is the Langmuir isotherm constant that relates to the energy of adsorption.

To evaluate the adsorption capacity for a particular range of adsorbate concentration, the aforementioned equation (3.13) can be used as a linear form as follows:

$$\frac{1}{q_e} = \frac{1}{q_{max} b} \times \frac{1}{C_e} + \frac{1}{q_{max}} \qquad (3.14)$$

The values of Langmuir parameters, q_{max} and b were calculated from the slope and intercept of the linear plots of $1/q_e$ vs $1/C_e$

To check the feasibility of the isotherm, the dimensionless equilibrium parameter R_L was determined by using the following equation [8]

$$R_L = \frac{1}{1 + bC_0} \qquad (3.15)$$

where, C_0 and b are the initial fluoride concentration and Langmuir isotherm constant. For favorable adsorption, R_L value should be less than 1.

Freundlich isotherm

The Freundlich isotherm model is based on the multilayer adsorption of an adsorbate onto the heterogeneous surfaces of an adsorbent. The well-known expression for the Freundlich model is given as [9].

$$q_e = K_F C_e^{\,n} \qquad (3.16)$$

Where, K_F is the Freundlich constant [(mg/g) (L/mg)$^{1/n}$] related to the bonding energy, and n is the heterogeneity factor. The value of n varies with the heterogeneity of the adsorbent and for favorable adsorption process, n value should be less than unity.

The linear form of the Freundlich equation (3.16), which is commonly used to describe adsorption isotherm data,

$$\log(q_e) = \log K_F + n \log C_e \qquad (3.17)$$

The Freundlich isotherm constants K_F and n were calculated from the slope and the intercept of the plot of $\log q_e$ vs. $\log C_e$ which is a straight line.

Temkin isotherm

The Temkin isotherm was developed based on the assumption that the heat of adsorption would decrease linearly with the increase of coverage of adsorbent. Equation (3.18) shows the Temkin isotherm model where b is the constant related to the heat of adsorption, A_T is the Temkin isotherm constant, T is the temperature (K) and R is the ideal gas constant (8.314 J /mol.K) [10].

$$q_e = \frac{RT}{b} \ln(A_T C_e) \qquad (3.18)$$

Equation (3.18) was linearized as

$$q_e = B_T \ln A_T + B_T \ln C_e \qquad (3.19)$$

where $B_T = \frac{(RT)}{b}$

The plot of q_e vs. $\ln C_e$ generates a straight line and from the values of slope and intercept, the Temkin constants A_T and B_T were calculated.

Dubinin–Rasdushkevich isotherm

Dubinin–Rasdushkevich (DR) isotherm helps in understanding the type of adsorption from the data of fluoride both in the adsorbent and solution at equilibrium. DR equation can be written [11] as

$$\ln q_e = \ln Q_m - K_{DR}\varepsilon^2 \qquad (3.20)$$

where ε is the Polanyi potential, Q_m is the adsorption capacity (mg/g), K is the constant related to the adsorption energy, R is the gas constant (J/K.mol) and T is the temperature (K).

$$\varepsilon = RT \ln\left(1 + \left(\frac{1}{C_e}\right)\right) \qquad (3.21)$$

The plot of $\ln q_e$ against ε^2 gives a straight line and DR isotherm constants K and Q_m were calculated from the slope and intercept of the plot. The mean free energy of adsorption (E), defined as the free energy change when 1 mole of ion is transferred to the surface of the solid from infinity in solution can be calculated from the K_{DR} value using the following equation.

$$E = \frac{1}{\sqrt{2K_{DR}}} \qquad (3.22)$$

The magnitude of the mean free energy of adsorption (E) calculated from DR equation is useful for estimating the type of adsorption. The E value obtained from equation 3.22, which is in the energy range of an ion-exchange reaction, i.e., 8–16 kJ/mol [12].

Regeneration technique

The main objective of the present work is to develop an efficient adsorbent that can be reused thereby making it cost effective. For reusability, the adsorbed fluoride should be easily desorbed. 15 mg/L fluoride was adsorbed on a certain mass of adsorbent at optimum pH. Then the solution was filtered and the adsorbent was transferred to 100 mL of water and the pH was adjusted. Desorption studies were conducted in 250 mL conical flask by conditioning the suspension at that pH for 90 min. In the acidic pH range hardly any fluoride was leached. But as the pH was increased above optimum pH, the adsorbed fluoride starts to leach back into the solution. The desorbed adsorbent was washed with distilled water and dried overnight. The desorbed adsorbent was again used for fluoride removal to check the performance of the regenerated adsorbent. All the adsorbents considered here were used for regeneration study.

Process calculation

Generally adsorption process goes through different stages such as external mass diffusion of solute from the bulk of the system to the adsorbent surface, then the solute diffuses into the pores of adsorbent and finally sorption of solute occurs onto the surface of the pores. It is very difficult to design properly the adsorber size and performance until and unless all experimental data and rate controlling step are available. Therefore, empirical design procedures based on sorption equilibrium conditions are the most common method for predicting the size of adsorber and performance [13]. The schematic diagram of a single stage batch reactor design was shown in Figure 3.1. The design

objective is to reduce the fluoride contaminated solution of volume V (L) from an initial concentration of C_o to C_1 (mg/L). The amount of adsorbent is M in g, and the solute loading changes from q_o (mg/g) to q_1 (mg/g). At time $t = 0, q_o = 0$ and as time proceeds the mass balance equates the fluoride removal from the liquid to that picked by the solid. The mass balance equation may be written as [13]

$$V(C_o - C_t) = M(q_o - q_1) = Mq_1 \qquad (3.23)$$

Under equilibrium conditions, $C_1 \to C_e$ and $q_1 \to q_e$

Since the sorption studies confirmed that the equilibrium data for fluoride onto adsorbent fitted well in Langmuir isotherm, Langmuir equation can be used for q_1. Equation (3.23) can be rearranged as,

$$\frac{C_o - C_e}{q_1} = \frac{M}{V} = \frac{C_o - C_e}{q_e} = \frac{C_o - C_e}{\frac{Q_o b C_e}{1 + bC_e}} \qquad (3.24)$$

Except for 100 percentage removal conditions, equation (3.24) can be used to calculate the amount of dose required for the required percentage removal of fluoride from aqueous solution for any initial solution concentration.

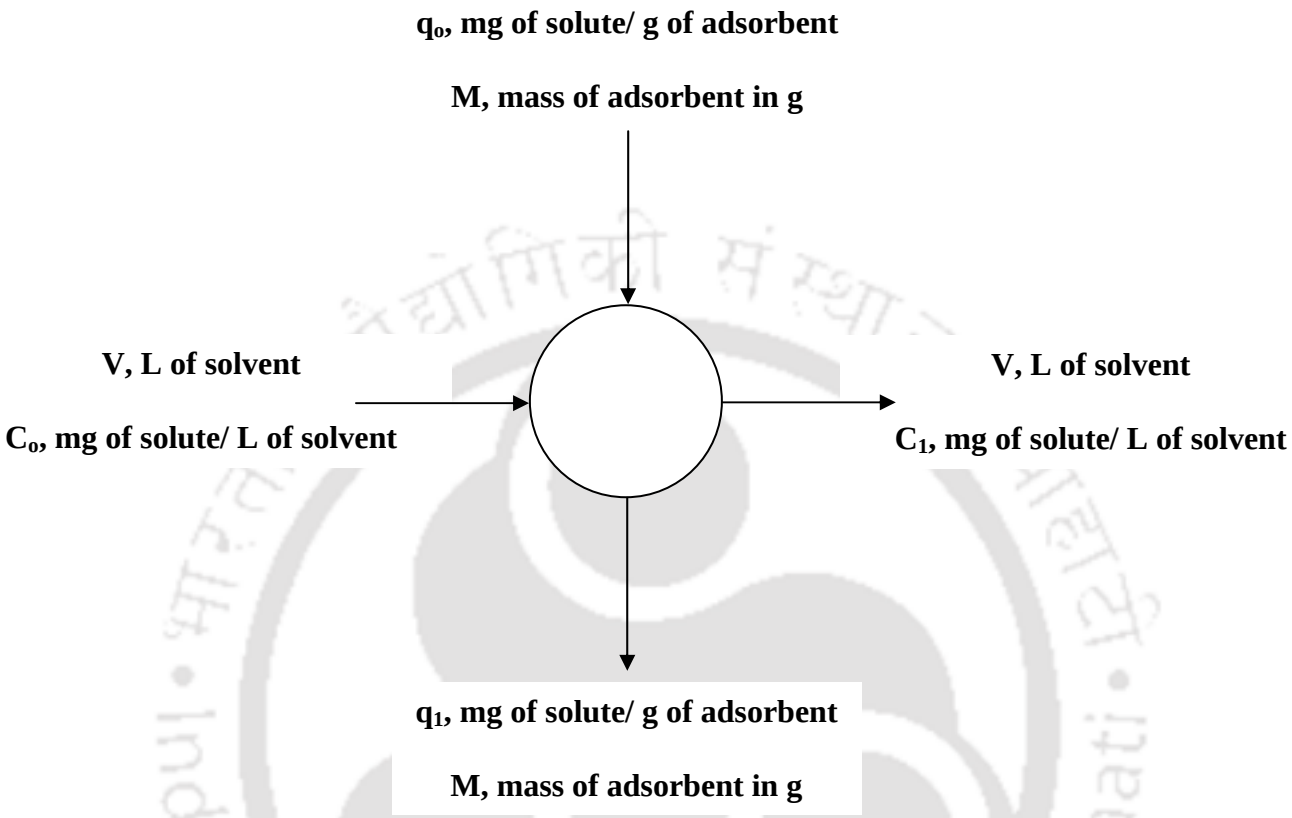

Figure 3.1: Single stage batch reactor design scheme

3.2 Fluoride removal by pyrophyllite*

Batch adsorption study is carried out to remove excess fluoride from water using pyrophyllite and described in this section. Effects of different adsorption parameters on fluoride adsorption were discussed and reported well in this section.

Effect of contact time and initial fluoride concentration

The rapid adsorption of fluoride took place within 20 minute and then adsorption became slow and almost reached equilibrium within 120 minute (Figure 3.2a). Further increase in contact time up to 24 hrs, removal of fluoride was increased by less than 1%. Thus, all the adsorption experiments were conducted for 120 minute. For initial concentration up to 6 mg/L, more than 85% removal and more than 83% for 10 mg/L was observed. The fluoride removal efficiency decreased with increase in initial fluoride concentration as with increase in fluoride concentration, competition for the active adsorption sites increased and the adsorption process will increasingly slow down. The rate of adsorption increased with initial fluoride concentration (Figure3.2b). The rates of adsorption in the initial rapid phase (Equation (3.25)) were found to be 0.046, 0.065, 0.085 and 0.095 mg/g min for initial fluoride concentrations of 4, 6, 8 and 10 mg/L, respectively. A similar trend was observed for the slower phase (Equation (3.26)) where the rates of adsorption were 1.9×10^{-4}, 6.5×10^{-4}, 7.7×10^{-4} and 1.35×10^{-3} mg/g min for initial fluoride concentrations of 4, 6, 8 and 10 mg/L, respectively.

* *The work is published in the following journals:*

A. Goswami, M.K.Purkait, Kinetic and equilibrium study for the fluoride adsorption using pyrophyllite, *Sep. Sci. Technol*. 46(11) (2011) 1797-1807

$$r_{rapid} = 0.0548 \ln C_o - 0.0309 \qquad R^2 = 0.993 \qquad (3.25)$$

$$r_{slower} = 1.8C_o - 5.2 \qquad R^2 = 0.9479 \qquad (3.26)$$

The adsorption of fluoride on pyrophyllite particles was governed by the ionic interaction. Aggregation of fluoride molecules with increasing contact time made it almost impossible for the fluoride molecules to diffuse deeper into the pyrophyllite structure at the highest energy sites. This aggregation prevents further adsorption of the fluoride molecules on pyrophyllite as mesopores get filled up and start offering resistance to diffusion [14]. This is the reason why rate of adsorption becomes slower at higher contact time.

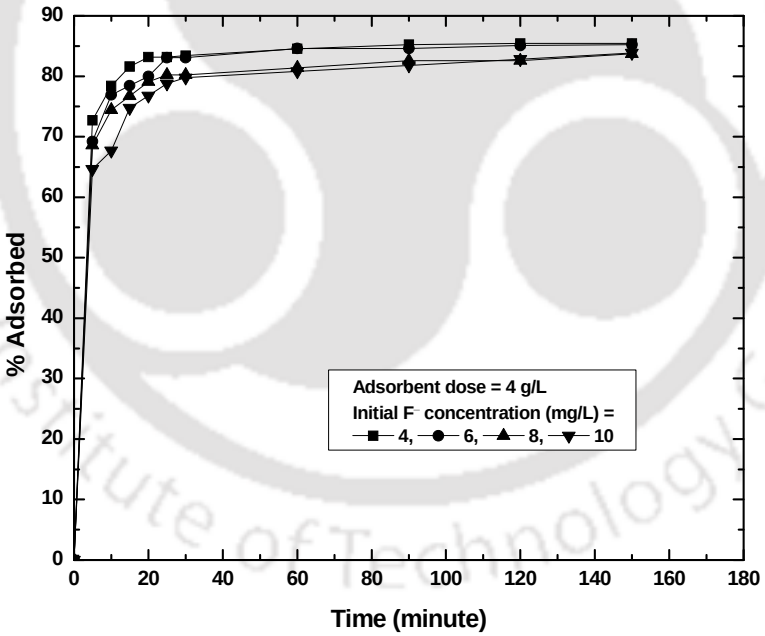

Figure 3.2a: Effect of contact time on fluoride adsorption by pyrophyllite

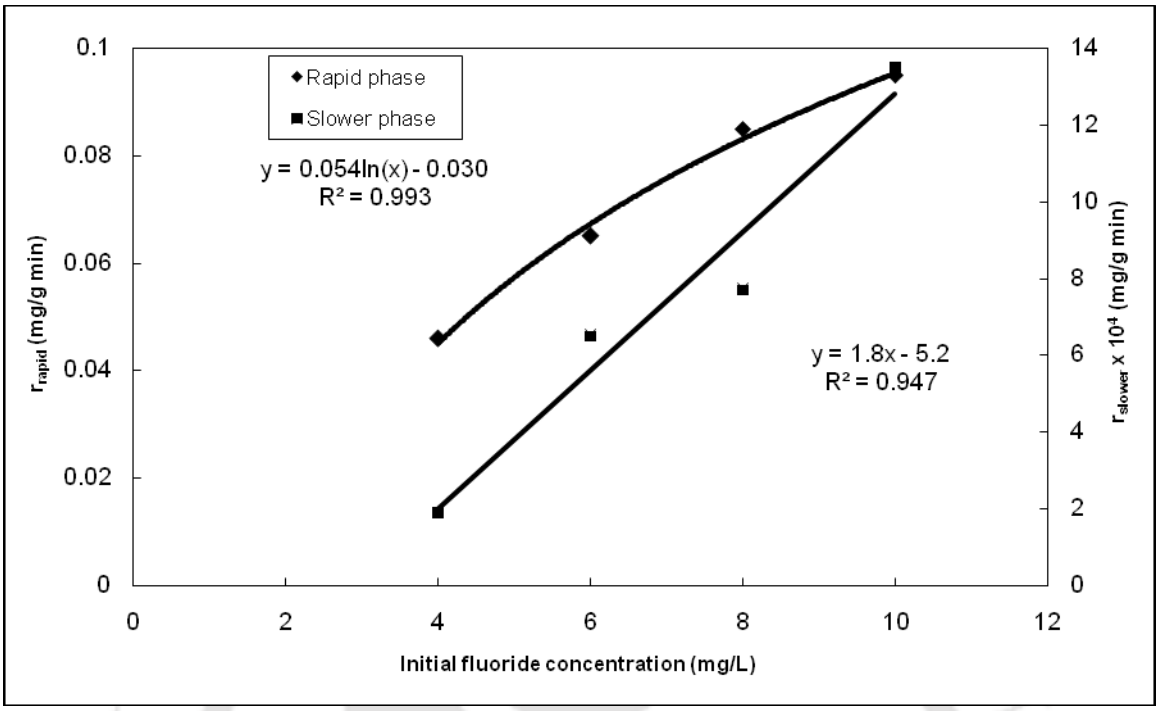

Figure 3.2b: Effect of initial fluoride concentration on the adsorption rate

Effect of adsorbent mass

The effect of adsorbent mass on the extent of fluoride adsorption for the initial concentration of 10 mg/L was studied and shown in Figure 3.3. The adsorbent dose was varied from 1 g/L to 6 g/L. The maximum fluoride removal of 84% was observed with the dosage of 4 g/L. This was due to the greater surface area or enhanced active sites. The percentage removal of fluoride decreased slightly (80%) with higher dose (> 4 g/L) of the adsorbent. It might happen that the higher adsorbent dose causes particles to aggregate, overlapping and overcrowding, resulting in a decrease of the availability of the surface area as well as the adsorption capacity.

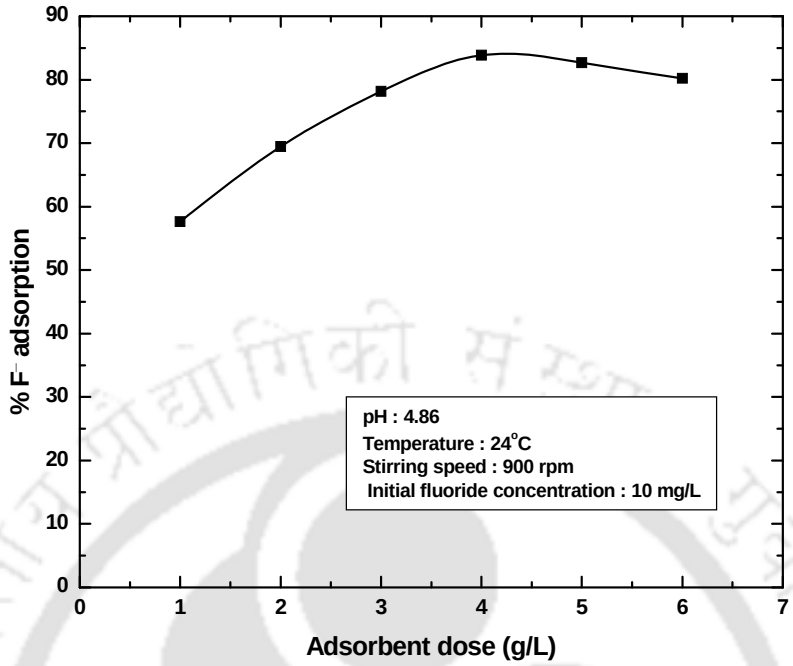

Figure 3.3: Variation of fluoride adsorption with adsorbent dose

Effect of pH

pH of the medium was one of the important parameters that significantly affect the extent of fluoride adsorption. The effect of pH on fluoride adsorption in pyrophyllite was shown in Figure 3.4. Fluoride removal by pyrophyllite was studied over a pH range of 2.8 – 11.2 for an initial fluoride concentration of 10 mg/L. From the figure, it was clear that maximum fluoride adsorption (84%) took place at pH 4.9, whereas 80% fluoride was adsorbed at pH upto 10. Again fluoride adsorption decreased (56%) at pH > 10. At acidic pH, only 36% fluoride was adsorbed. This was explained below.

ZPC of pyrophyllite was 5.12 (as discussed in Chapter 2, Figure 2.5), suggested that some weakly acidic groups were present on the surface of the adsorbent. In pyrophyllite, Al-OH bond plays the important role in fluoride adsorption. Fluorine ion

replaces hydroxyl ion and gets adsorbed. Acidic pH was maintained by adding 0.1 N HCl. At acidic pH, H^+ and Cl^- ions are present in solution. pH less than ZPC, the adsorbent was positively charged, hence F^- should be adsorbed by the adsorbent. But in actual case, when we add HCl to the F^- containing solution, the H^+ ion reacts with H_2O to form (hydronium ion) H_3O^+ which form hydrogen bond with F^- ion which is a stronger bond and present in solution. Between HCl and HF, tendency to exist Cl^- ion is greater than F^- ion in solution because HCl is a stronger acid than HF. That's why fluoride removing efficiency was decreasing in very low acidic pH (2.8-3.6).

Basic pH was maintained by adding 0.1 N NaOH. pH greater than ZPC, the adsorbent was negatively charged, hence, repulsion occurs between adsorbent and F^- ion. But in real case, pH more than ZPC, fluoride ion replaces hydroxyl ion of pyrophyllite and gets adsorbed, hence, increase the removing efficiency. But at very high basic pH (pH greater than 10), the equilibrium between Na^+ and F^- ion is effected due to extra addition of Na^+ ions and reverse reaction occurs (NaF forms) as NaF is a weak electrolyte. This is also explained from the ionization constant (pKa) value. Similar adsorption trend was also found by Sujana et al. (2009) [15], during fluoride adsorption using different geomaterials as adsorbent.

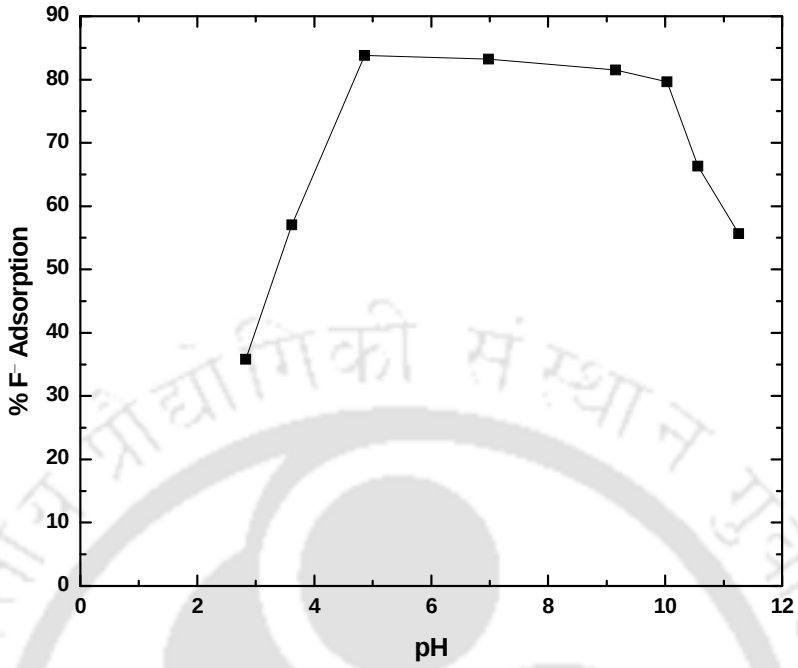

Figure 3.4: Effect of pH on the percentage adsorption of fluoride

Effect of temperature and thermodynamic study

Experiments were carried out using 10 mg/L fluoride solution at three different temperatures (24 ^{o}C, 40 ^{o}C and 60 ^{o}C) using 4 g of pyrophyllite per liter of solution and observed that with increase in temperature, adsorption capacity decreased from 84% to 72% and shown in Figure 3.5.

Thermodynamic parameters such as change in Gibb's free energy (ΔG^0), change in entropy (ΔS^0) and change in enthalpy (ΔH^0) were studied from the temperature effect on fluoride adsorption using equation 3.3 and 3.4b. The values of ΔH^0, ΔS^0 and ΔG^0 for 10 mg/L of fluoride solutions were shown in Table 3.2. The negative values of ΔH^0 and ΔG^0 indicated that the adsorption process was spontaneous and exothermic in

nature. The exothermic nature was also indicated by the decrease in the amount of adsorption with temperature (Figure 3.5). Negative change in entropy $\left(\Delta S^{o}\right)$ value indicated that the fluoride ions were organized on the adsorbent surface in less randomly fashion than in solution [16].

Table 3.2: Thermodynamic parameters of fluoride adsorption on pyrophyllite at different temperatures

Temperature (K)	$-\Delta H^{o}$ (kJ/mol)	$-\Delta S^{o}$ (J/K mol)	$-\Delta G^{o}$ (kJ/mol)
297			3.84
313	15.49	39.22	3.22
333			2.43

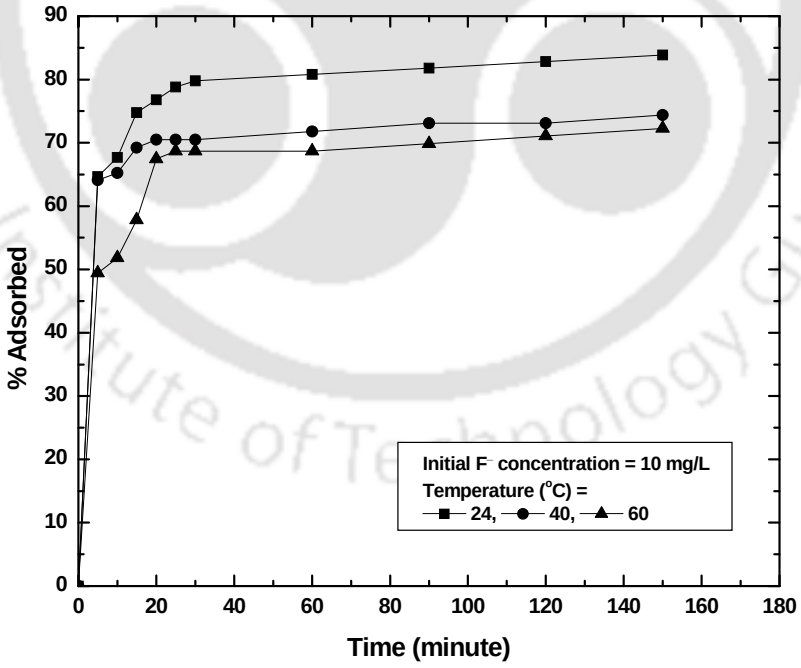

Figure 3.5: Effect of temperature on the extent of adsorption of fluoride

Mass transfer coefficient

The uptake of fluoride from the liquid phase to the solid phase is carried out by transfer of mass from former to the latter. The external mass transfer of adsorption of fluoride by pyrophyllite was analyzed using the external mass transfer model proposed by Furusawa and Smith [17]. The experimental data of fluoride adsorption were analyzed assuming a three step model:

(1) External mass transfer of fluoride ions from bulk solution to the pyrophyllite particle surface

(2) Intraparticle diffusion

(3) Adsorption at an interior site

In general, step (3) was rapid with respect to the first two steps [17]. For fully turbulent mixing (Reynolds number = 13.3×10^4), intraparticle diffusion was also very high. Hence, it may be assumed that step (1) was rate determining step. The change in concentration of fluoride with respect to time can be expressed by:

$$-\frac{dC}{dt} = k_S S\left(C_t - C_s\right) \qquad (3.27)$$

Where, k_S is the external mass transfer coefficient (m/s) between bulk liquid and outer surface of particles, S is the external surface area of pyrophyllite particle per unit volume of the particle free slurry (m^2/m^3) and C_s is the concentration of liquid at outer surface of pyrophyllite. In this case, S was experimentally determined by the BET surface area measurement.

As time $t \to 0$, $C_s \to 0$ and $C \to C_0$. Thus equation (3.27) became:

$$\left[\frac{d\left(C_t/C_o\right)}{dt}\right]_{t=0} = -k_S S \qquad (3.28)$$

The external mass transfer coefficient k_S was calculated from the slope of C_t/C_o versus time *t* using the experimental kinetic data for the first initial rapid phase process of 20 min where the external mass transfer was dominant. The calculated values of external mass transfer coefficient were shown in Table 3.3. It was observed from the table that the mass transfer coefficient of fluoride increased with increase in initial fluoride concentration.

Table 3.3: External mass transfer coefficient for the adsorption of fluoride at 24°C

Concentration (mg/L)	**$k_s \times 10^{13}$ (m/s)**
4	4.52
6	6.39
8	8.35
10	9.34

Effect of turbulence

Turbulence was an important parameter in adsorption phenomena influencing the distribution of the solute in the bulk solution and the formation of the external boundary film. Agitation speed of 500, 900 and 1500 rpm (Reynolds number, $N_{\mathrm{Re}} = 4.4\times10^4$, 8×10^4 and 13.3×10^4, respectively) were used within contact time of 120 minutes. With increasing Reynolds number from 4.4×10^4 to 13.3×10^4, the percentage removal of fluoride decreased from 85.8% to 72.2% as shown in Figure 3.6. During adsorption, the fluoride molecules were adsorbed on external surface of the pyrophyllite particle and then

the pores. The rate of surface adsorption mechanism was very fast in comparison with the intra particle diffusion. With increasing turbulence, the fluoride ion get detached from the surface of the adsorbent, thus decreasing its removal efficiency. Hence with increase in turbulence, removal efficiency of the adsorbent decreased.

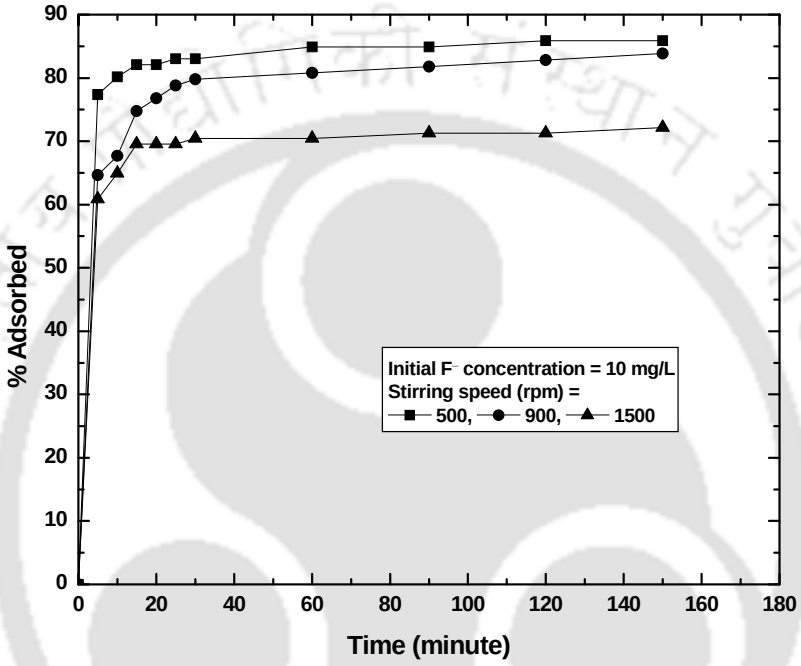

Figure 3.6: Effect of stirring on the percentage adsorption of fluoride

Other ions effect

Naturally fluoride contaminated water contains several other ions like sulphate, nitrate, chloride, bicarbonate and carbonate which can equally compete in the adsorption process. In order to investigate the effect of interfering such ions on fluoride adsorption, varying concentration ranging from 100-500 mg/L of each ion were added separately from its sodium and ammonium salts. Adsorption experiments were performed in 10 mg/L fluoride solution. Figure 3.7 showed the effect of various ions on fluoride uptake by

pyrophyllite. It was observed that presence of chloride and nitrate ions had negligible effect on fluoride removal by pyrophyllite as these anions were outer-spherically sorbing anions [18]. Presence of sulfate ion reduced the fluoride removal efficiency slightly as sulfate ion was partially inner-sphere complex forming species. The decrease in fluoride adsorption with the increase in carbonate and bicarbonate ions concentration considered in this study (0 – 500 mg/L) was presumably due to the significant increase in pH of the solution (4.9> pH <12). It was also confirmed from our experiments that the fluoride removal efficiency decreased in highly alkaline pH.

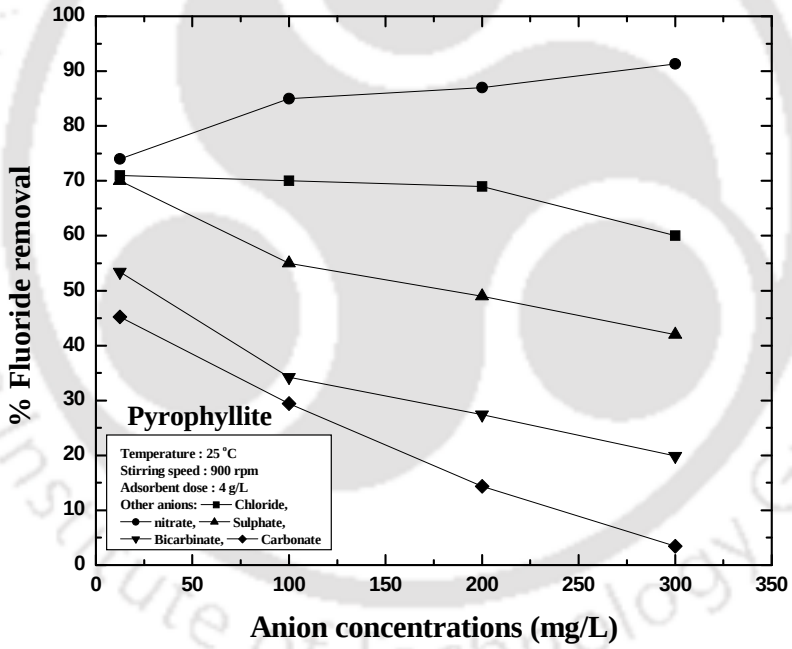

Figure 3.7: Effect of other ions on the extent of adsorption of fluoride

Kinetic study

Pseudo first order kinetic model

The adsorption rate constant k_1 and equilibrium adsorption capacity $q_{e,cal}$ of pseudo first order kinetic model was calculated from equation 3.8 and the obtained values were tabulated in Table 3.4. From the table, it may be concluded that the kinetics of fluoride adsorption on pyrophyllite was not probably following the pseudo first order kinetic model and hence not diffusion controlled phenomena.

Pseudo second order kinetic model

The constants of pseudo second order kinetic model and their corresponding regression coefficients (R^2) were calculated from equation 3.10 and tabulated in Table 3.4. The plot of pseudo second order model was shown in Figure 3.8. From the figure, it was observed that the values of regression coefficients are nearly unity (0.99) for all fluoride concentrations which confirmed that the sorption kinetics of fluoride followed pseudo second order process. It may also be found from Table 3.4 that the calculated q_e values were very close to that of experimentally obtained q_e. Thus it may be concluded that the adsorption of fluoride on pyrophyllite can be better explained by pseudo second order kinetic model than that of first order kinetic model.

Table 3.4: Different kinetic model parameters at 24°C

	Initial F^- concentration (mg/L)			
	4	**6**	**8**	**10**
Pseudo first order kinetics				
$q_{e,\ expt}$ (mg/g)	0.94	1.39	1.80	2.08
$q_{e,\ cal}$ (mg/g)	0.09	0.16	0.24	0.32
k_1 (min^{-1})	0.04	0.04	0.03	0.02
R^2	0.92	0.90	0.77	0.87
Pseudo second order kinetics				
$q_{e,\ cal}$ (mg/g)	0.95	1.39	1.80	2.09
k_2 (g/mg. min)	1.15	0.85	0.72	0.48
R^2	1.00	1.00	0.99	0.99
Intra particle diffusion (1st straight line)				
$k_{i,1}$ (mg/g $min^{1/2}$)	0.04	0.07	0.09	0.14
I_1 (mg/g)	0.72	0.98	1.29	1.29
R^2	0.92	0.93	0.97	0.96
Intra particle diffusion (2nd straight line)				
$k_{i,2}$ (mg/g $min^{1/2}$)	0.003	0.005	0.011	0.015
I_2 (mg/g)	0.90	1.33	1.67	1.89
R^2	0.90	0.85	0.96	0.98

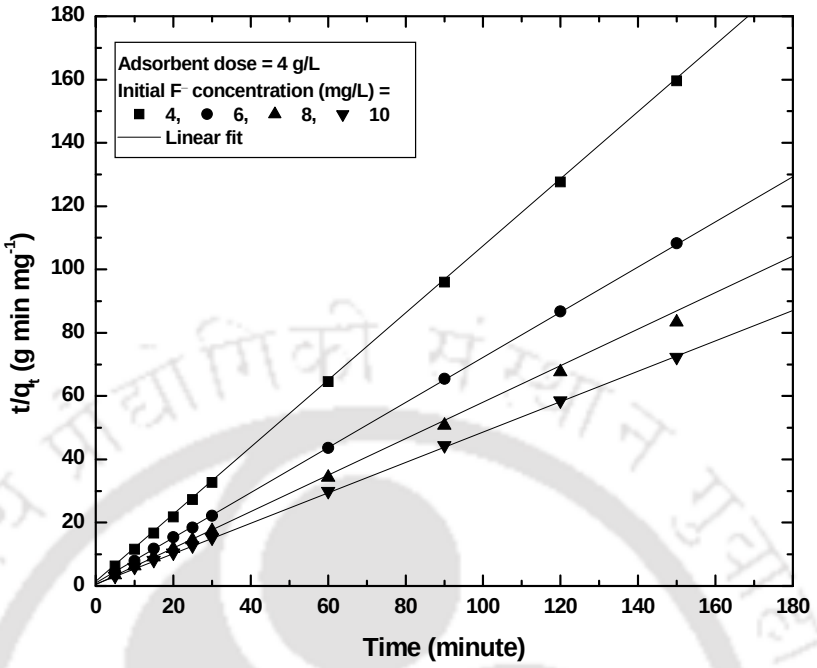

Figure 3.8: Pseudo second order kinetic model for the adsorption of fluoride

Intra particle diffusion model

The constants of intra particle diffusion model was calculated from the plot of intra particle diffusion model was shown in Figure 3.9. It was clear from the figure that there are two separate zones: first linear portion (phase I) and second linear part (phase II). In phase I approximately 80% of fluoride was rapidly uptaken by pyrophyllite within 25 min. This is attributed to the immediate utilization of the most readily available adsorbing sites on the adsorbent surface. Phase II may be attributed to very slow diffusion of the adsorbate from the surface site into the inner pores. Thus initial portion of fluoride adsorption by pyrophyllite may be governed by the initial intra particle transport of fluoride controlled by surface diffusion process and the later part controlled by pore

diffusion. The values of k_{i1} and k_{i2} obtained from the slope of linear plots were listed in Table 3.4. It is also observed from k_i values that k_{i1} (value of phase I) is higher than k_{i2} (value of phase II) indicating that initial step (phase I) is rapid followed by a slow step (phase II). The intercept of both the line did not pass through the origin at each concentration and the R^2 values of the concentrations were also less than 0.99. This concluded that mechanism of fluoride removal on pyrophyllite was complex and both, the surface adsorption as well as intra particle diffusion contribute to the rate determining step. Similar observations were found during the adsorption of crystal violet and brilliant green on the surface of kaolin [19] and fluoride adsorption by granular ferric hydroxide (GFH) [20].

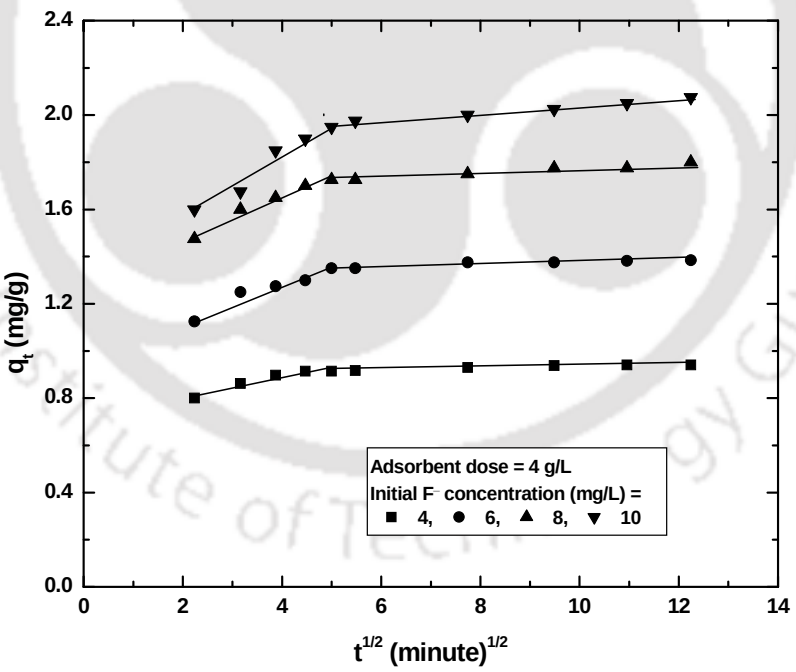

Figure 3.9: Intra particle diffusion model for adsorption of fluoride

Adsorption equilibrium

The Langmuir and Freundlich isotherm for fluoride adsorption system at 24oC was shown in Figure 3.10. The R_L values for the initial fluoride concentrations of 4 mg/L, 6 mg/L, 8 mg/L and 10 mg/L were calculated from equation 3.15 as 0.42, 0.32, 0.26 and 0.22 respectively. The R_L values indicated that the adsorption was more favorable for higher initial fluoride concentrations than the lower ones. This figure provided some information on the amount of pyrophyllite required to adsorb a particular mass of fluoride under the specified system conditions. From the figure, it was clear that the maximum adsorption capacity of pyrophyllite for fluoride adsorption is 2.2 mg/g. In order to evaluate the best fitted isotherm to the experimental equilibrium data, linear coefficients of determination and a non-linear χ^2 test, as described in the literature [21] were used. The χ^2 test statistic was basically the sum of the squares of the differences between the experimental data and data obtained from models, with each squared difference divided by the corresponding data obtained from models. The equivalent mathematical statement is:

$$\chi^2 = \sum \frac{(Q_e - Q_{e,m})^2}{Q_{e,m}} \qquad (3.29)$$

Where, $Q_{e,m}$ (mg/g) is the equilibrium capacity obtained by calculating from the model and Q_e (mg/g) is the experimental data of the equilibrium capacity. If data from the model are similar to the experimental data, χ^2 will be a small number; if they are different, χ^2 will be a large number. Therefore, it is necessary to analyze the data set using the χ^2 test to confirm the best-fitted isotherm for the sorption system.

The chi-square statistic, χ^2 and regression coefficient, R^2 were obtained and shown in Table 3.5. The Langmuir isotherm exhibited lower χ^2 values than the Freundlich. Therefore, Langmuir isotherm is the best fitted isotherm than Freundlich isotherm for the adsorption of fluoride in pyrophyllite.

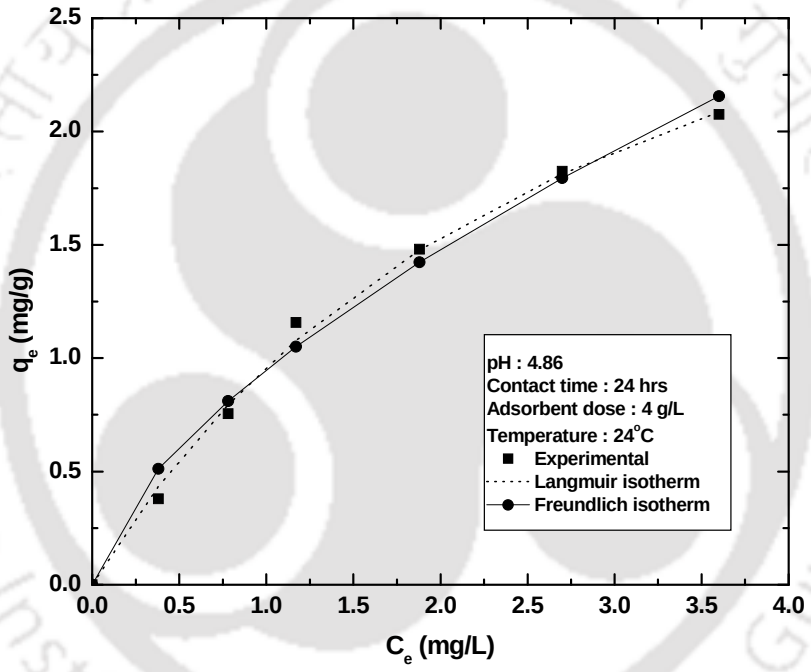

Figure 3.10: Langmuir and Freundlich adsorption isotherms for fluoride adsorption

Table 3.5: Langmuir and Freundlich isotherm constants for the adsorption of fluoride on pyrophyllite at 24°C

Langmuir isotherm constant				**Freundlich isotherm constant**			
Q_o (mg/g)	b (L/mg)	R^2	χ^2	K_F $[(mg/g)(L/mg)^{1/n}]$	n	R^2	χ^2
3.79	0.34	0.99	0.006	0.95	0.64	0.99	0.03

Regeneration study

The main objective of the present work is to develop an efficient adsorbent that can be reused thereby making it cost effective. For reusability, the adsorbed fluoride should be easily desorbed. 10 mg/L fluoride was adsorbed on 4 g/L adsorbent at pH 4.9. Then the solution was filtered and the adsorbent was transferred to 100 mL of water and the pH was adjusted. Desorption studies were conducted in 250 mL conical flask by conditioning the suspension at that pH for 90 min. In the acidic pH range hardly any fluoride was leached. But as the pH was increased above pH 4.9, the adsorbed fluoride starts to leach back into the solution. At around pH 11.9, more than 89% of the adsorbed fluoride was desorbed in about 90 minute. The adsorption performance of regenerated adsorbent showed that the adsorption efficiency was decreased from 83 to 65 percentages with 10 mg/L of initial fluoride concentration as some of the pores of pyrophyllite were already occupied by fluoride particles.

Process design calculation

Figure 3.11 showed the amount of pyrophyllite required for the desired percentage removal of fluoride for different solution volumes. From the figure it was observed that for initial fluoride concentrations of 1.9, 5.8 and 10 mg/L and 95 % removal of fluoride, the amount of pyrophyllite required was estimated to be 3.4 g to 34.9 g, 4.2 g to 42.8 g and 4 g to 40.1 g for solution volume of 1 L to 10 L respectively. The inset of the figure showed the volume of fluoride free water treated with 1 g adsorbent mass. It was clear from the figure that with low initial fluoride concentration, more volume of water was treated with unit mass of adsorbent. This study will give an idea to design an adsorber column.

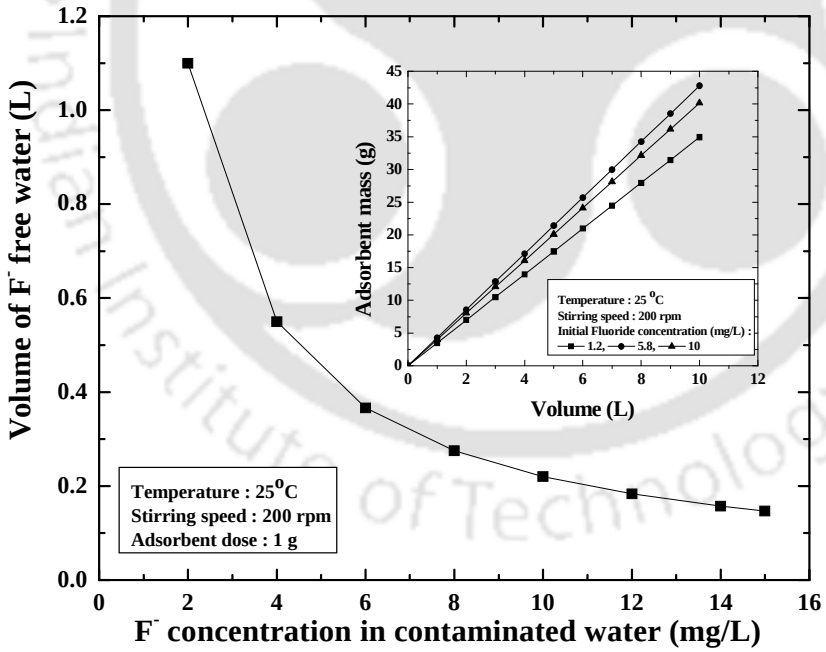

Figure 3.11: Volume of fluoride contaminated water treated with unit mass of pyrophyllite (Adsorbent mass (M) against volume of solution treated (L))

3.3 Fluoride removal by acidic alumina[†]

Acidic alumina was used as an adsorbent for fluoride removal. The adsorption process was studied with different process parameters such as temperature, stirring speed, pH, adsorbent dose and contact time and discussed detail in this section.

Variation of fluoride adsorption with contact time

Figure 3.12 showed the variation of fluoride adsorption with contact time during the adsorption process. It was observed from the figure that rapid adsorption of fluoride took place within 20 minutes of adsorption and then adsorption became slow and almost reached equilibrium within 90 min. Initially adsorbent active sites were vacant and fluoride was adsorbed into the active sites rapidly. As time proceeds, the numbers of active sites of the adsorbent were decreased and then adsorption became slow and equilibrium was reached slowly. With an increase in contact time up to 24 hrs, fluoride removal percentage was increased by less than 1%. Therefore, further experiments were conducted with a contact time of 90 minutes. More than 90% fluoride was adsorbed for all the cases. It was observed that for lower initial fluoride concentration, adsorption was fast. The percent removal of fluoride decreased with increase in initial fluoride concentration and took longer time to reach equilibrium. With increase in fluoride concentration, competition for the active adsorption sites increased and the adsorption process was increasingly slow down.

[†] *The work is published in following journals:*

A. Goswami, M. K. Purkait, The defluoridation of water by acidic Alumina, *Chem. Eng. Res. and Design* 90(2012) 2316-2324.

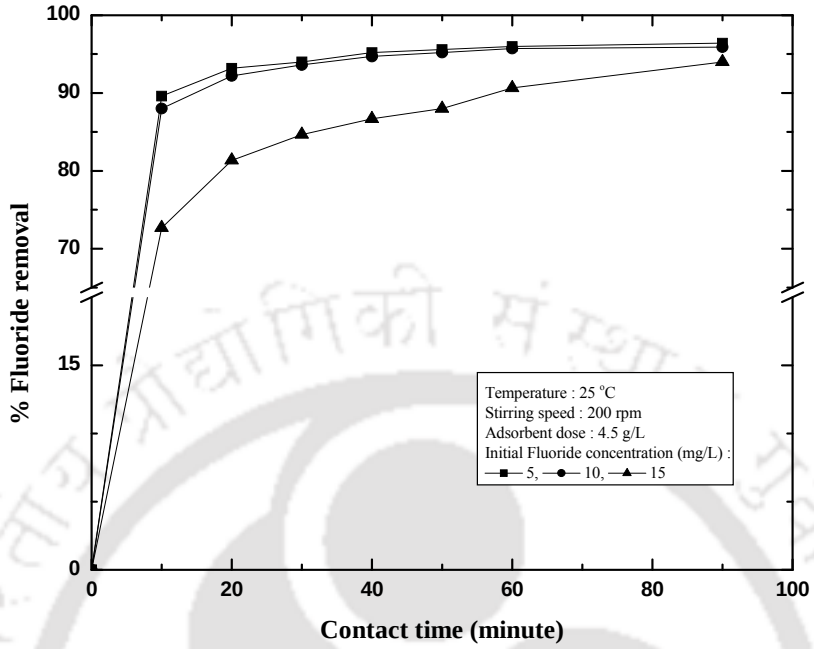

Figure 3.12: Effect of contact time on fluoride adsorption using acidic alumina

Variation of fluoride adsorption with adsorbent dose

Adsorbent dose is an important parameter for fluoride removal. With increase in alumina dose (varying from 1 g/L to 5 g/L), the residual fluoride concentration was decreased and permissible limit was achieved. The variation of residual fluoride concentration with different adsorbent dose was plotted in Figure 3.13. From the figure, it was observed that 4.5 g/L alumina was required to maintain the permissible limit of for 5 mg/L, 10 mg/L and 15 mg/L initial fluoride concentrations. Initially, the residual fluoride concentration was decreased sharply with increase in adsorbent dose (upto 1.5 g/L) and thereafter it was almost constant in case of 5 mg/L initial fluoride concentration. The sharp decrease in fluoride concentration was due to the greater surface area and

availability of more adsorption sites of adsorbent. With increase in time, the number of active sites on the adsorbent and the bulk fluoride concentration were decreased and reached in equilibrium. Therefore, the amount of residual fluoride concentration was stagnant with further increase in adsorbent dose.

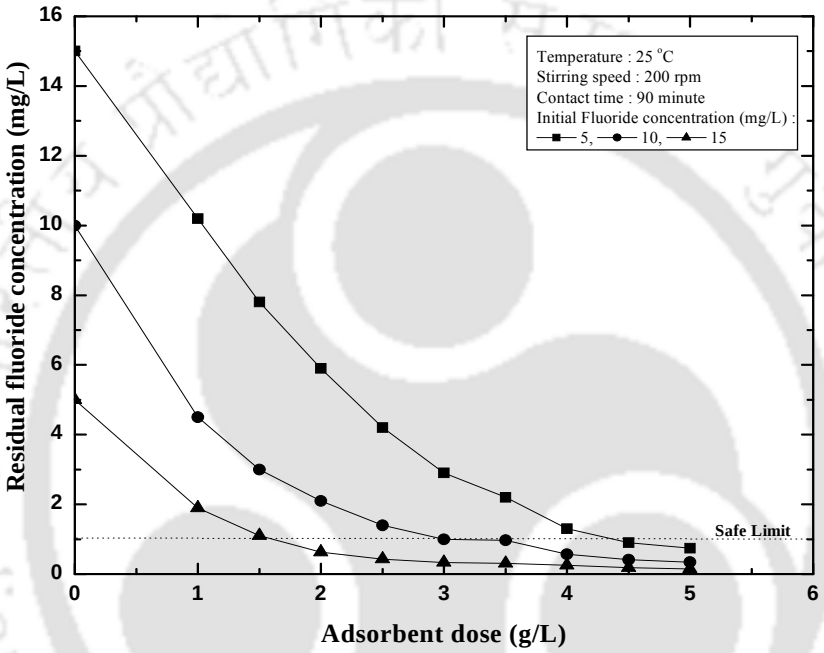

Figure 3.13: Variation of adsorbent dose on the removal of fluoride

Variation of fluoride adsorption with solution pH

pH is an important parameter influencing the sorption process at water–sorbent interfaces. To determine the optimum pH for maximum removal of fluoride, equilibrium sorption of fluoride with initial fluoride concentration of 15mg/L was investigated over a pH range of 2.24 - 10.73. The effect of pH on the extent of fluoride adsorption was shown in Figure 3.14. It was observed that the adsorption of fluoride on alumina was

strongly pH dependent. The percentage fluoride adsorption was increased with pH, reaching maximum at pH 4.4, and then decreased slowly upto the pH value of 9. Beyond pH 9, the percentage removal decreased sharply. Initially, as the pH increased from 2.24 to 4.4 ($pH < pH_{ZPC} = 5.1$), the fluoride adsorption increased due to the positive surface charge of alumina which attracts the negatively charged fluoride ion and became maximum at pH 4.4. Fluoride removal was decreased gradually below pH 4.4 due to the formation of weakly ionized hydrofluoric acid which reduces the columbic attraction between fluoride and the adsorbent surface. This was also due to the formation of positively charged alumina complexes (AlF^{2+} and AlF_2^+) [22] which were repelled from the positively charged alumina (alumina.H+). The sharp decrease in percentage fluoride adsorption beyond pH 9 was due to the stronger competition of hydroxide ions to the active sites of alumina and also the electrostatic repulsion of anionic fluoride by the negatively charged alumina surface as $pH > pH_{ZPC}$. The almost flat portion of the curve i.e., at pH 5 - 9, was due to the replacement of hydroxyl ion by fluoride ion as the hydroxyl ion concentration was less in that pH range. Beyond pH 9, the hydroxyl ion concentration was more which affects the fluoride removal capacity of the adsorbent.

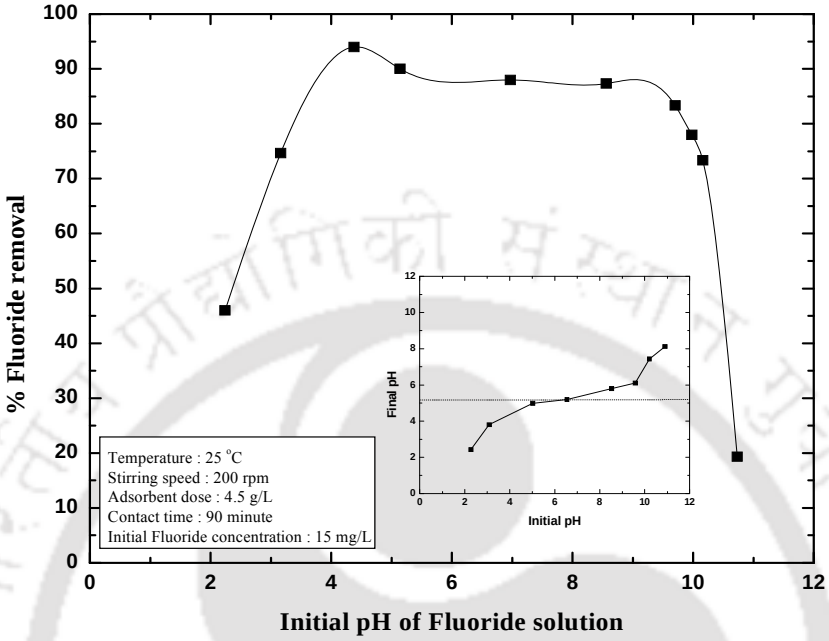

Figure 3.14: Effect of pH on the percentage adsorption of fluoride using acidic alumina

Variation of stirring speed on fluoride adsorption

Stirring is an important parameter in adsorption phenomena, influencing the distribution of the solute in the bulk solution and the formation of external boundary layer. Three different stirring speeds (100, 200 and 300 rpm) were used to observe the fluoride adsorption phenomenon. With increase in stirring speed from 100 - 300 rpm, amount of fluoride removal was changed as 92, 94 and 92 percentage, respectively. That means only a negligible change was noticed with increase in turbulence. The effect of stirring speed on fluoride adsorption was shown in Figure 3.15. The slight increase in

percentage removal of fluoride at 200 rpm was explained by the fact that increasing agitation speed reduced the film boundary layer surrounding the adsorbent, thus increasing the external film transfer coefficient, and hence increasing the percentage of fluoride adsorption. High stirring speed increases the turbulence, fluoride ions get detached from the surface of the adsorbent, thus decreasing its removal efficiency. Hence with increase in turbulence, the removal efficiency of the adsorbent marginally decreased (~ 2 %).

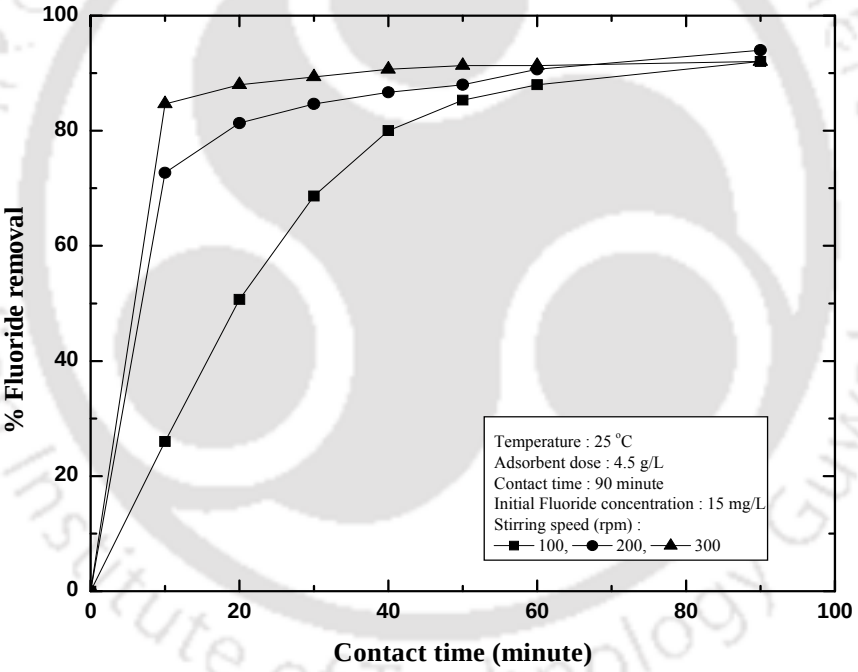

Figure 3.15: Effect of stirring speed on fluoride adsorption

Variation of fluoride adsorption with co-ions

The fluoride-contaminated drinking water is always associated with other co-ions like carbonate, chloride, sulphate, nitrate and bicarbonate, which can compete with fluoride ions during adsorption process for active sites on alumina. Thus, the effects of these competitive ions on the uptake of fluoride should be studied. Adsorption experiments were performed by adding 100 - 500 mg/L of carbonate, chloride, sulphate, nitrate and bicarbonate ions separately in 15 mg/L fluoride solution. Figure 3.16 showed the effect of various ions on fluoride uptake by alumina. The order of anions reducing the fluoride removal efficiency was observed as $HCO_3^- > CO_3^{2-} > SO_4^{2-} > NO_3^- > Cl^-$. It was observed that presence of chloride and nitrate ions had negligible effect on fluoride removal by alumina as these anions were outer-spherically sorbing anions [18]. Presence of sulfate ion reduced the fluoride removal efficiency slightly as sulfate ion was partially inner-sphere complex forming species and that is why it had a tendency to compete fluoride ion for forming the complexes with aluminum [23]. The decrease in fluoride adsorption with the increase in carbonate and bicarbonate ions concentration considered in this study (0 – 500 mg/L) was presumably due to the significant increase in pH of the solution (4.4>pH<12). It was also confirmed from our experiments on the effect of pH that the fluoride removal efficiency decreased in highly alkaline pH.

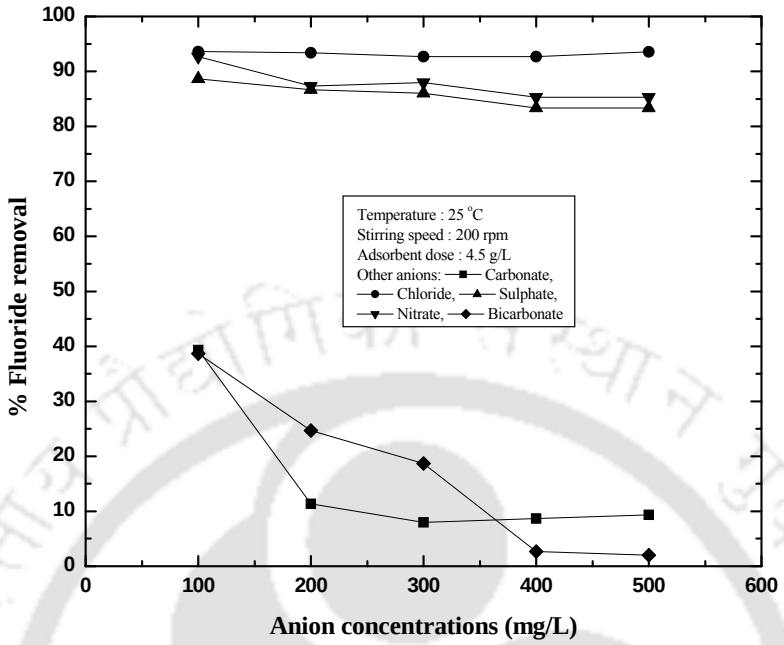

Figure 3.16: Effect of other anions on fluoride adsorption

Variation of fluoride adsorption with temperature and thermodynamic study

With increase in temperature from 25 °C to 55 °C, the percentage of fluoride adsorption was increased from 94% to 95.3% in case of 15 mg/L initial fluoride solution, indicating the endothermic behavior of adsorption (Figure 3.17).

Thermodynamic parameters such as free energy change, enthalpy change and entropy change were calculated and summarized in Table 3.6 for 15 mg/L initial fluoride concentration solution. Positive ΔH^0 value concluded the endothermic behavior of adsorption and negative ΔG^0 value indicated spontaneous nature of the adsorption process. The low value of ΔS^0 implied that no remarkable change in entropy occurred during the adsorption process. In addition, the positive value of ΔS^0 reflects the increased

randomness at the solid–solution interface during adsorption, and it also indicates the occurrence of ion replacement reactions. The low value of ΔH^0 indicated that the adsorption process was a physical adsorption process as heats of chemisorption generally falls into a range of 80 – 200 kJ/mol.

The activation energy (E_a) and sticking probability (S^*) were estimated from a plot of $\ln(1-\theta)$ vs $1/T$ using equations 3.5 and 3.6. The E_a for adsorption of fluoride onto alumina was calculated from the slope of the plot and found to be 95.13 kJ/mol.

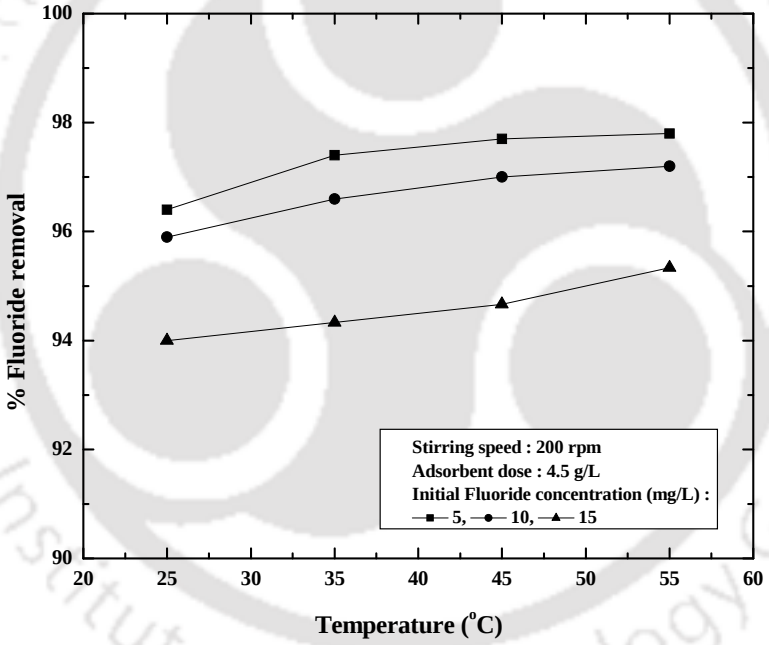

Figure 3.17: Effect of temperature on fluoride adsorption

Table 3.6: Thermodynamic parameters for fluoride adsorption using acidic alumina

Temperature (K)	**ΔH^o (kJ/mol)**	**ΔS^o (kJ/mol. K)**	**Ea (kJ/ mol)**	**S***	**$-\Delta G^o$ (kJ/mol)**
298					6.77
308	6.95	0.05	95.13	4.3×10^{-3}	7.23
318					7.69
328					8.15

Kinetics study on fluoride adsorption

The kinetics of fluoride adsorption onto alumina was evaluated using different models such as pseudo-first-order [4], pseudo-second-order [5] and intraparticle diffusion [6] models. The various parameters were calculated from the plots of the kinetic model equations and summarized in Table 3.7. Figure 3.18 showed the plots of different kinetic models. Among these models the criterion for their applicability is based on judgment on the respective correlation coefficient (R^2) and agreement between experimental and calculated value of q_e. The high values of R^2 (~1) and good agreement between two q_e values indicate that the understudy adsorption system follows pseudo-second-order kinetic model (Table 3.7 and Figure 3.18a). Another alternative method for kinetic evaluation of an adsorption process is intra-particle-diffusion model. According to conditions and equation presented in Table 3.7, it is seen that respective plot (plot of q_t versus $t^{1/2}$) gives only one line and the rate constant k_i was evaluated from the slope of the line (Figure 3.18b). Since the line did not pass through the origin, it indicates that the intraparticle diffusion was not the rate-controlling step.

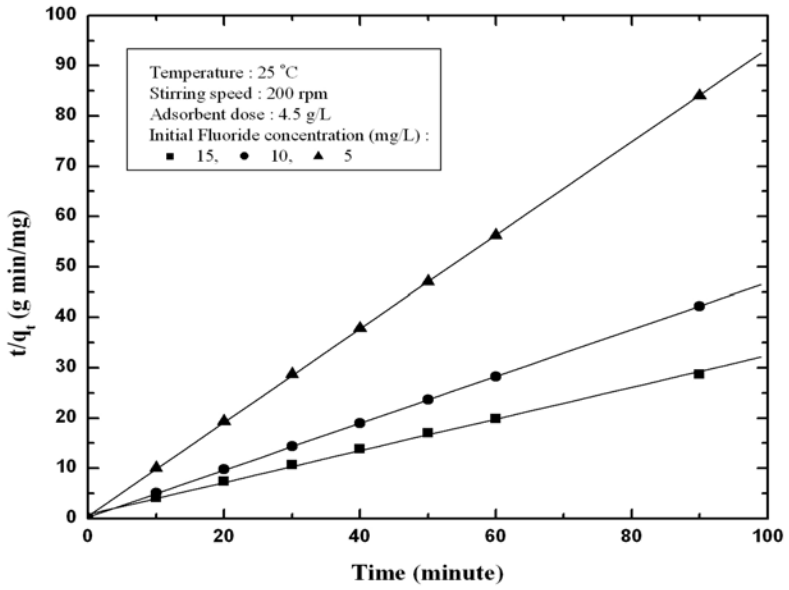

(a)

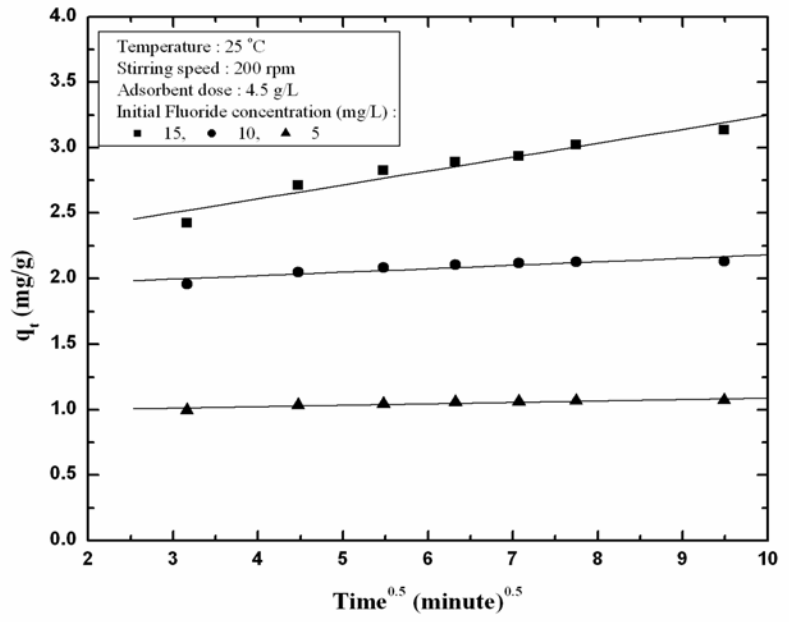

(b)

Figure 3.18: Kinetics of acidic alumina adsorbed fluoride (a) Pseudo second order (b) Intra particle diffusion

Table 3.7: Different kinetic model parameters at 25 oC for fluoride adsorption

Model	Equation	Plot	Parameters	Value		
				Initial F^- concentration (mg/L)		
				5	10	15
Pseudo first order	$\ln(q_e - q_t) = \ln q_e - k_1 t$	Plot the values of ln (q_e- q_t) versus t which gave a straight line with slope of (-k_1) and intercept ln (q_e) respectively.	$q_{e,\ expt}$ (mg/g) $q_{e,\ cal}$ (mg/g) k_1 (min^{-1}) R^2	1.07 0.12 0.05 0.98	2.13 0.37 0.07 0.98	3.13 0.92 0.03 0.97
Pseudo second order	$\frac{t}{q_t} = \frac{1}{k_2 q_e^{\ 2}} + \frac{t}{q_e}$	Plot the values of (t/q_t) versus t should give a straight line with slope of ($1/q_e$) and intercept ($1/k_2 q_e^2$).	$q_{e,\ cal}$ (mg/g) k_2 (g/μg. min) R^2	1.08 1.57 0.99	2.15 0.71 0.99	3.16 0.12 0.99
Intra particle diffusion	$q_t = k_i t^{0.5} + I$	Plot the values of (q_t) versus $t^{0.5}$ should give a straight line with slope (k_i) and intercept I.	k_i (mg/g $min^{1/2}$) I (mg/g) R^2	0.01 0.98 0.83	0.03 1.92 0.81	0.11 2.18 0.94

Adsorption equilibrium study on fluoride adsorption

Adsorption isotherms are essential to understand the nature of the interaction between adsorbate and the applied adsorbent. Two important isotherms viz Langmuir [7] and Freundlich [9] isotherms were investigated in this study (Figure 3.19). In the Langmuir model, Q_o is the maximum adsorption capacity (mg/g) and b is the Langmuir adsorption constant (L/mg). In the Freundlich model, K_F is the Freundlich constant [(mg/g) $(L/g)^{1/n}$] related to the bonding energy, and n is the heterogeneity factor. The value of n varies with the heterogeneity of the adsorbent and for favorable adsorption process; the value of n_F should be less than unity. All the isotherm constants and their correlation coefficients were reported in Table 3.8. The adsorption of fluoride on alumina followed Langmuir isotherm with high correlation coefficients (R^2 ~ 0.99). Hence, it can be concluded that Langmuir isotherm is the best isotherm to predict the adsorption of fluoride over alumina.

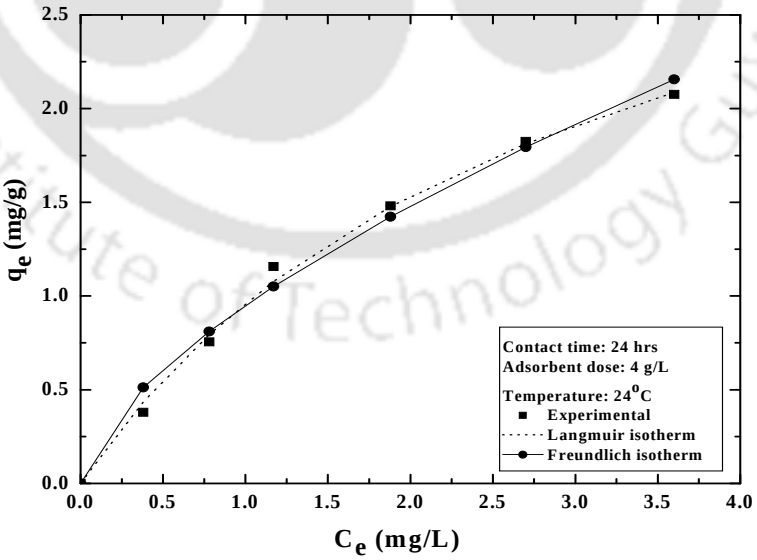

Figure 3.19: Various adsorption isotherms for fluoride adsorption on acidic alumina

Table 3.8: Langmuir and Freundlich isotherm constants for fluoride adsorption on acidic alumina

Isotherm	Equation	Plot	Parameters	Value
Langmuir	$q_e = \frac{Q_0 b C_e}{1 + b C_e}$	Plot the values of q_e versus C_e and find the constants with the help of curve expert software.	Q_o(mg/g) b (L/mg) R^2	8.4 1.08 0.99
Freundlich	$q_e = K_F C_e^{n_F}$	Plot the values of q_e versus C_e and find the constants with the help of curve expert software.	K_F[mg.g(L/mg)$^{1/n}$] n_F R^2	4.17 0.31 0.92

Regeneration of acidic alumina

Regeneration of acidic alumina makes the adsorption process cost effective. For reusability, 15 mg/L fluoride was adsorbed on 4.5 g/L adsorbent at pH 4.4. Then the solution was filtered and the adsorbent was transferred to 100 mL of water and the pH was adjusted. Desorption studies were conducted in 250 mL conical flask by conditioning the suspension at that pH for 90 min. In the acidic pH range hardly any fluoride was leached. But as the pH was increased above pH 4.4, the adsorbed fluoride starts to leach back into the solution. At around pH 11, more than 85% of the adsorbed fluoride was desorbed in about 90 min. After that the desorbed adsorbent was washed with 0.1 M *HCl* for activation. The mechanism of regeneration was described in introduction section. Initial tests with regenerated adsorbent showed that the adsorption efficiency was

decreased from 94 to 85 percentage with 15 mg/L of initial fluoride concentration as some of the pores of alumina was already occupied by fluoride particles. It is well known that better extent of adsorption and desorption was achieved in continuous mode of adsorption using a column. Therefore, it is recommended that column study for the removal of fluoride using present adsorbent will improve the performance of both adsorption and desorption.

Process design calculation

Equation 3.26 can be used to calculate the amount of adsorbent required for the required percentage removal of fluoride from aqueous solution for any initial solution concentration. Figure 3.20 showed the amount of alumina required for the desired percentage removal of fluoride for different solution volumes. From figure 3.20, for initial fluoride concentrations of 6, 10 and 14 mg/L and for 95 percentage removal of fluoride, the amount of alumina required was estimated to be 1.14 g to 11.4 g, 1.04 g to 10.4 g and 0.99 g to 9.91 g for solution volume of 1 L to 10 L respectively. The inset of figure 3.20 showed the volume of fluoride free water treated with 1 g adsorbent mass. It was clear from the figure that with low initial fluoride concentration, more volume of water was treated with unit mass of adsorbent. This study will give an idea to design an adsorber column.

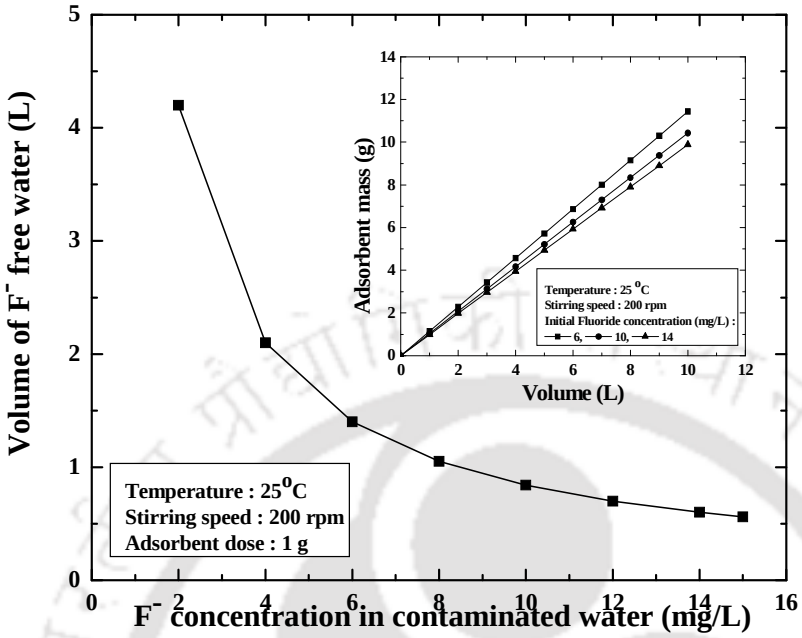

Figure 3.20: Volume of treated water using unit mass of acidic alumina

Section 3.4 Fluoride removal by Schwertmannite

In this section, fluoride contaminated water was treated with Schwertmannite (Sh) which was an iron-oxyhydroxy sulfate mineral synthesized in the laboratory. The detailed adsorption parameters were studied and reported well in this section.

Extent of fluoride adsorption with contact time

The variation of percentage fluoride adsorption with contact time was plotted in Figure 3.21. Rapid percentage fluoride adsorption took place within 30 minutes and then the adsorption became slow and reached equilibrium within 90 minute. Initially adsorbent active sites were vacant and fluoride was adsorbed into the active sites rapidly. As time proceeds, the numbers of active sites of the adsorbent were decreased and then adsorption became slow and equilibrium was reached. With an increase in contact time up to 24 hrs, fluoride removal percentage was not increase by 1%. Therefore, further experiments were conducted with contact time of 120 minutes. More than 85% fluoride was adsorbed for all the cases.

Extent of fluoride adsorption with adsorbent doses

The variation of residual fluoride concentration with varying adsorbent doses was plotted in Figure 3.22. From the figure, it was found that with increase in Sh dose from 1 g/L to 4 g/L, the residual fluoride concentration was decreased gradually. From the figure, it was observed that 3 g/L Sh was required to maintain the BIS permissible limit for 5 mg/L initial fluoride concentration.

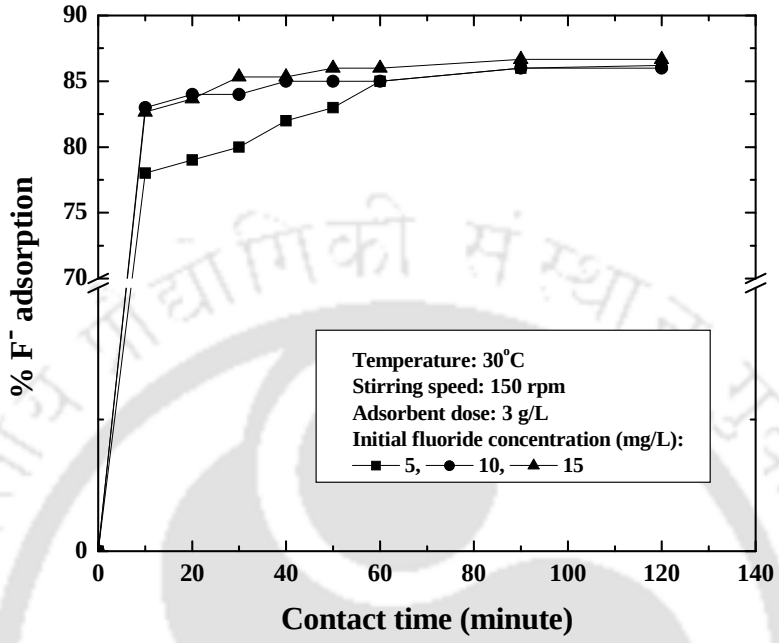

Figure 3.21: Effect of contact time on fluoride adsorption by Sh

Initially, the residual fluoride concentration was decreased sharply with increase in adsorbent dose (upto 3 g/L) and thereafter it was almost constant. The sharp decrease in fluoride concentration was due to the greater surface area and availability of more adsorption sites of adsorbent. With increase in time, the number of active sites on the adsorbent and the bulk fluoride concentration were decreased and reached in equilibrium.

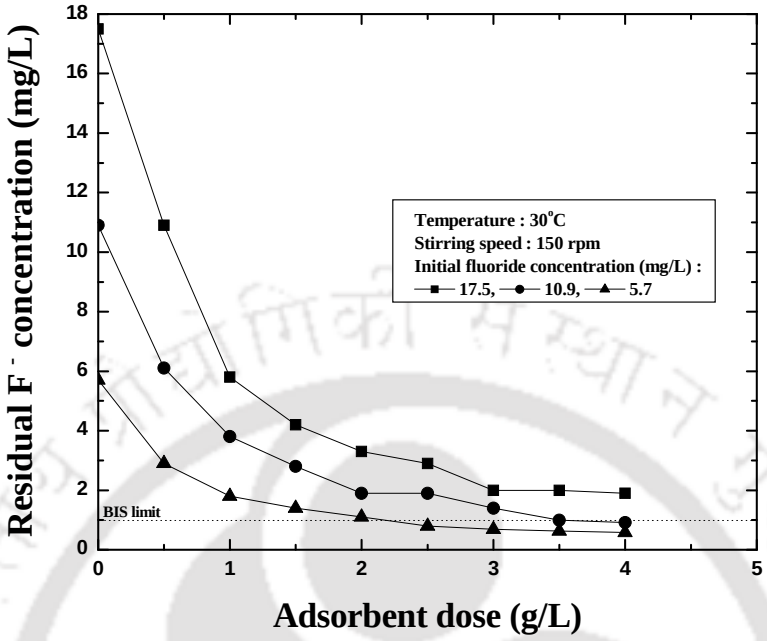

Figure 3.22: Variation of adsorbent dose on residual fluoride concentration

Extent of fluoride adsorption with pH

The percentage removal of fluoride with pH was shown in Figure 3.23. To determine the optimum pH for maximum removal of fluoride, equilibrium sorption of fluoride with initial fluoride concentration of 5 mg/L was investigated over a pH range of 2.7 - 11.4. From the figure, it was observed that maximum adsorption take place at pH 3.6. Above pH 3.6, an increase in pH causes decrease in percentage removal of fluoride concentration. To understand the fluoride adsorption behavior under different pH values, the following reactions are considered [24]

$$HF \leftrightarrow H^+ + F^- \qquad (3.30)$$

$$\equiv SOH + H^+ \leftrightarrow SOH_2^+ \qquad (3.31)$$

$$\equiv SOH + OH^- \leftrightarrow \equiv SO^- + H_2O \quad (3.32)$$

$$\equiv SOH_2^+ + F^- \leftrightarrow \equiv SF + H_2O \quad (3.33)$$

$$\equiv SOH + F^- \leftrightarrow \equiv SF + OH^- \quad (3.34)$$

where $\equiv SOH$, $\equiv SOH_2^+$ and $\equiv SO^-$ are the neutral, protonated and deprotonated sites on Sh and $\equiv SF$ is the active site-fluoride complex. Equation (3.30) expresses the ionization of HF in solution at low pH. Because HF is weakly ionized (p*K*a = 3.2) in solution at low pH values, the corresponding uptake of fluoride is reduced when pH≤3.6, since a fraction of fluoride becomes unavailable for adsorption. When the adsorption system (fluoride solution/Sh) is operated at pH > 3.6 the reaction sites become deprotonated according to equation (3.32) leading to a reduction in fluoride adsorption due to increased repulsive forces between the negatively charged fluoride ions and the deprotonated sites. According to Equation (3.34), fluoride adsorption on active sites is expected to cause an increase in solution pH. This was not observed in our case since Sh adsorbent had a strong tendency to lower the pH of solution. If hydroxyl ions were released, they may have competed fluoride for the adsorption sites.

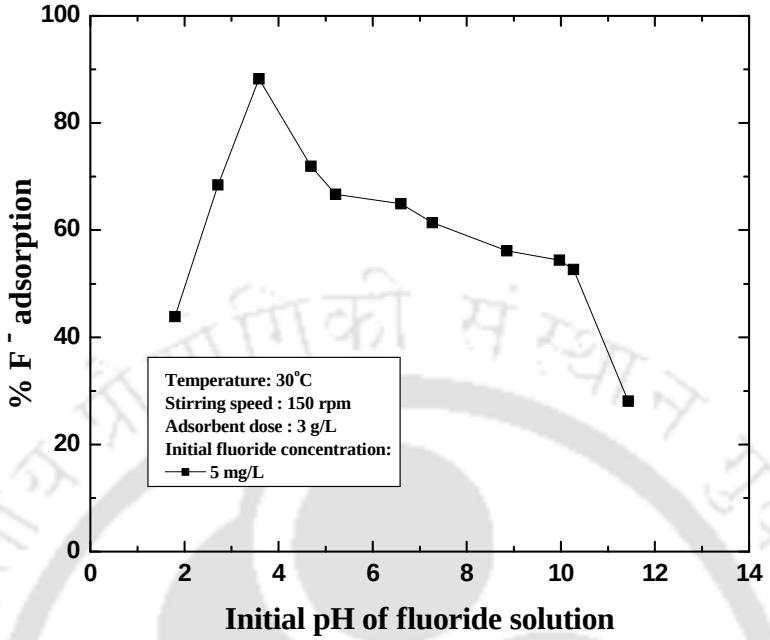

Figure 3.23: Effect of pH on the percentage adsorption of fluoride using Sh

Extent of fluoride adsorption with varying stirring speed

The change in fluoride removal efficiency with different stirring speeds (100, 150 and 200 rpm) were studied to observe the fluoride adsorption phenomenon. With increase in stirring speed from 100 - 200 rpm, amount of fluoride removal percentage was changed as 84, 86 and 82 respectively which indicated that only a negligible change was noticed with increase in turbulence. The slight increase in percentage removal of fluoride at 150 rpm was explained by the fact that increasing agitation speed reduced the film boundary layer surrounding the adsorbent, thus increasing the external film transfer coefficient, and hence increasing the percentage of fluoride adsorption. Stirring speed more than 150 rpm, the % removal of fluoride was decreased. At high stirring speed

turbulence increases and fluoride ions get detached from the surface of the adsorbent, thus decreasing its removal efficiency. That is why with increase in stirring speed upto 200 rpm, the fluoride removal efficiency of the adsorbent marginally decreased (~ 2 %).

Extent of fluoride adsorption in presence of other ions

Presence of other ions such as chloride, phosphate and bicarbonate in water along with fluoride ion will affect the fluoride removal efficiency by Sh. Figure 3.24 showed the effect of such ions on fluoride uptake by Sh. It was observed that presence of chloride ion had negligible effect on fluoride removal by Sh as this anion was outer-spherically sorbing anions. Presence of phosphate ion reduced the fluoride removal efficiency slightly as phosphate ions were partially inner-sphere complex forming species and that is why it had a tendency to compete fluoride ion for forming the complexes with the adsorbent. The decrease in fluoride adsorption in presence of bicarbonate ions was presumably due to the significant increase in pH of the solution (pH<11). It was also confirmed from the effect of pH that the fluoride removal efficiency decreased in highly alkaline pH (> 10).

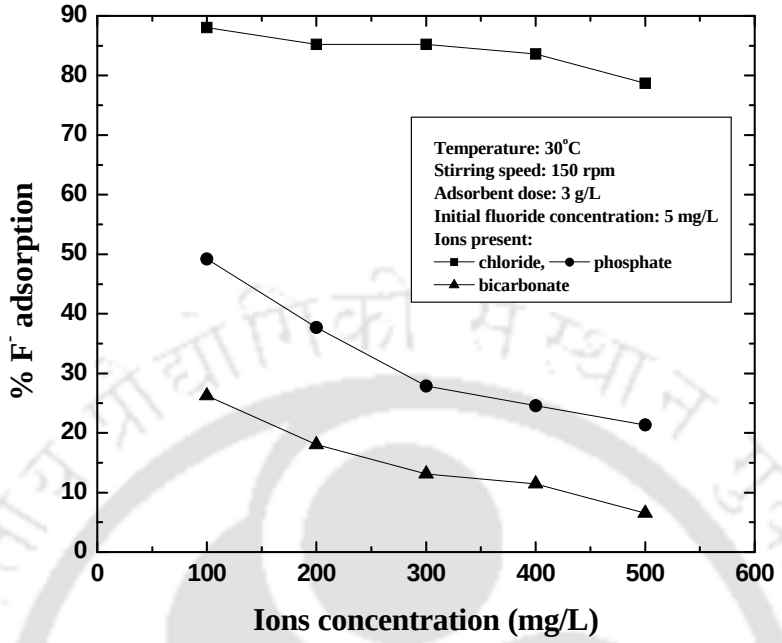

Figure 3.24: Fluoride removal in presence of various co-ions

Extent of fluoride adsorption with temperature and thermodynamic study

Table 3.9 summarized the thermodynamic parameters of 5 mg/L initial fluoride concentration solution. From the table, it was observed that negative ΔH^0 value concluded the exothermic behavior of adsorption and negative ΔG^0 value indicated spontaneous nature of the adsorption process. The low value of ΔS^0 implied that no remarkable change in entropy occurred during the adsorption process. In addition, the negative ΔS^0 value indicated that the fluoride ions were organized at the solid–solution interface during adsorption. The exothermic behavior of adsorption was also confirmed by the decrease of fluoride adsorption efficiency with temperature and shown in Figure 3.25.

Table 3.9: Thermodynamic parameters for fluoride adsorption on Sh

Temperature (K)	**$-\Delta H^o$ (kJ/mol)**	**$-\Delta S^o$ (kJ/mol. K)**	**$-\Delta G^o$ (kJ/mol)**
303	77.62	0.24	4.81
313			2.41
323			0.007

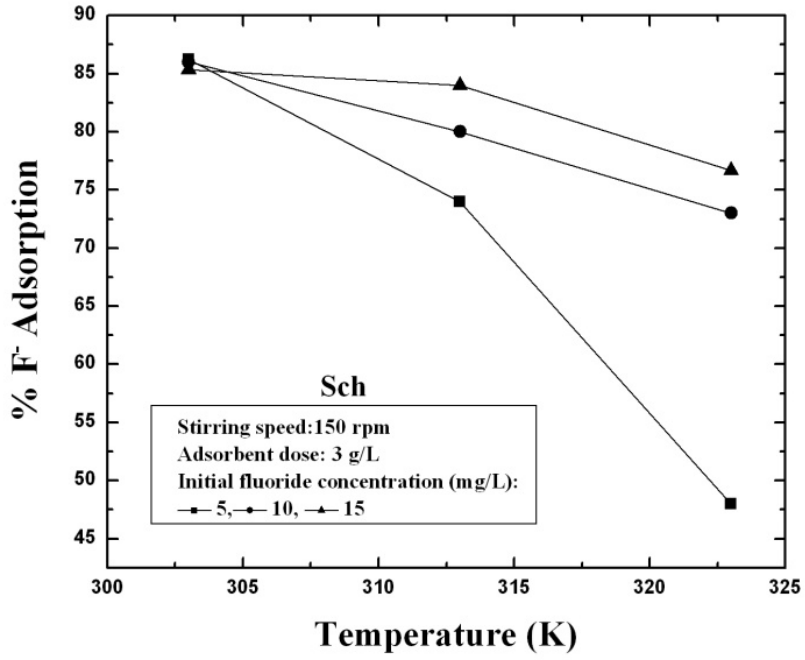

Figure 3.25: Effect of temperature on fluoride removal efficiency

Kinetics study of fluoride adsorption by Sh

The kinetics study of fluoride adsorption by Sh was studied with pseudo first order, pseudo second order and intra particle diffusion models of adsorption and plotted in Figure 3.26. The kinetics constant values of pseudo first order, pseudo second order and intra particle diffusion models were tabulated in Table 3.10. From the table, it was observed that the experimental and calculated values of q_e for pseudo first order kinetics was not similar which concluded that the kinetics of fluoride adsorption on Sh was not followed by the pseudo first order kinetic model and hence not diffusion controlled phenomena.

Table 3.10: Kinetic model parameters for fluoride adsorption on Sh

Model	**Parameters**	**Initial F^- concentration (mg/L)**		
		5	**10**	**15**
Pseudo first order	$q_{e,\ expt}$ (mg/g)	1.44	2.87	4.33
	$q_{e,\ cal}$ (mg/g)	0.38	0.12	0.32
	k_1 (min^{-1})	0.05	0.02	0.04
	R^2	0.90	0.86	0.89
Pseudo second order	$q_{e,\ cal}$ (mg/g)	1.45	2.88	4.35
	k_2 (g/mg. min)	0.41	0.71	0.43
	R^2	0.99	1	1
Intra particle diffusion	k_i (mg/g $min^{1/2}$)	0.02	0.01	0.02
	I (mg/g)	4.11	2.75	1.26
	R^2	0.70	0.84	0.84

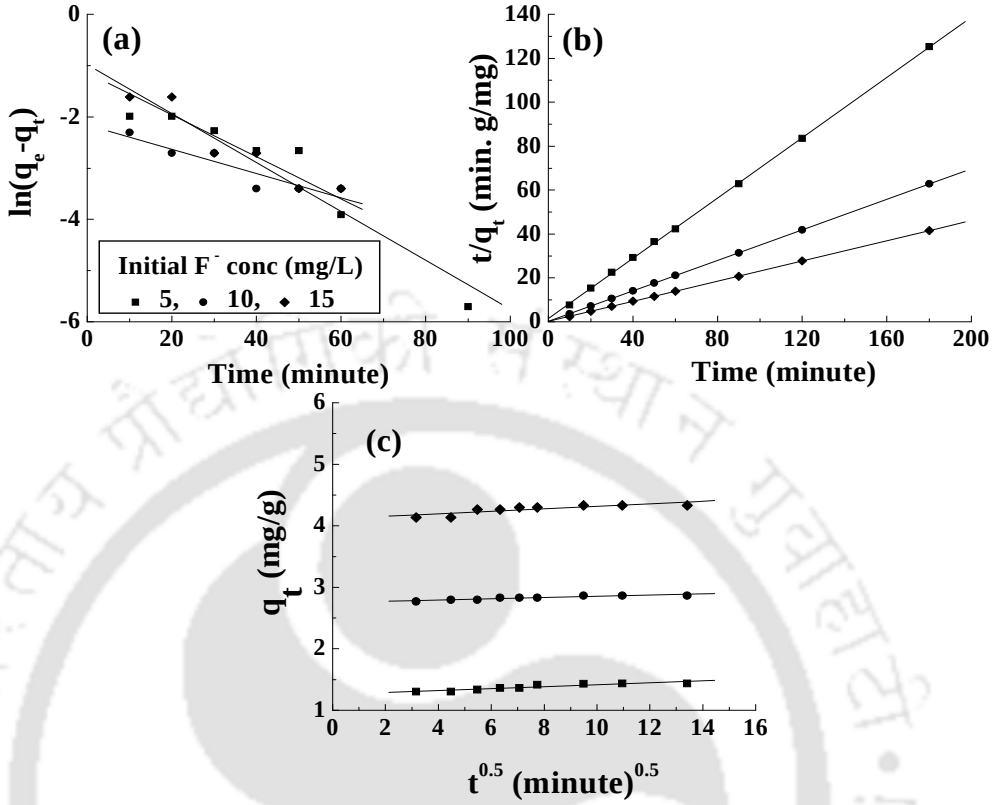

Figure 3.26: Kinetics of Sh adsorbed fluoride (a) Pseudo first order (b) Pseudo second order (c) Intra particle diffusion

It was also observed that the value of regression coefficient is unity for all the cases of adsorption which confirmed that the sorption kinetics of fluoride adsorption followed pseudo second order kinatics which was also found from table that the calculated q_e values were very close to that of experimentally obtained q_e. Thus it was concluded that the adsorption of fluoride on Sh could be better explained by pseudo second order kinetic model than that of first order kinetic model. To verify the rate limiting step of adsorption, intra particle diffusion model was studied. According to this model, if

adsorption of a solute is controlled by intra particle diffusion process, the plot of q_t versus $t^{0.5}$ should be a straight line passed through origin. From the figure, it was observed that the line did not pass through the origin, which indicated that the intraparticle diffusion was not the rate-controlling step.

Equilibrium study of Sh adsorbed fluoride system

Adsorption isotherms describe the relation between adsorbate concentration and its accumulating capacity on the adsorbent surface at constant temperature. So, in order to optimize the design of an adsorption system to remove fluoride from water, it is essential to establish the most appropriate isotherm correlation for the equilibrium curve. Accordingly, the conformity experimental results with four of the most conventional isotherm models viz. Langmuir, Freundlich, Temkin and Dubinin–Rasdushkevich (DR) isotherms were considered for this adsorption system.

Figure 3.27 showed the adsorption isotherms of Sh adsorbed fluoride solution. The isotherm constants were tabulated in Table 3.11. From the table, it was concluded that Langmuir and Temkin isotherms were fitted well with the fluoride adsorption system with Langmuir adsorption capacity of 12.35 mg/g. The magnitude of the mean free energy of adsorption (E) was calculated from DR equation which was useful for estimating the type of adsorption. The E value obtained was 2.12 kJ/mol, which was not in the energy range of an ion-exchange reaction, i.e., 8–16 kJ/mol [12].

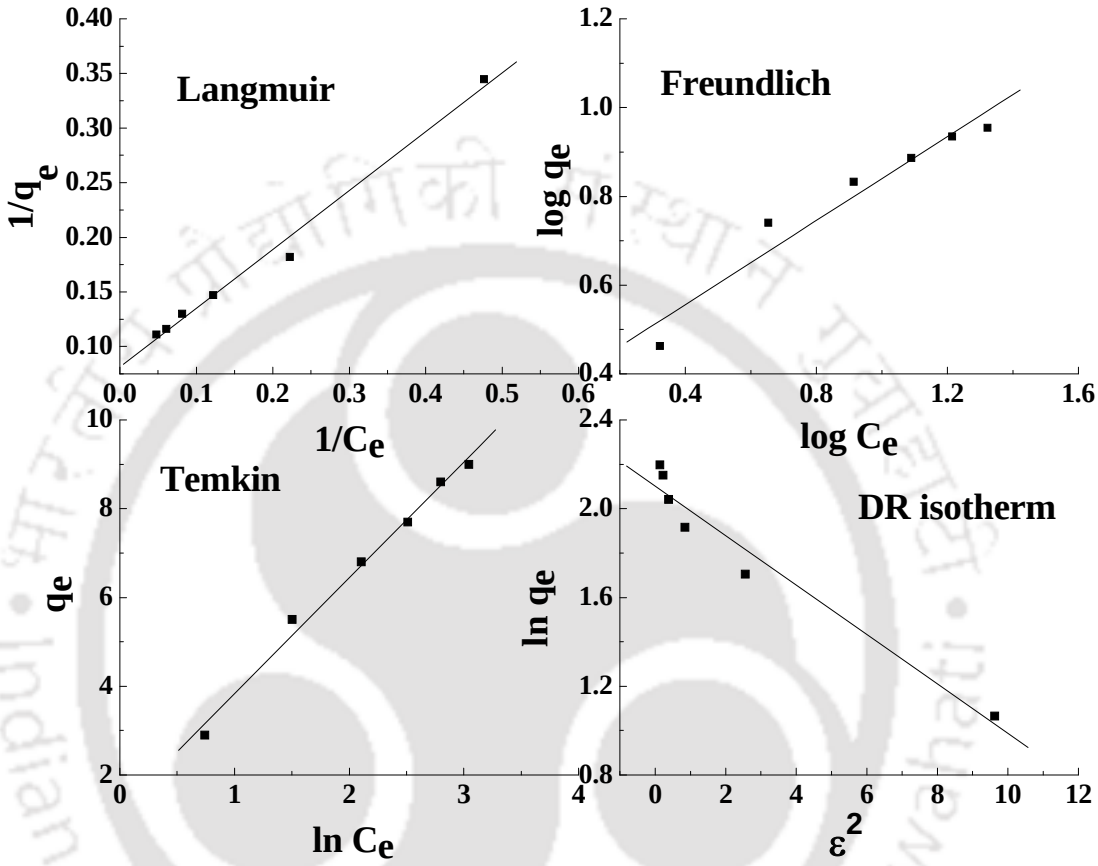

Figure 3.27: Adsorption isotherms of Sh - fluoride system

Table 3.11: Equilibrium isotherm constants of Langmuir, Freundlich, Temkin and DR isotherms for fluoride adsorption

Model	**Isotherm constants**		
Langmuir	q_{max} (mg/g)	b (L/mg)	R^2
	12.35	0.15	0.99
Freundlich	K_F [mg.g (L/mg)$^{1/n}$]	n_F	R^2
	1.44	0.48	0.94
Temkin	A_T	B_T	R^2
	1.59	2.61	0.99
DR - isotherm	K_{DR}	q_m	R^2
	0.11	8.17	0.95

Regeneration study of fluoride adsorbed Sh

Regeneration of Sh was done by fluoride adsorbed Sh particles in basic pH solution of pH 11.5. At this pH, more than 90% of the adsorbed fluoride was desorbed in about 90 min. After that the desorbed adsorbent was washed with distilled water and dried overnight. The desorption of fluoride adsorbed Sh particles were not so effective at acidic pH. Initial tests with regenerated adsorbent showed that the adsorption efficiency was decreased from 80 to 65 percentage with 5 mg/L of initial fluoride concentration as some of the pores of Sh was already occupied by fluoride particles.

Process calculation

Except for 100 percentage removal conditions, Equation 3.26 can be used to calculate the amount of dose required for the required percentage removal of fluoride from aqueous solution for any initial solution concentration. Figure 3.28 (inset) showed the amount of Sh required for desired percentage removal of fluoride for different solution volumes. From figure 3.28 (inset), for initial fluoride concentrations of 5, 10 and 15 mg/L and for 95 percentage removal of fluoride, the amount of Sh required was estimated as 0.98 g to 9.8 g, 1.11 g to 11.1 g and 1 g to 10 g for solution volume of 1 L to 10 L respectively. It was also clear from the figure that with low initial fluoride concentration, more volume of water was treated with a unit mass of adsorbent. This study will give an idea to design an adsorber column.

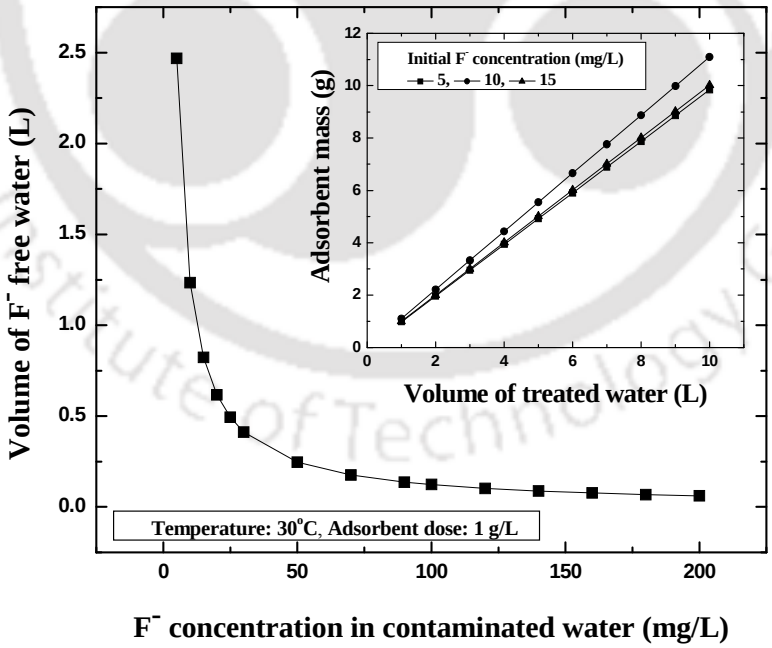

Figure 3.28: Variation of volume of fluoride free water using Sh

3.5 Fluoride removal by Nanomagnetite aggregated schwertmannite

Treatment of fluoride contaminated water is done by applying a novel nanomagnetite aggregation process through the formation procedure of iron oxide hydroxide, i.e. schwertmannite. The new adsorbent prepared is called NMSh particles. The adsorption parameters were studied in detail and presented in this section.

Role of contact time on fluoride adsorption

During adsorption, the change in residual fluoride concentration in water with time was plotted in Figure 3.29. It was observed that the concentration of fluoride decreased sharply within 10 minutes of adsorption and then adsorption became slow and almost reached equilibrium within 90 min. Initially all the adsorbent active sites were vacant and fluoride was adsorbed into the active sites rapidly. As time proceeds, the numbers of active sites of the adsorbent were decreased and then adsorption became slow and equilibrium was reached. The residual fluoride concentration was almost stagnant after 180 minutes. Therefore, further experiments were conducted with a contact time of 180 minutes.

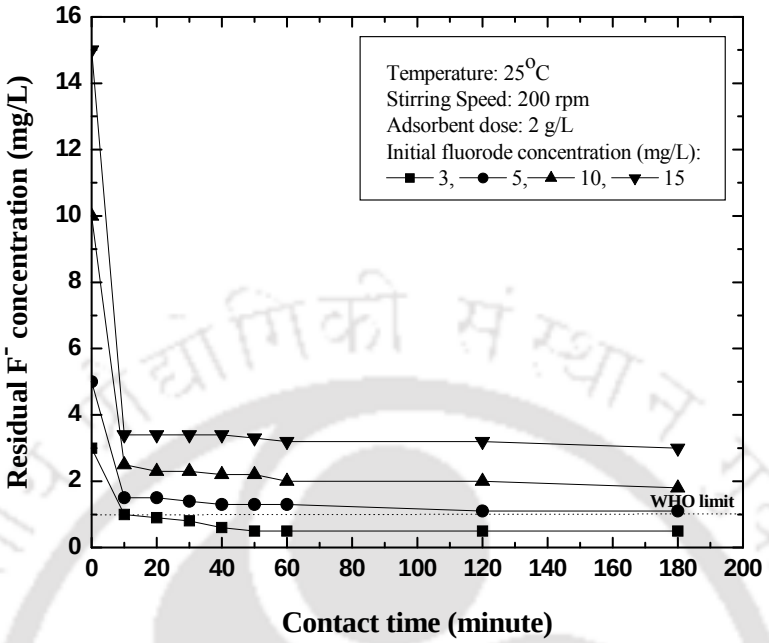

Figure 3.29: Effect of contact time on fluoride adsorption by NMSh

Role of adsorbent doses on fluoride adsorption

The change in residual fluoride concentration with varying NMSh mass was studied and plotted in Figure 3.30. Adsorbent dose is an important parameter for all adsorption processes. In this study, NMSh mass was varied from 1 g/L to 4 g/L. From the figure, it was observed that 2.0 g/L NMSh was required to maintain the WHO permissible limit for 5 mg/L initial fluoride concentration. Initially, the residual fluoride concentration was decreased sharply with increase in adsorbent dose (upto 1.5 g/L) and thereafter it was almost constant in case of 5 mg/L initial fluoride concentration.

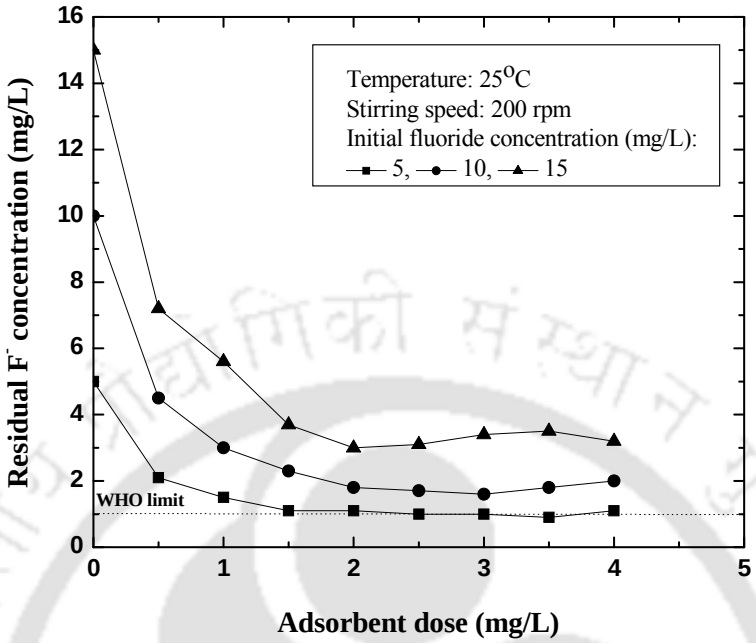

Figure 3.30: Residual fluoride concentration with varying adsorbent dose

Role of pH on fluoride adsorption by NMSh

To determine the optimum pH for maximum removal of fluoride, equilibrium sorption of fluoride with initial fluoride concentration of 15 mg/L was investigated over a pH range of 2.6 – 11.8. The effect of pH on the extent of fluoride adsorption was shown in Figure 3.31. It was observed that the adsorption of fluoride on NMSh was strongly pH dependent. The percentage fluoride adsorption was increased with pH, reaching maximum at pH 5.73, and then decreased slowly upto the pH value of 9.4. Beyond pH 9.4, the percentage removal decreased sharply. Initially, as the pH increased from 2.6 to 3.3 ($pH < pH_{ZPC} = 3.6$), the fluoride adsorption increased due to the positive surface charge of NMSh which attracts the negatively charged fluoride ion and became maximum at pH 5.8. Fluoride removal was decreased gradually below pH 5.8 due to the

formation of weakly ionized hydrofluoric acid which reduces the columbic attraction between fluoride and the adsorbent surface. The sharp decrease in percentage fluoride adsorption beyond pH 9.4 was due to the stronger competition of hydroxide ions to the active sites of NMSh and also the electrostatic repulsion of anionic fluoride by the negatively charged NMSh surface as pH > pH_{ZPC}. The almost flat portion of the curve i.e., at pH 7.1- 9.4, was due to the replacement of hydroxyl ion by fluoride ion as the hydroxyl ion concentration was less in that pH range. Beyond pH 9.4, the hydroxyl ion concentration was more which affects the fluoride removal capacity of the adsorbent.

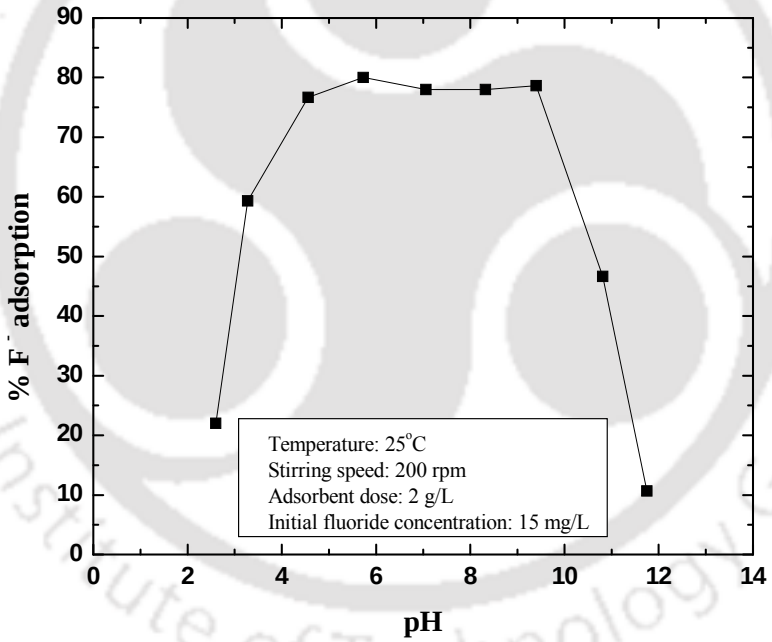

Figure 3.31: Effect of pH on the percentage adsorption of fluoride using NMSh

Role of varying stirring speed on fluoride adsorption

Three different stirring speeds (100, 200 and 300 rpm) were used to observe the fluoride adsorption phenomenon. With increase in stirring speed from 100 - 300 rpm,

amount of fluoride removal was changed as 82.7, 80 and 75.3 percentage, respectively. The effect of stirring speed on fluoride adsorption was shown in Figure 3.32. During adsorption, the fluoride molecules were adsorbed on the external surface of the adsorbent and then the pores. The rate of surface adsorption mechanism was very fast in comparison with the intraparticle diffusion. At low stirring speed, equilibrium was achieved in longer time than higher stirring speed. With increase in stirring speed, the fluoride ions get detached from the surface of the adsorbent, thus decreasing its removal efficiency.

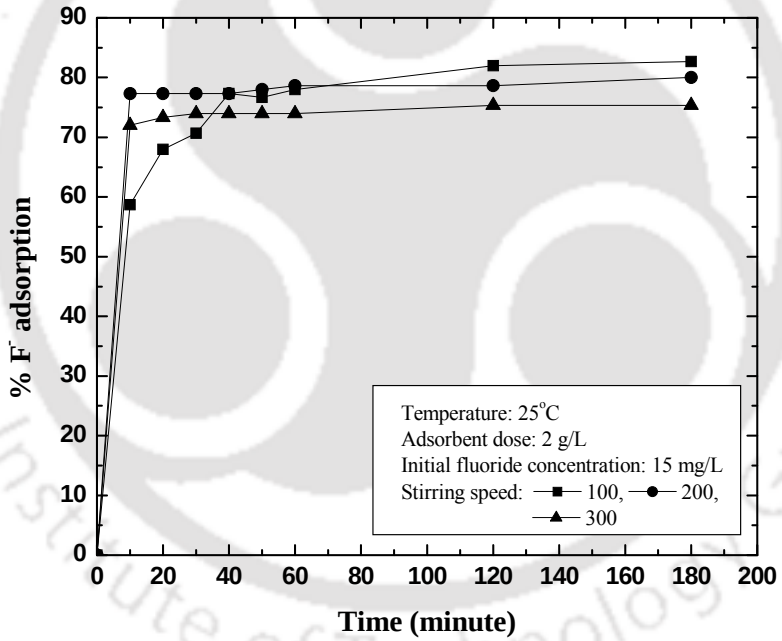

Figure 3.32: Effect of stirring speed on fluoride adsorption

Role of co-ions on fluoride adsorption

Figure 3.33 showed the effect of various ions on fluoride uptake by NMSh. It was observed that presence of chloride ion had negligible effect on fluoride removal as this

anion was outer-spherically sorbing anions. Presence of sulfate and phosphate ions reduced the fluoride removal efficiency slightly as sulfate and phosphate ions were partially inner-sphere complex forming species and that is why it had a tendency to compete fluoride ion for forming the complexes with the adsorbent. The decrease in fluoride adsorption in presence of carbonate and bicarbonate ions was presumably due to the significant increase in pH of the solution (pH<11). It was also confirmed from our experiments on the effect of pH that the fluoride removal efficiency decreased in highly alkaline pH (> 10).

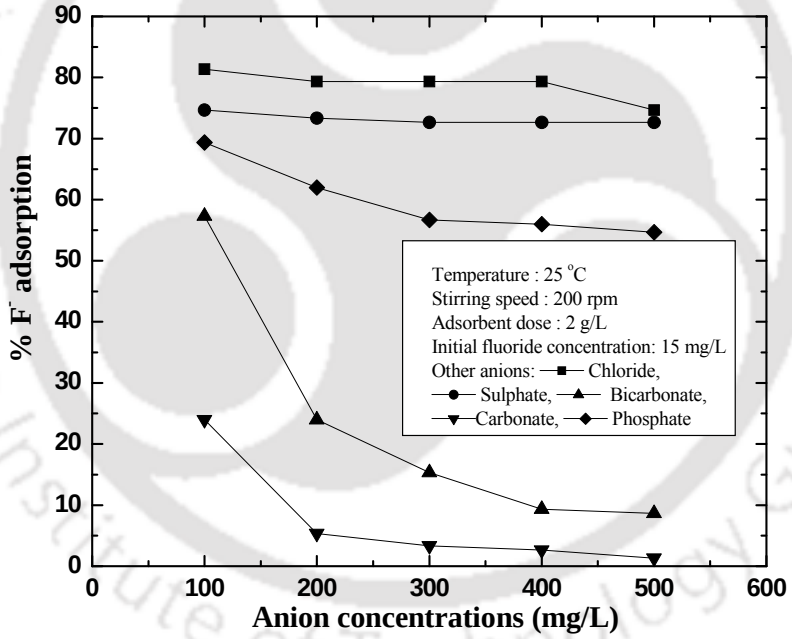

Figure 3.33: Presence of co-anions on the extent of fluoride adsorption

Calculation of thermodynamic parameters on fluoride adsorption

Thermodynamic parameters such as free energy change, enthalpy change and entropy change were calculated to evaluate the thermodynamic feasibility and the

spontaneous nature of the process. Table 3.12 summarized the thermodynamic parameters of 15 mg/L initial fluoride concentration solution. Positive ΔH^0 value concluded the endothermic behavior of adsorption and negative ΔG^0 value indicated spontaneous nature of the adsorption process. The endothermic nature of adsorption was also confirmed with increase in percentage fluoride adsorption from 80% to 83.3% with temperature shown in Figure 3.34. The low value of ΔS^0 implied that no remarkable change in entropy occurred during the adsorption process. In addition, the positive value of ΔS^0 reflects the increased randomness at the solid–solution interface during adsorption, and it also indicates the occurrence of ion replacement reactions.

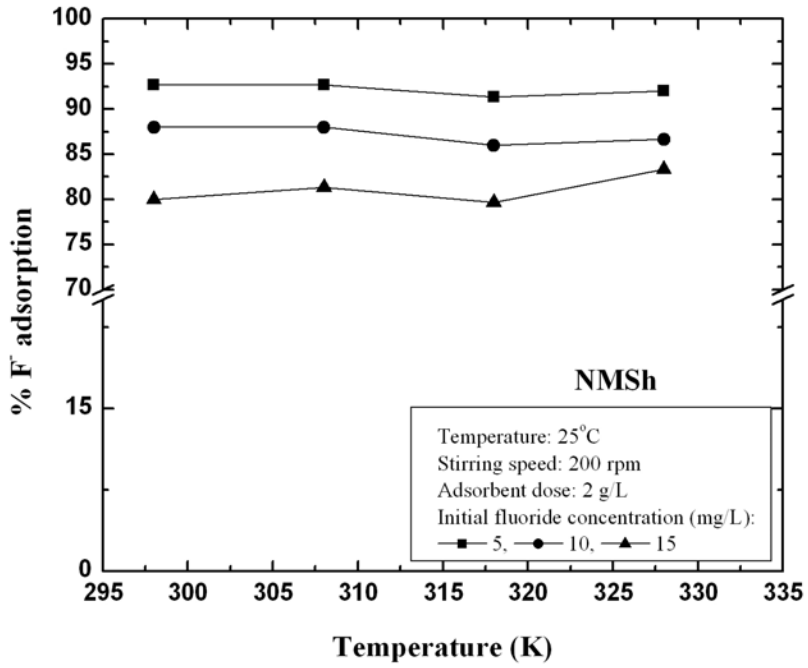

Figure 3.34: Effect of temperature on fluoride adsorption

The activation energy (E_a) and sticking probability (S^*) were estimated from a plot of $\ln(1-\theta)$ vs $1/T$. The E_a for adsorption of fluoride onto NMSh was calculated from the slope of the plot and found to be 73.2 kJ/mol.

Table 3.12: Thermodynamic parameters for fluoride adsorption on Sh

Temperature (K)	**ΔH^o (kJ/mol)**	**ΔS^o (kJ/mol. K)**	**Ea (kJ/ mol)**	**S* (x10^2)**	**-ΔG^o (kJ/mol)**
298					3.45
308	6.19	0.03	73.19	2.58	3.77
318					4.09
328					4.42

Kinetics study of fluoride adsorption by NMSh

The kinetics of fluoride adsorption onto NMSh was evaluated using different models such as pseudo-first-order [4], pseudo-second-order [5] and intraparticle diffusion [6] models. The various parameters were calculated from the plots of the kinetic model equations and summarized in Table 3.13. Among these models the criterion for their applicability is based on judgment on the respective correlation coefficient (R^2) and agreement between experimental and calculated value of q_e. The high values of R^2 (~1) and good agreement between two q_e values indicate that the understudy adsorption system followed pseudo-second-order kinetic model (Table 3.13).

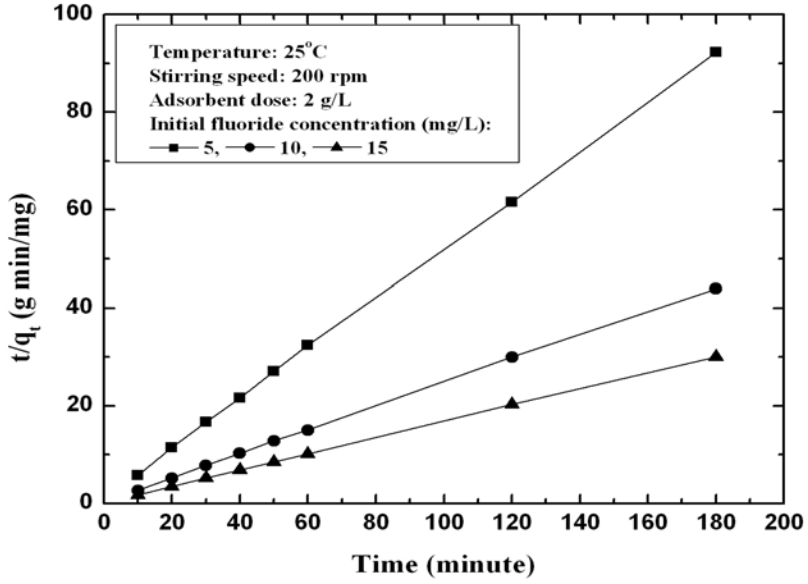

(a)

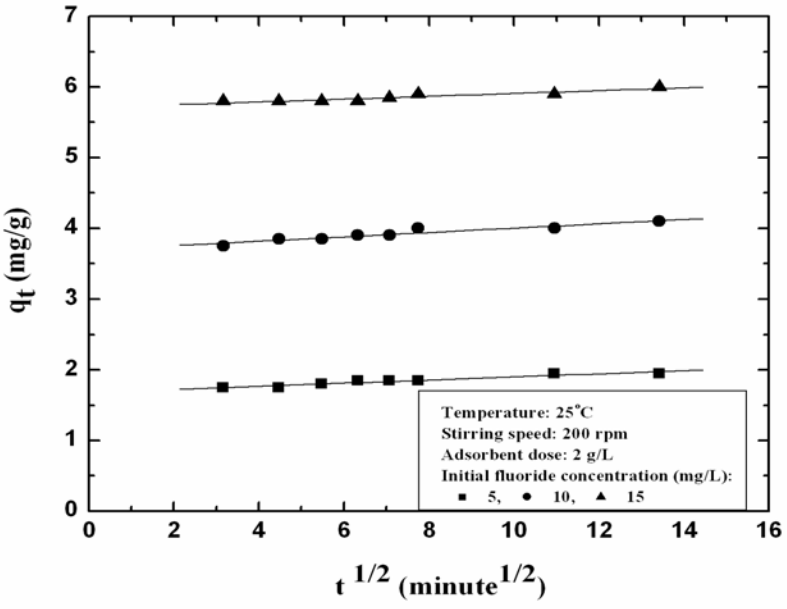

(b)

Figure 3.35: Kinetics of NMSh adsorbed fluoride system (a) Pseudo second order kinetic model (b) Intra particle diffusion model

It was also confirmed from Figure 3.35(a). Another alternative method for kinetic evaluation of an adsorption process is intra-particle-diffusion model. According to conditions and equation presented in Table 3.13, it is seen that respective plot (plot of q_t versus $t^{1/2}$) gives only one line and the rate constant k_i was evaluated from the slope of the line (Figure 3.35 b). Since the line did not pass through the origin, it indicates that the intraparticle diffusion was not the rate-controlling step.

Adsorption equilibrium study of NMSh adsorbed fluoride system

Adsorption equilibrium study for NMSh adsorbed fluoride system was studied with the help of Langmuir, Freundlich, Temkin and Dubinin–Rasdushkevich (DR) isotherms. The isotherms were plotted in Figure 3.36. The isotherm constants were tabulated in Table 3.14. From the table, it was concluded that the fluoride adsorption system was followed by both Langmuir and Temkin isotherm models with Langmuir adsorption capacity of 17.24 mg/g.

Table 3.13: Various kinetic model parameters at 25 ^{o}C on NMSh

Model	Equation	Plot	Parameters	Initial F^- concentration (mg/L)		
				5	**10**	**15**
Pseudo first order	$\ln(q_e - q_t) = \ln q_e - k_1 t$	Plot the values of ln (q_e- q_t) versus t which gave a straight line with slope of (-k_1) and intercept ln (q_e).	$q_{e,\ expt}$ (mg/g)	1.07	2.13	3.13
			$q_{e,\ cal}$ (mg/g)	0.12	0.37	0.92
			k_1 (min^{-1})	0.05	0.07	0.03
			R^2	0.98	0.98	0.97
Pseudo second order	$\frac{t}{q_t} = \frac{1}{k_2 q_e^{\ 2}} + \frac{t}{q_e}$	Plot the values of (t/q_t) versus t should give a straight line with slope of ($1/q_e$) and intercept ($1/k_2 q_e^2$).	$q_{e,\ cal}$ (mg/g)	1.08	2.15	3.16
			k_2 (g/µg. min)	1.57	0.71	0.12
			R^2	0.99	0.99	0.99
Intra particle diffusion	$q_t = k_i t^{0.5} + I$	Plot the values of (q_t) versus $t^{0.5}$ should give a straight line with slope (k_i) and intercept I.	k_i (mg/g $min^{1/2}$)	0.01	0.03	0.11
			I (mg/g)	0.98	1.92	2.18
			R^2	0.83	0.81	0.94

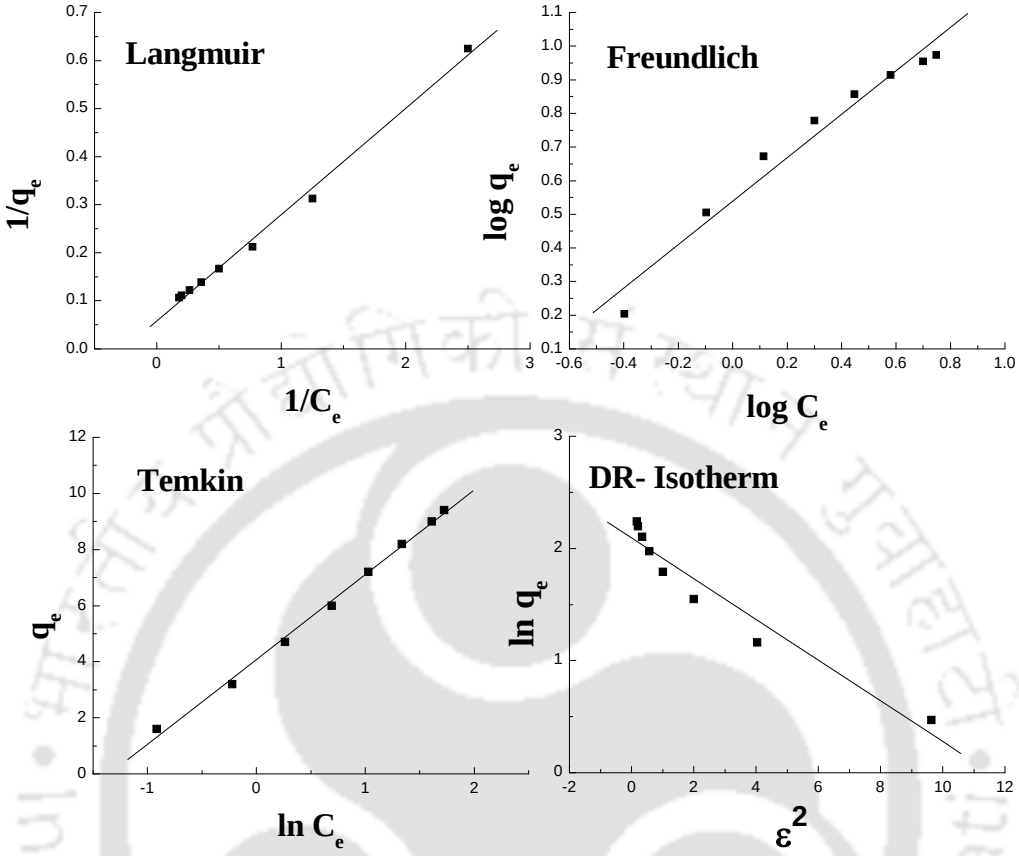

Figure 3.36: Adsorption isotherms of NMSh adsorbed fluoride system

The mean free energy of adsorption (E), defined as the free energy change when 1 mole of ion is transferred to the surface of the solid from infinity in solution can be calculated from the K value using equation (3.23). The magnitude of the mean free energy of adsorption (E) calculated from DR equation is useful for estimating the type of adsorption. The E value obtained was 15.8 kJ/mol, which are in the energy range of an ion-exchange reaction, i.e., 8–16 kJ/mol [12].

Table 3.14: Langmuir, Freundlich, Temkin and DR isotherm constants for fluoride adsorption on NMSh

Model	**Isotherm constants**		
Langmuir	q_{max} (mg/g)	b (L/mg)	R^2
	17.24	0.26	0.99
Freundlich	K_F [mg.g (L/mg)$^{1/n}$]	n_F	R^2
	1.71	0.65	0.97
Temkin	A_T	B_T	R^2
	3.85	3.03	0.99
DR-isotherm	K_{DR}	q_m	R^2
	0.18	8.11	0.94

Regeneration study of NMSh

Generally fluoride ion has a tendency to replace hydroxyl ion since their ionic sizes are almost same. That is why, for regeneration, basic solution is preferred. At pH 11.8, more than 85% of the adsorbed fluoride was desorbed. After that the desorbed adsorbent was washed with distilled water and dried overnight. The regenerated adsorbent was used as an adsorbent for 15 mg/L fluoride solution and found that adsorption efficiency was decreased from 80 to 65 percentage as some of the pores of NMSh was already occupied by fluoride particles.

Process calculation

This study was helpful in designing a single batch reactor design scheme. Using equation 3.26, we calculate the amount of dose required for 95% fluoride removal from

aqueous solution for any initial solution concentration. Figure 3.37 (inset) showed the amount of NMSh required for desired percentage removal of fluoride for different solution volumes. From figure 3.37 (inset), for initial fluoride concentrations of 4, 8 and 12 mg/L and for 95 percentage removal of fluoride, the amount of NMSh required was estimated as 1.07 g to 10.7 g, 1.01 g to 10.1 g and 0.96 g to 9.6 g for solution volume of 1 L to 10 L respectively. It was also clear from the figure that with low initial fluoride concentration, more volume of water was treated with a unit mass of adsorbent. This study will give an idea to design an adsorber column.

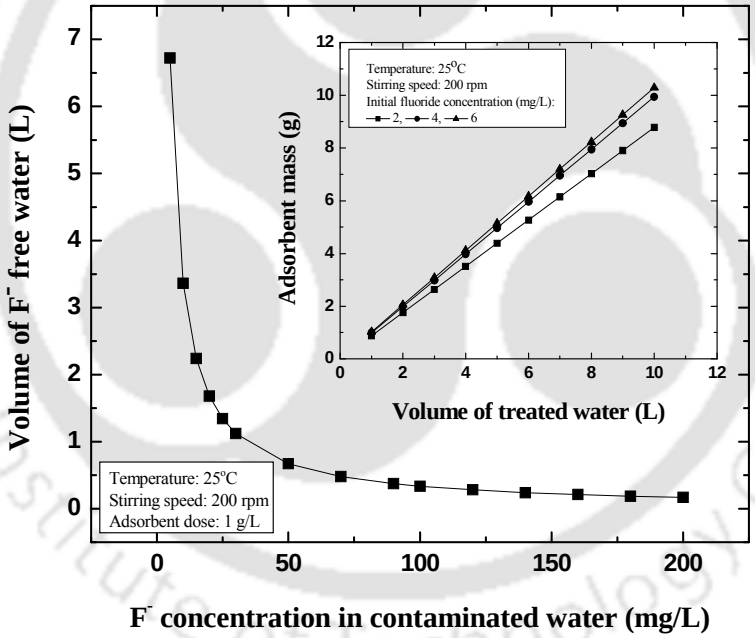

Figure 3.37: Volume treated water using NMSh

3.6 Performance analysis of various adsorbents used for fluoride removal

Adsorption is considered as a cheap and easy handling water treatment process. The adsorption technique is mainly depends on the nature and type of adsorbent used for the purpose. Different types of adsorbents were used for defluoridation of water. These include mainly biosorbents, natural materials, metal oxides and hydroxides, some nano adsorbents and many more. The adsorption efficiency of all these kinds of adsorbents was different. The adsorption capacity of an adsorbent depends on several factors including initial fluoride concentration of the solution. Hence for a same adsorbent, if the experimental condition is varied, the performance of that particular adsorbent was varied accordingly.

In this study, four different adsorbents were selected to study the fluoride adsorption performance. Result obtained is compared with the available literatures. A comparison of various adsorbents used for defluoridation are analyzed and reported in this section.

Karthikeyan et al. [25] studied Fluoride removal by montmorillonite clay. They observed that fluoride uptake was found maximum at pH 2, and it decreased with increase in pH. The material with particle size of 75 μm exhibited maximum percentage of fluoride adsorption compared to the other particle sizes. The Langmuir maximum sorption capacity for fluoride was found to be 1.485 - 1.910 mg/g at different temperatures. Fluoride removal was found to be adversely affected only in the presence of HCO_3^-. Another study was conducted by Tor [26] for the defluoridation of aqueous solution using montmorillonite. The maximum removal of fluoride was obtained at pH 6.

Below pH 5, adsorption was not favourable due to the formation of weakly ionised hydrofluoric acid in acidic conditions. At higher pH, above pHpzc (6.5), the fluoride sorption decreased due to the negative charge of the montmorillonite surface. The fluoride saturation capacity of montmorillonite was reported 0.263 mg/g at room temperature. The interaction between the metal oxides at the surface of montmorillonite and fluoride ions was accounted for the uptake of fluoride by the sorbent.

According to Sarkar et al. [27], laterite was selected as defluoridating agent. The pHpzc of laterite was reported 3.98 and was found to be responsible for fluoride adsorption. Lowering of pH enhanced fluoride removal from the solution. Fluoride adsorption decreased from 0.2014 to 0.1586 mg/g as the solution pH increased from 2.1 to 6.7, and decreased on further rise in pH above 7.5. The Langmuir sorption capacity of laterite for fluoride was 0.8461 mg/g at 303 K. Zhang et al. 2011 [28] studied the defluoridation of water by calcium chloride modified natural zeolite (CZ). They observed that maximum fluoride adsorption capacity of the modified zeolite was 1.766 mg/g at an initial fluoride concentration of 100 mg/L. The adsorption system followed pseudo second order kinetics and intra particle diffusion model and the experimental data fitted well to both Langmuir and Freundlich isotherm models. According to Thakre et al. [29], magnesium incorporated bentonite clay (MB) was used as defluoridating agent. It works effectively over wide range of pH and showed maximum fluoride removal capacity of 2.26 mg/g at an initial fluoride concentration of 5 mg/L. The experimental data fitted well into Langmuir adsorption isotherm and follows pseudo first order kinetics. Thermodynamic study suggested that fluoride adsorption on MB is spontaneous and endothermic in nature.

Pyrophyllite used in this study was basically a clay material, naturally available and hence cheap and environment friendly. The $Al-OH$ bonds present in pyrophyllite might have a capacity of fluoride adsorption. The study concludes that the fluoride adsorbed by pyrophyllite followed both Langmuir and Freundlich isotherms with Langmuir adsorption capacity of 2.2 mg/g which was better adsorption performance than many other adsorbents [30]. It also gives a comparative fluoride adsorption capacity even without any surface modification as in case of bentonite [29].

Ghorai and Pant [31] investigated the removal of fluoride using activated alumina (AA) (Grade OA-25) in batch and continuous operations. An adsorption capacity of 1.45 mg/gm was obtained at pH 7. Percentage fluoride removal increased in the pH range from 4 to 7 and decreased thereafter. Silicates and hydroxyl ions were considered to compete more strongly with fluoride ions for alumina exchange sites at pH > 7, whereas, at pH < 7, the soluble alumino-fluoro complexes were formed resulting in the presence of aluminium ions in the treated water. Early saturation and lower fluoride removal was observed at higher flow rate and at higher concentration. There was a marginal decrease in the uptake capacity after each regeneration cycle. Regeneration procedure resulted in 85% efficiency with the grade of AA studied. A loss of 5% in uptake capacity of AA was observed after five cycles. The same workers also employed granulated activated alumina for the sorption of fluoride [32]. The removal of fluoride was maximum (69.5%) at pH 7 and was independent of sorbent dose and initial fluoride concentration. The Langmuir maximum sorption capacity was found to be 2.41 mg/g.

Lee et al. [33] used γ alumina as defluoridating agent. Equilibrium fluoride ion adsorption data over the adsorbent samples obtained at 30^{o}C at initial fluoride

concentrations ranging from 20 - 250 mg/L. The adsorption system followed Langmuir isotherm with adsorption capacity of 6.36 mg/g. Pseudo second order kinetics was followed by the system. According to Jagtap et al. [34], it was observed that mesoporous alumina works effectively over wide range of pH and showed a maximum adsorption capacity 8.264 mg/g at initial fluoride concentration of 5 mg/L which is much better than the conventional alumina. The experimental data fitted well in Langmuir isotherm and follows pseudo-second order kinetics. Thermodynamic study reveals that fluoride adsorption on mesoporous alumina is spontaneous and exothermic process.

Maliyekkal et al. [35] also modified alumina with manganese oxide to prepare manganese-oxide-coated alumina (MOCA) and investigated the potential of sorbent for defluoridation of drinking water by batch and continuous mode experiments. Adsorption of fluoride on to MOCA was found to be much faster than that of AA at the initial period of time and was almost constant after 3 hrs. Optimum removal of fluoride ions occurred in a pH range of 4 – 7. Results indicate that fluoride adsorption rate and adsorption capacity of MOCA are far superior to that of activated alumina (AA), which was used as the base material for MOCA preparation. The MOCA can be effectively regenerated using 2.5% NaOH as eluent. The Langmuir equilibrium model was found to be suitable for describing the fluoride sorption on AA and MOCA. The maximum fluoride uptake capacity for MOCA and AA was found to be 2.85 and 1.08 mg/g, respectively. The kinetic results showed that the fluoride sorption to MOCA followed pseudo - secondorder kinetics with a correlation coefficient greater than 0.98.

Bansiwal et al. [36] modified the mesoporous alumina by coating copper oxide to enhance the defluoridation of water. The copper oxide coated alumina (COCA) was

synthesised by impregnating alumina with copper sulphate solution followed by calcination at 450 ^{o}C in presence of air. The adsorption capacity of COCA for fluoride obtained from the Langmuir model was 7.22 mg/g, which was three times higher than that of unmodified AA (2.232 mg/g).

The acidic alumina used in the present work follow Langmuir isotherm with adsorption capacity of 8.4 mg/g [37] which is far better than many activated alumina even after modification.

Metal oxide-hydroxide plays an important role in defluoridation of water. According to Kumara et al. [38] granular ferric hydroxide (GFH) was used for defluoridation of water. The adsorption capacity of 7 mg/g was observed for fluoride on GFH at pH 6 – 7 at 25^{o}C. Fluoride adsorption was found to decrease sharply above pH 8 as the surface charge becomes more negative (pHzpc of GFH is 8). The fluoride adsorption onto GFH was attributed to the interaction of fluoride with singly co-ordinated FeOH surface groups and the mechanism of fluoride adsorption was described as an exchange reaction against OH^- of the surface groups. The OH/F exchange has also found to suggest that the fluoride ion can be considered as fully located in the surface of GFH.

Granular zirconium-iron oxide (GZI) was successfully prepared using the extrusion method, and its defluoridation performance was systematically evaluated by Dou et al. [39]. The GZI was composed of amorphous and nano-scale oxide particles. The Zr and Fe were evenly distributed on its surface, with a Zr/Fe molar ratio of 2.3. The granular adsorbent was porous with high permeability potential. Moreover, it had excellent mechanical stability and high crushing strength, which ensured less material breakage and mass loss in practical use. In batch tests, the GZI showed a high adsorption capacity

of 9.8 mg/g under an equilibrium concentration of 10 mg/L at pH 7.0. The GZI performed well over a wide pH range of 3.5 - 8.0, and especially well at pH 6.0-8.0, which was the preferred range for actual application. Fluoride adsorption on GZI followed pseudo-second-order kinetics and could be well described by the Freundlich equilibrium model.

In this study Schwertmannite (Sh) which is an iron oxide hydroxide was used as an adsorbent for fluoride removal. The fluoride adsorption system follows pseudo second order kinetics and spontaneous in nature. Langmuir adsorption isotherm was followed by the system with an adsorption capacity of 12.3 mg/g [40] which is better than GZI.

Apart from this, nanotechnology has emerged as a promising technology in past decade in various fields. Likewise, use of nanoparticles as sorbents for water treatment is also gaining wide attention in recent years. Carbon nanotubes (CNTs) have attracted huge interest since their discovery. Their small sizes, large surface area, high mechanical strength and remarkable electrical conductivities make them potential materials for a wide range of promising applications.

Aligned carbon nanotubes (ACNTs), were prepared by catalytic decomposition of xylene using ferrocene as catalyst, and their performance was evaluated for fluoride removal from water [41]. Both the surface and inner cavities of ACNTs were found to be readily accessible for fluoride sorption. A broad pH range of 3 - 9 was found optimum for fluoride removal. The highest adsorption capacity of ACNTs occurred at pH 7.0 and reached 4.5 mg/g at equilibrium fluoride concentration of 15 mg/L.

Wang et al. [42] performed defluoridation experiments employing nano-scale aluminium oxide hydroxide as sorbent, taking into account the advantage of higher

surface area of nanoparticles as compared to the traditional micron-sized materials. The maximum Langmuir defluoridation capacity of nano-AlOOH was found to be 3.26 mg/g. The adsorption of fluoride onto nano-AlOOH was strongly pH dependent. The fluoride adsorption increased with the rise in pH, reaching a maximum of 96.7% at pH 6.8, and then decreased with further increase in pH. The pHzpc of the sorbent was reported as 7.8, which was responsible for the sorption of fluoride at acidic pH and low efficiency in alkaline medium was explained by the repulsion between the negatively charged surface and fluoride. To utilize the advantage of granular form of Fe–Al–Ce adsorbent, Chen et al. [43] used acrylic–styrene copolymer latex as a binder for Fe–Al–Ce and spray-coated it onto sand in a fluidized bed. The introduction of latex was found to increase the stability of the coated layer. The granules had spherical shape and high stability with size about 2–3 mm and coating thickness up to 200 μm. The coating amount was from 3% to 36%. Granule stability was found to decrease and adsorption capacity increased with increase in coating amount. The results of FTIR analysis indicated that the latex could react with active hydroxyl on the Fe–Al–Ce adsorbent, which led to a decrease of the adsorption capacity. For the optimal stability and adsorption capacity, a coating amount of 27.5% was suggested. Coated granules with a coating amount of 27.5% had a fluoride adsorption capacity of 2.22 mg/g (coated granules) at pH 7.0 and initial fluoride concentration of 0.001 M.

The feasibility of nano-alumina was evaluated for fluoride removal from aqueous solutions [18]. The maximum sorption capacity of nano-alumina for fluoride was found to be 14.0 mg/g at 25 ^{o}C. Maximum fluoride removal occurred at pH 6.15. Fluoride sorption was mainly influenced by the presence of PO_4^{3-}, SO_4^{2-} and CO_3^{2-}. Pathak et al.

[44] successfully standardized the preparation of a variety of nano-sized inorganic oxides through thermolysis of a polymeric based aqueous precursor solution of the desired inorganic ions. The obtained Fe_3O_4, Al_2O_3 and ZrO_2 nano-sized oxide powders were incorporated in the matrix of activated charcoal through adsorption and used as the adsorbing bed for the removal of trace amounts of fluoride and various other pollutants. The charcoal embedded fine powders of the inorganic oxides have been able to remove fluoride/ arsenite and arsenate ions from industrial wastewater up to 0.01–0.02 mg/L levels.

Based on this concept we have prepared nanomagnetite particles and embedded on the surface of Sh [45]. The new adsorbent, NMSh followed pseudo second order kinetics and Langmuir isotherm model with an adsorption capacity of 17.24 mg/g. The comparison of different adsorbents mentioned above was tabulated in Table 3.15. From the table it was concluded that NMSh should be a better adsorbent for defluoridation of water.

Table 3.15: Comparison of fluoride adsorption capacities of different adsorbents

Adsorbent	**pHzpc**	**Isotherm Followed**	**Adsorption capacity (mg/g)**	**Concentration range(mg/L)**	**Contact time**	**pH**	**Temperature**	**Reference**
Montmorillonite	2.5	Langmuir	1.485	3.0	50 min	neutral	30^{o}C	[25]
Montmorillonite	6.5	Langmuir	0.263	2.0 – 120.0	180 min	6.0	25 ^{o}C	[26]
Laterite	3.98	Langmuir	0.8461	10.0 – 50.0	-	7.5	303 K	[27]
CZ	-	Langmuir	1.766	100.0	-	6.0	25 ^{o}C	[28]
MB	-	Langmuir	2.26	5.0	12 hr	-	25 ^{o}C	[29]
Pyrophyllite	**5.12**	**Langmuir**	**2.2**	**2.0 – 12.0**	**180 min**	**4.9**	**25 ^{o}C**	**Present work [30]**
Activated alumina	-	Langmuir	1.45	2.5 – 14.0	-	7.0	-	[31]
γ alumina	-	Langmuir	6.36	20.0 – 250.0	-	-	30 ^{o}C	[33]
Mesoporous alumina	-	Langmuir	8.264	5.0	-	-	25 ^{o}C	[34]
MOCA	7.2	Langmuir	2.851	2.5 – 30.0	180 min	7.0	30 ± 2 ^{o}C	[35]
COCA	-	Langmuir	7.22	10.0	24 hr	-	30 ± 1 ^{o}C	[36]
Acidic Alumina	**5.1**	**Langmuir**	**8.4**	**2.0 -15.0**	**90 min**	**4.4**	**25 ^{o}C**	**Present work [37]**
GFH	7.5	Langmuir	7.0	1.0 – 100.0	24 hr	6.0	25 ± 2 ^{o}C	[38]
GZI	-	Langmuir	9.8	10.0	-	7.0	-	[39]
Sh	**-**	**Langmuir**	**12.3**	**5.0 – 30.0**	**120 min**	**3.6**	**30 ^{o}C**	**Present work [40]**
ACNT	-	Langmuir	4.5	15.0	180 min	7.0	25 ^{o}C	[41]
Nano-AlOOH	7.8	Langmuir	3.259	3.0 – 35.0	6 hr	5.2	298 K	[42]
Fe-Al-Ce	-	Langmuir	2.22	0.001 M	36 hr	7.0	25 ^{o}C	[43]
Nano alumina	7.2	Langmuir	14.0	1.0 – 100.0	24 hr	6.15	25 ± 2 ^{o}C	[18]
NMSh	**3.6**	**Langmuir**	**17.24**	**2.0 – 15.0**	**90 min**	**5.7**	**25 ^{o}C**	**Present work [45]**

3.7 Summary

The initial concentration of fluoride present in water indicates the contamination level of the source water and depending on that the treatment time and adsorbent mass come into the picture as one of the most dependent variables. Adsorption is mainly a combination of mass transfer and ion exchange process and it mainly depends on the surface area, ionic charge of the adsorbent and the adsorbate molecules. During adsorption process, pH is the most important parameter which depicts the overall effect of different ion-ion interactions. Hence, several parameters like initial fluoride concentration, duration of experiment, adsorbent mass, temperature, stirring speed, pH and other ions effect were investigated during adsorption treatment of fluoride contaminated water. The excerpts obtained from the experimental results are presented below separately for four different adsorbents.

Pyrophyllite

The current study highlighted that pyrophyllite had considerable potential for fluoride removal from aqueous solution. It was found that pyrophyllite showed significant fluoride removal efficiency (85%) at pH 4.9. Maximum fluoride adsorption capacity was found to be 2.2 mg/g at an initial fluoride concentration of 10 mg/L. The experimental data fitted well with Langmiur adsorption isotherm and the value of equilibrium parameter "R_L" suggested that fluoride adsorption by pyrophyllite was favorable. Presence of other ion effects the fluoride removal efficiency. Kinetic study reveals that fluoride adsorption by pyrophyllite follow pseudo second order kinetic model and both intra-particle diffusion as well as surface diffusion steps was involved during

fluoride uptake. The mass transfer coefficient increased from 4.52×10^{-13} to 9.34×10^{-13} when initial fluoride concentration increases from 4 mg/L to 10 mg/L. The negative values of ΔG^o and ΔH^o values suggest that the fluoride adsorption by pyrophyllite was a spontaneous process and exothermic in nature. Low cost of pyrophyllite made this material a potential candidate for defluoridation of water.

Acidic alumina

The present work showed that alumina which is acidic in nature had a considerable potential for fluoride removal from aqueous medium. Around 94 percentage fluoride was adsorbed by alumina at pH 4.4. Kinetic study revealed that fluoride adsorption process was controlled by pseudo-second-order rate equation and intraparticle diffusion was not the rate-controlling step. From EDX study, `it was concluded that fluoride adsorption onto alumina was mostly due to surface adsorption. Thermodynamic study concluded that the fluoride adsorption process was spontaneous, feasible and endothermic nature with activation energy of 95.13 kJ/mol which were fallen in physical adsorption process range. The equilibrium data was fitted with Langmuir and Freundlich isotherm models. Langmuir isotherm model was fitted well to this system with an adsorption capacity of 8.4 mg/g of adsorbent. The performance of alumina towards fluoride was decreased with the presence of other ions. The interference of carbonate and bicarbonate ions was more than that of chloride, nitrate and sulfate ions. The spent adsorbents were regenerated with basic solutions and regenerated adsorbents showed very good adsorption efficiencies. Finally, the process calculation shown here will be helpful in designing a batch adsorber.

Schwertmannite (Sh)

It has been successfully demonstrated that Sh can be potentially used for fluoride removal from aqueous solutions by adsorption. The permissible limit defined by WHO for defluoridation was achieved by 3 g/L adsorbent dose in 90 minute contact time at a pH 3.6. Kinetic study revealed that fluoride adsorption process was controlled by pseudo second order rate equation and intraparticle diffusion was not the rate-controlling step. Thermodynamic study concluded that the fluoride adsorption process was spontaneous, feasible and exothermic nature. The equilibrium isotherm data was best fitted with Langmuir and Temkin isotherm models with an adsorption capacity of 12.5 mg/g of adsorbent. The performance of Sh towards fluoride adsorption was decreased with the presence of phosphate and bicarbonate ions. The spent adsorbents were regenerated with basic solutions and regenerated adsorbents showed good adsorption efficiencies.

Nanomagnetite schwertmannite (NMSh)

In this study, batch adsorption experiments were carried out to remove fluoride from aqueous solution using synthesized NMSh. NMSh was prepared by introducing nanomagnetite in ordinary schwertmannite, which is a composite of ferromagnetic and paramagnetic materials. This new property improves the fluoride adsorption efficiency. The permissible limit defined by WHO for defluoridation was achieved by 2 g/L adsorbent dose in 90 minute contact time at a pH 5.73. Kinetic study revealed that fluoride adsorption process was controlled by pseudo-second-order rate equation and intraparticle diffusion was not the rate-controlling step. Thermodynamic study concluded that the fluoride adsorption process was spontaneous, feasible and endothermic nature

with activation energy of 73.19 kJ/ mol which were fallen in physical adsorption process range. The equilibrium isotherm data was best fitted with Langmuir and Temkin isotherm models with an adsorption capacity of 17.24 mg/g of adsorbent. The performance of NMSh towards fluoride was decreased with the presence of other ions. The interference of phosphate, carbonate and bicarbonate ions was more than that of chloride and sulfate ions. The spent adsorbents were regenerated with basic solutions and regenerated adsorbents showed good adsorption efficiencies. Finally, the process calculation shown here will be helpful in designing a batch adsorber. This study will also help to run a continuous fluoride adsorption set up which gives the real life of the adsorbent. The results of magnetic removal of fluoride using the new adsorbent indicated that nano magnetite aggregation process not only improves the magnetic property, but also provides a highly-promoted fluoride adsorption capacity compared to the other adsorbents.

Although several studies such as study of temperature dependent isotherms, mathematical modeling, detailed adsorption mechanisms have not covered, but the above preliminary investigations will be helpful for selecting adsorbents and designing a fluoride removal unit in real practice.

3.8 References

[1] Namasivayam, C., Kavitha, D., 2002. Removal of Congo red from water by adsorption onto activated carbon prepared from coir pith, an agricultural solid waste. Dyes and Pigments 54, 47–58.

[2] Igwe, J.C., Abia, A.A., 2007. Studies on the effects of temperature and particle size on bioremediation of AS (III) from aqueous solution using modified and unmodified coconut fiber. Global Environ. Res. 1, 22-26.

[3] Lagergren, S., 1898. Zur theorie der sogenannten adsorption gelöster stoffe, Kungliga Svenska Vetenskapsakademiens. Handlingar 24, 1-39.

[4] Blanchard, G., Maunaye, M., Martin, G., 1984. Removal of heavy metals from waters by means of natural zeolites. Water Res. 18, 1501-1507.

[5] Weber, J.W.J., Morriss, J.C., 1963. Kinetics of adsorption on carbon from solution. J. Sanit. Eng. Div. Am. Soc. Civil Eng. 89, 31–60.

[6] Langmuir, I., 1918. The adsorption of gases on plane surfaces of glass, mica and platinum. J. American Chem. Soc. 40, 1361-1403.

[7] Hall, K.R., Eagleton, L.C., Acrivos, A., Vermeulen, T., 1966. Pore and solid diffusion kinetics in fixed-bed adsorption under constant pattern conditions. Ind. Eng. Chem. Fund. 5, 212–223.

[8] Freundlich, H., 1907. Uber die Adsorption in Lösungen. Zeitschrift für Physikalische Chemie 57, 385–470.

[9] Temkin, M.J., Pyzhev, V., 1940. Kinetics of ammonia synthesis on promoted iron catalysts. Acta Physicochimica U.R.S.S. 12, 217–222.

[10] Dubinin, M.M., Radushkevich, L.V., 1947. Equation of the characteristic curve of activated charcoal. Chem Zentr 1, 875-889.

[11] Helfferich, F., 1962. Ion Exchange. McGraw-Hill, New York, USA.

[12] O¨ zacar, M., Sengil, I.A., 2004. Equilibrium data and process design for adsorption of disperse dyes onto Alunite, Environ. Geo. 45, 762–768.

[13] Weber, W.J., 1972. Physicochemical Processes for Water Quality Control. Wiley-Interscience, New York.

[14] Mall, I.D., Srivastava, V.C., Agarwal, N.K., Mishra, I.M., 2005. Adsorptive removal of malachite green dye from aqueous solution by bagasse fly ash and activated carbon kinetic study and equilibrium isotherm analyses. Colloids Surf., A Physicochem. Eng. Asp. 264, 17-28.

[15] Sujana, M.G., Pradhan, H.K., Anand, S., 2009. Studies on sorption of some geomaterials for fluoride removal from aqueous solutions. J. Hazard. Mater., 161, 120–125.

[16] Purkait, M.K., Maiti, A., DasGupta, S., De, S., 2007. Removal of congo red using activated carbon and its regeneration. J. Hazard. Mater. 145, 287-295.

[17] Furusawa, T., Smith, J.M., 1973. Fluid-particle and intraparticle mass transport rates in slurries. Ind. Eng. Chem. Fundam. 12, 197-203.

[18] Kumar, E., Bhatnagar, A., Kumar, U., Sillanpää, M., 2011. Defluoridation from aqueous solutions by nano-alumina: characterization and sorption studies. J. Hazard. Mater. 186, 1042–1049.

[19] Nandi, B.K., Goswami, A., Purkait, M.K., 2009. Removal of cationic dyes from aqueous solutions by kaolin: Kinetic and equilibrium studies. App. Clay Sci. 42, 583-590.

[20] Kumara, E., Bhatnagara, A., Jia, M., Junga, W., Lee, S.H., Kim, S.J., Lee, G., Songd, H., Choie, J.Y., Yange, J.S., Jeona, B.H., 2009. Defluoridation from aqueous solutions by granular ferric hydroxide (GFH). Water Res. 43, 490-498.

[21] Ho, Y., Chiu, W., Wang, C., 2005. Regression analysis for the sorption isotherms of basic dyes on sugarcane dust. Bioresour. Technol. 96, 1285-1291.

[22] Clifford, D., Matson, J., Kennedy, R., 1978. Activated alumina: Rediscovered "adsorbent" for fluoride, humic acids and silica. Ind. Wat. Eng. 15, 6-12.

[23] Eskandarpour, A., Onyango, M.S., Ochieng, A., Asai, S., 2008. Removal of fluoride ions from aqueous solution at low pH using schwertmannite. J. Hazard. Mater. 152, 571–579.

[24] Onyango, M.S., Kojima, Y., Aoyi, O., Bernardo, E.C., Matsuda, H., 2004. Adsorption equilibrium modeling and solution chemistry dependence of fluoride removal from water by trivalent-cation-exchanged zeolite. J. of Colloid and Interf. Sci. 279, 341–350.

[25] Karthikeyan, G., Pius, A., Alagumuthu, G., 2005. Fluoride adsorption studies of montmorillonite clay. Indian J. Chem. Technol. 12, 263–272.

[26] Tor, A., 2006. Removal of fluoride from an aqueous solution by using montmorillonite. Desalination 201, 267–276.

[27] Sarkar, M., Banerjee, A., Pramanick, P.P, Sarkar, A.R. ,2006. Use of laterite for the removal of fluoride from contaminated drinking water. J. Colloid Interface Sci. 302, 432–441.

[28] Zhang, Z., Tan, Y., Zhong, M., 2011. Defluorination of wastewater by calcium chloride modified natural zeolite. Desalination, 276, 246 - 252.

[29] Thakre, D., Rayalu, S., Kawade, R., Meshram, S., Subrt, J., Labhsetwar, N., 2010. Magnesium incorporated bentonite clay for defluoridation of drinking water. J. Hazard. Mater. 180, 122-130.

[30] Goswami, A., Purkait, M.K., 2011. Kinetic and Equilibrium study for the fluoride adsorption using Pyrophyllite. Sep. Sci. Tech. 46, 1797-1807.

[31] Ghorai, S., Pant, K.K., 2004. Investigations on the column performance of fluoride adsorption by activated alumina in a fixed-bed. Chem. Eng. J. 98,165–173.

[32] Ghorai, S., Pant, K.K., 2005. Equilibrium, kinetics and breakthrough studies for adsorption of fluoride on activated alumina. Sep. Purif. Technol. 42, 265–271.

[33] Lee, G., Chen, C., Yang, S.T., Ahn, W.S., 2010. Enhanced adsorptive removal of fluoride using mesoporous alumina. Micropor. Mesopor. Mater. 127, 152-161.

[34] Jagtap, S., Yenkie, M.K.N., Labhsetwar, N., Rayalu, S., 2011. Defluoridation of drinking water using chitosan based mesoporous alumina. 2011, Micropor. Mesopor. Mater. 142, 454-463.

[35] Maliyekkal, S.M., Sharma, A.K., Philip, L., 2006. Manganese-oxide-coated alumina: A promising sorbent for defluoridation of wate. Water Res. 40, 3497–3506.

[36] Bansiwal, A., Pillewan, P., Biniwale, R.B., Rayalu, S.S., 2010. Copper oxide incorporated mesoporous alumina for defluoridation of drinking water. Micropor. Mesopor. Mater. 129, 54–61.

[37] Goswami, A., Purkait, M.K., 2012. The defluoridation of water by acidic alumina. Chem. Eng. Res. Desig. 90, 2316 -2324.

[38] Kumar, E., Bhatnagar, A., Ji, M., Jung, W., Lee, S.H., Kim, S.J., Lee, G., Song, H., Choi, J.Y., Yang, J.S., Jeon, B.H., 2009. Defluoridation from aqueous solutions by granular ferric hydroxide (GFH). Water Res. 43, 490–498.

[39] Dou, X., Zhang, Y., Wang, H., Wang, T., Wang, Y., 2011. Performance of granular zirconiumeiron oxide in the removal of fluoride from drinking water. Water Res. 45, 3571- 3578.

[40] Goswami A, Purkai, M.K., Preparation and characterization of nanoporous schwertmannite for defluoridation of water, Submitted to Water Res., (2nd Feb, 2013).

[41] Li, Y.H., Wang, S., Zhang, X., Wei, J., Xu, C., Luan, Z., Wu, D., 2003. Adsorption of fluoride from water by aligned carbon nanotubes. Mater. Res. Bull. 38, 469–476.

[42] Wang, S.G., Ma, Y., Shi, Y.J., Gong, W.X., 2009. Defluoridation performance and mechanism of nano-scale aluminum oxide hydroxide in aqueous solution. J. Chem. Technol. Biotechnol. 84, 1043–1050.

[43] Chen, L., Wu, H.X., Wang, T.J., Jin, Y., Zhang, Y., Dou, X.M., 2009. Granulation of Fe-Al-Ce nano-adsorbent for fluoride removal from drinking water by spray coating on sand in a fluidized bed. Powder Technol. 193, 59–64.

[44] Pathak, A., Panda, A.B., Tarafdar, A., Pramanik, P., 2003. Synthesis of nano-sized metal oxide powders and their application in separation technology. J. Indian Chem. Soc. 80, 289–296.

[45] Goswami A, Purkai, M.K., Defluoridation of contaminated drinking water using nano magnetite schwertmannite, submitted to J. Hazard. Mater, (27th Feb, 2013).

Chapter 4

Chemical treatment followed by microfiltration for defluoridation

This chapter is divided into three sections. Section 4.1 describes the chemical treatment method used to remove fluoride from fluoride contaminated water. The membrane filtration technique for defluoridation is discussed in section 4.2. Essential raw materials for membrane preparation, procedure of preparing ceramic microporous membranes and their characterization techniques are discussed here. Chemical precipitation followed microfiltration technique is reported in section 4.3.

4.1: Chemical treatment method

Chemical treatment method includes the chemical precipitation technique which is the most common method for defluoridation of water. It is an easy handling and cheap method of defluoridation. Earlier this method is known as Nalgonda technique which is a two step process. In step 1, precipitation occurs by lime dosing which is followed by a second step in which alum is added for coagulation. When alum is added to water, essentially two reactions occur. In the first reaction, alum reacts with some of the alkalinity to produce insoluble aluminium hydroxide $[Al(OH)_3]$. In the second reaction, alum reacts with fluoride ions present in the water.

Unfortunately, this technique is not preferable as it removes only a smaller portion of fluoride (18 – 33%) in the form of precipitates and converts a greater portion of ionic fluoride (67 – 82%) into soluble aluminium fluoride complex ion, and therefore this technology is erroneous. Also, as the soluble aluminium fluoride complex is itself

toxic, adoption of Nalgonda technique for defluoridation of water is not desirable [1]. Hence, in this work, chemical precipitation technique without using alum is applied to remove fluoride from contaminated water.

4.1.1 Experimental methods

The chemical precipitation experiments were carried out in batch mode. 100 mL of 500 mg/L fluoride solution was taken in a 250 mL conical flask and a measured amount of $CaCl_2$ was added to it. The parameters which affect the extent of chemical precipitation were molar ratio, pH, presence of other ions and performances of different types of calcium salts were studied. After adding $CaCl_2$, the solution was placed in a shaker at 200 rpm for complete mixing for 10 minutes. The samples taken out were centrifuged at 9000 rpm for 30 minutes. The fluoride ion concentration left after precipitation, also called residual fluoride concentration was measured with fluoride ion electrode. The measurement procedure of fluoride ion was described in chapter 3, section 3.1.

4.1.2 Mechanism of fluoride removal

Fluoride is removed by adding an alkali compound such as lime or hydrated lime to adjust the water pH to the point where the fluoride exhibits minimum solubility. Then the precipitated fluoride is removed by a proper solid–liquid separation technique such as sedimentation and filtration [2].

For fluoride removal, lime is added as coagulant. By adding a calcium salt to the water (e.g. lime, calcium chloride), the solubility of CaF_2 is exceeded and fluoride is converted from the aqueous solution into solid crystal. The process includes the following reactions:

$$Ca(OH)_2 \rightarrow Ca^{2+} + 2OH^- \qquad (4.1)$$

$$Ca^{2+} + 2F^{-} \rightarrow CaF_2 \qquad (4.2)$$

Presently, the cheapest way to remove fluoride from water is to produce calcium fluoride (CaF_2) by adding lime or another calcium salt, such as $CaCl_2$. When stoichiometric amount of calcium salt is added to the fluorinated water, precipitation is not occurred satisfactorily. This result is obtained in practice because of high ionic strength, slow nucleation and low pH of the solution. Hence, the amount of calcium salt added often exceeds the stoichiometric amount. The CaF_2 particles are too fine to be sedimented, hence it is very difficult to agglomerate the precipitate and hence the solution is filtered through a microfiltration membrane for total separation.

4.1.3 Performance of chemical treatment method

Effect of molar ratio

Effect of $[Ca^{2+}/F^{-}]$ molar ratio on fluoride removal was illustrated in Figure 4.1. The molar ratio was varied from 0.5 to 3.0. It was observed from the figure that with increase in molar ratio, the residual fluoride concentration was decreasing gradually. When the $[Ca^{2+}/F^{-}]$ molar ratio was 0.5, the residual fluoride concentration of 21.8 mg/L in the solution was observed. The residual fluoride concentration was decreased gradually to 8.7, 6.6, 5.7, 5.5 and 5.6 mg/L with increase in $[Ca^{2+}/F^{-}]$ molar ratio to 1, 1.5, 2, 2.5 and 3 respectively. This indicated that the effective removal of fluoride can be achieved so long as $[Ca^{2+}/F^{-}]$ molar ratio was greater than 2. Further increase in molar ratio did not reduce residual fluoride ion concentration. This was also explained with the help of reaction stoichiometry discussed in 4.1.3. Hence, $[Ca^{2+}/F^{-}]$ molar concentration ratio of 2 was considered for further experiments.

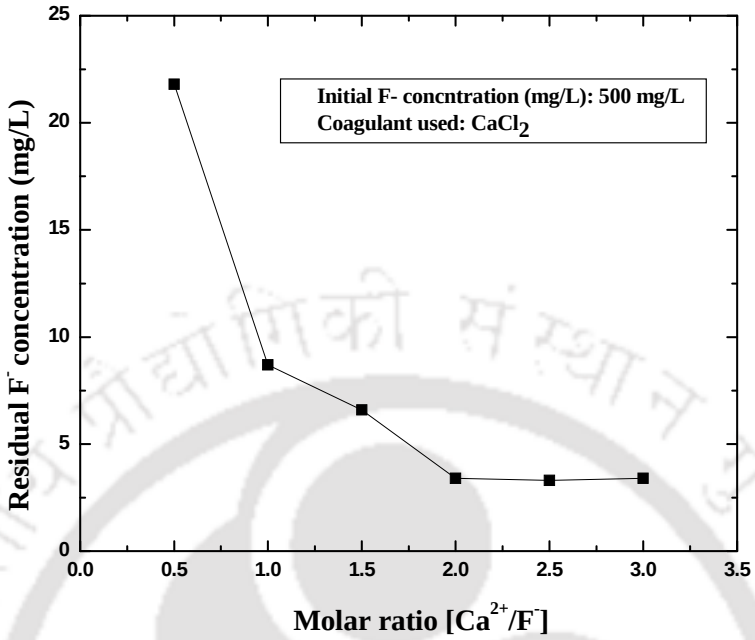

Figure 4.1: Effect of molar ratio on fluoride precipitation

Effect of pH

Solution pH is one of the most important parameter in the chemical precipitation technique. Depending on the pH, different interfacial properties and reaction routes may be found [3, 4]. Effect of pH on fluoride precipitation was shown in Figure 4.2. At extreme acidic pH, (pH 2.6), the residual fluoride concentration was 136 mg/L. With increase in pH, the residual fluoride concentration was decreased. The residual fluoride concentration in solution was in the range of 0.49 to 0.86 mg/L at pH range of 5.2 - 11.1. The defluoridation permissible limit was achieved at pH 6.3 and 11.1. Hence further experiments were conducted at this two pH values. At this pH range, fluoride ion binds with calcium ion completely. At very low pH, incomplete precipitation occurs due to

formation of HF. Again, at very high pH (pH, 11), the residual fluoride concentration was more in solution due to the formation of $Ca(OH)_2$ species.

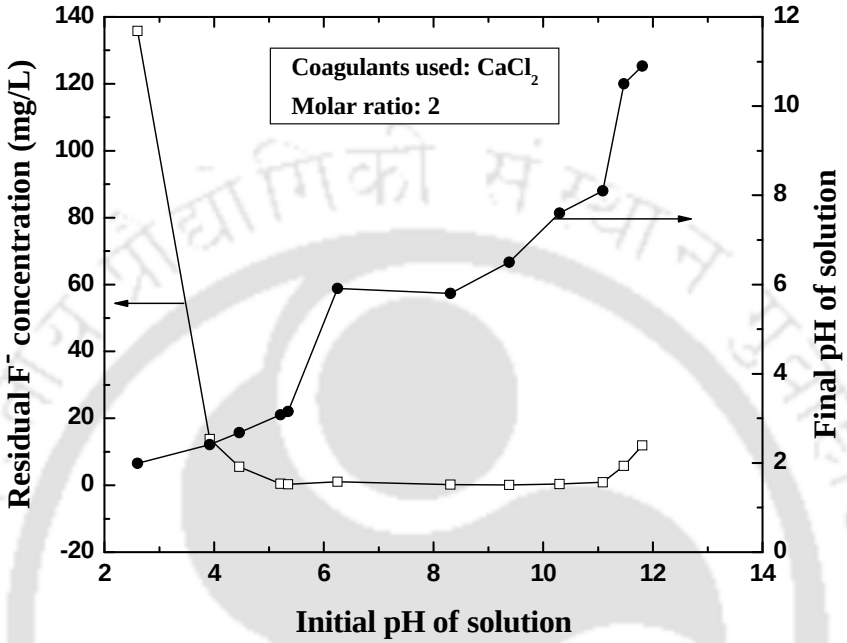

Figure 4.2: Effect of pH on fluoride precipitation

Types of calcium salts

To examine the chemical treatment efficiency, three types of most common calcium salts, $CaCl_2$, $Ca(OH)_2$ and $Ca(NO_3)_2$, were used, respectively to precipitate fluoride ion. The performance of different calcium salts on fluoride precipitation was plotted in Figure 4.3. From the figure, it was observed that the best fluoride removal efficiency was achieved with $CaCl_2$ followed by $Ca(NO_3)_2$ and $Ca(OH)_2$. Hence $CaCl_2$ was chosen as good precipitating agent of fluoride.

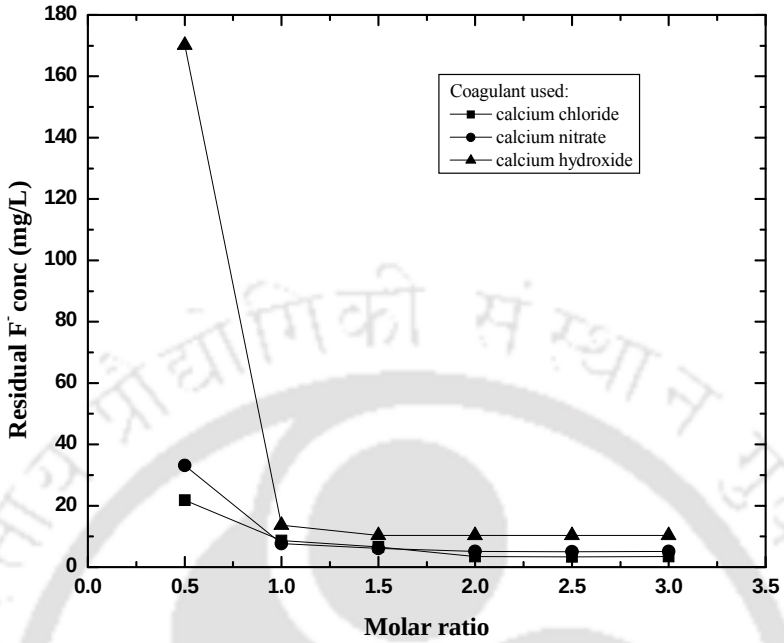

Figure 4.3: Variation of fluoride precipitation for different calcium salts

Effect of presence of co-ions

Various types of salts are present in wastewater apart from fluoride. The most common ions present in fluoride containing wastewater include sulfate, nitrate and phosphate. The effect of these ions on the fluoride precipitation was shown in Figure 4.4. From the figure, it was noticed that residual fluoride concentration was increased with increase concentration of nitrate, sulfate and phosphate from 100 – 500 mg/L. The effect of residual fluoride concentration was more in presence of phosphate as there was strong competition for calcium ion between phosphate and fluoride followed by sulfate and nitrate.

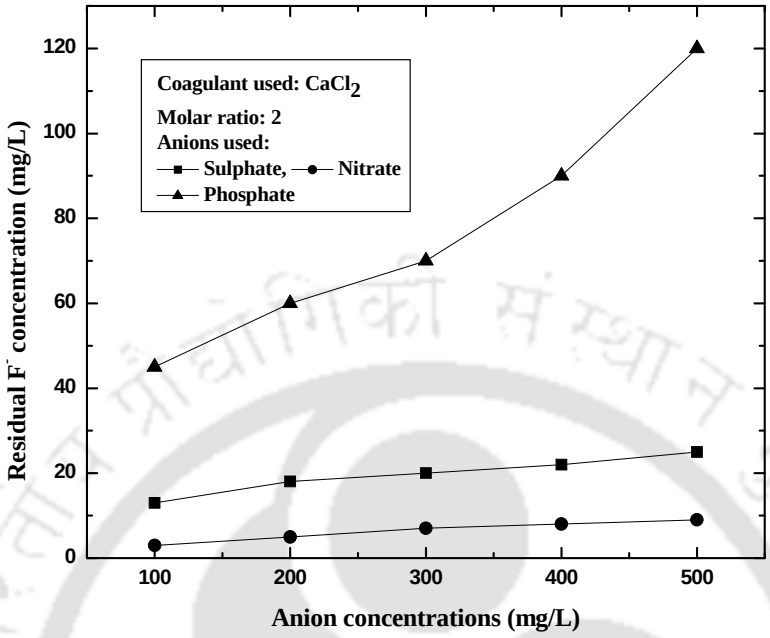

Figure 4.4: Effect of other ions on fluoride precipitation

4.1.4 Characterization of precipitate

In the chemical precipitation technique, a white fine precipitate was obtained and characterized with FESEM, EDX and XRD to confirm that the produced precipitate was calcium fluoride (CaF_2) and the texture of precipitate. The size of the precipitate was analyzed by Laser particle size analyzer (LPSA). From the FESEM picture (Figure 4.5a), it was observed that the precipitate formed were not in regular shape. The composition of the precipitate was confirmed by the EDX shown in Figure 4.5b. The EDX result confirmed that the obtained precipitate contain fluoride along with calcium ion. The XRD was shown in Figure 4.5c. The sharp peaks at 28, 47 and 55 two theta value confirmed that the formed precipitate was calcium fluoride. Figure 4.5d showed the particle size distribution of the precipitate formed during chemical treatment. From the figure it can be

viewed that most of the particles generated during the treatment were in the range of 10 µm with volume % of more than 5. Some of the bigger size particles were also formed due to the agglomeration of fine particles so that particle size distribution had two other nodes, one at 100 µm and the other at 1000 µm with the volume percentage of 1.4 and 2, respectively. This observation undoubtedly supported the agglomeration of precipitates.

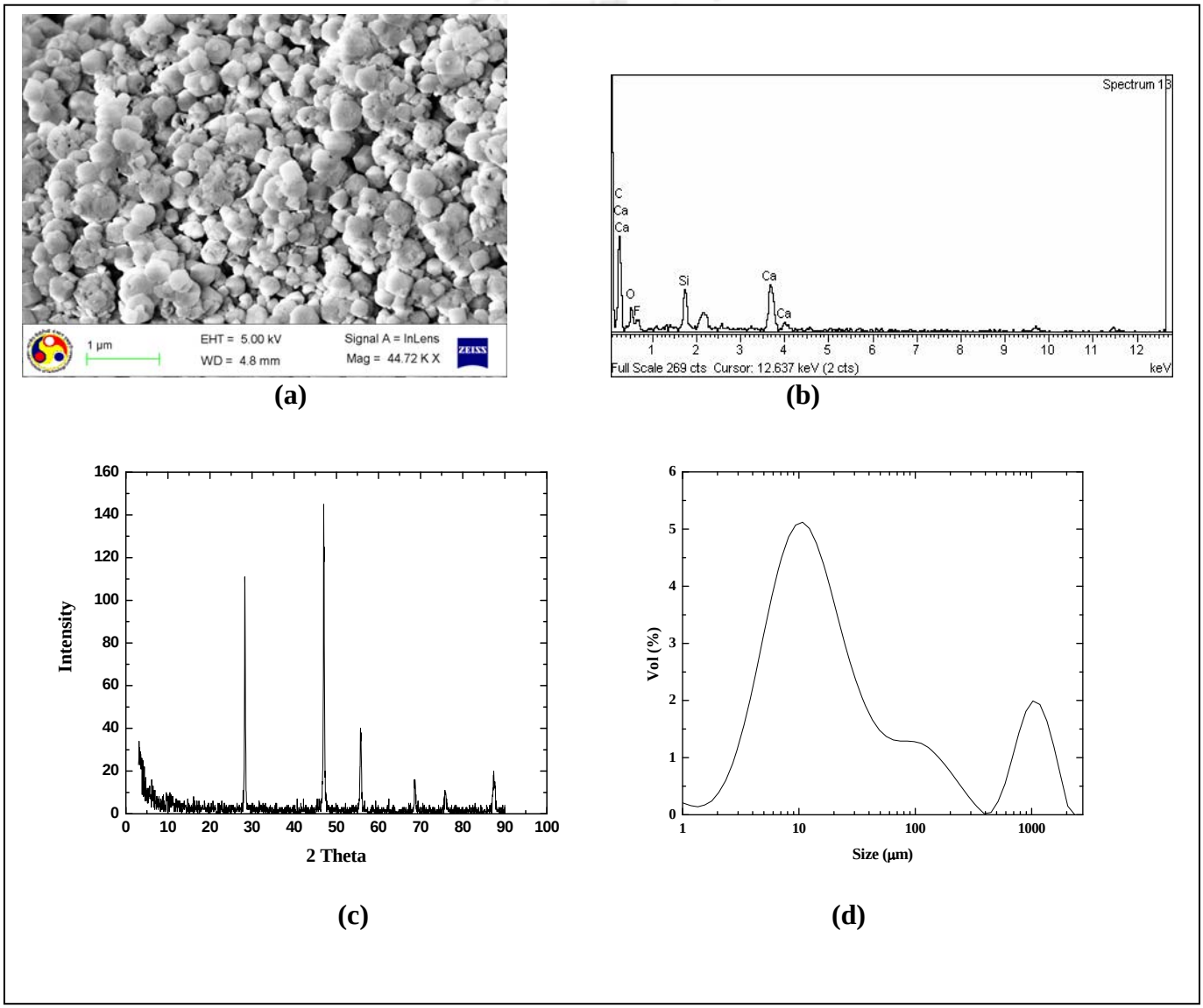

Figure 4.5: Characterization of precipitate formed during chemical precipitation. (a) FESEM picture of precipitate, (b) EDX of the precipitate, (c) XRD and (d) particle size distribution of precipitate.

4.2 Membrane filtration technique

4.2.1. Raw materials

The raw material used in the synthesis of ceramic membrane was tabulated in Table 4.1. Inorganic raw materials such as kaolin, quartz, calcium carbonate, sodium carbonate, boric acid and sodium metasilicate were used to synthesize ceramic membrane. Different raw materials used in this work for the fabrication of inorganic membrane serve for different functional attributes. Kaolin provides low plasticity and high refractory properties to the membrane. Quartz contributes for mechanical and thermal stability of the membrane. Regulation of porous texture in the ceramic is realized by calcium carbonate which under sintering conditions would dissociate into CaO and release CO_2 gas. The path taken by the released CO_2 gas thereby creates the porous texture of the inorganic membrane and contributes to the membrane porosity during the sintering process. On the other hand, sodium carbonate and boric acid acts as a colloidal agent and improves dispersion properties of the inorganic precursors thereby addressing homogeneity in the membrane structure. Boric acid also increases membrane mechanical strength by the formation of metallic metaborates at sintering temperatures. In a similar way, sodium metasilicate acts as binder by creating silicate bonds among the elements to induce higher mechanical strength in the ceramic membrane [5, 6]. Kaolin and sodium metasilicate are obtained from CDH India. Quartz is collected from Research Lab Fine Chem Industry, India. All other inorganic precursors such as calcium carbonate, boric acid, sodium carbonate are obtained from Merck, India. All these raw materials used for inorganic fabrication are graded at least 99.5% pure and used without further purification.

Table 4.1: Composition of ceramic microfiltration membrane

Material	Composition (wt%)	Sources
Kaolin	40	CDH, India
Calcium carbonate (calcite)	25	MERCK, India
Quartz	15	Research-Lab Fine Chem Ind, India
Sodium carbonate	10	MERCK, India
Boric acid	5	RANBAXY, India
Sodium meta silicate	5	GSC Lab Testing & Allied Ind, India

4.2.2. Membrane preparation

The membrane fabrication process is initialized by thorough mixing of dry inorganic raw materials (Table 4.1) followed by addition of distilled water to prepare a paste. The paste is then cast over gypsum in the shape of a circular compact disk using a SS316 ring of 55 mm inner diameter and 5 mm thickness. Subsequently, the ring is carefully removed and the paste is kept under distributed pressure of 2 kg for 24 hrs to prevent the propagation deformation and drive homogeneity in the inorganic matrix. The paste is then subjected to two different sequential heat treatment steps. Firstly, the circular mold is dried at room temperature for 24 hrs. After that it is dried at 100°C for 12 hrs in a hot air oven followed by drying at 250°C for 24 hrs. During the transition from 100°C to 250°C, low heating rate is maintained in order to eliminate the induction of thermal stresses generated due to loss of moisture. The second heat treatment step involves the heating of the membrane from 250°C to desired sintering temperature at a heating rate of 2°C/min. Then the membrane is kept for 5 hrs for sintering. Sintering of

membranes at 950°C are done. Subsequent cooling of the membrane is conducted by atmospheric cooling procedure adopted by switching off the muffle furnace that is previously maintained at desired sintering temperature. After sintering, membranes achieved hard, rigid and porous texture. Finally, the fabricated membrane is polished with silicon carbide abrasive paper (C-220) to obtain a smooth, flat micro-filtration membrane of diameter 52.5 mm and thickness 4.5 mm. Figure 4.6 represents the schematic for the membrane preparation procedure.

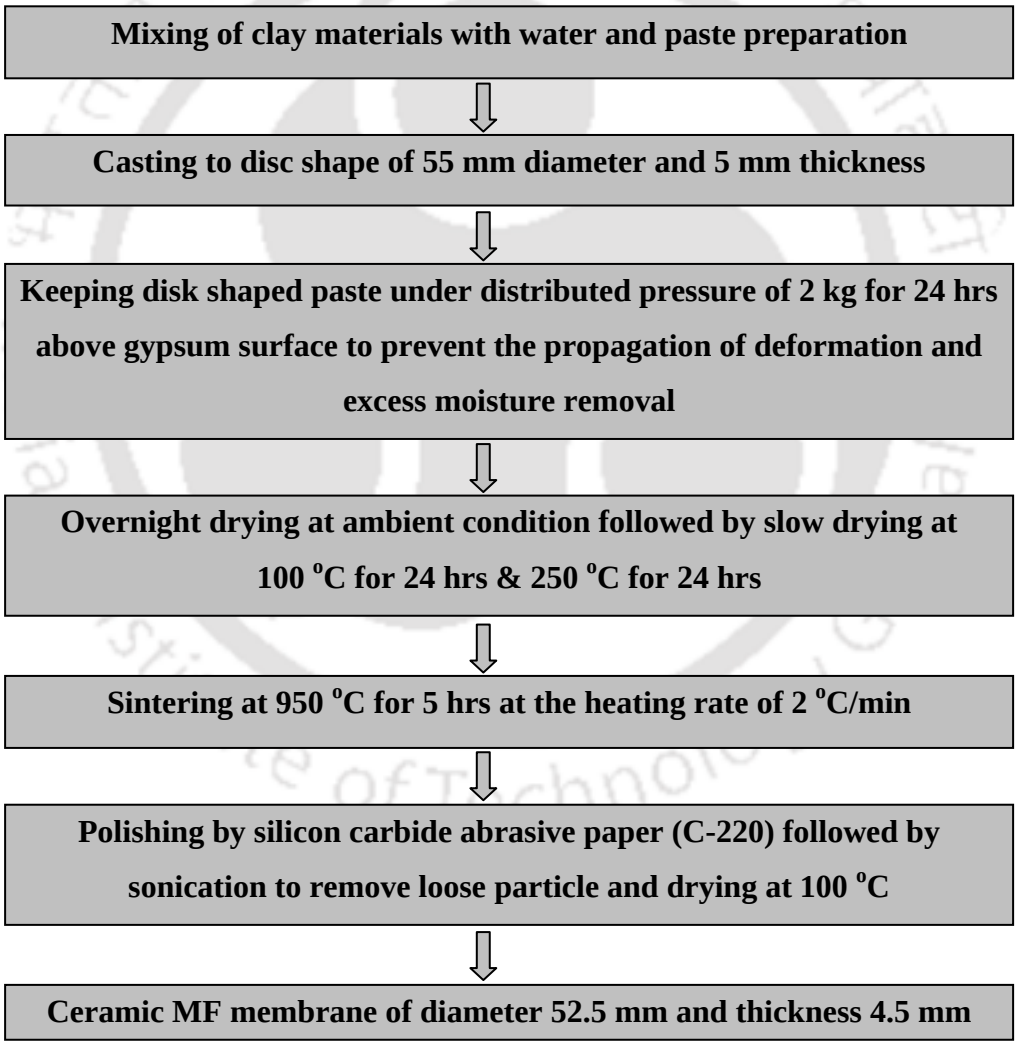

Figure 4.6: Schematic representation of the membrane preparation procedure

4.2.3 Characterization techniques

Structural characterizations

The structural characterization of membranes involves thermogravimetric analysis (TGA), differential thermal analysis (DTA), X ray diffraction analysis (XRD), morphological study using scanning electron microscope (SEM), total porosity determination, structural density measurement and evaluation of pore size distributions from SEM images.

Thermogravimetric analysis

TGA and DTA (*Make: Mettler Toledo, USA; Model: TGA/SDTA 851^e*) of the sample mixtures were conducted to identify the temperature regimes where predominant weight losses (and hence transformations) occur in the membrane. Thereby, an insight could be gained to analyze the effect of various temperature regimes on the porous structure, pore diameter and mechanical strength of the membrane. TGA and DTA were carried out by heating the dry inorganic powder mixture in a α - alumina crucible from room temperature to 1000^{o}C at a heating rate of 10^{o}C per minute.

XRD analysis

XRD analysis was conducted to evaluate the extent of different phase transformations that occurred during sintering.

Surface morphology

Membrane morphological studies were carried out using SEM (*Make: Oxford, UK; Model: LEO 1430VP*) to analyze the presence of possible defects and estimate the membrane pore size. The estimation of average membrane pore size (d_s) and pore size distribution from SEM micrographs was carried out using ImageJ software (Version

1.40). Individual pore diameters were measured for about 500 pores using ImgeJ software for different pores visible in the SEM [7]. Since pore size distribution and average pore size distribution values are critically dependent on the sampling procedure, five SEM pictures were evaluated using the software. These micrographs were taken randomly from the selected sections of the membranes in order to obtain pore size distributions representing the existing porous texture of the membrane. The area average pore diameter (d_s) from SEM analysis of the membrane was evaluated by assuming cylindrical porous texture of the membrane as;

$$d_s = \left[\frac{\sum_{i=1}^{n} n_i d_i^{\,2}}{\sum_{i=1}^{n} n_i} \right]^{0.5} \qquad (4.3)$$

Where, n is the number of pore, d_i is the pore diameter (μm) of i^{th} pore.

Porosity and structural density

The total porosity of the membrane was estimated using Archimedes principle. The experimental procedure involved the measurement of the volume of the wetting liquid that displaced air in a dry membrane after equilibrating the membrane with water for 12 hrs. Total porosity (ε_m) and structural density (ρ_{mem}) of the membrane were estimated using the following equations [8]:

$$\varepsilon_m(\%) = \left[\frac{w_1 - w_2}{\rho_{water}} \right] \times \frac{100}{v_{mem}} \qquad (4.4)$$

$$\rho_{mem} = \frac{w_2}{v_{mem}} \qquad (4.5)$$

Permeation characterizations

Experimental set up

A schematic of experimental set up used for water permeation experiment is presented in Figure 4.7. The set up constitutes a Teflon tubular cell of 125 mL capacity with a flat circular teflon base plate that holds the ceramic membrane. The membrane was kept in the teflon casing and sealed with epoxy resin (*Mseal, Pidilite Industries Ltd, Mumbai, India*). During air permeation experiments, the outlet of the setup was connected to a gas flow meter using a silicon tube for measuring the gas flow rate at various trans-membrane pressure differentials. During liquid permeation experiments, the feed (de-ionized water) was filled in the tubular section from the top. The cell was pressurized with compressed air. The outlet of the setup was disconnected from the gas flow meter and liquid permeate was collected in a beaker. Liquid permeate flux was measured using a digital weight machine.

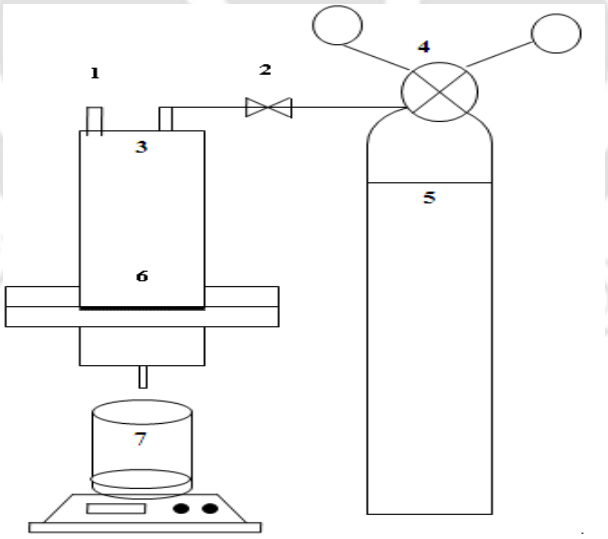

Figure 4.7: Experimental set up used for water permeation experiment

1: Feed inlet, **2:**Valve, **3:** Membrane cell, **4:** Regulator, **5:** Compressed air cylinder, **6:** Membrane, **7:** Permeate collector

Liquid permeation characteristics

Permeation experiments using pure water (deionised water) were carried out for the determination of the hydraulic permeability (P_m) and hydraulic pore diameter (d_l) of the membrane. The permeation tests involve the measurement of permeate liquid volume as a function of time at specific values of trans-membrane pressure drop (ΔP). The liquid flux was measured at an interval of 10 seconds to verify the variation of flux with time. These experiments were performed until the total liquid permeate collected was 80 mL at a specific pressure differential. Physical observations during liquid permeation tests confirmed that the flow rate did not vary during the 10 second intervals. All permeation experiments were conducted at a temperature of 25°C. Before conducting liquid permeation experiments, the membranes were compacted at ΔP of 310 kPa. These pressures were higher than the maximum operating pressure during experiments. Membrane compaction was carried out to obtain steady pure water flux through the membrane. The hydraulic permeability (P_m) and hydraulic pore radius (d_l) of the membranes were evaluated by assuming presence of cylindrical pores in the membrane matrix using the following expressions [9, 10]:

$$J_W = \frac{Q}{S.\Delta t} = \frac{\Delta P}{\mu_w}\frac{\varepsilon_m d_l^{\,2}}{32 l_m} = P_m \times \Delta P \qquad (4.6)$$

$$P_m = \frac{\varepsilon_m d_l^{\,2}}{32 \times l_m \times \mu_w} \qquad (4.7)$$

$$d_l = \left[\frac{32 \times \mu_W \times l_m \times P_m}{\varepsilon_m}\right]^{0.5} \qquad (4.8)$$

In equation (4.7), $\varepsilon_m d_l^2$ corresponds to effective permeable area factor that determines the actual permeable area available during filtration.

Chemical stability

All membranes were tested for their corrosion resistance using NaOH solution (pH 12.5) and HCl (pH 2) solution. The chemical resistance of the membrane was measured by measuring its weight after leaving the membrane in contact with the above solutions for seven consecutive days at atmospheric conditions and evaluating the net weight loss after drying the membrane. Further, porosity measurements before and after acid or alkali treatment were conducted in order to verify any change in the porosity when the membrane was exposed to corrosive environment. Energy Dispersive X- ray (EDX) analysis of the membranes before and after corrosion test was carried out to verify any change in elemental composition.

Characterization results

Characterization of clay materials

Major constituents of kaolin are alumina silicates with the following chemical composition (by wt %) SiO_2: 46.5 %, Al_2O_3: 39.5 % and H_2O: 14 %. Spectrum obtained from XRD analysis (*Make: Bruker Axs, USA; Model: D8 ADVANCE*) of kaolin is illustrated in Figure 4.8. The XRD spectrum was matched with the JCPDS [11] data base file (PDF-01-089-6538) which conveyed that the kaolin used in our work is ideal kaolinite ($Al_2Si_2O_5(OH)_4$). Particle size distribution (*Make: Malvern, USA: Model:*

Mastersizer 2000) of major inorganic materials such as kaolin, feldspar, calcium carbonate and quartz used for the membrane fabrication process are shown in Figure 4.9. From the figure, it can be observed that particle size varied from 18.67 - 0.224 μm for kaolin, 240 - 0.479 μm for feldspar, 16.257 - 0.296 μm for calcium carbonate and 37.24 - 1.18 μm for quartz. The average particle size of kaolin, feldspar, calcium carbonate and quartz were 2.37, 36.32, 4.108 and 8.4 μm, respectively.

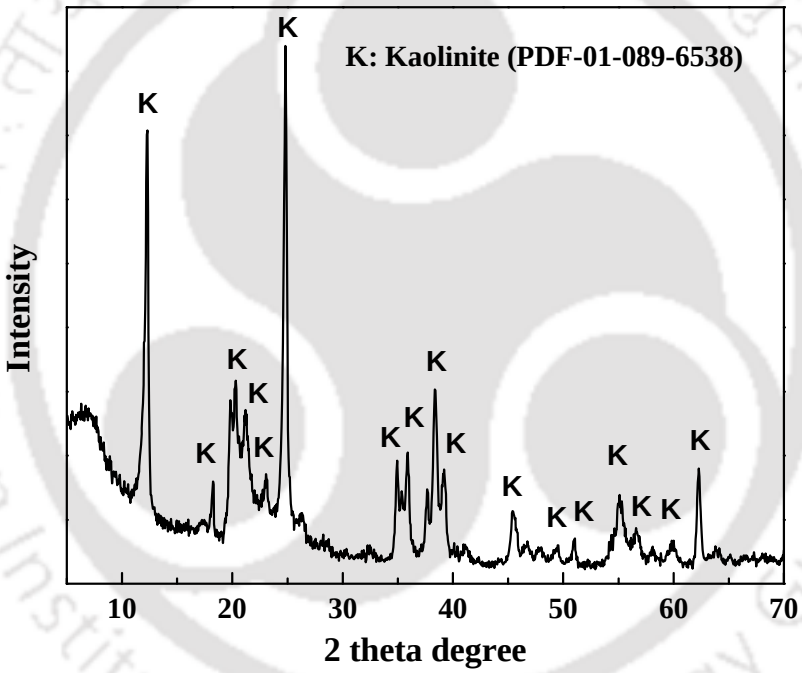

Figure 4.8: XRD diagram of kaolin powder

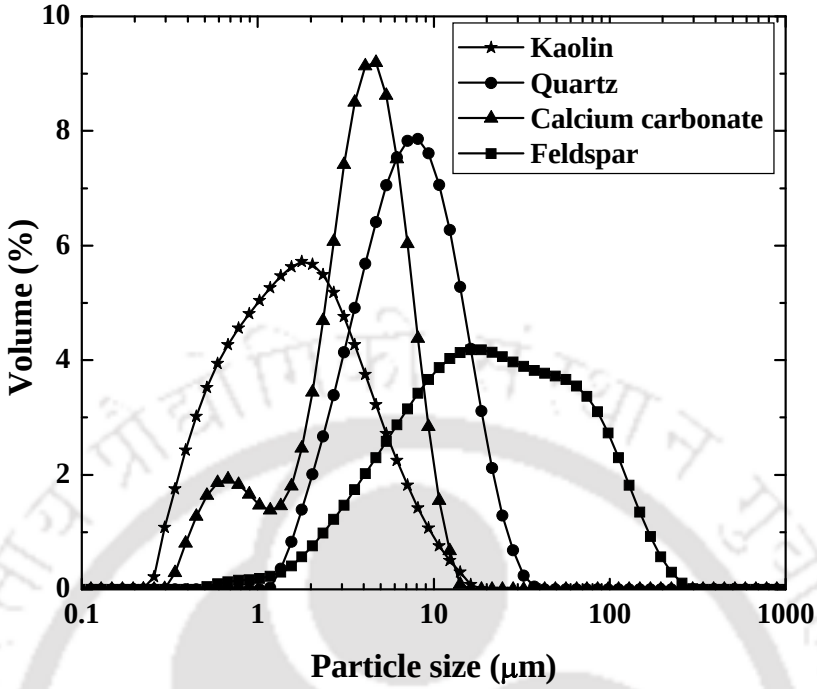

Figure 4.9: Particle size distribution for kaolin, quartz, $CaCO_3$ and feldspar

Structural characterization of membranes

Thermogravimetric analysis

Results obtained from TGA and DTA analysis are presented in Figure 4.10. The figure conveys that a highly non-linear variation exists in weight loss due to the presence of complex phase transformations and interactions. The total weight loss of the sample was observed to be about 28.5 %. About 2.5 % weight loss was observed below 105 ^{o}C due to the removal of weakly bonded water molecules in the sample mixture. This specific water loss was characterized by an endothermic peak at 105^{o}C in the DTA curve. The weight loss of the sample between 105 – 400 ^{o}C was around 4 %, which can be correlated with the pre-dehydration of kaolin and crystal water of boric acid. The pre-

dehydration process of kaolin takes place due to the reorganization of the octahedral layer and it first occurred at the OH of the surface [12]. The second endothermic peak in the DTA curve corresponds to the loss of structural hydroxyl groups at 513^{o}C. This was due to the transformation of kaolinite to metakaolinite according to the following reaction [13]:

$$Al_2O_3.2SiO_2.2H_2O\,(\text{kaolinite}) \rightarrow Al_2O_3.2SiO_2\,(\text{metakaolinite}) + 2H_2O \qquad (4.9)$$

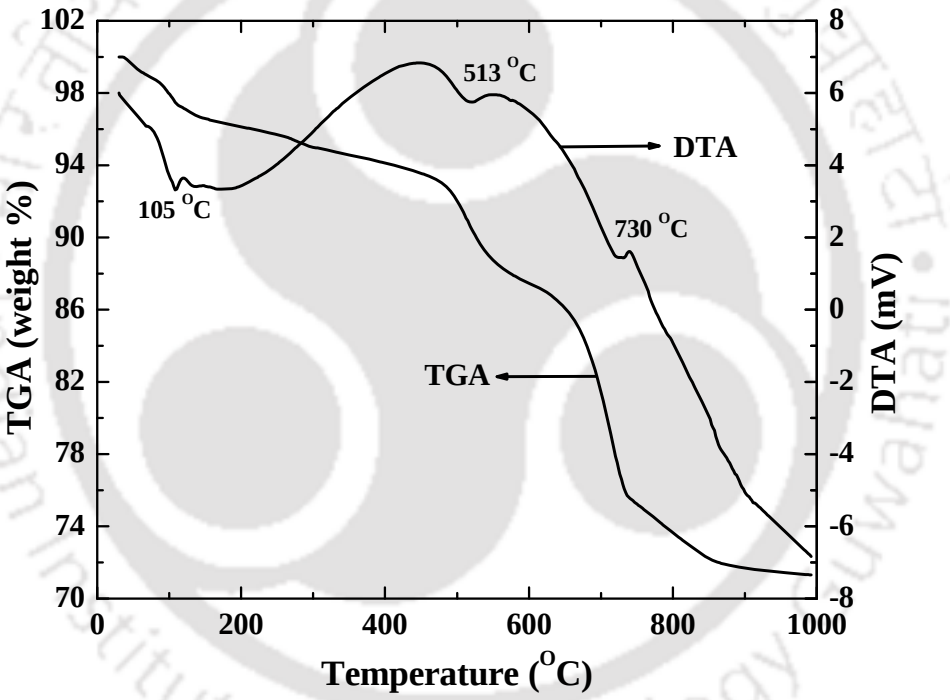

Figure 4.10: TGA-DTA curve of membrane powder

The formation of CO_2 (and hence enhancement of the porous structure of the membrane) occurred at 730 ^{o}C with a corresponding weight loss of 10 % in the temperature regime of 663 ^{o}C to 745 ^{o}C. This was due the calcination of $CaCO_3$ in this temperature regime. Calcinations of Na_2CO_3 started at temperature 800^{o}C and ended in temperature 843 ^{o}C

which corresponds to very minute loss of mass in the TGA curve. The sample corresponded to very insignificant weight loss above 843 ^{o}C as conveyed by the TGA curve. This result infers that minimum sintering temperature for the membrane fabrication should be above 843^{o}C. These observations further justified that all phase transformations were complete well below the chosen sintering temperature ranges (850 – 1000 ^{o}C). Hence, high sintering temperatures (more than 1100 ^{o}C) as presented in various works [14, 15, 16] were not required for the preparation of membranes using the chosen inorganic precursor formulations.

Phase characterization by XRD analysis

From the TGA - DTA analysis it was observed that above sintering temperature of 843^{o}C, almost no significant weight loss occurred. To verify this hypothesis, XRD analysis of membrane structure at temperatures higher than 843^{o}C was carried out. Figure 4.11 summarize XRD graphs for four different samples calcined at 25, 850, 900 and 1000^{o}C for 5 hrs in muffle furnace. The observation of peaks and trends in the XRD graphs of the figure conveyed that the inorganic mixture originally consisted of kaolinite, quartz and inyoite as main components. The XRD graph obtained for the sample calcined at 850 ^{o}C depicted that peaks corresponding to kaolinite disappeared due to conversion of kaolinite to metakaolinite. In this regard, it could be pointed out that the formation of metakaolinite was illustrated by TGA-DTA curve trends at a temperature of 513^{o}C. The other phases that appear are nephiline and quartz. Nephiline (Na_2O, Al_2O_3, $2SiO_2$) was produced by the reaction of sodium oxide (Na_2O) and metakaolinite at temperature of 800 ^{o}C [17]. A critical observation of the peaks at higher temperature revealed that no other significant phase transformation occurred above 850^{o}C to 1000^{o}C. This inferred

that the membrane skeletal structure constitutes mainly metakaolinite, quartz and nephiline. From the XRD analysis, it was concluded that a sintering temperature of 850^{o}C was sufficient for preparing the membranes. All XRD diffractogram graphs indicate no change in the peak trends corresponding to quartz, thereby inferring that quartz phase was not at all affected by sintering of inorganic materials within the temperature considered in this work. Therefore, the sintering temperature above 850^{o}C considered in this work was justified. Hence, the membrane used for this study was prepared at 950^{o}C.

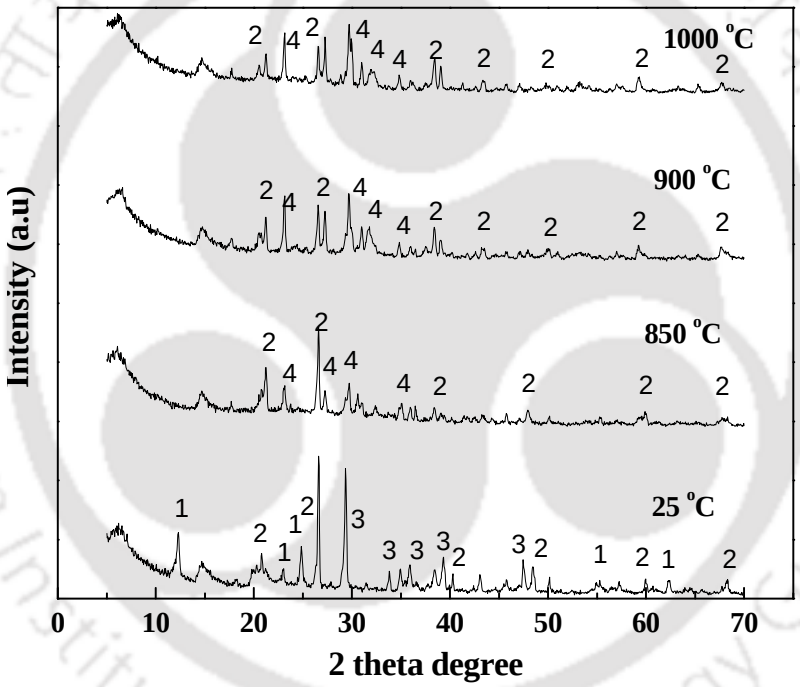

1: Kaolinite (PDF- 01-089-6538) **2**: Quartz (PDF-01-075-0443)

3: Inyoite (PDF-00-006-0361) **4**: Nephiline (PDF-00-019-1176)

5: Hydrogen Borate (PDF-00-022-1109) **6**: Sodium Calcium Silicate (PDF-00-002-0951)

Figure 4.11: XRD patterns of membrane powder at various sintering temperatures

Surface morphology

Result obtained from SEM analysis for membranes sintered at 950^{o}C temperature is shown in Figure 4.12. As observed in the figure, the ceramic substrates sintered at 950^{o}C were more consolidated due to the fact that sintering temperatures over 900^{o}C enabled greater agglomeration of particles to yield more dense structure. Due to this reason, the porosity of the membrane reduced with an increase in sintering temperature. An overall observation of the image shows that, for all the membranes maximum number of pores were within the range of 0.3 - 0.6 μm. A superficial observation of the SEM indicated that the membrane did not have any pinholes cracks and the maximum observable pore size of the surface is about 5 μm. These attributes of the membrane make it suitable for MF applications.

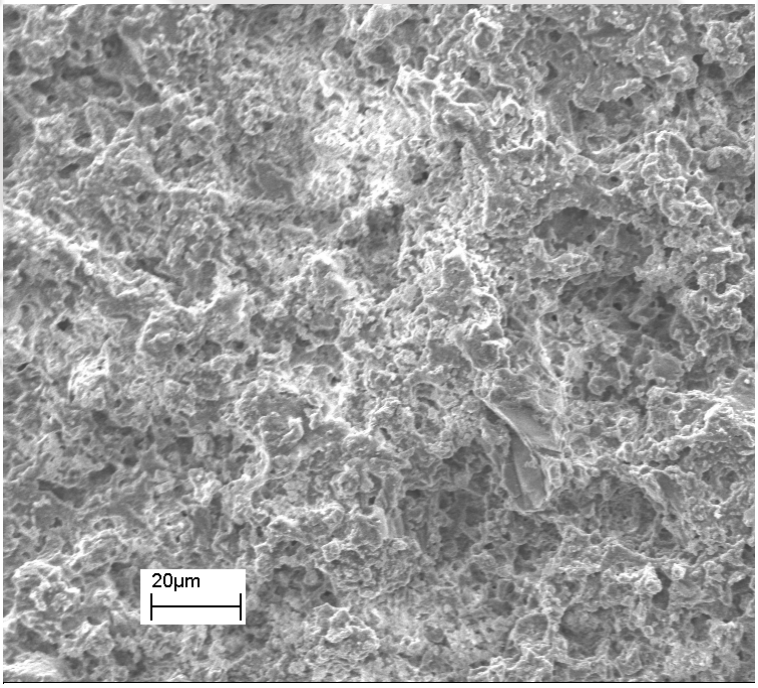

Figure 4.12: Top surface SEM images of prepared membrane at 950^{o}C sintering temperature

Pore size analysis based on SEM

Pore size distribution of the membranes obtained form SEM image analysis are shown in Figure 4.13. The average pore diameters of membranes were evaluated using equation 4.3 and found that the average pore diameter is 0.70 μm.

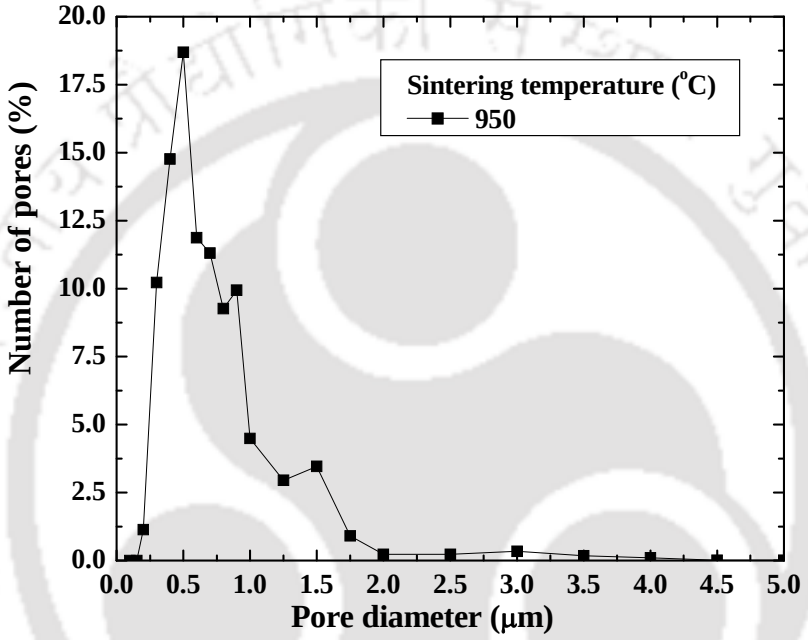

Figure 4.13: Pore size distributions (based on SEM) of prepared ceramic membranes at 950°C

Porosity and structural density

The variation of membrane porosity and structural density of membrane with varying sintering temperature are shown in Figure 4.14. From the figures it can be observed that structural density of the membrane increased with an increase in sintering temperature. However, the total porosity reduced with increasing sintering temperature. The porosity decreased from 42 - 33 % where as structural density increases from 1260 -

1360 kg/m^3 with an increase in sintering temperature from 850 - 1000^{o}C. When the sintering temperature was increased to 950^{o}C, porosity of the membrane decreased to 19.5 % where as structural density increased to1540 kg/m^3. This was due to the reason that higher sintering temperatures enable densification of the porous structure to enhance structural density and reduce membrane porosity. This was also reasoned with the fact that with increasing sintering temperature, the number of pores representing small pore sizes reduced and hence the overall pore volume and porosity decreased.

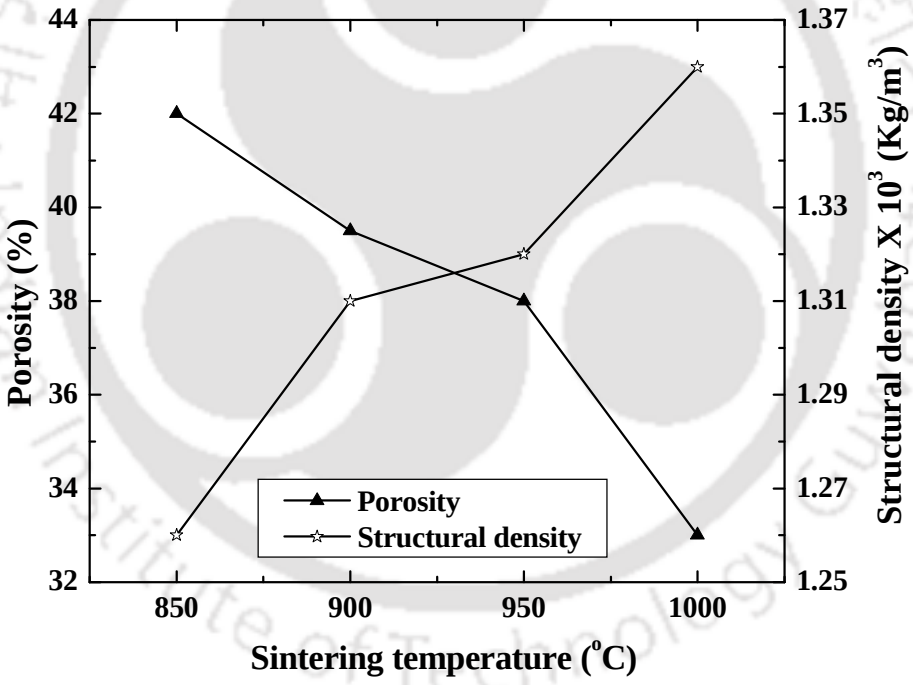

Figure 4.14: Variation of membrane porosity and structural density with varing sintering temperatures

Permeation characterization of membranes

Membrane compaction

The compaction profiles for different membranes prepared in this work are shown in Figure 4.15. From the figure, it can be observed that the PWF was initially high and declined gradually to reach a steady state value after 60 - 90 minutes. The reduction in PWF was due to the fact that the walls of the pores become closer, denser and uniform during compaction [18]. For the prepared membrane, the observed pure water flux at the beginning of compaction was 6.4×10^{-4} $m^3/m^2.s$ which subsequently reached to a steady state value of 5×10^{-4} $m^3/m^2.s$.

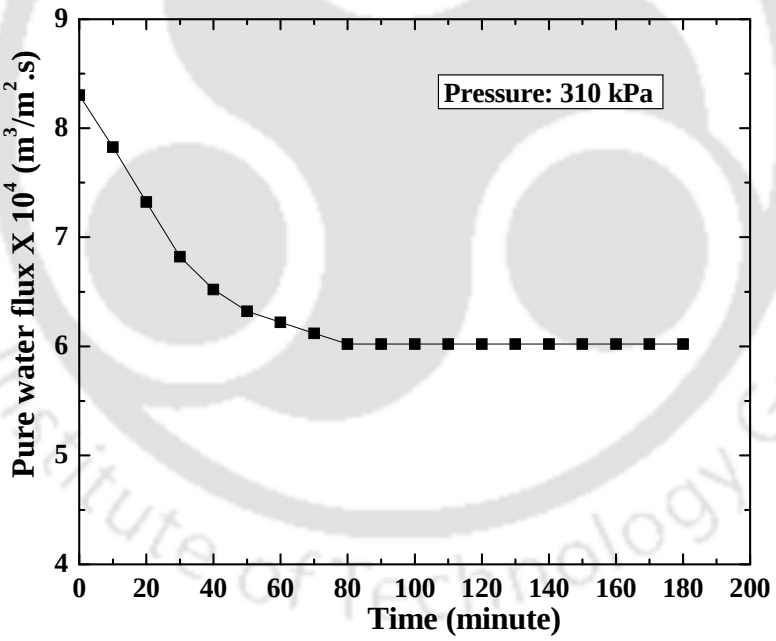

Figure 4.15: Variation of pure water flux with time during compaction study

Chemical stability

It was observed that the weight loss of membranes during chemical stability tests was not significant and was less than 4 % for all membranes. However, a maximum increase of 8 % in membrane porosity was observed for all membranes after both HCl and NaOH tests. Results obtained from EDX analysis is Tabulated in Table 4.2.

Table 4.2: EDX analysis of the synthesized membrane before and after corrosion test

Elements	Membrane (wt %)	Membrane after acid corrosion test (wt %)	Membrane after base corrosion test (wt %)
Oxygen	49.24	48.55	50.26
Sodium	7.96	7.21	8.43
Aluminum	11.84	12.60	11.32
Silicon	14.82	16.45	14.43
Calcium	16.14	15.19	15.56

It can be inferred from the table that the elemental composition of the membrane remains unchanged after acid and basic treatment. The observed trends in weight loss and EDX analysis during corrosion tests convey that the membranes possessed excellent corrosion resistance and are suitable for MF applications involving acidic and basic media.

4.2.4 Fluoride removal by microfiltration membrane

The experimental condition of fluoride removal by MF membrane is tabulated in Table 4.3.

Table 4.3: Experimental condition of fluoride removal by MF membrane

Parameters	Values
Pressure (kPa)	0 - 28.95
Initial fluoride concentration (mg/L)	5, 10
Time (min)	60
Temperature (^{o}C)	25

The variation of fluoride removal % separated by MF membrane directly was shown in Figure 4.16. From the figure, it was concluded that fluoride removal % was maximum for initial 5 minute in case of 10 mg/L and thereafter it was decreasing. This was due to the fact that the MF membrane used for fluoride separation was act as an adsorbent. Since the membrane contains Ca ion in its composition, initially that Ca ion binds with fluoride forming calcium fluoride and hence its concentration was decreasing initially. With time, Ca ion present in the membrane was saturated with fluoride; fluoride ion rejection was decreasing with time. Hence it was concluded that fluoride ion was not successfully separated by MF membrane as the size of the ion is also very small, about 0.133 nm. The flux of the membrane was almost constant after the separation experiment. It was clearly observed from Figure 4.17.

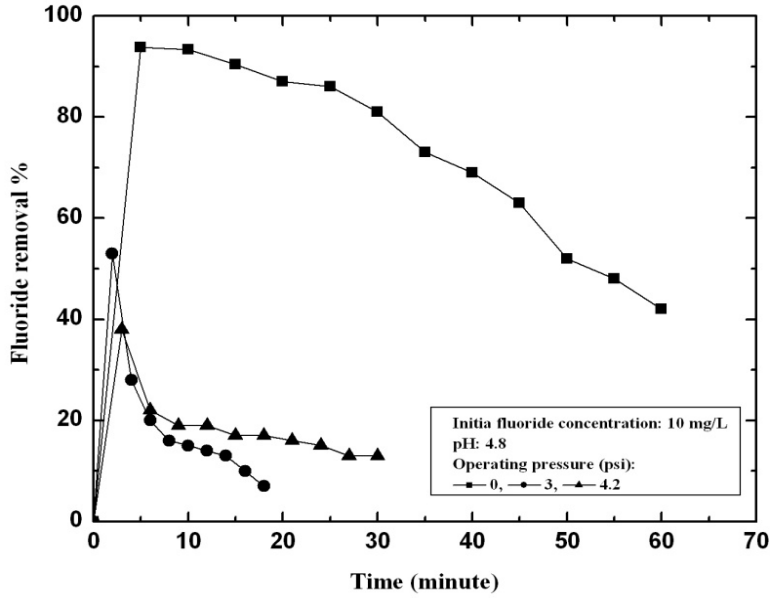

(a)

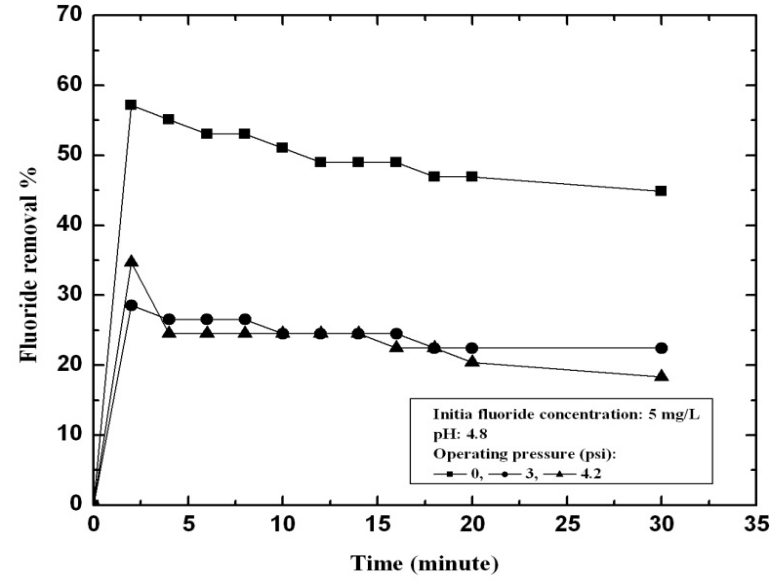

(b)

Figure 4.16: Fluoride removal by MF membrane (a) 10 mg/L initial fluoride solution (b) 5 mg/L initial fluoride solution

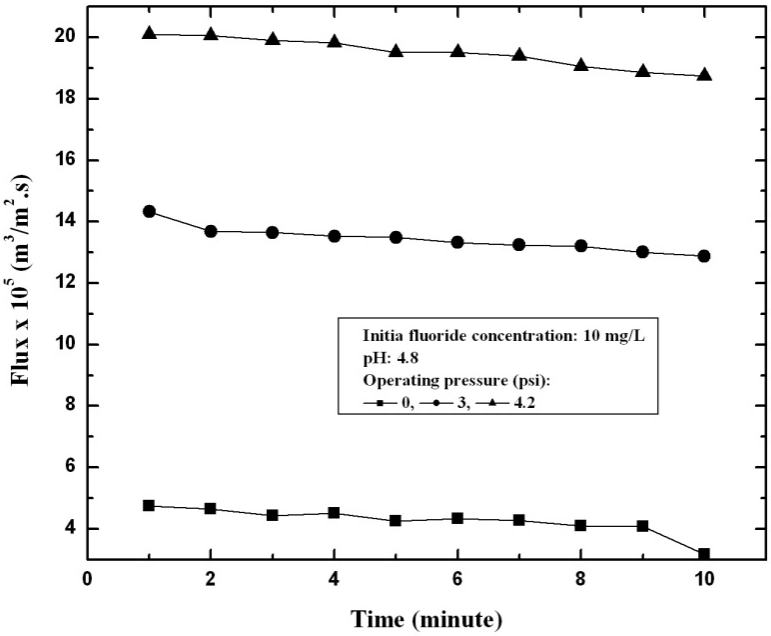

Figure 4.17: Variation of permeate flux with time during the MF technique

4.3 Chemical treatment followed by microfiltration

This section deals with the hybrid process adopted for the effective separation of fluoride contamination from drinking water using chemical precipitation followed by microfiltration. During precipitation, the precipitate obtained was very fine and due to its small particle size, it took longer time to settle down. Hence separation of such small precipitate was a major drawback. With the help of MF membrane prepared in the laboratory, it was easy to separate such fine precipitate. Hence a hybrid technique of chemical precipitation followed by microfiltration is applied to treat the fluoride contaminated water.

In this section, the applied aspect of the proposed combination method is verified with fluoride contaminated water. The contaminated water was first treated in a batch chemical precipitation process. The treated water along with the fine precipitate was then passed through a MF unit for further treatment. The schematic representation of the hybrid process is shown in Figure 4.18.

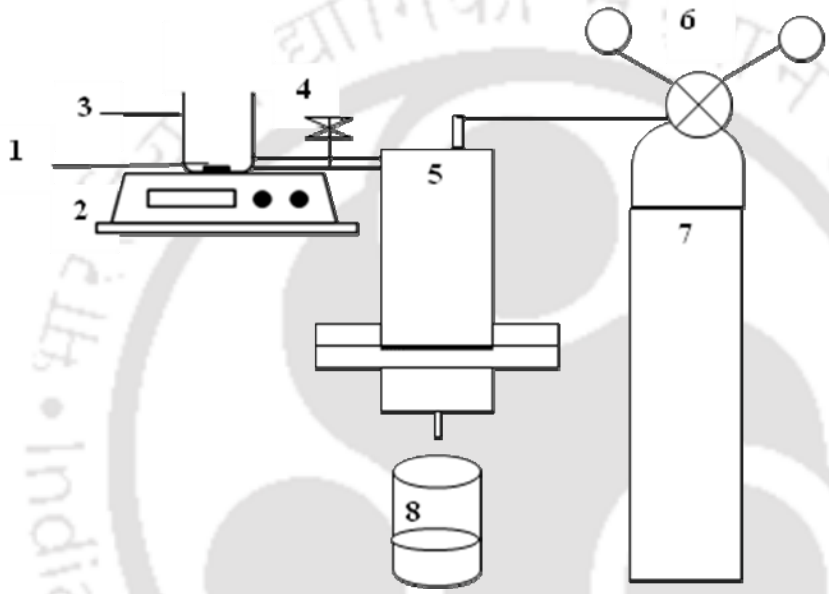

Figure 4.18: Schematic figure of combination technique

1: Magnetic needle; 2: Stirring plate; 3: Precipitation bath; 4: Outlet; 5: Membrane cell; 6: Regulator; 7: Compressed air cylinder; 8: Permeate collector

4.3.1 Experimental procedure

The chemical precipitation experiments were carried out in a batch mode. A 100 mL of 500 mg/L fluoride solution was taken in a 250 mL conical flask and a measured amount of $CaCl_2$ was added to it. The effects of parameters which affect the chemical precipitation technique were molar ratio, pH, presence of other ions and effects of

different types of calcium salts were studied. After adding $CaCl_2$, the solution was placed in a shaker at 200 rpm for complete mixing for 10 minutes. The outlet of the precipitation technique was introduced into the membrane cell. The ceramic membrane prepared by paste method sintered at 950^oC was used in the MF cell. The membrane cell was pressurized by N_2 gas upto 28.95 kPa. During the experiments the pressure was kept constant and after every 5 min interval, the permeate was collected and the flux (J) was measured using following equation.

$$J = \frac{Q}{A \times t} \qquad (4.9)$$

Where Q is the volume of permeate, A is the effective membrane area and t is the time of permeation. Permeate conductivity, pH and concentrations of fluoride was measured to ensure water quality for drinking purpose.

4.3.2 Experimental results of hybrid technique

Removal performance of fluoride

This subsection elaborately discusses the performance of the hybrid process for the treatment of fluoride contaminating water. The chemical treatment followed by MF experiment was conducted with conditions mentioned in section 4.3.1. The performance of chemical precipitation and MF was analyzed separately in terms of removal efficiency of fluoride, conductivity and pH of the treated water. Table 4.4 clearly shows the experimental observation of percentage removal of fluoride during chemical precipitation.

Table 4.4: Removal performance of fluoride by hybrid technique

Transmembrane pressure (0 kPa)		Transmembrane pressure (20.68 kPa)		Transmembrane pressure (28.95 kPa)	
Time (minute)	**Fluoride concentration (mg/L)**	**Time (minute)**	**Fluoride concentration (mg/L)**	**Time (minute)**	**Fluoride concentration (mg/L)**
0	0.86	0	0.86	0	0.86
5	0.86	3	0.86	1	0.86
10	0.87	6	0.82	2	0.81
15	0.86	90	0.80	3	0.82
20	0.82	12	0.83	4	0.85
25	0.8	15	0.85	5	0.86
30	0.82	18	0.81	6	0.86

It was observed from the table that no significant change in residual fluoride concentration was observed during the separation process.

Permeate flux profile after MF experiments

The suspended solution was subjected to microfiltration at conditions mentioned in section 4.3.1. Permeate flux and quality was measured and analyzed. Figure 4.19 shows the permeate flux profile during MF. It was observed that the permeate flux was declined with time for all the operating pressure differentials. For an example at 0 kPa pressure, the permeate flux was declined from 7.4×10^{-6} to 3.9×10^{-6} $m^3/m^2.s$ at the end of 3.5 minutes of MF experiment. The similar trend was also noticed for the experiments operated at 20.68 and 28.95 kPa. In such cases the flux was declined from 1.6×10^{-4} to 1.01×10^{-4} $m^3/m^2.s$ and from 2.5×10^{-4} to 1.3×10^{-4} $m^3/m^2.s$, for the transmembrane

pressure differentials of 20.68 and 28.95 kPa, respectively. It can be found that at higher pressure differentials, the flux declination was more. The decline in flux with time is due to the fact that the deposition of suspended particles over the membrane surface restrict the permeate flux by blocking the active pores of the membranes. With time amount of particle deposition becomes more which causes the lower permeate flux. Again, increase in permeate flux with pressure is due to the more driving force.

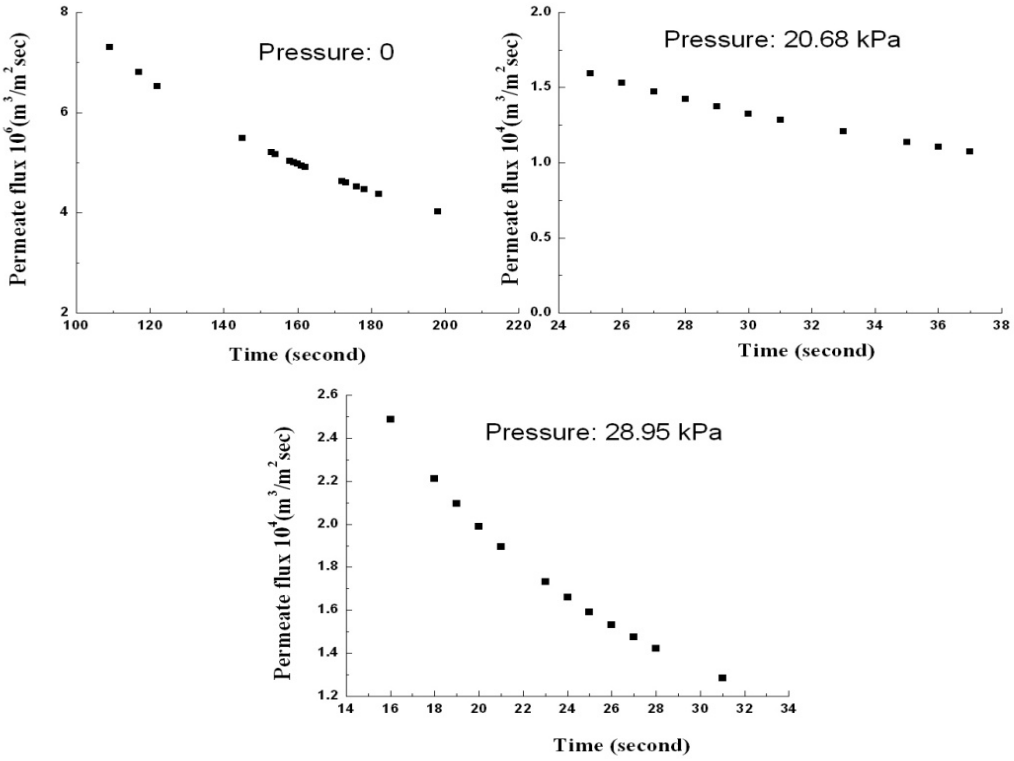

Figure 4.19: Flux variation after separation of chemical precipitate

The quality of chemical precipitation solution and permeate after MF was measured in terms of conductivity, pH, total dissolve solids (TDS) and concentration of fluoride and shown in Table 4.5. It may be seen that after chemical treatment, the final concentration of fluoride was in the safety limit recommended by WHO. However, the solution pH, TDS and conductivity were beyond the recommendable limit. It was noticed that the pH was around 8.1 while conductivity and TDS were found 0.43 mS/cm and 1325 mg/L, respectively, after the chemical treatment for 10 minutes. Hence, the treated water could not be used for drinking purpose after chemical treatment. Furthermore, the suspended particles generated during the treatment as discussed earlier also reflected the improper quality of treated water for drinking purpose. Therefore, after the completion of chemical treatment, a further treatment was necessary to retain the drinking water quality in terms of pH, conductivity and TDS as specified in the Table 4.5. In view to this, microfiltration was considered as an alternative in combination with the chemical treatment to overcome the situation. It was observed that after the MF treatment, the pH, conductivity and TDS were found 7.2, 0.3 mS/cm and 580 mg/L, respectively.

It was also observed that there were no noticeable changes in the final concentrations of fluoride in the permeate collected after the MF treatment. It was finally confirmed that precipitation followed by microfiltration for the treatment of water with fluoride contamination could be an effective alternative to combat with the drinking water problem associated with such type of contamination in near future.

Table 4.5: Quality of chemical precipitation solution and permeate of MF

Parameters	After chemical treatment	After microfiltration	Drinking water specification [19]
pH	8.1	7.2	6.5 - 8.2
Conductivity (mS/cm)	0.43	0.3	0.2 - 2.0
TDS (mg/L)	1325	580	500 - 700
Concentration of fluoride (mg/L)	0.86	0.86	1.5

4.4 Summary

The drinking water contaminated with significant amount of fluoride was treated by Chemical precipitation followed by microfiltration technique. In this investigation, Calcium chloride was used as precipitating agent and ceramic microfiltration membrane prepared by paste method was used in the MF technique, respectively. The followings are the excerpts of the present investigation:

Chemical treatment method

The current study highlighted that the chemical precipitation technique is very much effective for higher concentration fluoride water stream discharged by many industries. In this technique, 500 mg/L initial fluoride concentration water was chosen and calcium chloride was used as precipitating agent. The maximum fluoride was precipitated at $[Ca^{2+} / F^{-}]$ molar ratio of 2 at pH range of 6.5 – 11.1. The use of other precipitating agents concluded that the performance of calcium chloride was better than

calcium hydroxide and calcium nitrate. The fluoride precipitation was affected in presence of phosphate, sulfate and nitrate ions. The characterization of the precipitate confirmed the presence of both calcium and fluoride ions in the precipitate.

MF technique

In this technique, ceramic membrane was prepared by paste method at 950 ^{o}C sintering temperature with average pore diameter of 0.7 μm. From the study, it was found that MF separation of fluoride solution was not so much effective as the membrane pore diameter is more than the size of the fluoride ion. Also due to the presence of calcium ion in the membrane composition, the MF membrane used in the separation behaves like an adsorbent.

Chemical precipitation followed by microfiltration

In this technique, a combination of chemical precipitation along with microfiltration was used to treat fluoride contaminating water. The fine precipitate obtained in chemical treatment process was separated completely by using a MF membrane which acts as a filtering media. The pressure applied to the membrane is in the range of 0 – 28.95 kPa. The flux was decreasing with increase in time as some of the pores of the membrane were blocked by the fine precipitates. The permeate collected at the end of membrane filtration was in the drinking water range.

All the above mentioned findings might be useful for the further advancement of the hybrid technique to design a drinking water treatment system in continuous mode.

4.5 References

[1] Nayak, P., 2002. Review aluminum: impacts and disease. Envtl. Res. Sec. 89, 101–115.

[2] Meenakshi, Maheshwari, R.C., 2006. Fluoride in drinking water and its removal. J. Hazard. Mater. B137, 456-463.

[3] Matis, K.A., Mavros, P., 1991. Recovery of metals by ion floatation from dilute aqueous solutions. Sep. Purif. Methods. 20, 1-48.

[4] Lin, M.C., Liu, J.C., 1996. Adsorbing colloid flotation of As (V) – Feasibility of utilizing streaming current detector. Sep. Sci. Technol. 31, 1629-1641.

[5] Nandi, B.K., Uppaluri, R., Purkait, M.K., 2008. Preparation and characterization of low cost ceramic membranes for microfiltration applications. App. Clay Sci. 42, 102 - 110.

[6] Saffaj, N., Persin, M., Younsi, S.A., Albizane, A., Cretin, M., Larbot, A., 2006. Elaboration and characterization of micro-filtration and ultra-filtration membranes deposited on raw support prepared from natural Moroccan clay: Application to filtration of solution containing dyes and salts. Appl. Clay Sci. 31, 110 - 119.

[7] Chakrabarty, B., Ghoshal, A.K., Purkait, M.K., 2008. SEM Analysis and Gas Permeability Test to Characterize Polysulfone Membrane Prepared with Polyethylene Glycol as Additive. J. Colloid Interf. Sci. 320, 245 - 253.

[8] Mulder, M., 1991. Basic Principles of Membrane Technology, Kluwer Academic Publishers, Dordrecht.

[9] Cheryan, M., 1998. Ultrafiltration and Microfiltration Handbook. Technomic Publishing Co. Inc. Lancaster, Pennsylvania.

[10] Baker, R.W., 2004. Membrane Technology and Applications. John Wiley & Sons Ltd, West Sussex, England.

[11] JCPDS (Joint Committee for Powder Diffraction Studies), 1997. Powder Diffraction File of Inorganic Phases, International Center for Diffraction Data, Swarthmore, PA, USA.

[12] Balek, V., Murat, M., 1996. The emanation thermal analysis of kaolinite clay minerals. Thermochim. Acta., 282 – 283, 385 - 397.

[13] Chena, Y.F., Wang, M.C., Hon, M.H., 2006. Phase transformation and growth of mullite in kaolin ceramics. J. Afri. Earth Sci. 46, 245 - 252.

[14] Masmoudia, S., Larbot, A., Feki, H.E., Amara, R.B., 2007. Elaboration and characterisation of apatite based mineral supports for microfiltration and ultrafiltration membranes. Cer. Inter. 33, 337-344.

[15] Jedidi, I., Khemakhem, S., Larbot, A., Amar, R.B., 2009. Elaboration and characterization of fly ash based mineral supports for microfiltration and ultrafiltration membranes. Cer. Inter. 35, 2747 - 2753.

[16] Khemakhem, S., Larbot, A., Amar, R.B., 2009. New ceramic microfiltration membranes from Tunisian natural materials: Application for the cuttlefish effluents treatment. Cer. Inter. 35, 55 - 61.

[17] Wang, M.C., Wu, N.C., Hon, M.H., 1994. Preparation of nepheline glass-ceramics dental porcelain. Materials Chemistry and Physics. 37, 370 – 375.

[18] Porter, M.C., 1989. Handbook of industrial membrane technology. Noyes Publications, Westwood, New Jersey, U.S.A.

[19] WHO (World Health Organization), 1984. Guidelines for Drinking Water Quality (vol. II): Health Criteria and Supporting Information, World Health Organization, Geneva, Switzerland.

Chapter 5

Removal of arsenic using copper (II) oxide nanoparticles*

This chapter discusses the preparation and characterization of copper (II) oxide nanoparticles. Arsenic contaminated water was treated with synthesized copper (II) oxide nanoparticles as adsorbent. The process parameters such as temperature, stirring speed, pH, nanoparticles dose and contact time were studied in detail. Adsorption kinetics and thermodynamic behavior were studied and reported. Langmuir and Freundlich isotherm models were used to observe the equilibrium behavior of the system. A regeneration technique was proposed in order to reuse the spent adsorbents. Finally, a calculation procedure was reported for determining the amount of adsorbent required for treating the volume of arsenic contaminating water as well as volume treated by unit mass of adsorbent.

5.1 Experimental

5.1.1 Materials

A round bottom flask along with reflux condenser on a heating mantle (JSGW, 200W) was used as experimental set up for synthesizing the Copper (II) oxide nanoparticles. Double distilled water was used in the batch experiments. All chemicals including Cupric Chloride (Merck, India), Sodium Hydroxide (Qualigens India Ltd),

* This work is published in following journals

A. Goswami, P. K. Raul and M. K. Purkait, Arsenic adsorption using copper (II) oxide nanoparticles, *Chem. Eng. Res. and Design*. 90(2012) 1387-1396.

capping solvent (SRL, Mumbai), Arsenic trioxide (Loba chemicals), acetone (Loba chemicals), ethanol and arsenic trioxide were analytical grade and used without further purification.

5.1.2 Preparation of cupper (II) oxide nanoparticles

3.4 g Cupric Chloride ($CuCl_2$), 1.6 g Sodium Hydroxide (NaOH) and 2 g capping solvent were mixed with 200 mL ethanol in a round bottom flask fitted with reflux condenser. The mixture was heated for 16 hrs (around 75 ^oC) and allowed to cool to room temperature. The supernatant was decanted and the product was washed with double distilled water and acetone. The dark brown precipitate was centrifuged and washed with ethanol, acetone and hot water. Finally, the product was dried at room temperature and heated to 110 ^oC before being weighed for adsorption experiments.

5.1.3 Method

Batch experiments were carried out using 250 mL conical flask at ambient temperature (25 ± 2 ^oC). 1 mg/L concentration of arsenic solution was prepared by dissolving an accurately weighed quantity (1.0 mg) of arsenic trioxide in 1 L of deionised water. Solutions of desired concentration were obtained by successive dilution of the stock solution. Standard technique was used to determine the remaining arsenic concentration using atomic absorption spectrophotometer. The effect of contact time on arsenic adsorption using copper (II) oxide nanoparticles was observed by agitating 100, 200, 500 and 1000 µg/L of arsenic solution with 1 g of adsorbent, separately at room temperature (25 ^oC). Different doses of adsorbent (0.25 – 2.0 g/L) were used to observe its effect on arsenic adsorption. Temperature effect was studied at 25 ^oC, 40 ^oC and 50 ^oC

while pH effect was studied by maintaining different pH (varying from 3.6 to 11.6) of the solution. Stirring effect was performed by maintaining three different speeds viz. 150, 200 and 250 rpm to observe its effect on arsenic adsorption. A common adsorbent dose of 1 g/L, stirring speed of 200 rpm, initial arsenic concentration of 100 µg/L and pH 7 was used for adsorption experiments. In order to study the adsorption isotherm, 0.1 g of adsorbent was kept in contact with 100 mL arsenic solution of different concentrations (500, 600, 700, 800 and 1000 µg/L) at pH 7 for 24 hrs with constant shaking and at ambient temperature of 25 ± 2 ^{o}C . After 24 hrs, the solution attains equilibrium and the amount of arsenic adsorbed (µg/g) on the surface of the adsorbent was determined by the difference of the two concentrations. Duplicate experiments were carried out for all the operating variables studied and only the average values were taken into consideration.

5.1.4 Characterization techniques and measurement

Prepared Copper (II) oxide nanoparticles were characterized using X-ray diffractometer (D8 ADVANCE, Bruker Axs) to know its structural feature. A BET surface analyzer (SA 3100, Beckman Coulter) was used to measure nitrogen adsorption isotherm at 77 K. Before measurement, the sample was degassed using Helium at 200 ^{o}C for 2 hrs. The BET surface area, total pore volume, average pore radius, micropore area were obtained from the adsorption isotherms. The size and morphology of copper (II) oxide nanoparticles were observed by 200 KV Transmission Electron Microscope (JEOL JEM 2100). Fourier transform infrared spectroscopy (FTIR, Make: Perkin Elmer, USA, Model: LR 64912C) was used to analyze the organic functional groups of the adsorbent. The point of zero charge (pH_{ZPC}) of copper (II) oxide used for adsorption experiment was determined by using solid to liquid ratio of 1:1000. For this, 0.1 g of copper (II) oxide

was added to 100 mL of 0.01M NaCl solution with varying pH from 2 to 12 and stirred for 48 hrs. Final pH of the solution was plotted against initial pH of the solution and pH_{ZPC} was measured. A digital pH meter (Eutech Instruments, pH 510) was used to measure the pH of the solution. Shaking incubator (Daihan Labtech Co. Ltd) was used for shaking all the adsorption experiments. Arsenic (III) concentration of the solution was determined by Atomic absorption spectrophotometer (Model No. 240 FF, Varian, Netherlands).

5.2 Results and discussion

5.2.1 Characterization of adsorbent

The shape of copper (II) oxide prepared by thermal refluxing method was determined by TEM and shown in Figure 5.1a. From the figure, it was clear that copper (II) oxide formed was in cylindrical shape. The specific surface area of the copper (II) oxide determined from BET surface area analyzer was 52.11 m^2/g. Figure 5.1b showed the pore size distribution curve of adsorbent based on the nitrogen equilibrium adsorption isotherm at 77 K. It was found from the figure that copper (II) oxide exhibited a wide distribution of pores. About 87.61% of total pores were in the range of pore diameter below 40 nm with total pore volume of 0.117 mL/g nm, indicating a very high mesopore volume. The second fraction of pores appeared in the field from 50 to 150 nm. In this range, the pore volume was 0.002 mL/g nm with only 12.39% of the total pore volume indicating the existence of the macropores. Chemical composition of copper (II) oxide nanoparticles was determined by X-ray diffraction (XRD) and shown in Figure 5.1c. The XRD pattern matched with that of single phase monoclinic copper (II) oxide with broad

peaks at 2θ = 35.55°, 38.55°, 48.75°, 53.4° and 61.4° which were matched with JCPDS file no. 801917. Peaks at 2θ = 16.2° and 32.4° indicated the presence of $Cu_2Cl(OH)_2$ (paratacamite). The Fourier transform infrared spectroscopy (FTIR) of copper (II) oxide was shown in Figure 5.1d. The major peaks were observed at 517, 1019, 1631 and 3442 cm^{-1} and identified as Cu-O, C-O, C-O and O-H group respectively. The point of zero charge (pH_{ZPC}) of copper (II) oxide was plotted and discussed in subsequent section. It was observed that pH_{ZPC} value of copper (II) oxide nanoparticles was at pH 6.8 which concluded that the adsorbent surface had a positive charge (weekly cationic) in aqueous medium.

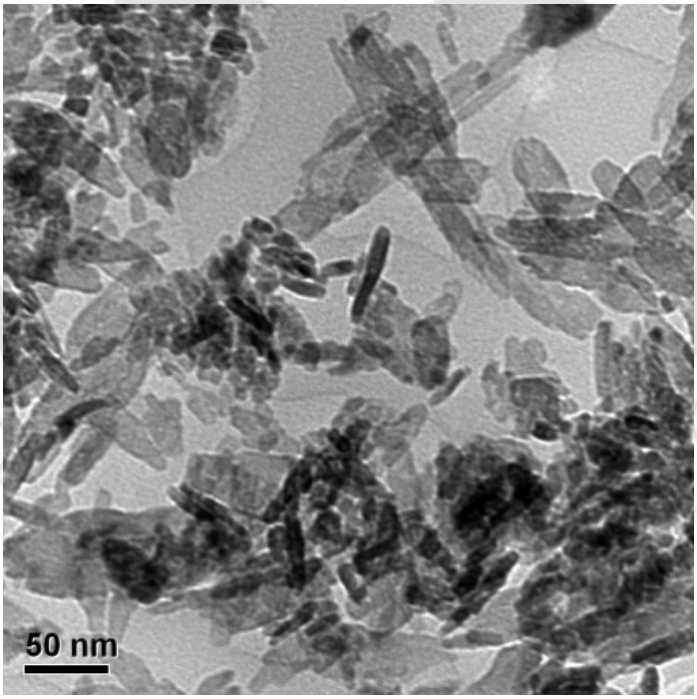

Figure 5.1a: TEM picture of copper (II) oxide nanoparticles before adsorption.

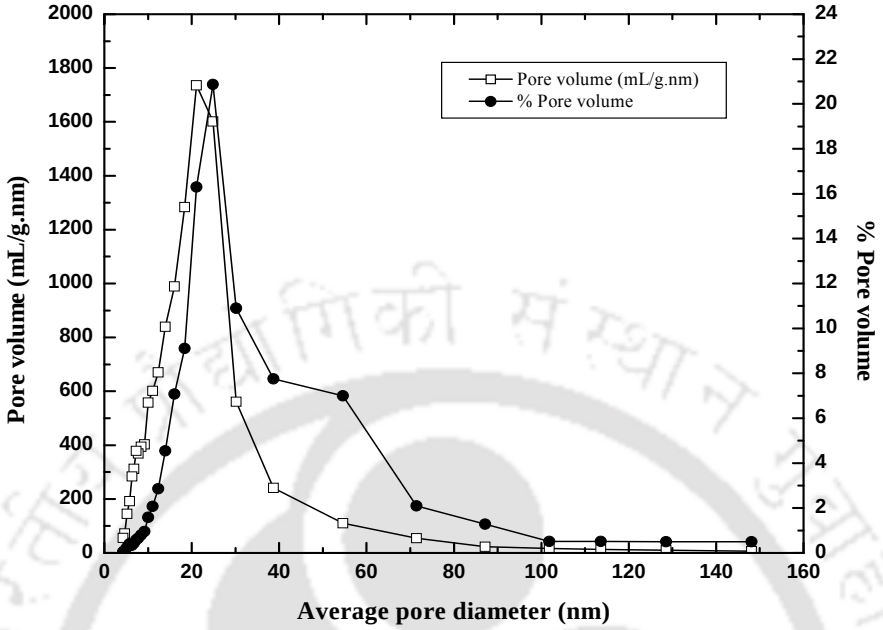

Figure 5.1b: Pore size distribution of copper (II) oxide nanoparticles

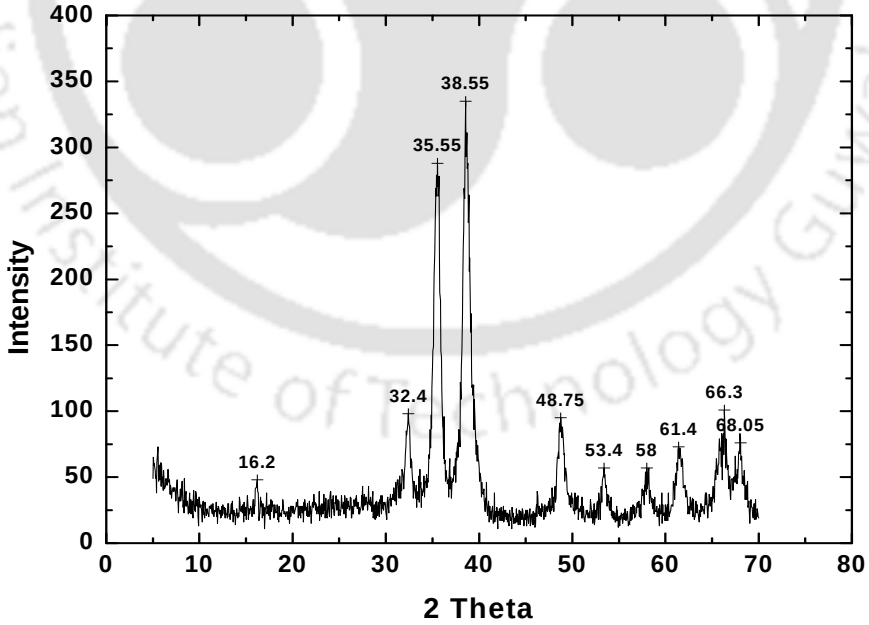

Figure 5.1c: XRD of copper (II) oxide nanoparticles

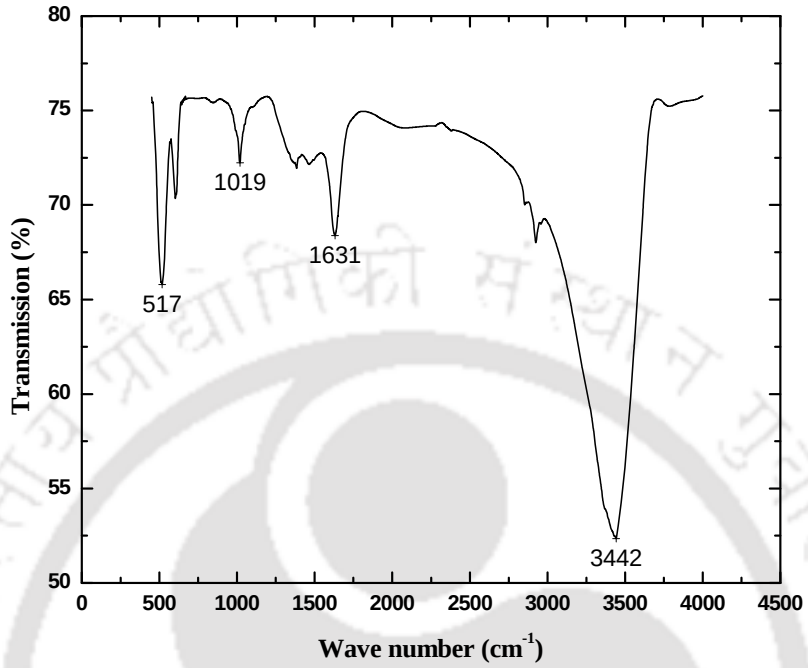

Figure 5.1d: Fourier transform infrared spectroscopy of copper (II) oxide nanoparticles

5.2.2 Effect of contact time and initial concentration

The rapid adsorption of arsenic took place within 100 minutes of adsorption, then adsorption became slow and almost reached equilibrium within 300 min (Figure 5.2a). With an increase in contact time up to 24 hrs, removal of arsenic was increased by less than 1%. Thus, further experiments were conducted within 3 hrs. For the initial concentration up-to 1000 µg/L, more than 92 % removal was observed within 3 hrs. 100 % removal efficiency was achieved for initial concentration up to 200 µg/L. It was evident that for lower initial concentrations of arsenic, adsorption was very fast. The percent removal of arsenic decreased with increase in initial concentration and took

longer time to reach equilibrium. With increase in arsenic concentration, competition for the active adsorption sites increased and the adsorption process will increasingly slow down. The rate of adsorption increased with initial arsenic concentration (inset of Figure 5.2a). The rate of adsorption in the initial rapid phase (equation 5.1a) were found to be 0.99, 1.86, 4.3 and 8.1 µg/g.min for initial arsenic concentration of 100, 200, 500 and 1000 µg/L, respectively. Similar trend was observed for the slower phase (equation 5.1b) where the rate of adsorption were 0.0011, 0.0156, 0.0778 and 0.1833 µg/g.min for initial arsenic concentration of 100, 200, 500 and 1000 µg/L, respectively.

$$r_{rapid} = 0.007C_0 + 0.269 \qquad R^2 = 0.999 \qquad (5.1a)$$

$$r_{slower} = 0.205C_o - 22.79 \qquad R^2 = 0.998 \qquad (5.1b)$$

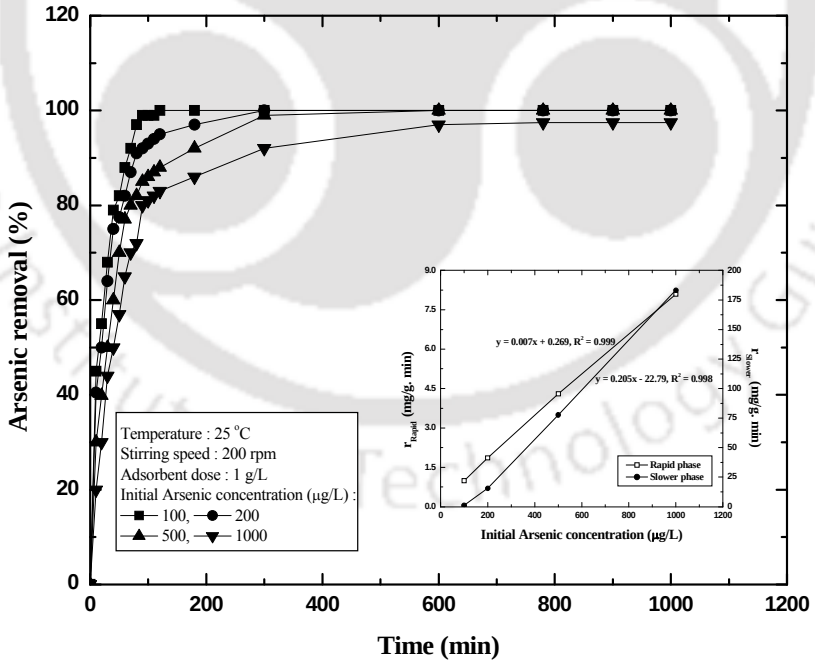

Figure 5.2a: Effect of contact time on arsenic adsorption (inset: Effect of initial arsenic concentration on adsorption rate).

5.2.3 Adsorbent dose effect

Adsorbent dose is an important parameter for arsenic removal by adsorption. The copper (II) oxide dose (varying from 0.25 g/L to 2.0 g/L) on the percentage removal of arsenic at four different initial concentrations 100, 200, 500 and 1000 µg/L was shown in Figure 5.2b. It was observed that arsenic removal increased with increasing adsorbent dose up to 1 g/L and then rate of increase was slow down. Initially, rapid increase in adsorption with the increase in adsorbent dose up to 1 g/L can be attributed to greater surface area and availability of more adsorption sites. After this critical dose, the extent of adsorption is increasingly slow down due to the fact that although there is increasing number of active sites but there is shortage of adsorbate in the solution. Hence, after 1 g/L adsorbent dose, increase in percentage removal of arsenic was marginal.

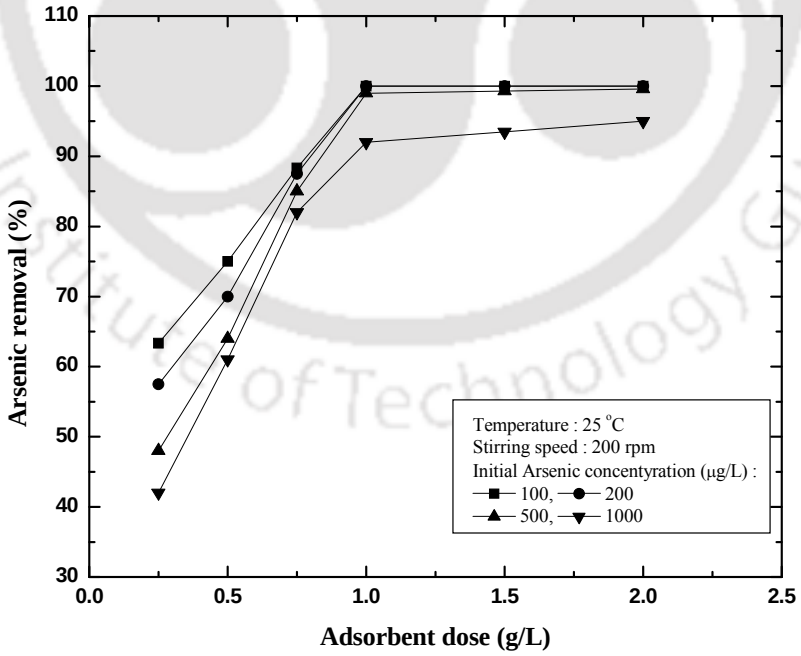

Figure 5.2b: Variation of adsorbent dose on the removal of arsenic

5.2.4 pH effect

The percentage of arsenic removal was a function of equilibrium pH which was shown in Figure 5.2c. The dominant species of arsenic in aqueous solution correlate closely with the solution pH. Trivalent arsenic is stable at pH 0 – 8 as neutral H_3AsO_3, while $H_2AsO_3^-$, AsO_3^{3-} and AsO_3^{3-} exist as stable species in the pH range of 8 – 12, 12 – 13, and 13 – 14, respectively. In this study, pH of 100 µg/L arsenic feed solution was varied from 3.6 to 11.6. It was observed from the figure that almost 100% arsenic was removed from water at pH more than 8 while arsenic removal percentage was less (75%) in acidic pH.

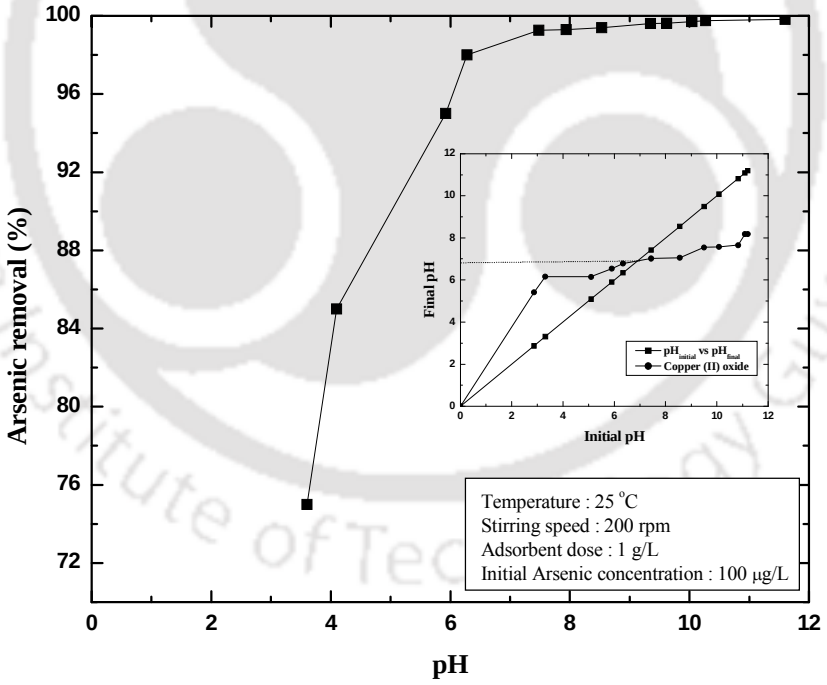

Figure 5.2c: Effect of pH on the percentage adsorption of arsenic (inset: pH_{ZPC} of copper (II) oxide nanoparticles)

In acidic conditions, the adsorbent surface was highly protonated (less than pH_{ZPC}) and such a situation was not favorable for arsenic (III) removal as neutral H_3AsO_3 was more dominating. With increase in pH (more than pH_{ZPC}), the degree of protonation of the surface reduced gradually and $H_2AsO_3^-$, AsO_3^{3-} and AsO_3^{3-} species were present in solution. Hence percentage removal of arsenic was more.

5.2.5 Stirring speed effect

Stirring is an important parameter in adsorption phenomena, influencing the distribution of the solute in the bulk solution and the formation of the external boundary layer. Experiments showed that the percentage removal of arsenic using copper (II) oxide nanoparticles at three different stirring speeds viz. 150, 200 and 250 rpm had no influence on arsenic adsorption. It was observed that stirring speed more than 110 rpm, there was no increase in the percentage adsorption of arsenic which ensures that the solid was completely and homogenously suspended in the solution and hence, stirring speed had no significant effect on adsorption rate [1, 2]. It was also cleared that external diffusion was not the rate limiting step in this adsorption process.

5.2.6 Competing anions

Presence of other anions such as phosphate and sulfate can have a significant effect on arsenic adsorption onto many adsorbents. The results of the competing anion studies were shown in Table 5.1. The presence of sulfate ion at very high concentrations (1 mM or 280 mg/L), decreased the percentage of arsenic removal (by less than 10%).

Removal of arsenic was decreased by more than 20% when phosphate concentrations were greater than 0.2 mM. From Table 5.1, it was concluded that sulfate ion had a significantly lower affinity than arsenic to Copper (II) oxide nanoparticles while phosphate ion had somewhat higher affinity, but lower than that of arsenic. The concentrations of competing anions in this study were much higher than those likely to be encountered in groundwater. Thus, Copper (II) oxide nanoparticles were able to remove arsenic even at exceptionally high concentrations of the competing anions used in this study.

Table 5.1: Effect of competing anions on arsenic adsorption.

Arsenic concentration (μg/L)	Competing ion concentration (mM)	% Arsenic removal in the presence of	
		Sulphate	Phosphate
500	0	95	95
	0.2	82	70
	1	75	60
1000	0	93	93
	0.2	94	80
	1	86	60

5.2.7 Temperature effect and thermodynamic study

With increase in temperature from 25 ^{o}C to 50 ^{o}C, arsenic adsorption percentage was also increased from 92 % to 99 % indicating the endothermic behavior of adsorption.

The thermodynamic parameters viz. Gibb's free energy (ΔG^0), entropy (ΔS^0) and enthalpy (ΔH^0) changes for the adsorption process were determined for 100 µg/L initial arsenic concentration solution and tabulated in Table 5.2. From the table, it was found that positive ΔH^0 value concluded the endothermic behavior of adsorption and negative ΔG^0 value indicated spontaneous nature of the adsorption process. The low value of ΔS^0 implied that no remarkable change in entropy occurred during the adsorption process. In addition, the positive value of ΔS^0 reflects the increased randomness at the solid–solution interface during adsorption, and it also indicates the occurrence of ion replacement reactions. The higher value of ΔH^0 indicated that the adsorption process was a physico-chemical adsorption process rather than a pure physical or chemical adsorption process as heats of chemisorption generally falls into a range of 80 – 200 kJ/mol.

Table 5.2: Thermodynamic parameters for arsenic adsorption.

Temperature (^{o}C)	ΔH^o (kJ/mol)	ΔS^o (kJ/K mol)	$-\Delta G^o$ (kJ/mol)
298			5.48
313	120.78	0.42	11.84
323			16.07

5.2.8 Kinetic study

The kinetics of arsenic adsorption onto copper (II) oxide was evaluated using different models such as pseudo-first-order, pseudo-second-order and intraparticle diffusion models discussed in Section 3.1 in chapter 3. Fitting the adsorption experimental data to these models, various parameters were calculated and reported in Table 5.3. Among these models the criterion for their applicability is based on judgment on the respective correlation coefficient (R^2) and agreement between experimental and calculated value of q_e. The high values of R^2 (~1) and good agreement between two q_e values indicate that the adsorption system followed pseudo-second-order kinetic model (Table 5.3).

Another alternative method for kinetic evaluation of an adsorption process is intra-particle-diffusion model. According to the model, the mass transfer rate can be expressed as a function of the square root of time (*t*). The details of the model was discussed in Section 3.1 in chapter 3.

Figure 5.3 represents q_t versus $t^{0.5}$ plot for initial arsenic concentrations of 100, 200, 500 and 1000 µg/L. This is represented by three steps. The first sharper portion was attributed to the diffusion of arsenic through the solution to the external surface of adsorbent. The second portion described the gradual adsorption stage, where intraparticle diffusion was rate limiting. The third portion was attributed to the final equilibrium stage for which the intraparticle diffusion started to slow down due to the extremely low arsenic concentration left in the solution. The rate of uptake might be limited by the size of adsorbate molecule, concentration of the adsorbate and its affinity to the adsorbent, diffusion coefficient of the arsenic in the bulk phase, the pore-size distribution of the

adsorbent. As seen from the figure, the plots were not linear over the whole time range, implying that more than one process affected the adsorption. The multiple natures of these plots could be explained by boundary layer diffusion, which gave the first portion and the intraparticle diffusion that gave further two linear portions. If the intraparticle diffusion was the only rate-controlling step, the plot passed through the origin; if not, the boundary layer diffusion controlled the adsorption to some degree. It could be deduced that there were three processes that controlled the rate of molecules adsorption but only one was rate limiting in any particular time range. The slope of the linear portion indicated the rate of the adsorption. The lower slope corresponded to a slower adsorption process. One could observe that the diffusion in bulk phase to the exterior surface of adsorbent, which started at onset of the process, was the fastest. The second portion of the plot seemed to refer to the diffusion into mesopores and the third one with the lowest slope to adsorption into micropores. This implied that the intraparticle diffusion of arsenic into micropores was the rate-limiting step in the adsorption process on copper (II) oxide nanoparticles, particularly over long contact time periods.

Table 5.3: Various kinetic model parameters for arsenic adsorption at 25 ^{o}C

Model	Equation	Plot	Parameters	Value			
				Initial arsenic concentration (μg/L)			
				100	200	500	1000
Pseudo first order kinetics	$\ln(q_e - q_t) = \ln q_e - k_1 t$	Plot the values of ln (q_e- q_t) versus t which gave a straight line with slope of (-k_1) and intercept ln (q_e) respectively.	$q_{e,\ expt}$ (μg/g)	100	200	500	975
			$q_{e,\ cal}$ (μg/g)	112.17	113.29	320.54	742.48
			k_1 (min^{-1})	0.04	0.02	0.01	0.02
			R^2	0.94	0.94	0.92	0.94
Pseudo second order kinetic	$\frac{t}{q_t} = \frac{1}{k_2 q_e^{\ 2}} + \frac{t}{q_e}$	Plot the values of (t/q_t) versus t should gave a straight line with slope of ($1/q_e$) and intercept ($1/k_2 q_e^{\ 2}$).	$q_{e,\ cal}$ (μg/g)	101.01	203.25	512.82	1014.41
			k_2 (x 10^3) (g/μg. min)	1.37	0.41	0.09	0.03
			R^2	0.99	0.99	0.99	0.99

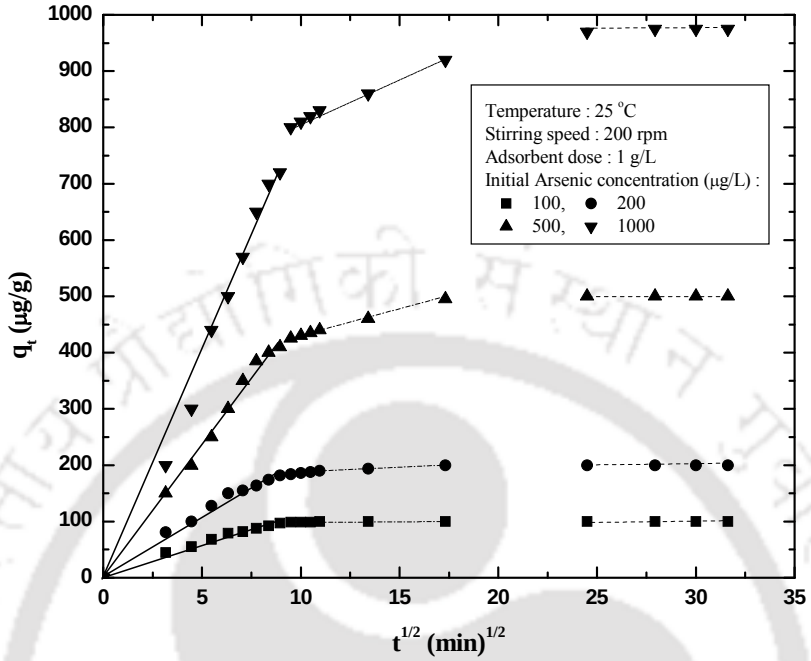

Figure 5.3: Intra particle diffusion kinetic model for the adsorption of arsenic

5.2.9 Equilibrium study

Adsorption equilibrium was studied with the help of Langmuir and Freundlich isotherm models. The details of these isotherms were discussed in section 3.1 in chapter 3.

Both the isotherms for arsenic - copper (II) oxide nanoparticles at 25 °C were shown in Figure 5.4. It was observed from the figure that maximum adsorption capacity of copper (II) oxide on arsenic adsorption is 1086.2 µg/g. The maximum adsorption capacity was comparable to the adsorption capacities of other arsenic removal adsorbents (Table 5.4). From Table 5.4, it was cleared that there was a huge difference between the adsorption capacities and the surface area of the two adsorbents, although both the two adsorbents were almost same in nature. The adsorption capacity of an adsorbent mainly depends on

the adsorbent surface area and the initial adsorbate concentration. The technique adopted in this work is quite different to that of Martinson and Reddy, 2009 [3] which gives a lower surface area (38.7% less). In Martinson and Reddy, they have used 0.1-100 mg/L of arsenic, whereas 500-1000 µg/L (0.5-1.0 mg/L) was used in this work which was very less compared to them and were in the range of actually available in arsenic contaminated drinking water. The Langmuir adsorption capacity was more in case of Martinson and Reddy than the present work. This was due to large surface area of adsorbent and more initial concentration of adsorbate. Correlation coefficients for Langmuir and Freundlich adsorption isotherms were calculated by fitting the experimental adsorption equilibrium data and summarized in Table 5.5. From the table, it is concluded that Langmuir isotherm fitted well than Freundlich isotherm.

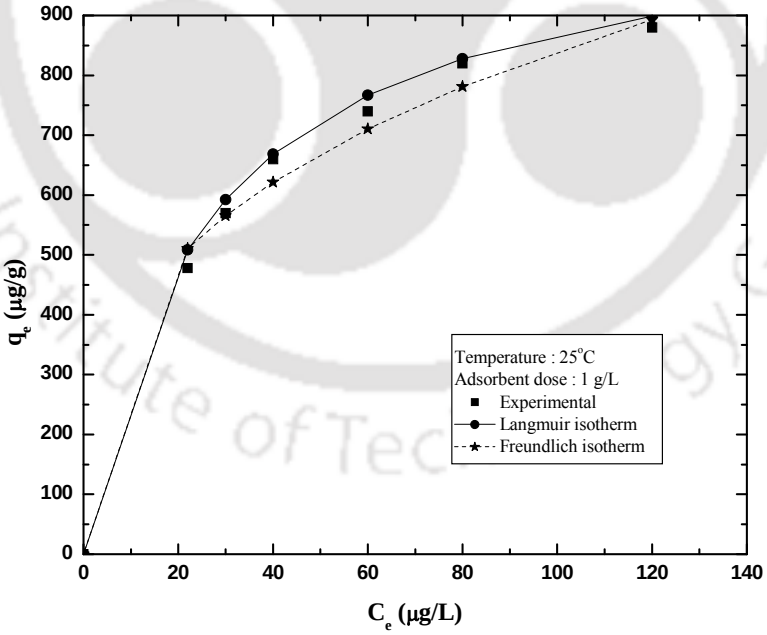

Figure 5.4: Equilibrium isotherm model for arsenic adsorption.

Table 5.4: Comparison of arsenic adsorption capacity of copper (II) oxide with some reported adsorbents.

Adsorbent	Concentration range	Surface area (m^2/g)	Models used to calculate q_e	q_e (mg/g)	References
Pine wood char	10–100 μg/L	2.73	Langmuir	0.0012	[4]
Iron oxide uncoated Sand	100-800 μg/L	-	Langmuir	0.006	[5, 6]
Iron oxide coated sand	100 μg/L	10.6	Langmuir	0.041	[7]
Activated alumina	1 mg/L	370	Langmuir	0.18	[8]
Manganese ore	-	-	Langmuir	0.53	[9]
Iron oxide coated cement (IOCC)	0.7-13.5 mg/L	-	Langmuir	0.67	[10]
Cupric oxide nanoparticles	0.1-100 mg/L	85±1	Langmuir	26.9	[3]
Copper (II) oxide	**0.5-1.0 mg/L**	**52.11**	**Langmuir**	**1.0862**	**Present work**

Table 5.5: Langmuir and Freundlich isotherm constants for arsenic adsorption

Langmuir isotherm constant			Freundlich isotherm constants		
Q_o (μg/g)	b (L/μg)	R^2	K_F [μg.g (L/μg)$^{1/n}$]	n_F	R^2
1086.2	0.04	0.99	184	0.33	0.97

5.2.10 Regeneration of adsorbent

Preliminary regeneration experiments were carried out using spent copper (II) oxide adsorbent using 0.2 M and 0.5 M NaOH solution. 13.5% and 25 % arsenic was recovered from 200 µg/L arsenic solution with 0.2 M and 0.5 M NaOH solution, respectively. The lower percentage of desorption of arsenic was due to the strong attraction between adsorbent active sites and arsenic molecule. To check the efficiency of the regenerated adsorbents, copper (II) oxide was washed thoroughly in distilled water and dried properly under sunlight for 24 hrs. The regenerated adsorbents were used for adsorption of 100 µg/L of arsenic at adsorbent dose of 1 g/L for a contact time of 3 hrs. Results showed that only about 4% decrease in adsorption efficiency was observed.

5.2.11 Process calculation

The process design calculation of arsenic - copper (II) oxide nanoparticles was studied. The details of the calculation procedure was discussed in section 3.1 of chapter 3.

Figure 5.5 showed the volume of arsenic free water treated with 1 g adsorbent mass. It is clear from the figure that with low initial arsenic concentration, more volume of water may be treated with unit mass of adsorbent. From inset of Figure 5.5, for initial arsenic concentrations of 300, 400 and 500 µg/L and for 95% removal of arsenic, the amount of copper (II) oxide required was estimated to be 1.63 g to 16.3 g, 1.10 g to 11.01 g and 0.94 g to 9.40 g for solution volume of 1 L, to 10 L respectively. This study will give a preliminary idea to design an adsorber for the removal of arsenic from drinking water.

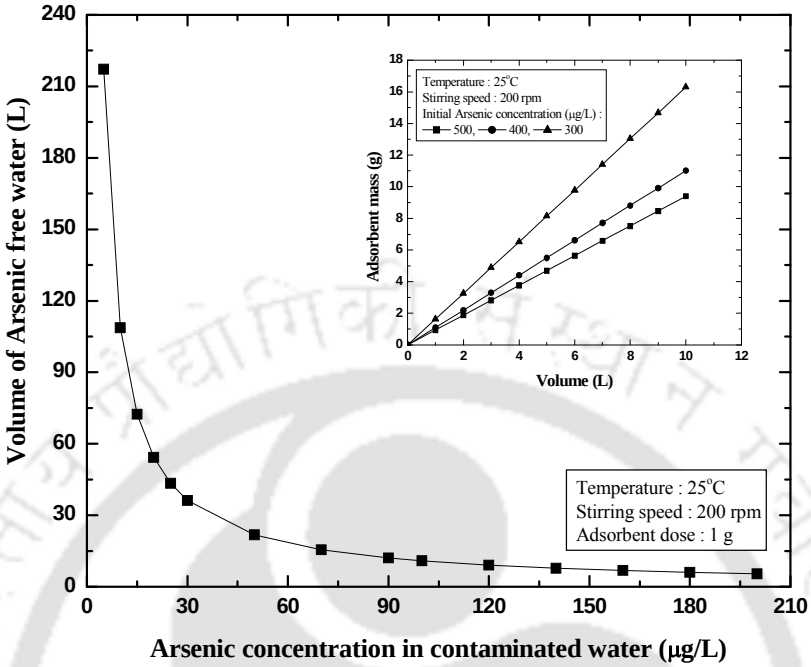

Figure 5.5: Volume of arsenic contaminated water treated with unit mass of adsorbent (inset: Adsorbent mass (M) against volume of solution treated (L)).

5.3 Summary

Arsenic poisoning is a major problem in today's life. To reduce its concentration in drinking water, different metal based compounds were explored as arsenic adsorbents. In the present study, copper (II) oxide nanoparticles were prepared by thermal refluxing technique and used as an adsorbent for arsenic removal from water. Characterization of the adsorbent using TEM, BET, XRD and FTIR implied that the prepared adsorbent was in nano size and had excellent adsorption behavior with surface area of 52.11 m^2/g.

Systematic adsorption experiments were carried out with different process parameters such as contact time, adsorbent mass, pH, temperature and stirring speed and found that copper (II) oxide had very good efficiency towards arsenic adsorption. Thermodynamic parameters and adsorption kinetics were studied in detailed to know the nature and mechanism of adsorption. Results showed that the adsorption process followed pseudo second order kinetic and endothermic behavior. Adsorption equilibrium was studied with Langmuir and Freundlich isotherm models. The adsorption process followed Langmuir isotherm with an adsorption capacity of 1086.2 µg/g. A regeneration study was proposed in order to reuse the adsorbent for better economy of the process.

5.4 References

[1] Rodrı´guez, A., Ovejero, G., Mestanza, M., Garcı´a, J., 2010. Removal of Dyes from Wastewaters by Adsorption on Sepiolite and Pansil. Ind. Eng. Chem. Res. 49, 3207–3216.

[2] Anbia, M., Ghassemian, Z., 2011. Removal of Cd(II) and Cu(II) from aqueous solutions using mesoporous silicate containing zirconium and iron. Chem. Eng. Res. Des. 89 (11) 2770-2775.

[3] Martinson, C.A., Reddy, K.J., 2009. Adsorption of arsenic (III) and arsenic (V) by cupric oxide nanoparticles. J. Colloid Interf. Sci. 336, 406–411.

[4] Mohan, D., Pittmann Jr., C.U., 2007. Arsenic removal from water/wastewater using adsorbents—A critical review. J. Hazard. Mater. 142, 1–53.

[5] Gupta, V.K., Saini, V.K., Jain, N., 2005a. Adsorption of As (III) from aqueous solutions by iron oxide-coated sand. J. Colloid Interf. Sci. 288, 55–60.

[6] Gupta, V.K., Mittal, A., Krishnan, L., 2005b. Use of waste materials, bottom ash and de-oiled soya, as potential adsorbents for the removal of amaranth from aqueous solutions. J. Hazard. Mater. 117, 171–178.

[7] Thirunavukkarasu, O.S., Viraghavan, T., Suramanian, K.S., 2003. Arsenic removal from drinking water using iron-oxide coated sand. Water Air Soil Pollut. 142, 95–111.

[8] Fryxell, G.E., Liu, J., Hauser, T.A., Nie, Z., Ferris, K.F., Mattigod, S., Gong, M., Hallen, R.T., 1999. Design and synthesis of selective mesoporous anion traps. Chem. Mater. 11, 2148–2154.

[9] Chakravarty, S., Dureja, V., Bhattacharyya, G., Maity, S., Bhattacharjee, S., 2002. Removal of arsenic from groundwater using low cost ferruginous manganese ore. Water Res. 36, 625–632.

[10] Kundu, S., Gupta, A.K., 2006. Arsenic adsorption onto iron oxide-coated cement (IOCC): regression analysis of equilibrium data with several isotherm models and their optimization. Chem. Eng. J. 122, 93– 106.

Chapter 6

Conclusions and Scope of Future Work

This chapter summarizes the inferences drawn from various works presented in this thesis. Also, some suggestions towards the scope for future research are outlined.

Conclusions

In this thesis, different techniques for defluoridation of water are presented. Four different adsorbents viz; pyrophyllite, acidic alumina, schwertmannite and nanomagnetite aggregated schwertmannite were used for defluoridation of water. Calcium chloride, calcium hydroxide and calcium nitrate were used to precipitate fluoride from water. A microfiltration membrane is prepared and used for the separation of byproducts obtained during defluoridation by precipitation. At last, arsenic removal was investigated using synthesized copper (II) oxide nanoparticles. The major conclusions drawn from each of the work is presented below

Fluoride adsorption using pyrophyllite

- It was found that pyrophyllite showed significant fluoride removal efficiency (85%) at pH 4.9, for the initial fluoride concentration of up to 10 mg/L.
- Maximum fluoride adsorption capacity was found to be 2.2 mg/g
- The experimental data fitted well with Langmiur adsorption isotherm and the value of equilibrium parameter "R_L" suggested that fluoride adsorption by pyrophyllite was favorable.

- Presence of sulphate ion reduces the fluoride removal efficiency by around 5%.
- Kinetic study reveals that fluoride adsorption by pyrophyllite follow pseudo second order kinetic model and both intra-particle diffusion as well as surface diffusion steps was involved during fluoride uptake. The mass transfer coefficient increased from 4.52 × 10-13 to 9.34 × 10-13 when initial fluoride concentration increases from 4 mg/L to 10 mg/L.
- The negative values of ΔG^o and ΔH^o suggest that the fluoride adsorption by pyrophyllite was a spontaneous process and exothermic in nature.
- Low cost of pyrophyllite made this material a potential candidate for defluoridation of water.

Removal of Fluoride using acidic alumina

- The current study dictated that alumina which is acidic in nature had a fluoride removal efficiencies of around 94% at pH 4.4 for initial concentration of up to 10 mg/L.
- Kinetic study revealed that fluoride adsorption process was controlled by pseudo-second-order rate equation and intraparticle diffusion was not the rate-controlling step.
- From EDX study, `it was concluded that fluoride adsorption onto alumina was mostly due to surface adsorption.
- Thermodynamic study concluded that the fluoride adsorption process was spontaneous, feasible and endothermic nature with activation energy of 95.13 kJ/ mol which were fallen in physical adsorption process range.

- Langmuir isotherm model was fitted well to this system with an adsorption capacity of 8.4 mg/g of adsorbent.
- The performance of alumina towards fluoride was decreased with the presence of other co-ions. The interference of carbonate and bicarbonate ions was more than that of chloride, nitrate and sulfate ions.
- The spent adsorbents were regenerated with basic solutions and regenerated adsorbents showed very good adsorption efficiencies.

Defluoridation using nanoporous schwertmannite (Sh)

- It has been successfully demonstrated that Schwertmannite can be potentially used for fluoride removal from aqueous solutions by adsorption. The permissible limit defined by WHO for defluoridation was achieved by 3 g/L adsorbent dose in 90 minute contact time at a pH 3.6.
- Kinetic study revealed that fluoride adsorption process was controlled by pseudo second order rate equation and intraparticle diffusion was not the rate-controlling step.
- Thermodynamic study concluded that the fluoride adsorption process was spontaneous, feasible and exothermic nature.
- The equilibrium isotherm data was best fitted with Langmuir and Temkin isotherm models with an adsorption capacity of 12.35 mg/g of adsorbent.
- The performance of Schwertmannite towards fluoride adsorption was decreased with the presence of phosphate and bicarbonate ions. The spent adsorbents were

regenerated with basic solutions and regenerated adsorbents showed good adsorption efficiencies.

Defluoridation using nano magnetite aggregated schwertmannite(NMSh)

- NMSh was prepared by introducing nanomagnetite in ordinary schwertmannite, which is a composite of ferromagnetic and paramagnetic materials. This new property improves the fluoride adsorption efficiency. The permissible limit defined by WHO for defluoridation was achieved by 2g/L adsorbent dose in 90 minute contact time at a pH 5.73.
- Kinetic study revealed that fluoride adsorption process was controlled by pseudo-second-order rate equation and intraparticle diffusion was not the rate-controlling step.
- Thermodynamic study concluded that the fluoride adsorption process was spontaneous, feasible and endothermic nature with activation energy of 73.19 kJ/ mol which were fallen in physical adsorption process range.
- The equilibrium isotherm data was best fitted with Langmuir and Temkin isotherm models with an adsorption capacity of 17.24 mg/g of adsorbent.
- The performance of NMSh towards fluoride was decreased with the presence of other ions. The interference of phosphate, carbonate and bicarbonate ions was more than that of chloride and sulfate ions.
- The spent adsorbents were regenerated with basic solutions and regenerated adsorbents showed good adsorption efficiencies.

- The results of indicated that nanomagnetite aggregation process not only improves the magnetic property, but also provides a highly promoted fluoride adsorption capacity compared to the other adsorbents.

Chemical treatment followed by microfiltration technique

- Drinking water contamination caused by the significant presence of fluoride ion was successfully treated with chemical precipitation technique.
- Effective removal of fluoride took place at $[Ca^{2+} / F^{-}]$ molar ratio of 2.
- pH was considered as one of the most important parameter in fluoride precipitation technique. The effective fluoride precipitation took place at pH range of 6.3-11.1.
- Presence of phosphate ion influences more in the removal of fluoride ion followed by sulfate and nitrate ions.
- Ceramic microfiltration membrane prepared by paste method followed by sintering at 950 °C was used for separating the fluoride contaminated water.
- Microfiltration membrane was not so effective for separating fluoride from water as the pore size of the membrane was bigger than the fluoride ion.
- Hence, microfiltration membrane was used for the separation of precipitate formed during chemical treatment process.
- The fine precipitate of calcium fluoride was completely removed from the suspended solution of chemical treatment process.

- The residual fluoride concentration of the suspended solution was not affected by the membrane separation.
- The permeate quality followed the drinking water specification which was a major achievement of this process.

Arsenic adsorption using copper (II) oxide nanoparticles

- Copper (II) oxide was found to be a potential nano-adsorbent for arsenic removal from water. The sorption of arsenic onto copper (II) oxide was found to be highly pH dependent. 100 percent arsenic was adsorbed for up to 200 µg/L initial arsenic concentrations using 1 g/L adsorbent dose and a contact time of 300 min.
- The percentage adsorption was decreased with increase in initial arsenic concentration. Presence of phosphate and sulfate ions reduced arsenic adsorption percentage by more than 20 percent and less than 10 percent respectively, on the surface of copper (II) oxide nanoparticles.
- Thermodynamic studies concluded that the process of sorption of arsenic species was feasible, spontaneous and endothermic in nature with ΔH^{o} value 120.78 kJ/mol which was fallen in the physico – chemical adsorption process range.
- The pseudo second order kinetic model was found to best correlate to the experimental data for arsenic adsorption. The rate determining step was found to be controlled by both surface sorption as well as intraparticle diffusion.

- Equilibrium sorption data showed excellent fit to Langmuir isotherm model than Freundlich isotherm model with an adsorption capacity of 1086.2 µg/g which indicated monolayer sorption on the homogeneous surface of the nano-adsorbent.
- The spent adsorbents were regenerated with NaOH solutions and regenerated adsorbents showed very good adsorption efficiencies. The process calculation shown here will be helpful to know about the adsorbent requirement for treating the volume of arsenic contaminated water.

Recommendations for future work

Research findings in this work provided a good number of insights with respect to adsorbent selection, preparation and their utilization in fluoride and arsenic removal. Followings are few recommendations for further scope of research:

- Exploration of low cost better adsorbent from various natural sources for enhanced fluoride removal efficiencies.
- Utilization and / or modification of agricultural/municipal waste toward adsorbent for water treatment.
- Details investigations on temperature dependent isotherms and kinetic parameters
- Establishment of adsorption mechanism for various nanoparticles
- Fluoride removal performance in adsorber columns and development of breakthrough curve.

- Development of mathematical modeling to predict the adsorption kinetics and column performance.
- The proposed hybrid technique may be investigated to remove other contaminants of drinking water like arsenic and other heavy metals.
- A continuous system of the hybrid process for the treatment of fluoride and other contaminants may be a further scope of the work.
- Detailed investigation of different combinations of other techniques like adsorption, precipitation, ion exchange would be undoubtedly the furthermore realistic contribution to the advancement along with their comparative cost analysis.
- The disposal of sludge formed during chemical precipitation process is really a problem from the environmental point of view. Either a suitable treatment technology or proper utilization of the byproducts has to be developed. This would also be an additional scope of research.

Error Analysis

The errors in experimentally measured quantities and in parameters calculated from those measurements are important in that they determine the accuracy of calculation and predictions using those quantities. There are two types of errors viz. systematic error and random error. Systematic errors are the results of faulty assumptions or improper experimental measuring techniques. In this work, care was taken in eliminating systematic errors by appropriately designing the experiments and adopting qualified methods for analysis of the data. On the other hand, random errors result from variation in the precision of measuring parameters and the slight variations that occur in successive measurements made by the same observer under nearly identical conditions. Random errors cannot be eliminated. The focus of the error analysis presented in this section is on the random errors.

In most of the experiments performed in this work, the quantities that are measured directly are concentrations of fluoride and arsenic and permeate flux during microfiltration.

Error in the measurement of concentration

Concentration of fluoride in aqueous medium is determined using fluoride ion meter and that of for arsenic is determined using AAS as discussed in Chapter 2 and Chapter 5 respectively. Calibration curves were prepared by taking known values of concentrations of fluoride and arsenic. From the respective calibration curve of fluoride and arsenic it is seen that the standard deviation of the predicted value from actual value

of concentration is more than 0.9917 for both the cases. Thus, every measurement of concentration in synthetic solution is associated with an error of 0.83 % whose effect on removal values can be ignored.

Error in the measurement of permeate flux

The errors in the values of permeate flux are related to the errors in the measurements used to calculate those values. In this section, statistical analysis is used for estimation of the uncertainty associated with the values of permeate flux. Determination of standard deviation is generally considered to be one of the best methods to estimate the uncertainty which is based on the following method:

If u_1, u_2, ..., u_N are the N results of the measurements of a particular quantity u, then the mean value of u (i.e. $\bar{u}$), is defined by

$$\bar{u} = \frac{u_1 + u_2 + ... + u_N}{N} = \frac{1}{N}\sum_{i=1}^{N} u_i \qquad \text{(I)}$$

The uncertainty in the result is usually expressed as "root-mean-squared-deviation", which is denoted as Δu, which is computed using the following Eq. (II):

$$\Delta u = \sqrt{\frac{(u_1 - \bar{u})^2 + (u_2 - \bar{u})^2 + ... + (u_N - \bar{u})^2}{N-1}} \qquad \text{(II)}$$

Since in the present work, membrane was cleaned thoroughly after and before each experimental run, the performance of all the membranes were checked through pure water flux (PWF) measurement, hence uncertainties involved in the PWF measurements are reported here.

The uncertainties involved in different experimental measurements for (PWF) for different membranes are estimated and shown in Table ER1.

Table ER1: Values of uncertainties estimated in PWF measurements for membranes prepared at 950 ^{o}C and operated at 310 kPa of transmembrane pressure

Membrane used	**Run 1** **WPF** ($m^3/m^2.sec$) $\times 10^4$	**Run 2** **WPF** ($m^3/m^2.sec$) $\times 10^4$	**Run 3** **WPF** ($m^3/m^2.sec$) $\times 10^4$	**ū** **WPF** ($m^3/m^2.sec$) $\times 10^4$	Δu	**Uncertainties (%)**
Paste method	5.01	5.04	4.96	5	0.041	0.807

Bibliography

Ms. Aparajita Goswami was born in 1982 in Guwahati, Kamrup District, Assam. She obtained her B. E (2003) in Chemical Engineering from Assam Engineering College under Gauhati University and M. Tech (2006) in Petroleum Refining and Petrochemicals from Dibrugarh University, Assam, India. After her M. Tech, she has joined as Assistant Project Engineer in the Dept of Chemical Engineering, IIT Guwahati (2006 - 2009). Thereafter, she was a research scholar in the same Department. Her current interest is on treatment of wastewater including contaminated drinking water using adsorption techniques. Her research publications are listed below.

International Journals:

A. Goswami, M. K. Purkait, The defluoridation of water by acidic Alumina, *Chem. Eng. Res. and Design* 90(2012) 2316-2324.

A. Goswami, P. K. Raul and M. K. Purkait, Arsenic adsorption using copper (II) oxide nanoparticles, *Chem. Eng. Res. and Design*. 90(2012) 1387-1396.

A. Goswami, M.K.Purkait, Kinetic and equilibrium study for the fluoride adsorption using pyrophyllite, *Sep. Sci. Technol*. 46(11) (2011) 1797-1807.

A. Goswami, J. Nath, M.K.Purkait, Cloud Point Extraction Of Nitrobenzene Using TX-100, *Sep. Sci. Technol*. 46(5) (2011), 744-753.

B. K. Nandi, **A. Goswami**, M. K. Purkait, Removal of cationic dyes from aqueous solution by kaolin: kinetic and equilibrium studies, *Applied Clay Sci.*, 42 (2009) 583-590.

B. K. Nandi, **A. Goswami**, M. K. Purkait, Adsorption characteristics of brilliant green dye on kaolin, *J. Haz. Mat*, 161 (2009) 387-395.

B. K. Nandi, **A. Goswami**, A. K. Das, B. Mondal, M. K. Purkait, Kinetic and equilibrium studies on the adsorption of crystal violet dye using kaolin as an adsorbent, *Sep. Sci. Technol.*, 43 (2008) 1382–1403.

Manuscripts Communicated:

A. Goswami and M.K. Purkai, Preparation and characterization of nanoporous schwertmannite for defluoridation of water, Submitted to *Water Research*, (2nd Feb, 2013).

A. Goswami and M.K. Purkai, Defluoridation of contaminated drinking water using nano magnetite schwertmannite, submitted to *J. Haz. Mat*, (27th Feb, 2013).

A. Goswami, D. Mandal, M.K. Purkait, Treatment of colored effluent using surfactant modified bamboo leaves powder, submitted to *Sep. Sci. Technol*., (26th Sept, 2012).

Book Chapter:

Aparajita Goswami and Mihir Kumar Purkait, Kaolin as an adsorbent for color removal, Book: Sorption processes and pollution, Publisher: Presses universitaires de Franche-Comt, ISBN 978-2-84867-304-2, Chapter 8, page 215-230, (2010).

International Conference Presentations:

Aparajita Goswami, Mihir K Purkait, Defluoridation of water by Schwertmannite, *7TH CUTSE Conference*, 6-7 November 2012, Curtin University Sarawak Campus, Malaysia.

Aparajita Goswami, Mihir K Purkait, Nanomagnetite aggregated schwertmannite for Fluoride adsorption, *International conference on Nanomaterials & Nanotechnology (ICNANO-2011),* 18-21 December 2011, Conference centre at University of Delhi, Delhi, India.

A. Goswami, C.R. Medhi, M.K. Purkait, Treatment of Toxic coloured dye effluent using kaolin as adsorbent, *International Congress on Environmental Research (ICER-08),* 18 – 20 Dec., 2008, BITS Pilani - Goa Campus, Goa, India.

National Conference Presentations:

Aparajita Goswami, Prasanta K Raul, Mihir K Purkait, A new Approach of Preparation of Cupric Oxide Nanoparticles, *Recent Trends in Engineering & Education (RTEE-2010),* 28-29 Jan, 2010, NITTTR, Kolkata, India.

B.K. Nandi, **A. Goswami**, M.K. Purkait, Treatment of Colored effluent using low cost adsorbent, *Indian Chemical Engineering Congress (CHEMCON-2007),* 27 – 30 Dec., 2007, Kolkata, India.

Awards:

Best paper award in Chemical Engineering for the paper entitled **"**Defluoridation of water by Schwertmannite**",** presented in *7TH CUTSE Conference***,** Curtin University Sarawak Campus, Malaysia.

Appendix A

Responses to the comments made by national and abroad reviewers

<u>Corrections suggested by abroad examiner</u>

Q1: Author may wish to present drinking water standards of fluoride in India, US and WHO.

A1: Drinking water standards of fluoride in India, US and WHO are presented below [26].

Country wise drinking water standards of fluoride	Minimum limit (mg/L)	Maximum limit (mg/L)
India	0.6	1.2
US	0.6	0.9
WHO	0.6	1.5

[26] World Health Organization (WHO), 2008. Guidelines for Drinking water Quality, third ed., vol. 1. WHO, Geneva.

Q2: To present comparison of various treatment methods conducted by author in a graph may be useful.

A2: In this thesis, various techniques such as adsorption with pyrophyllite, acidic alumina, Sh and NMSh, chemical precipitation (CP), microfiltration (MF) and chemical precipitation followed by microfiltration (CPMF) were used to treat fluoride contaminating water. The performance of individual techniques were plotted in a graph and shown in Fig.A1. From the

graph, it may be concluded that MF technique is not preferable for defluoridation. The performance of all the four adsorbents as well as CP and CPMF was better than MF technique. In case of CP, removal of fine precipitate formed during the process was a major disadvantage of the process. Hence CPMF technique might be preferable than CP.

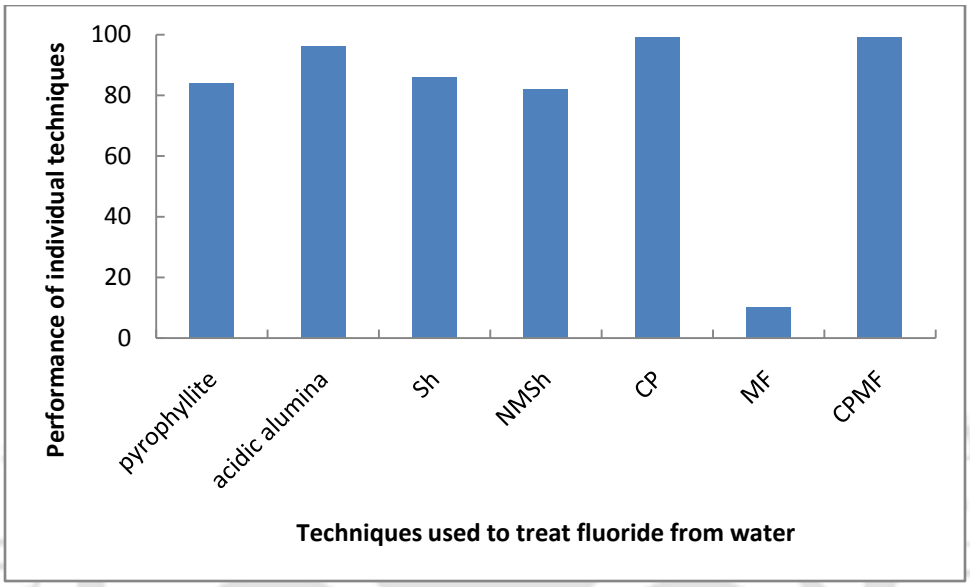

Fig. A1: Comparison of various treatment methods used to treat fluoride contaminated water

Q3: Please present some preliminary cost comparison of various treatment methods for defluoridation.

A3: In this thesis, adsorption, chemical precipitation and chemical treatment followed by microfiltration techniques are described. Selection of these processes was mainly depended on the cost of the individual technique. From the literature, it was found that the cost of adsorption process was cheap as its cost mainly depends on the cost of the adsorbent. In this study, pyrophyllite was used which was a low cost and easily available clay material. The cost of acidic alumina was also very cheap. The preparation cost of Sh and NMSh was also economic as it contains only common synthetic chemicals. The cost of chemical precipitation technique was

also not as high as it depends on mainly the cost of the precipitating agent. In this technique, calcium chloride, calcium hydroxide and calcium nitrate which were common laboratory chemicals were used. In case of membrane preparation, inorganic membranes were prepared using kaolin as the basic raw material. The cost of the kaolin was very marginal. If we compare all these three techniques, adsorption was considered as the cheapest technique. This is due to the fact that in case of chemical precipitation, the separation of the precipitate from the solution was very difficult due to its smaller size of the precipitate. Again in case of membrane preparation by paste method, high temperature furnace is required for sintering the prepared membranes which is a major point. In case of adsorption, no furnace is required as well as no precipitate is formed, hence the separation cost is minimal.

Q4: Please discuss limitations of treatment methods.

A4: Following lines may be read in introduction section after section1.5 of the thesis.

"The above mentioned techniques described in section 1.5 have some advantages and disadvantages. The main disadvantage of chemical coagulation precipitation is the generation of unwanted precipitate and its disposal. Electrocoagulation process was not cost effective as it consumes electricity, again electrode corrosion and formation and disposal of sludge problem. Physical process such as ion exchange process is very costly, so it is not economical. Membrane separation processes have different operation modes such as reverse osmosis, nanofiltration, ultrafiltration and microfiltration. The disadvantages of membrane processes are low economic viability, high maintenance cost, fouling, scaling and membrane fouling problem. Based on the advantages and disadvantages discussed above, the adsorption is widely accepted technology as it is the most efficient, easy, cost effective and fast process."

Q5: Authors conducted batch study in thesis. Author may wish to touch upon continuous reactor study.

A5: This study was focused to observe the performance and fluoride removal capacity of proposed processes. The effect of various process parameters on the extent of adsorption was also reported. Apart from isotherm and kinetic study, a calculation method was presented to know the information on the amount of adsorbent requirement. This information is sufficient to know the details of the process for designing an adsorber column. However, investigation on fluoride removal is our ongoing work and continuous study will be done in due course.

Q6: Chemical precipitation using lime or calcium carbonate will produce large amount of sludge. Please address sludge disposal in the thesis.

A6: We agree with the reviewer. Chemical precipitation using lime or calcium carbonate produce large amount of sludge of calcium fluoride which creates a major disposal problem. The following lines may be read in **section 4.1.4** of the thesis.

"This sludge can safely be added to a landfill. The other uses of this sludge is to be used as raw material in cement plants, in the production of hydrofluoric acid, which is made from CaF_2 by the action of sulfuric acid. CaF_2 precipitate is used in laboratory instruments as a window material for both infrared and ultraviolet radiation."

Q6: Title of thesis deals with fluoride removal. However arsenic removal is included in thesis. Author may wish to discuss why arsenic removal is included in the thesis.

A7: We agree with the reviewer that Title of thesis deals with fluoride removal. However, arsenic removal is included in thesis. This is because, in present situation, fluoride and arsenic

pollution in water is severely affected by the people of India. Hence a preliminary study on arsenic removal is incorporated to the present thesis.

Corrections suggested by national examiner

Q1: Since regeneration studies have been carried out, a detailed analysis of the hysteresis study in adsorption could have given a thorough insight about the feasibility of the material.

A1: We agree with the reviewer. The BET analysis of the adsorbents show the hysteresis study in adsorption. In case of acidic alumina, the hysteresis study shows the feasibility of fluoride adsorption. Following plot shows the hysteresis plot of acidic alumina. Similarly the hysteresis study of pyrophyllite, Sh and NMSh also confirmed the feasibility of fluoride adsorption.

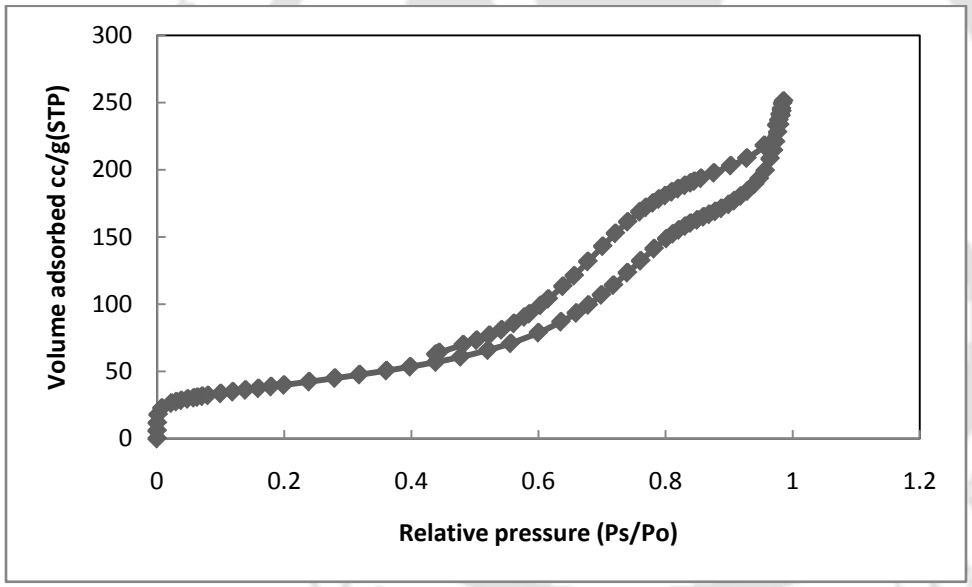

Q2: The effect of multistage (more than one stage) in different flow patterns such as cross current, counter current processes have not been discussed. For one stage, adsorption was found to be 84% but for multistage, the adsorption might show an increment.

A2: We agree with the reviewer. In this work, the fluoride removal performance of various adsorbents was investigated using single stage batch adsorption. The adsorption of fluoride in single stage operation was found to be 84%. The adsorption performance might be increased using multiple stages of adsorption. However, these stage variations were not included within the scope of this work.

Q3: The significance of pH_{zpc} is not well understood.

A3: The zero point charge (pH_{ZPC}) is a concept relating to the phenomenon of adsorption, and it describes the condition when the electrical charge density on a surface is zero. It is usually determined in relation to an electrolyte's pH, and the pH_{ZPC} value is assigned to a given substrate or colloidal particle. In other words, pH_{ZPC} is (usually) the pH value at which a solid submerged in an electrolyte exhibits zero net electrical charge on the surface.

When the pH is lower than the pH_{ZPC} value, the system is said to be "below the pH_{ZPC}." Below the pH_{ZPC}, the acidic water donates more protons than hydroxide groups, and so the adsorbent surface is positively charged (attracting anions). Conversely, above pH_{ZPC} the surface is negatively charged (attracting cations/repelling anions). Zero point charge is of fundamental importance in surface science. For example, in the field of environmental science, it determines how easily a substrate is able to adsorb potentially harmful ions like fluoride, arsenic.

At pH_{ZPC}, the colloidal system exhibits zero zeta potential (i.e., the particles remain stationary in an electric field), minimum stability (i.e., exhibits maximum coagulation/flocculation rate), maximum solubility of the solid phase, maximum viscosity of the dispersion, and other peculiarities.

Q4: In page 113, as the stirring speed increases from 100-200 rpm the maximum adsorption is observed to increase from 92% to 94% but after that there is a sudden decrease to 92% as the speed increases to 300 rpm. At higher rpm, the removal rate of fluoride increases. Give suitable reasons for the same.

A4: Stirring speed is an important parameter in sorption phenomena, which has a serious action on the distribution of the solute in the bulk solution and the formation of the external boundary film. The effect of stirring on the uptake of fluoride by acidic alumina was studied at different stirring speeds (100-300 rpm). From Fig. 3.15, it can be observed that stirring speed significantly affects the sorption of fluoride, thus confirming that the influence of external diffusion on the sorption kinetic control plays a significant role. The percent of fluoride adsorbed was found to increase from 92% to 94% with increased in agitation speed from 100 rpm to 200 rpm, thus confirming that the influence of external diffusion on the sorption kinetic control plays a significant role. With increasing the stirring speed, the rate of diffusion of fluoride molecules from bulk liquid to the boundary layer surrounding the particle becomes higher because of an enhancement of turbulence and a decrease of thickness of the liquid boundary layer. Also it is clear that while increasing the speed from 200 to 300 rpm, the percent removal of fluoride was decreased to 92%. This decrease in percent removal may be attributed to an increase desorption tendency of fluoride molecules and/or having similar speed of adsorbent particles and adsorbate ions. This desorption tendency may be attributed to high mixing speed which means more energy input and higher shear force causing break of bonds between fluoride and the adsorbent.

Q5: From the R^2 values, it is observed that 2^{nd} order kinetics give a better fit. What does it signify?

A5: All the adsorption processes follow pseudo second order kinetics which signifies that chemisorption occurs. The pseudo-second-order rate expression was used to describe chemisorption involving valence forces through the sharing or exchange of electrons between the adsorbent and adsorbate as covalent forces, and ion exchange. In recent years, the pseudo-second-order rate expression has been widely applied to the adsorption of pollutants from aqueous solutions. The advantage of using this model is that there is no need to know the equilibrium capacity from the experiments, as it can be calculated from the model. In addition, the initial adsorption rate can also be obtained from the model.

Q6: It is not clear whether the adsorption process is chemisorption or physisorption process. Since the mass transfer is involved and if reaction is also involved, a detailed derivation of Fick's law from normal mass balance and with proper boundary conditions should have been done with the evaluation of Hatta number.

A6: The relative magnitudes of rate of reaction and the rate of physical mass transfer are expressed in terms of Hatta number. It is defined as,

$$\mathrm{Ha} = \left(\frac{\text{maximum rate of reaction of A in the film per unit interfacial area}}{\text{maximum rate of phsical mass transfer per unit interfacial area}}\right)^{1/2} \quad (1)$$

If the reaction is second-order, the Hatta number (Ha) is defined as,

$$\mathrm{Ha} = \frac{\left(D_A k_2 C_B^{bulk}\right)^{1/2}}{k_L} \quad (2)$$

where k_2 is the reaction rate constant, D_A is the diffusivity of reactant A and k_L is the inter phase mass transfer coefficient. In pyrophyllite (A) – fluoride (B) adsorption system, surface

area of pyrophyllite is 424 m^2/g, particle size of pyrophyllite is 116.7 µm. From Fick's law of diffusivity,

$$J_A = -D_A \frac{dC_A}{dr} \qquad (3)$$

Where J_A flux, D_A is the diffusivity of A, $\frac{dC_A}{dr}$ is the concentration gradient in r direction.

At $t \rightarrow 0$, $C_A \rightarrow 0$, and at $t \rightarrow t$, $C_A \rightarrow C_t$ Rearranging Equation 3,

$$\frac{d\left(C_t/C_o\right)}{J_A} = -\frac{dr}{D_A}$$

Flux J_A is calculated as

$$J_A = \frac{1}{\text{Surface area} \times \text{time}}$$

Flux J_A is varied according to time. Diffusivity (D_A) is calculated from the slope of C_t/C_o versus J_A. For 4 mg/L initial fluoride concentration, k_2= 1.15 g/mg.min, C_B= 0.64 mg/L , k_L=4.52 × 10^{-13} m/s, D_A= 2.9175 × 10^{-12} m^2/s

$$Ha = \frac{\left[\frac{(2.9175 \times 10^{-12} \times 60)m2}{\min} \times \frac{1.15g}{mg}.\min \times 0.64 \times 10^3 mg/m3\right]^{1/2}}{4.52 \times \frac{10^{-13}m}{s}}$$

$$Ha = 7.944 \times 10^8$$

Since $Ha \gg 1$, the adsorption of pyrophyllite – fluoride reaction may be considered as chemisorption.

A7: Our industries generally prefer continuous processes. Thus the breakthrough curve analysis could have given us a better picture.

A7: We agree with the reviewer. Please see answer 5 of abroad reviewer. The study was completed only in batch mode of operation. Continuous study of fluoride removal was not incorporated in the thesis. Hence it is difficult to analyze breakthrough curve. The continuous study of fluoride adsorption will be done in due course of time.

Q8: The most of the experiments were carried out in 250 ml conical flask. Scaling up problems of the process should be incorporated in the thesis.

A8: We agree with the reviewer. In our study batch experiments were carried out using 250 mL conical flask. Following lines are added in the thesis.

During experiment, we calculate thermodynamic parameters (ΔH, ΔG and ΔS) for all the adsorption systems. Adsorption kinetics was studied and rate of mass transfer coefficient was also calculated. The adsorption capacity of adsorbents was calculated from the adsorption equilibrium study. In case of pyrophyllite, thermodynamic study concluded that the fluoride adsorption system was spontaneous and exothermic in nature. From kinetic study, it confirmed that the system followed pseudo second order kinetic model which indicate chemisorption is dominating. Also it concluded that both surface adsorption as well as intra particle diffusion contributes to the rate determining step. From adsorption equilibrium study, it was found that Langmuir isotherm was fitted well with the fluoride adsorption system. This basic information must be helpful for scaling up the process. However development of breakthrough curve might be more helpful for scaling up the process.

Q9. In page 233, the conclusion of the thesis is nothing but the summary of the thesis. So this is to be corrected.

A9: Conclusion section is restructured with quantification of major findings. Please see revised conclusion (Chapter 6)